Title
INTENSITY ANALYSIS OF LOW ENERGY ELECTRONS DIFFRACTED FROM SINGLE .CRYSTAL SURFACES

Author
Farrell, Helen Honora.

Publication Date
1969-11-01

UCRL-19087

INTENSITY ANALYSIS OF LOW ENERGY ELECTRONS DIFFRACTED FROM SINGLE CRYSTAL SURFACES

Helen Honora Farrell
(Ph. D. Thesis)

November 1969

AEC Contract No. W-7405-eng-48

LAWRENCE RADIATION LABORATORY
UNIVERSITY of CALIFORNIA BERKELEY

UCRL-19087

DISCLAIMER

TABLE OF CONTENTS

INTENSITY ANALYSIS OF LOW ENERGY ELECTRONS DIFFRACTED FROM SINGLE CRYSTAL SURFACES

Helen Honora Farrell

Inorganic Materials Research Division, Lawrence Radiation Laboratory,
and Department of Chemistry
University of California, Berkeley, California

ABSTRACT

The intensities of several of the low index low energy electron diffraction beams from the (100) faces of aluminum and palladium have been measured. These have been compared with data already existing in the literature for several other face centered cubic (fcc) metals. Diffraction mechanism based on multiple scattering theory have been assigned to the various intensity maxima observed in the very low energy region. Model calculations of the intensities based on simple multiple scattering theory have been performed. The agreement between the calculated and the observed values was limited by the degree of sophistication of the model atomic potentials employed. The intensities of the LEED beams from the structured surfaces on palladium and platinum have been measured and compared with trends predicted from multiple scattering theory. Simple calculations have been performed for oxygen chemisorbed on the (100) face of the body centered cubic (bcc) metals in the primary stage of oxidation. One model has been suggested on the basis of the calculations and existing experimental data.

I. INTRODUCTION

Experimental low-energy electron diffraction (LEED) studies of metals have a long history which dates back to the Davisson-Germer experiment in 1927.[1] In the following years, LEED has been used to observe qualitative changes in the nature of the surfaces such as those that occur upon heat treatment or the adsorption of gases. However, unlike in the case of the x-ray diffraction, quantitative theoretical interpretation of the diffraction features has been incomplete or only partially satisfactory, particularly in the very low energy ($< \sim 100$ V) region. The relatively large values of atomic scattering cross sections for low energy electron diffraction necessitate the consideration of multiple scattering phenomena. Recently, McRae[2] has developed a formally complete and self consistent theory of dynamical low energy electron diffraction. In the subsequent months, there have been published a large number of theoretical papers[2-10] and calculations[11-14] which have all considered the importance of multiple scattering in analyzing the intensities of the diffraction spots to obtain information about the arrangement of atoms in the surface. A number of theoretical approaches have been developed, but little work has yet been done correlating theory with actual experimental data.

The intensities of several of the low index low energy electron diffraction beams from the (100) faces of aluminum and palladium have been measured. These have been compared with data already existing in the literature for several other face centered cubic (fcc) metals. Diffraction mechanisms based on multiple scattering theory have been assigned to the various intensity maxima observed in the very low energy region. Model calculations of the intensities based on simple multiple scattering theory have been performed. The agreement between the calculated

and the observed values was limited by the degree of sophistication of the model atomic potentials employed. The intensities of the LEED beams from structured surfaces on palladium and platinum have been measured and compared with trends predicted from multiple scattering theory. Simple calculations have been performed for several different models to identify the possible atomic positions for oxygen chemisorbed on the (100) face of the body centered cubic (bcc) metals in the primary stage of oxidation. One model has been suggested on the basis of the calculations and existing experimental data.

II. THEORY

A. Introduction

Many of the unique characteristics of low energy electron diffraction in the energy range 0-500 eV owe their existance to the large scattering cross sections that are involved. Particularly at very low electron energies, 0-100 eV, these cross sections may be of the order of square angstroms. As a consequence, there will be substantial amplitudes scattered into the non-forward directions, and the probability that the electron will be found in the transmitted beam will be significantly less than unity. This results in a high probability that an electron will be incapable of penetrating very deeply into a solid under these conditions before it is scattered, either elastically or inelastically, out of the forward scattered beam. Therefore, most of the intensity that is back-scattered out of the crystal comes from either the surface or the neighborhood of the surface. This, of course, makes low energy electron diffraction an ideal tool for studying the structure of surfaces.

Unfortunately, the very aspect that makes low energy electron diffraction valuable for surface structure analysis also complicates this analysis. That is, because the scattering cross sections are large, not only will the electron be scattered predominantly from the vicinity of the surface, but it will also have a significant probability of being scattered more than once. This phenomenon is known as multiple scattering and its importance vitiates the applicability of the kinematic theory of diffraction which has been used so successfully in the x-ray case where only single scattering or kinematic events are important.

One of the interesting consequences of the fact that scattering is confined to the vicinity of the surface is that the full three dimensional periodicity of the crystal is not experienced by the electron. We therefore are dealing with a potential which has essentially perfect periodicity in the two dimensions parallel to the surface but has imperfect periodicity, perpendicular to the surface. This perfect two dimensional periodicity insures that diffraction will occur and that the electron will be scattered only into certain discrete rods or beams, destructive interferences having taken place along all other directions in space.

More concisely, as has been noted by Boudreaux and Heine,[6] the only exact quantum number in the system is that component of the wave vector, $\vec{K}_{\|}$ or $\vec{K}_{xy}$, which is parallel to the surface and this is indeterminant to the extent of adding any reciprocal lattice vector that is parallel to the surface in the usual sense of the Bloch theorem. Due to the imperfect periodicity perpendicular to the surface however, that the component of the wave vector, $\vec{K}_{\perp}$ or $\vec{K}_{z}$, that is perpendicular to the surface is not constrained to take on only certain discrete values as it would be in the x-ray diffraction case.

However, when only elastic scattering is considered, this perpendicular component is defined by the parallel component and the condition that the total magnitude of the wave vector must be conserved. If the incident electrons are characterized by a total wave vector, $\vec{K}^{0}$, then the components parallel to and perpendicular to the surface may be denoted as $\vec{K}^{0}_{\|}$ and $\vec{K}^{0}_{\perp}$ respectively. In a similar manner, a diffraction beam may be characterized by $\vec{K}'$ with components $\vec{K}'_{\|}$ and $\vec{K}'_{\perp}$. Now, the constraint on the parallel component may be written as

$$\vec{K}'_{\|} = \vec{K}^{0}_{\|} + \vec{G}_{\|} \qquad (1)$$

where $\vec{G}_{\|}$ is some reciprocal lattice vector parallel to the surface. If the surface has rectangular or square symmetry, $\vec{G}_{\|} = 2\pi(\hat{x}\ \frac{h}{a_x} + \hat{y}\ \frac{k}{a_y})$ where h and k are integers x and y are unit vectors in the x and y directions and a_x and a_y are the primitive translational vectors of the surface lattice net in the x and y directions respectively. The z direction has been taken as being perpendicular to the surface. (It is frequently customary to index the diffracted beams with these two integers h and k. For example, the specularly reflected beam is denoted as the (00) beam as it is associated with the null reciprocal lattice vector parallel to the surface. One could then write $\vec{K}'$ as $\vec{K}^{hk}$.)

In free space, the energy of the electron is directly proportional to the square of the total wave vector as $E = \hbar^2 |\vec{K}|^2/2m$ where $\hbar$ is Plancks constant divided by 2π and m is the mass of the electron. Therefore, the constraint that the scattering must be elastic may be written as

$$|\vec{K}'|^2 = |\vec{K}^\circ|^2 \tag{2a}$$

or

$$|\vec{K}_{\|}'|^2 + |\vec{K}_{\perp}'|^2 = |\vec{K}^\circ|^2 \tag{2b}$$

Rearranging Eq. 2b, $K_{\perp}'$ may be determined as

$$\vec{K}_{\perp}^{hk} = \pm \sqrt{|K^\circ|^2 - |G_{\|}^{hk}|^2 - |K_{\|}^\circ|^2} \tag{3}$$

Note that $K_{\perp}'$ may be either positive or negative, corresponding to a diffraction beam directed either into or out of the crystal. Real vaules of $K_{\perp}'$ correspond to travelling waves or allowed states in the crystal while complex or imaginary values correspond to dampèd or evanescent waves at the surface and forbidden states in the bulk of the crystal.

There are actually an infinite number of solutions to Eq. 3.[11] First, there are those within the Ewald sphere where $|\vec{K}^\circ|^2 > |\vec{K}_{\|}'|^2$.

The Ewald sphere is that surface in reciprocal space with a radius of $|\vec{K}^{\circ}|$. When within this sphere, $\vec{K}'_{\perp}$ is real, at least when not in a band gap where it may assume complex values.[15] In the following, the states characterized by real values of $K'_{\perp}$ will be referred to as "allowed" states. Secondly, there are those solutions that lie outside of the Ewald sphere where $|\vec{K}^{\circ}|^2 < |\vec{K}'_{\parallel}|^2$. For these cases, $\vec{K}'_{\perp}$ is purely imaginary and the associated eigenfunctions are strongly damped. Note that $\vec{K}'_{\perp}$ may be either positive or negative, corresponding to diffraction beams directed both into and out of the crystal. As most low energy electron diffraction studies are made as a function of electron energy, it is of value to inspect Eqs. 1,2 and 3 for their energy dependence. Equation 2 states the necessity that the diffracted beam have a wave vector of the same magnitude as the incident beam for elastic scattering whereas Eq. 1 states that the parallel component may contain some reciprocal lattice vector. It may therefore be seen that at a low enough beam voltage these two equations may not be fulfilled simultaneously with real values of $\vec{K}'_{\perp}$ except for the null reciprocal lattice vector. In this region, only the transmitted and the specularly reflected beams are allowed. All other beams will be forbidden, or evanescent. Upon going to higher energies, the magnitude of the wave vector becomes large enough to accomodate the smallest reciprocal lattice vector, and the first order diffraction beams will be allowed in addition to the transmitted and specularly reflected beams. At still higher voltages, higher order diffraction beams will come into existance. From this viewpoint, LEED may be arbitrarily categorized into regions characterized by the allowed diffraction beams. When a diffraction beam first appears, the component of its wave vector perpendicular to the surface will have zero magnitude, and the emergent beam

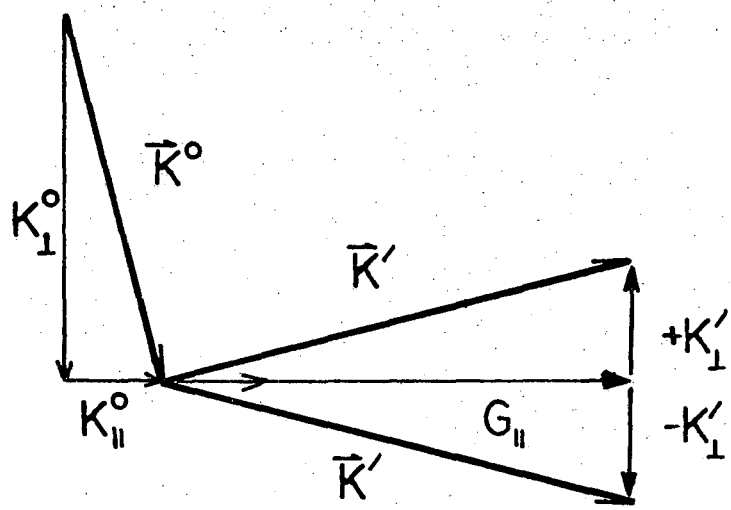

Fig. II-1. Wave vectors for the incident beam and two diffraction beams showing their components parallel and perpendicular to the surface. Note that $\vec{K}'_\parallel = \vec{K}^o_\parallel + \vec{G}_\parallel$.

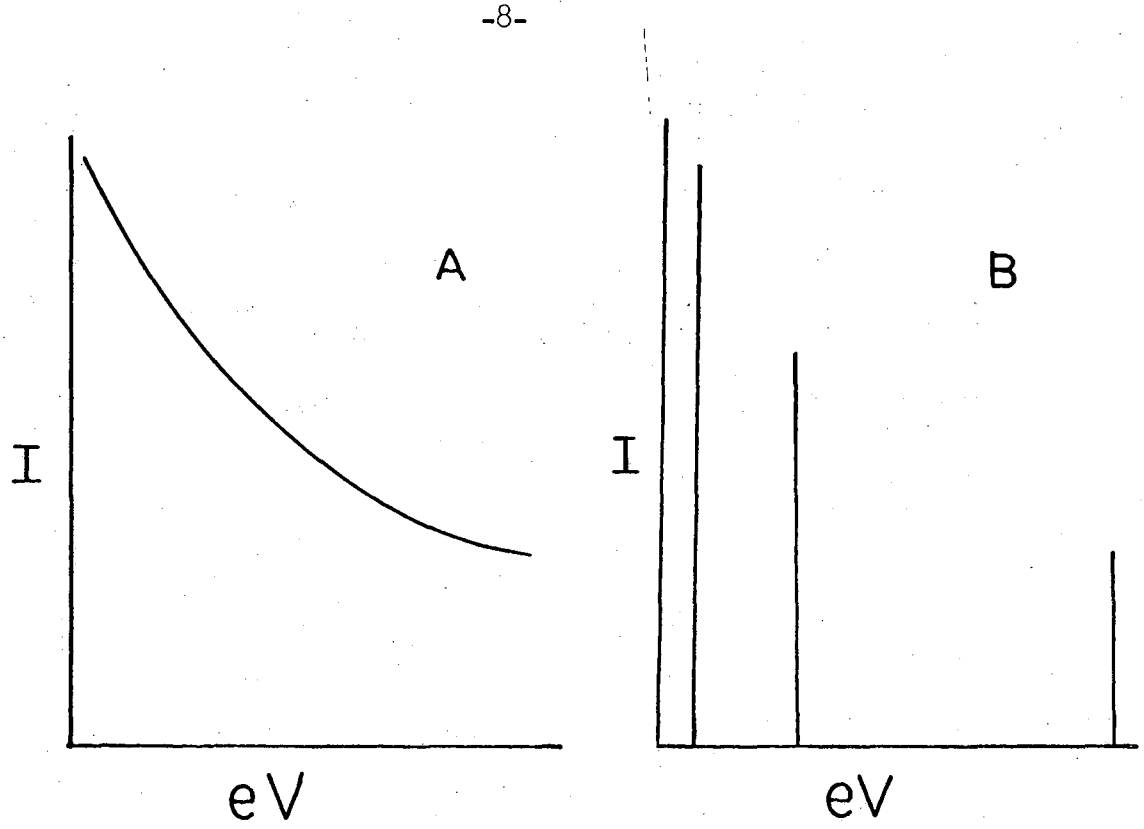

Fig. II-2. A) Intensity of the (00) beam as a function of energy in the pure two dimensional diffraction limit.

B) Intensity of the (00) beam as a function of energy in the pure three dimensional diffraction limit.

will lie in the surface. At a slightly higher energy, $|\vec{K}_{\perp}|$ will have a finite value and diffraction beams directed both into and out of the surface will appear. As the energy is increased, the angle that these new beams will make with the surface increases and these beams will assymtotically approach the axis of the incident or specularly reflected beam. Viewing only the back scattered beams, upon increasing the electron energy one would first see new diffraction beams appear parallel to the surface of the crystal and then rise up out of this surface and sweep through space towards the specularly reflected beam. These considerations arise solely from the symmetry, that is, the two dimensional periodicity parallel to the surface. They are completely independent of the nature of the surface other than its symmetry and the dimensions of its unit cell parallel to the surface.

Information about dimensionalities perpendicular to the surface and about the type of scattering centers involved is, however, contained in the intensities of these diffraction beams. To appreciate the possible variations in these beam intensities, let us consider two limiting cases.

1) Pure Two-Dimensional Diffraction Limit

The first case is that in which there are no periodic modulations in the potential in the direction perpendicular to the surface that are experienced by the electron. This is essentially the two dimensional grating problem. Here if one monitored the intensities of the back-diffracted beams as a function of electron energy, one would find, at best, a monotonic variation. Conceptually, this situation could occur if the scattering cross sections were sufficiently large that the electrons never penetrated the first atomic layer of the surface.

2) Pure Three Dimensional Diffraction Limit

The second limiting case arises in the opposite limit where the cross sections for back scattering are quite small so that the electron can penetrate deeply into the crystal before being scattered. In this case, the effect of the surface can be ignored and the electron will be diffracted predominently in an environment where it is subjected to the full three-dimensional periodicity of the crystal. Now the perpendicular component of the reciprocal lattice vector is no longer free to assume a continuum of values but is limited to certain discrete values by this periodicity in the z direction. This constraint on $\vec{K}'_{\perp}$ may be expressed in a manner similar to Eq. 2 as

$$\vec{K}'_{\perp} = \vec{K}^{\circ}_{\perp} + \vec{G}_{\perp} \qquad (4)$$

where $\vec{G}_{\perp}$ is some reciprocal lattice vector perpendicular to the surface. Note that the combination of Eqs. 2 and 4 is just the Bragg equation for x-ray diffraction expressed in reciprocal space.

If one were to look at the intensities of the diffracted beams in this limit, it would be observed that they were zero except at those points where Eqs. 2 were met simultaneously.

3) The Nature of Low Energy Electron Diffraction

We now have two extreme cases, one where the intensity varies smoothly with electron energy, and the other where the intensity varies abruptly being zero except at certain discrete energies and points in space. Reality for LEED is, of course, somewhere in between. There are modulations in the beam intensities, some, but not all, corresponding to maxima predicted by Eq. 4. Furthermore, particularly at low beam voltages, there is usually finite intensity in these diffraction beams at energies that do not correspond to any diffraction condition. These

observations may be explained by the fact that, even though the scattering cross sections are rather large, they are not so large that the electron does not have a finite probability of penetrating the first and even several of the top most atomic layers parallel to the surface. Consequently, the electron may experience some degree of the full three dimensional periodicity of the crystal.

However, the observation of intensity maxima at energies other than those predicted from Eq. 4 indicate that the situation is not so simple as outlined above. As mentioned before, the very fact that the scattering cross sections are reasonably large can lead to multiple scattering events. These may be envisioned in the following manner. As the amplitudes of the non-transmitted diffraction beams are substantial, and as the cross sections are large, the diffracted beams themselves may act as primary beams or electron sources. Consequently, we must consider diffraction conditions of the form of Eq. 4, but between diffracted beams rather than only between the primary, or incident, beam and a diffraction beam.

We therefore have the new condition

$$\vec{K}''_{\perp} = \vec{K}'_{\perp} + \vec{G}_{\perp} \tag{5}$$

where both $\vec{K}'_{\perp}$ and $\vec{K}''_{\perp}$ are wave vector components corresponding to diffraction beams. Note that Eq. 4 may be considered as a special case of Eq. 5. The analogous condition for the parallel components

$$\vec{K}'_{\parallel} = \vec{K}'_{\parallel} + \vec{G}_{\parallel} \tag{6}$$

is always met. This is guaranteed by Eq. 2.

For sufficiently large cross sections, still more phenomena can be

observed. For example, when the condition expressedin Eq. 5 is met between two diffraction beams, a subsidiary maximum may be observed in a third beam, even though no appropriate diffraction condition is met. This is because all of the beams are more or less coupled for sufficiently large cross sections, and an increase in the intensity of one of them may result in an increase in the intensity of another.

The actual intensity maxima that are observed may be arbitrarily categorized into three different types on the basis of the associated diffraction conditions.

1) Kinematic or Single Diffraction: The first group is comprised of those maxima whose positions are predicted by Eq. 4. This is the kinematic or single scattering case, and peaks should appear at these positions even in the limit of negligible multiple scattering.

2) Double Diffraction: In this case, we have those peaks whose positions are predicted by Eq. 5 rather than Eq. 4. This is a simple multiple scattering situation and may be called the double diffraction case as it necessitates only two successive scattering events.

3) Tertiary and High Order Scattering: This case contains all intensity maxima not directly predicted by Eqs. 4 and 5. Observation of these phenomena should be limited to those situations where multiple scattering is quite strong. One would expect when inelastic scattering was important that maxima of this type would be experimentally observed only with some difficulty.

Although the division of intensity maxima into these three different categories presents a useful classification scheme, it is rather artificial as higher order scattering events may contribute to the intensities of maxima classified as either kinematic or double diffraction even though only one or two events need be considered to predict their positions.

B. Computational Procedures to Evaluate the Scattered Low Energy Electron Beam Intensities

From the above considerations, we see that the geometry of the scattered beams is uniquely defined by the dimensions and two-dimensional symmetry of the crystal surface, and by the energy and angle of incidence of the primary beam. Further, we now know that intensity maxima may appear in these diffraction beams when certain diffraction conditions are met. However, the relative magnitude of these intensity maxima and their precise relationship to the chemical nature and exact positions of the scattering centers can only be determined through a more quantitative investigation of the scattering phenomena.

There are a number of different approaches currently popular in the literature, but they all involve, either explicitly or implicitly finding a solution in some degree of approximation to the Schroedinger equation. It should be emphasized that while many of these approaches appear formalistically different, they are all concerned with the same physical phenomena. They differ primarily in their viewpoint and in the nature of their approximations. The current literature on theoretical calculations of the intensity of LEED beams may be roughly subdivided into two parts on the basis of their starting points.

The first group begins with the differential form of the Schroedinger equation

$$(\nabla^2 + K^2)\, \psi\ (\vec{r}, \vec{K}) = u(\vec{r})\, \psi\ (\vec{r}, \vec{K}) \qquad (7)$$

where K is the magnitude of the wave vector, and $u(\vec{r})$ is $2m/\hbar^2$ times the potential. In general, both the potential and the eigenfunction are expanded in a Bloch or Fourier series and the resulting set of linear inhomogeneous equations are then solved for the coefficients of the eigenfunctions. Frequently, these solutions are obtained for the eigenfunctions

within the crystal and those in free space are determined by matching $\psi(\vec{r},\vec{K})$ and its first derivative at the surface. Variations on this approach have been employed by Hirabayashi and Takeishi,[16] Boudreaux and Heine,[6] Hoffmann and Smith,[12] Jeppson and Marcus,[11] and Ohtsuki[10] among others. Historically, this method has its roots in the works of Bethe[17] and Von Laue.[18]

The second basic approach begins with the integral form of the Schroedinger equation

$$\psi(\vec{r},\vec{K}) = \psi^{\circ}(\vec{r},\vec{K}) - \frac{1}{4\pi} \int_{\vec{r}'} G(\vec{r},\vec{r}')\, u(\vec{r}')\, \psi(\vec{r}',\vec{K})\, d^3 r' \quad (8)$$

where $\psi^{\circ}(\vec{r},\vec{K})$ is the incident beam, $G(\vec{r},\vec{r}')$ is a Greens function and $u(\vec{r}')$ is the potential defined above. An excellent description of the transformation of the differential form of the Schroedinger equation to its integral form is given by Merzbacher.[19] The effect of the integral operator, $\int_{\vec{r}'} d^3 r'\, G(\vec{r},\vec{r}')\, u(\vec{r}')$ on the eigenfunction $\psi(\vec{r}',\vec{K})$ may be regarded as a projection or an evolution of this eigenfunction from a point $\vec{r}'$ to another point $\vec{r}$. As the solution appears also on the right hand side of Eq. 8 under the integral sign, an iterative procedure is often followed. Alternatively, the quantities involved in the integral may be expanded in some appropriate basis set, such as partial waves, the integral solved, and the resulting set of coupled linearly dependent equations resolved as in the case of the differential Schroedinger equation approach. The integral equation, or Greens' function, approach has been utilized by McRae,[2] Kambe,[7,8] and Beeby[9] among others. Historically it is similar to the dynamical theory of x-ray diffraction developed by Darwin.[12]

Regardless of the starting point, there are several basic assumptions employed by most authors. The first is that the incident or primary beam of electrons may be represented as a plane wave. As the actual wave is

presumably coherent for hundreds to thousands of Angstroms,[21] this is probably not a bad approximation.

The second assumption is that the crystal has perfect periodicity parallel to the surface. The degree of perfection required perpendicular to the surface varies from paper to paper. The neglect of the existance of ledges and other surface imperfections is not important in a qualitative discussion though there is some evidence that surface damange can change the results in actual situations.[21]

It is frequently assumed that the electrons that are elastically scattered into the region exterior to the crystal are contained in a number of discrete beams whose wave vectors are defined by Eqs. 1 and 3. While this is definitely true far away from a scattering center, it is not necessarily true in the immediate vicinity thereof. However, calculations performed by McRae[2] for the case of isotropic scatterers indicate that deviations from a plane wave nature may be negligible.

Further, the lattice is generally assumed to be static. This assumption is not valid except perhaps for those materials having a large atomic weight and a high Debye temperature. (see Appendix III).

Inelastic scattering is usually either ignored, or considered on as simple a basis as possible. When considered, it is usually represented as atomic excitations and collective phenomena, such as plasma resonances, are usually neglected. The lack of a detailed consideration of inelastic scattering is somewhat dangerous, particularly as it is frequently the dominent scattering mechanism.[22]

The last assumption is that the scattering is non-relativistic. This is a reasonably good assumption for low energies and light atoms, but further investigation into its validity under other situations is necessary.

From the first assumption, we may write the incident beam as

$$\psi^{\circ}(\vec{r},\vec{K}) = e^{i\vec{K}^{\circ}\cdot\vec{r}} \tag{9}$$

From the secondassumption, that of perfect two dimensional periodicity parallel to the surface of the crystal, we may express the potential of the crystal as a Fourier expansion

$$u(\vec{r}) = \Sigma_{G\|} \; V_{G\|}(z) \; e^{-i\vec{G}\|\cdot\vec{r}\|} \tag{10}$$

where $\vec{G}_{\|}$ is a reciprocal lattice vector parallel to the surface and z is the coordinate perpendicular to the surface. There are several alternate expressions for $V_{G_{\|}}(z)$ which will be used below. The first is in the limit of perfect three dimensional periodicity,

$$V_{G_{\|}}(z) = \Sigma_{G_{\perp}} V_G \, e^{-i\vec{G}_{\perp}\cdot\vec{z}} \tag{11}$$

where $\vec{G}_{\perp}$ is some reciprocal lattice vector perpendicular to the surface and $\vec{G} = \vec{G}_{\|} + \vec{G}_{\perp}$. This expansion will be used in the x-ray or kinematic limit, and for the matching calculations.

The second expansion of $V_{G_{\|}}(z)$ is an integral Fourier expansion

$$V_{G_{\|}}(z) = \int_{-\infty}^{+\infty} d\gamma \; V_G \; e^{-\vec{\gamma}\cdot\vec{z}} \tag{12}$$

where $\vec{G} = \vec{G}_{\|} + \vec{\gamma}$ and $\vec{\gamma}$ is some continuously varying parameter in the z direction. This expression is useful near the surface where the periodicity in the z direction is weak or non-existant. Further, when the potential is expressed as a sum of scattering centers

$$u(\vec{r}) = \sum_{s} W_s(\vec{r} - \vec{R}_s) \tag{13}$$

where the summation is either over layers, or atomic sites, then

$$u(\vec{r}) = \sum_{G,s} W_{s,G} \; e^{-i\vec{G}\cdot(\vec{r}-\vec{R}_s)} \tag{14}$$

and

$$V_G = \Sigma_s W_{s,G} e^{+i\vec{G}\cdot\vec{R}_s} \qquad (15)$$

where the summation over G can be taken to formally include an integration over γ. This expansion is important when there are two or more atoms per unit cell. Below, the structure factor terms, $e^{i\vec{G}\cdot\vec{R}_s}$, will usually be carried implicitly in V_G.

Another result of the second assumption is that like the potential the wave function may be expressed as a Fourier expansion

$$\psi(\vec{r},\vec{K}) = \Sigma_{G_\parallel} A_{G_\parallel}(z) e^{i(\vec{K}^\circ_\parallel + \vec{G}_\parallel)\cdot\vec{r}_\parallel} . \qquad (16)$$

This is a result of Bloch's theorem for two dimensional periodicity. As for $V_{G_\parallel}(z)$, $A_{G_\parallel}(z)$ may be expressed as a discrete or continuous Fourier expansion as the situation warrents. Again, $\vec{G} = \vec{G}_\parallel + \vec{G}_\perp$ or $\vec{G} = \vec{G}_\parallel + \vec{\gamma}$ will be used, and Σ_G will be taken to contain an implicit summation over $\vec{G}_\perp$ or integration over γ as is appropriate to the circumstances. With this in mind, we may write

$$\psi(\vec{r},\vec{K}) = \Sigma_G A_G e^{i(\vec{K}^\circ+\vec{G})\cdot\vec{r}} \qquad (17)$$

It is instructive to consider the calculational procedures in the limit of negligible multiple scattering. More extensive calculations must reduce to these solutions for very small cross sections and these results serve as a basic frame of reference within which multiple scattering phenomena may be discussed. In addition, general techniques can be outlined, with a minimum of detail.

In the kinematic limit, when multiple scattering is insignificant, it may be assumed that the electron has a much greater probability of being found in the primary, or transmitted beam than in any other. In addition it may be assumed that the electron penetrates deeply enough into the crystal

to experience its full three dimensional periodicity, and that surface effects are negligible. We therefore may use the three dimensional expansion of the potential and wave function.

Substituting equations 10,11 and 17 into the differential form of the Schroedinger equation, there results

$$(\nabla^2 + K^2)\,\Sigma_G A_G\, e^{i(\vec{K}^\circ + \vec{G})\cdot r} = \Sigma_{G''} V_{G''}\, e^{-\vec{G}''\cdot\vec{r}} \times \Sigma_{G'} A_{G'}\, e^{i(\vec{K}^\circ+\vec{G}')\cdot\vec{r}}$$

which becomes

$$\Sigma_G \{(K^2 - |\vec{K}^\circ + \vec{G}|^2)\; A_G - \Sigma_{G'} V_{G'-G} A_{G'}\}\, e^{i(\vec{K}^\circ+\vec{G})\cdot\vec{r}} = 0. \qquad (19)$$

As the functions $e^{i(\vec{K}^\circ+\vec{G})\cdot r}$ form a linearly independent basis set, we need only consider the set of equations

$$(K^2 - |\vec{K}^\circ+\vec{G}|^2)A_G - \Sigma_G V_{G'-G} A_{G'} = 0. \qquad (20)$$

In this limit, it is not necessary to solve simultaneously this total set of equations in order to determine the amplitudes, A_G, as we have made the assumption that $A_0 \gg A_G$. Therefore Eq. 20 becomes

$$(K^2 - |\vec{K}^\circ+\vec{G}|^2 - V_0)\, A_G - V_G A_0 = 0 \qquad (21)$$

or

$$A_G = \frac{V_G}{(K^2 - |\vec{K}^\circ+\vec{G}|^2 - V_0)}\, A_0 \qquad (22)$$

This is essentially the x-ray result, that the amplitudes of the various diffraction beams are proportional to a Fourier coefficient in the expansion of the potential.

We obtain a similar result by using the integral equation approach. There, assuming that $A_0 \gg A_G$ is the same as making the first Born approximation. That is, we may substitute $\psi^\circ(\vec{r},\vec{K})$ for $\psi(\vec{r},\vec{K})$ under the integral

sign on the right hand side of Eq. 8. Making this approximation and substituting Eq. 10 and 11 into Eq. 8 we obtain

$$\psi(\vec{r},\vec{K}) \cong -\int_{\vec{r}'}\int_{\vec{K}'} d^3K' \frac{e^{i\vec{K}'\cdot(\vec{r}-\vec{r}')}}{|\vec{K}'|^2 - |\vec{K}^\circ|^2} \sum_G V_G\, e^{-i\vec{G}\cdot\vec{r}'}\, e^{i\vec{K}^\circ\cdot\vec{r}'} d^3r' \tag{23}$$

where the spectral form of the Greens function is used (see the following section). Utilizing the following two equations

$$\int_{\vec{r}} e^{i\vec{Q}\cdot\vec{r}}\, d^3r = \delta(\vec{Q}); \quad \vec{Q} = \vec{K}^\circ - \vec{G} - \vec{K}' \tag{24}$$

and

$$\int_{\vec{K}'} d^3K' \frac{e^{i\vec{K}'\cdot\vec{r}}}{|\vec{K}'|^2 - |\vec{K}^\circ|^2}\, \delta(\vec{K},\vec{K}^\circ - \vec{G}) = \frac{e^{i(\vec{K}^\circ - \vec{G})\cdot\vec{r}}}{|\vec{K}^\circ - \vec{G}|^2 - |\vec{K}^\circ|^2} \tag{25}$$

we obtain

$$\psi(\vec{r},\vec{K}) = \Sigma_G \frac{V_G}{|\vec{K}^\circ|^2 - |\vec{K}^\circ - \vec{G}|^2}\, e^{-i(\vec{K}^\circ - \vec{G})\cdot\vec{r}} \tag{26}$$

where, by a comparison with Eq. (17) and (22) it may be seen that the relative amplitudes are identical with those from the differential form of the Schroedinger equation.

1. Differential Equation Approach

One of the earliest non-kinematic LEED calculations was performed by Hirabayashi and Takeishi.[16] They used the differential equation approach in an extension of Von Laue's[18] dynamical theory. An explicity accounting of the termination of the crystal periodicity at the surface was made by utilizing the forms for the potential and wave function given in Eqs. 10 and 16. Substituting these equations into the differential form of the Schroedinger equation, and proceeding as in the kinematic case, they obtained;

$$\frac{d^2 A_{G_\parallel}(z)}{dz^2} + \cdot [(\vec{K}^2 - |\vec{K}^\circ_\parallel + \vec{G}_\parallel|^2) - V_0(z)] A_{G_\parallel}(z)$$

$$- \sum_{G_\parallel \neq G_\parallel} V_{G_\parallel - G'_\parallel} A'_{G_\parallel}(z) = 0 . \qquad (27)$$

This set of coupled first order differential equations in $A_{G_\parallel}(z)$ could conceivably be solved for the amplitudes of the various diffraction beams. However, Hirabayashi and Takeishi did not attempt a completely self consistent solution, but rather made the approximation $|A_0(z)| \gg |A_G(z)|$, i.e. that the intensity of the incident beam is much stronger than that of any of the diffracted beams. Numerical calculations were performed for the specularly reflected beam in the case of graphite and were compared with experimental results. The agreement is not bad in the region above 100eV but becomes progressively worse at lower voltages. This is not unexpected as the approximation $|A_0(z)| \gg |A_G(z)|$ becomes less valid at lower energies. This paper is of vital significance as it was the first to attempt a dynamical treatment of low energy electron diffraction. Not only did it illustrate that reasonable agreement with experimental data could be obtained at higher energies by considering only a limited number of beams, but it further underlined the fact that the amplitudes of the diffracted beams are not negligible relative to that of the incident beam in the very low energy region. The condition that $A_G(z) \sim A_0(z)$ is precisely that which is associated with multiple scattering, and it is this condition which necessitates a more self consistent treatment of the problem.

A related but more complete method has gained considerable popularity recently, particularly among the solid state physicists. This is the wave matching approach where the wave equation is first solved within the perfectly infinite crystal and then the eigenfunctions outside of the crystal are determined by matching these wave functions and their normal derivatives

at the surface. In this approach, the primary problem is identical with that of determining the energy band structure within the crystal, but only for that energy and that component of the wave vector, $\vec{K}_{\|}^{o}$, parallel to the surface which characterize the incident beam. This method has the advantage that it may draw upon much of the knowledge accumulated about energy band calculations. It is particularly applicable to uncontaminated and unreconstructed surfaces, and leads to a clear insight into the relationship between reflected intensities and the band structure of the solid. The wave function inside the solid may be expressed as a linear combination of the Bloch functions for the perfect bulk crystal, as in Eq. 17. However, there are the restrictions that the energy of these functions must be that of the incident beam and that the component of their wave vector parallel to the surface must be both real and equal to that of the incident beam to within a parallel reciprocal lattice vector.

There are actually an infinite number of Bloch waves satisfying these conditions. First, there are those within the Ewald sphere. The component of their wave vector that is perpendicular to the surface may be either real or complex depending respectively on whether or not they are in a band gap. When complex, the imaginary component must always be chosen such that the total wave will be an evanescent or a damped wave incapable of being transmitted by the crystal. Secondly, there are those Bloch waves that lie outside of the Ewald sphere. The perpendicular components of their wave vectors are pure imaginary and they are strongly damped. Fortunately, in actual calculations the contributions from those terms outside of the Ewald sphere are small and, when the cross sections are not very large, only those within or those whose distance from the Ewald sphere is less than a few reciprocal lattice vectors need be considered.

The first phase of the problem within the framework of this approach is to solve the wave equation within the crystal. Inserting equations 10,

11, and 17 into the differential form of the Schroedinger equation, there results

$$(\nabla^2 + K^2) \quad \Sigma_G A_G \; e^{i(\vec{k} + \vec{G})\cdot \vec{r}} = \Sigma_{G''} V_{G''} e^{-i\vec{G}''\cdot \vec{r}} \times \Sigma_{G'} A_{G'} e^{i(\vec{k}+\vec{G}')\cdot\vec{r}} \tag{28}$$

which, upon performing the indicated differentiation and then rearranging, becomes

$$\Sigma_G \quad \{(K^2 - |\vec{k}-\vec{G}|^2 - V_0)A_G - \sum_{G'\neq G} V_{G'-G}A_{G'}\} e^{i(\vec{k}+\vec{G})\cdot\vec{r}} = 0 \tag{29}$$

or, as the traveling wave terms, $e^{i(\vec{k}+\vec{G})\cdot\vec{r}}$, are linearly independent

$$(K^2 - |\vec{k} - \vec{G}|^2 - V_0) \; A_G - \sum_{G'\neq G} V_{G'-G} A_{G'} = 0 . \tag{30}$$

This set of linearly dependent equations in the amplitudes, A_G, has solutions if and only if the secular determinent is equal to zero, i.e.

$$\begin{vmatrix} (K^2 - |\vec{k} - \vec{G}_{\|}|^2 - V_0) & -V_{G_{12}} & \cdots \\ -V_{G_{21}} & (K^2 - |\vec{k}-\vec{G}_{22}|^2 - V_0) & \\ \vdots & & \end{vmatrix} = 0 \tag{31}$$

The relative values of the amplitudes A_G, may be determined as cofactors of the secular matrix,[23] and their absolute values then determined from the normalization condition

$$\Sigma_G |A_G|^2 = 1. \tag{32}$$

Again, the above solution is essentially identical with that for an energy band problem with the exception that those solutions which attenuate, or are damped, are also considered.

The second phase of the problem is to match the wave function and its first derivative with respect to the surface normal within the crystal to that wave function and its derivative that are exterior to the crystal.

In this manner, the amplitude of the diffracted beams in free space may be determined. The matching equations are

$$\psi(\vec{r},\vec{K}) = \psi_B(\vec{r},\vec{K}); \quad z < z_s \tag{33a}$$

$$\psi(\vec{r},\vec{K}) = \psi_E(\vec{r},\vec{K}); \quad z > z_s \tag{33b}$$

$$\psi_B(\vec{r},\vec{K})\,|_{\vec{r}=\vec{r}_s} = \psi_E(\vec{r},\vec{K})|_{\vec{r}=\vec{r}_s} \tag{34}$$

and

$$d\psi_B(\vec{r},\vec{K})/dz|_{\vec{r}=\vec{r}_s} = d\,\psi_E\,(\vec{r},\vec{K})/dz|_{\vec{r}=\vec{r}_s} \tag{35}$$

when $\psi_B(\vec{r},\vec{K})$ is the wave function in the bulk of the crystal, $\psi_E(\vec{r},\vec{K})$ is that exterior to the crystal, and $\vec{r}_s$ is the coordinate of the crystal surface.

The simplest case, the two beam case at normal incidence where only the transmitted and the specularly reflected beams are allowed, has been discussed in detail by Boudreaux and Heine.[6] The development is as follows. Within the crystal, the Bloch function is given by

$$\psi_B(\vec{r},\vec{K}) = A_0\, e^{i\vec{K}\cdot\vec{z}} + A_{\vec{G}_\perp}\, e^{i(\vec{K}-\vec{G}_\perp)\cdot\vec{z}} \tag{36}$$

where K is given by equation 31. When $\vec{K} = \vec{G}_\perp/2$, we are at the end of a Brillouin zone and consequently in an energy gap. For the smallest $G_\perp$, this corresponds to the first Bragg reflection. Away from the gap, the wave function within the crystal is predominantly that of a traveling wave directed into the crystal, and $A_0 > A_{G_\perp}$. The coefficient of the back reflected wave, $A_{G_\perp}$, is given, to a first order, by Eq. 22 for the kinematic case.

However, within the band gap the waves are strongly coupled and a simple perturbation approach is no longer valid. It may be shown that within the gap, A_0 and $A_{G_\perp}$ have the same magnitude, and differ at most

only by a phase factor, 2ϕ, i.e.

$$|A_0|\, e^{+i\phi} = |A_{G_\perp}|\, e^{-i\phi} \tag{37}$$

where ϕ varies from 0 to $\pm \pi/2$ from one edge of the gap to the other.[6] The sign of ϕ depends upon the sign of $V_{G_\perp}$. Further, at energies inside of the gap, there are no corresponding real values of $\vec{K}$. This is a direct consequence of Eq. 31 and has the physical significance that there are no traveling waves allowed within the crystal at these energies. There are, however, complex values of $\vec{K}$ that are allowed that correspond to evanescent or damped waves that are localized at the surface of the crystal. It follows then that

$$\vec{k} = \vec{K}_R + i\,\vec{K}_M \tag{38}$$

where $\vec{K}_M$ is the imaginary part of $\vec{k}$ and $\vec{K}_R$ is the real part. $|\vec{K}_R|$ is equal to $|\vec{G}_\perp|$ within the gap and $|\vec{K}_M|$ is zero at the edges of the gap. Within the gap, the Bloch function inside of the crystal is

$$\psi_B(\vec{r},\vec{K}) = |A|\,\{e^{i\phi}\, e^{-K_M z}\, e^{i\vec{G}_\perp\cdot\vec{z}/2} \tag{39a}$$

or

$$+ e^{-i\phi}\, e^{-K_M z}\, e^{-i\vec{G}_\perp\cdot\vec{z}/2}\}$$

$$\psi_B(\vec{r},\vec{K}) = |A|\, e^{-K_M z} \cos(\vec{G}_\perp\cdot\vec{z}/2 + \phi) \tag{39b}$$

The wave function outside of the crystal is

$$\psi_E(\vec{r},\vec{K}) = e^{i\vec{K}^\circ\cdot\vec{z}} + A'\, e^{-i\vec{K}^\circ\cdot\vec{z}} \tag{40}$$

By matching ψ_B and ψ_E and their first derivatives at the surface, the value of A', the amplitude of the specularly reflected beam may be determined. It is found that $|A'|$, the magnitude back reflected amplitude, is equal to unity. This is not unexpected as all of the electrons striking the crystal must be back reflected at energies within the band gap as there are no allowed travelling waves within the crystal in this region. When inelastic scattering is taken into account, $|A'|$ of course will be

less than unity. As the band gap is of width V_G, it follows that, to a first approximation this also will be the width of the Bragg peak. Similar arguments hold at higher beam voltages and for other diffraction beams. Consider the case where a higher order diffraction beam characterized by $\vec{K}' = \vec{K}'_{\parallel} + \vec{K}'_{\perp}$ met a diffraction condition of the form

$$2\vec{K}'_{\perp} = \vec{G}_{\perp} \tag{41}$$

The higher order diffraction beam will behave in a similar manner to the specularly reflected beam discussed above. At this point, there is a band gap, and no traveling waves with $\vec{K}'$ are allowed in the crystal.[6] Consequently, the electron must be either reflected out of the crystal or, alternatively, scattered into some beam for which there is an allowed state. Actual calculations have been performed using variations on this wave matching technique. Hoffman and Smith[12] have applied this approach to the problem of calculating the intensities of the (00), (01) and (11) diffraction beams from the 100 face of aluminum at normal incidence. They used a 27 term Fourier expansion of the potential with a 10 eV inner potential correction and a constant 2.5 volts imaginary part of the potential to simulate inelastic scattering. In addition to Bragg peaks predicted by kinematic theory, they found secondary peaks associated with multiple scattering phenomena. While the agreement with experimental data is imperfect, it does illustrate the validity of this approach for real problems.

Model calculations using the wave matching approach have been performed by Carpart[13] and by Marcus and Jepsen[11] for simple cubic crystals. Marcus and Jepson effected the solution of the one-dimensional linear differential equations given in Eq. 27 through the use of a propoagation matrix. They used a potential of point ions of charge Z in a sea of uniform negative charge. The calculations were performed for non-normal incidence. Their

published results show both the band structure and the reflected intensities. The strong correlation between the band structure and the intensities is quite obvious. The several types of multiple scattering phenomena discussed above are well represented. Carpart has used a pure wave matching approach. His calculations are particularly important as they were performed for a cubic ensemble of S- wave scatterers. This same model potential was used by McRae[2] in the first self consistent dynamical LEED calculations using the integral equation approach. The strong agreement between the results of these two approaches substantiates their fundamental similarities. It is of interest to note that while the S-wave scatterer potential is an easy model in the integral equation approach, it is a particularly difficult model within the differential equation approach. This is because all of the Fourier coefficients have the same magnitude and consequently, a large number of terms must be carried. Consequently, the claim is made that the achieved agreement constitutes rather important evidence that the method can be used for real situations. Carpart's work also includes a band structure calculation and again, there is a definite relationship between the band structure and the beam intensities.

The detailed results of these model calculations will be considered in Appendix I along with those from the integral equation method.

2. Integral Equation Approach

While the differential form of the Schroedinger equation has been employed in a number of different approaches that are related to the determination of the band structure of solids, the integral form is conceptually more concerned with the scattering mechanisms from a number of different scattering centers. Further, the previous approach is most easily handled when the crystal has perfect three dimensional symmetry

right up to the surface, while the following method initially assumes nothing about the periodicity of the system in the direction normal to the surface.

Assuming the potential to be formally expressible as a sum of individual scattering centers as in Eq. 13, the integral form of the Schroedinger equation becomes a sum of integral equations

$$\psi(\vec{r},\vec{K}) = \psi^{\circ}(\vec{r},\vec{K}) + \sum_{s} \int_{\vec{r}'} G(\vec{r},\vec{r}')\, W_s\,(\vec{r}'-\vec{R}_s)\, \psi(\vec{r}',\vec{K}')\, d^3r' \qquad (42)$$

where, if all of the centers are identical, only one integral need be evaluated. The formal solution is now independent from the total symmetry or lack thereof, of the problem. However, as most LEED problems do have a two dimensional symmetry parallel to the surface, it is useful to introduce this as it results in some simplification of the problem. This symmetry is explicitly assumed when Eqs. 14 and 17 for the potential and the wavefunction are substituted into Eq. 42 which then becomes

$$\psi(\vec{r},\vec{K}) = \psi^{\circ}(\vec{r},\vec{K}) + \sum_{s,g,g'} \int_{\vec{r}'} \left[G(\vec{r},\vec{r}')\, V_{s,g-g'}(z)\, e^{-i(\vec{g}-\vec{g}')\cdot\vec{r}'\|} \times A_{g'}(z)\, e^{i(\vec{K}^{\circ}\| + \vec{g}')\cdot\vec{r}'\|}\, d^3r' \right] \qquad (43)$$

Here, g has been used to indicate $G_{\|}$ in order to avoid confusion with the Greens' function $G(r,r')$. The terms of the structure factor, $e^{i(\vec{g}-\vec{g}')\cdot\vec{R}_s}$, have been absorbed into $V_{s,g-g'}(z)$. The Greens function has several different acceptable forms; among others it may be used as an expansion of spherical harmonics or in its spectral form

$$G(\vec{r},\vec{r}') = \int_{\vec{K}'} d^3K' \, \frac{e^{i\vec{K}'\cdot(\vec{r}-\vec{r}')}}{|\vec{K}'|^2 - |\vec{K}^{\circ}|^2} \,. \qquad (44)$$

Substituting this spectral form of the Greens function into Eq. 43 and integrating over $\vec{r}_{\|}$, there results

$$\psi(\vec{r},\vec{K}) = \psi^{\circ}(\vec{r},\vec{K}) - 2 \sum_{s,g,g'} \int_{z} \left[dz' \, V_{g-g'}(z') \, A_{g'}(z') \right.$$

$$\left. \times \int_{\vec{K}'} d^{3}K' \; \frac{e^{i\vec{K}'_{z}\cdot(\vec{z}-\vec{z}')}}{|\vec{K}'|^{2} - |\vec{K}^{\circ}|^{2}} \; e^{i\vec{K}'_{\|}\cdot\vec{r}_{\|}} \; \delta\left(\vec{K}'_{\|}, \vec{K}^{\circ}_{\|} + \vec{g}\right) \right] . \qquad (45)$$

Using the properties of the delta function to first integrate over $K'_{\|}$ and then over $\vec{k}'_{z}$, one obtains,

$$\psi(\vec{r},\vec{K}) = \psi^{\circ}(\vec{r},\vec{K}) - 4\pi \sum_{s,g,g'} \left[\frac{e^{i(\vec{K}^{\circ}_{\|} + \vec{g} + \vec{k}_{g})\cdot\vec{r}}}{2 i k_{g}} \right.$$

$$\left. \times \int_{z'} V_{g-g'}(z') \; A_{g'}(z') \right] \qquad (46)$$

Here, $|k_{g}| \equiv \sqrt{|\vec{K}^{\circ}|^{2} - |\vec{K}^{\circ}_{\|} + \vec{g}|^{2}}$ is the component of K' perpendicular to the surface.

This formal solution illustrates several points about the integral equation approach. The use of symmetry and the expansion of the potential into a sum of individual potentials have been mentioned above. Further, the solution may usually be expressed as a sum of plane wave states characterized by the appropriate parallel reciprocal lattice vector. The amplitudes in these states are, of course, dependent upon the nature of the potential and the geometry of the crystal. Moreover, they are inversely proportional to the perpendicular component, $|\vec{K}'_{\perp}| = |\vec{k}_{g}|$, of the diffracted wave vector. This is a direct consequence of the imposition of perfect two dimensional symmetry on the Greens function.

Kambe[7] has shown how to derive a specific form of the Green's function that is particularly tailored to this problem as

$$G(\vec{r},\vec{r}') = \Sigma_g \frac{e^{i(\vec{K}^\circ_{\parallel} + \vec{g} + \vec{k}_g) \cdot (\vec{r}-\vec{r}')}}{2i\, k_g} \cdot \quad (47)$$

In addition, he has given an excellent discussion of the relationship between the Green's function and the integral equation approach.

Kambe has also developed a solution to the integral form of the Schroedinger equation.[8] Key to the whole approach is the particular choice of the form of the potential. As in Eq. 13, it is assumed that the potential can be expressed as a sum of potentials centered at particular atomic positions. Further it is assumed that these potentials are of the "muffin-tin" type; specifically, that the total potential is contained in a series of spherically symmetric non-overlapping globes and that there is a constant potential between these spheres of zero value. As the wave function and its first derivative must both be continuous, it follows that at the surface of these spheres, the wave functions that are inside any given sphere must match those that are external to it. Moreover, because there is no potential between the spheres, any outgoing wave that leaves a sphere must travel unperturbed, at least until it enters another sphere. Therefore, by knowing $\psi(\vec{r},\vec{K})$ at the surface of the sphere, its value in free space may be calculated in the following manner.

Using the property that the potential is a sum of spherical potentials and is zero in between, the integral over all space may be reduced to a sum of integrals over the spheres as in Eq. 42. Using the form of the Schroedinger equation $(\nabla^2 + K^2)\,\psi(\vec{r},\vec{K}) = W_s(\vec{r})\,\psi(\vec{r},\vec{K})$, these sphere potentials in the integral equation may be replaced with the differential operator $\nabla^2 + K^2$. Ordinarily, there would be little advantage to this procedure as the potential term carries the important information about the scattering process. However, in this case it is assumed that the information

is already contained in the wave functions under the integral sign. That is, it is assumed that the $\psi(\vec{r},\vec{K})$ on the right hand side of Eq. 42 has already been determined as solutions to the differential form of the Schroedinger equation where the potential employed is that of the sphere under consideration. Green's theorem is used to transform the volume integrals to surface integrals over the spheres. Then the eigenfunction and the Green's function terms are expanded in spherical harmonics and the integral solution is obtained. Kambe has shown that the results of this method are essentially identical with those of McRae, at least for the case of isotropic scatterers.

The first self-consistent dynamical theory of LEED to be published was that of E. G. McRae.[2a] This paper was particularly significant not only for the mathematical formalism, but also for the model calculations that it contained. These calculations qualitatively illustrated many of the important aspects of multiple scattering such as its dependence upon cross-section, angle of incidence, etc.

In many ways, McRae's derivation of a solution for the wave equation is similar to that of Kambe's. They both employ a Green's function approach, a "muffin tin" potential and both expand into spherical harmonics to perform the integration. However, McRae's approach differs in that the potential between the spheres is not constrained to have a zero value. In addition, Green's theorem is not evoked and only volume integrals are used. Further, $G(\vec{r},\vec{r}')$ is utilized in its real space expression rather than as an expansion of Bloch-like functions.

The salient feature of McRae's theory is the concept of the effective field $\psi^S(\vec{r},\vec{K})$. The total field is considered to be composed of the primary field, $\psi^\circ(\vec{r},\vec{K})$, and the fields emitted by all of the atoms,

$\Sigma_s \psi^s (\vec{r},\vec{K})$. Within this viewpoint, the effective field incident on any given atom is the sum of the primary field and all of the fields emitted by all of the other atoms. This is the basis of this self-consistent approach. The field emitted by any atom is a function of all of the fields emitted by all of the other atoms and, for sufficiently large cross-sections, multiple scattering of all orders is a logical consequence of this inter-dependence.

McRae's derivation begins with Lax's equations for the total field $\psi(\vec{r},\vec{K})$, and the effective field, $\psi^s(\vec{r},\vec{K})$

$$\psi(\vec{r},\vec{K}) = e^{i\vec{K}\cdot\vec{r}} - \Sigma_s \int_{\vec{r}'} \frac{e^{iK|\vec{r}-\vec{r}'|}}{|\vec{r}-\vec{r}'|} T(\vec{r}',\vec{r}_s)\, \psi^s(\vec{r}',\vec{K})\, d^3r' \qquad (48a)$$

$$\psi^s(\vec{r},\vec{K}) = e^{i\vec{K}\cdot\vec{r}} - \sum_{s\neq t} \int_{\vec{r}'} \frac{e^{iK|\vec{r}-\vec{r}'|}}{|\vec{r}-\vec{r}'|} T(\vec{r}',\vec{r}_s)\psi^s(\vec{r}',\vec{K})\, d^3r' \qquad (48b)$$

where the transition operator, $T(\vec{r}',\vec{r}_s)$ is defined by

$$T(\vec{r}',\vec{r}_s)\, \psi^s(\vec{r}') = V(\vec{r}'-\vec{r}_s)\, \psi(\vec{r}') \qquad (49)$$

An effective partial wave expansion scattering factor

$$\langle f^s(\vec{K}'\leftarrow\vec{K})\rangle = \sum_\ell \langle f^s{}_\ell(K)\rangle P_\ell(\vec{K}'\cdot\vec{K}) \qquad (50)$$

for the individual atoms is defined in terms of the transition operator and the plane wave amplitudes of the effective fields. Then the Green's function and the travelling wave exponentials are expanded in terms of spherical harmonics and the integral is executed. At this point, the two-dimensional periodicity of the crystal is evoked by requiring that the effective field have a Bloch like form

$$\psi^s(\vec{r}_\parallel,\vec{z}) = \phi^s(\vec{r}_\parallel,\vec{z})\, e^{i\vec{K}_\parallel\cdot\vec{r}_\parallel} \qquad (51)$$

where $\phi^s(\vec{r}_\parallel,\vec{z})$ has the periodicity of the surface. Again, the interplay between the two dimensional symmetry (expressed here through the effective field) and the nature of the Green's function results in a term of the

form $\Sigma_g (k_g^{-1}) \exp [i(\vec{g} + \vec{k}_g)\cdot(\vec{r}-\vec{r}_s)]$. As before, the solution may be expressed in the form

$$\psi(\vec{r},\vec{K}) = \psi^\circ(\vec{r},\vec{K}) + \sum_G A_G e^{i(\vec{K}^\circ_{\parallel} + \vec{g} + \vec{k}_g)\cdot\vec{r}} \qquad (52)$$

where

$$A_G = \frac{2\pi i}{\Omega} \Sigma_s \alpha_s^s \langle f^s(\vec{K}_g \leftarrow \vec{K})\rangle \; e^{i\vec{G}\cdot\vec{r}_s} \qquad (53)$$

where α^s is the ratio of the effective field at the s^{th} atom to the primary field at the same point, that is

$$\alpha^s = \phi^s \exp [-i\vec{K}^\circ\cdot\vec{z}_s]. \qquad (54)$$

An equation similar to Eq. 52 holds for the effective field. It should be noted that the effective atomic scattering factor and the effective field are interdependent so that both quantites must be calculated iteratively. This interdependence results from calculating the effective atomic scattering in terms of the plane wave amplitudes of the effective fields.

This formalism was used to calculate the intensity of the back diffracted electron beams from the (100) face of a hypothetical simple cubic crystal. A number of different intensity maxima were observed in the calculated plots. Their relation to the diffraction conditions expressed in Eq. 5 will be discussed in Appendix I.

McRae has studied the behavior of these intensity maxima, or peaks, as a function of cross section.[2] He has found that as the cross section is reduced, those peaks which are non-kinematic in nature diminish in intensity more rapidly than do those that are allowed in the kinematic limit. This is reasonable as the non-kinematic peaks have their origin in multiple scattering in contrast to the single scattering kinetmatic peaks. The smaller that one makes the cross sections, the more improbable multiple scattering will be relative to single scattering, all things else being equal. In addition to changes in the ratios of peak heights, McRae

has found that the peak positions may move when the cross sections are reduced. In the limit of small cross sections, the positions approach those predicted from the free electron model. This is to be expected as reducing the cross sections is essentially the same as reducing the interactions of the electron with the crystal. Therefore, the band gaps become more narrow and the coupling between different beams is diminished.

Both McRae[2] and Marcus and Jepsen[11] have considered the effect of non-normal incidence on the intensity vs energy curves. In general, those beams that are strongly coupled to other beams in a given energy range developed very pronounced fine structure when the degeneracy is broken by deviating from normal incidence. This is in sharp contrast to the kinematic case where maxima would be expected to move, but would not be expected to split and develop fine structure when the angle of incidence is varied. The development and variation of fine structure with changes in the angle of incidence has been observed experimentally.[24]

McRae has also studied the effect of introducing inelastic scattering by assigning a complex value to the scattering phase shift.[2] The effect was to change the shape and reduce the height of the peaks without changing their position or their base width. In addition, there is a tendency for inelastic scattering to discriminate against higher order multiple scattering events when that inelastic scattering is considered in the form of individual atomic excitations.

Ohtsuki has also considered the effect of inelastic scattering.[10] He has formally developed a theoretical approach to the LEED problem in the limit of strong absorption, that is, when the diffraction potential is small compared with the inelastic potential. His qualitative conclusions are similar to those of McRae. His formalism is sufficiently general to include bulk phenomena that are not well represented by individual atomic excitations.

When a surface structure is present, that is, when the surface layer is different from all of the underlying bulk layers, it is more convenient to use a detailed scattering approach such as the integral equation method rather than the differential equation, or band structure approach. The formalisms of McRae[2] and Kambe[8] may be used to effect a solution to this problem. In addition, several authors have approached this problem through the use of a scattering or transfer matrix.

Beeby[9] has developed a method where the amplitude of the diffracted beam is expressed as an infinite summation. This form is particularly interesting because of the physical interpretation of his result. The first term in the summation is the single scattering term. It represents the electron being scattered only once before leaving the crystal and would be the dominant term in the kinematic limit. The second term is a double scattering term. The electron is first scattered at a point r_1 and is then scattered again at a second point r_2 before leaving the crystal. The following terms correspond to higher order multiple scattering events. This approach is of course similar to an iterative Born expansion. The step wise picture leads to a fairly direct interpretation of the physical significance of the various terms.

McRae[3] has considered the problem in a similar manner. He has approached the problem as a generalization of Darwin's theory of diffraction.[20] Here, however, unlike Darwin, he has considered all beams to be coupled and has allowed for the possibility that the surface may differ from the bulk of the crystal. McRae[4] has considered, in particular, the case where only single and double diffraction are important. Like Beeby, he has expressed the amplitude of the diffracted beam as a summation

$$\underline{b_0} \cong \underline{b_1} + \underline{b_2} \qquad (55)$$

where $\underline{b}_0$ is a column vector whose components are the amplitudes of the plane wave components of the total wave field emitted by the crystal. The term $\underline{b}_1$ contains those contributions from single scattering events and may be regarded as a modified kinematical expression for the diffraction amplitude. The term $\underline{b}_2$ corresponds to double diffraction events where the electron has been scattered twice before leaving the crystal.

The physical meaning of the various terms is illustrated in Fig. II-3. The heavy line indicates the unique surface layer. The bulk layers that are chosen are to be considered as representative.

This approach has been suggested by Bauer,[25] among others, and should be useful where multiple scattering is weak, but not so weak as to place the problem in the kinematic limit. This situation could conceivably arise when inelastic scattering is strong, or when the number of diffraction beams is sufficiently large that the amplitude in any given beam is small.

When the surface layer has a periodicity that bears an integral multiple relationship to the periodicity of the bulk, fractional order beams will be diffracted back from the crystal. The only non-vanishing contributions from $\underline{b}_1$ to the intensity of these fractional order beams will come from the surface layer. This contribution will contribute little to the modulation of the intensity of these fractional order beams. Therefore, the contributions primarily from $\underline{b}_2$ will determine the structure of the intensity curves. Furthermore, according to McRae[4] the peak position should resemble a superposition of intensity curves for the integral order beams. Physically, one may regard this process in the following manner. The diffraction beams that are formed within the crystal have large amplitudes in the back direction in the neighborhood of band gaps. As these large amplitude integral order diffraction beams leave the crystal, they impinge

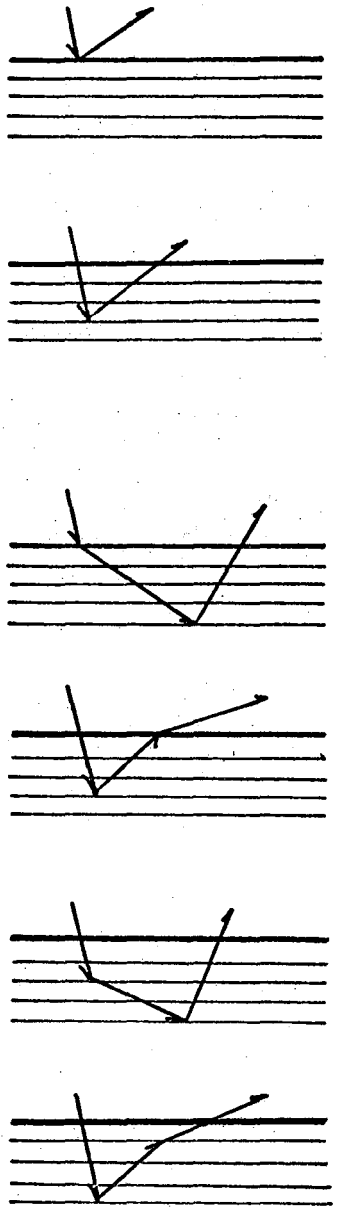

Fig. II-3. Schematic representation of several simple scattering processes involving the surface layer of atoms and/or bulk atomic layers.

upon the surface layer. Part of their intensity is lost by scattering at the surface layer into the fractional order beams. Thus, the surface layer serves to mix the intensities of the various beams. From these considerations, it is to be expected that surface structures with the same periodicity, but different chemical natures, should give rise to peaks in the same positions. The intensities of these peaks should of course be dependent upon the detailed nature of the scattering centers.

McRae and Winkler[5] have considered the case where a gas is adsorbed in register on a crystal. They find that when the surface layer differs significantly from the bulk, that the secondary or fractional order Bragg peaks are damped relative to the kinematically allowed Bragg peaks. This result may be interpreted in terms of destructive interference in the double diffraction terms because of the disparity between the surface and the bulk. The step wise diffraction picture formally developed by McRae[4] and Beeby[9] has been used earlier in a more intuitive form by Gafner.[14] He has carried out a multiple diffraction calculation for several of the diffraction beams from the Ni(111) face. The amplitudes of the waves which were formed at each diffraction event were adjusted to make their sum equal the incident amplitude multiplied by an adsorption factor to account for inelastic scattering. This is in contrast to the usual method of normalizing through intensities rather than amplitudes. The relative scattering factor was assumed to be unity for all scattering angles other than zero where it was given the value of 9. The step wise scattering process was considered in the following manner. The normally incident beam was diffracted into the several allowed diffraction beams at the first layer. The beams scattered into the crystal were allowed to undergo oscillatory diffraction between the first and second layer until all of

the beams had amplitudes less than some prescribed value. The beams that were scattered out of the crystal in this process were gathered up with those scattered back out of the incident beam. The beams that were scattered forward in this process were combined vectorially and oscillatory diffraction between layers 2 and 3 was allowed to proceed as in the preceding case. This process was continued until all beam amplitudes in the crystal had fallen below the prescribed limit. Despite the approximations and assumptions within this model (or, perhaps because of them), the agreement between the calculated and the experimentally observed intensity curves is quite encouraging.

III. EXPERIMENTAL

A. Apparatus

The low energy electron diffraction apparatus employed was of the post-acceleration type manufactured by Varian Associates.[26] The electron source was an indirectly heated bariated tungsten filament.[27] The electrons were electrostatically focused and then accelerated into a field free region containing the sample. Those electrons that were back scattered to within about 40° of the incident direction were intercepted by a detector system. The diffraction chamber was constructed of stainless steel. Visual and mechanical access to the chamber was obtained through several ports. High vacuum seals were made with stainless steel knife edge flanges and copper gaskets. The chamber was pumped by a 140 liter per second ionization pump. Forepumping was accomplished with cryogenic pumps containing a molecular sieve that were chilled with liquid nitrogen. An auxillary vacuum system could be used to admit controlled quantities of pure gases into the diffraction chamber.

The display system consisted of a set of grids and a fluorescent screen. The outermost grid was maintained at ground potential to ensure the field free nature of the sample region. The next grid closer to the screen was maintained at a negative potential, usually cathode potential. This grid was used as a velocity selector to reject those electrons scattered inelastically. The commercially available equipment contained only these two grids but in most of the work reported here, these were supplemented by a third grid. This extra grid was maintained at either ground or cathode potential and was used to improve resolution. Those electrons which successfully penetrated this system of grids were then

accelerated through five thousand volts onto the fluorescent screen where their kinetic energy was converted to visible light. The intensity detected on the fluorescent screen was a linear function of the current density in the region of interest.[28] This intensity was measured with a telephotometer[29] whose output was generally plotted as a function of electron energy, in electron volts, on an X-Y recorder.

The samples were attached to the sample holder by two strips of tantalum. These were gripped by stainless steel pressure contacts that were bolted to a ceramic rectangle mounted on the central shaft of the sample holder. In this manner, the sample was electrically isolated from the body of the chamber. The sample was heated by passing an electrical current through it. This current was carried by oxygen free high purity copper braids that were attached to high vacuum electrical feed throughs mounted in the base of the flange. The temperature of the sample was monitored with a platinum-platinum 10% rhodium thermocouple that was spot welded to the sample or to the sample holder in the vicinity of the sample. The thermocouple voltage was monitored through another set of high vacuum electrical feed throughs.

The central shaft was fastened to the stainless steel flange through a stainless steel knife edge bellows. By compressing or expanding these bellows, the sample could be translated into or out of the region of the electron beam. Further, the flexibility of these bellows allowed the sample to be rotated around the axis of the central shaft. A limited amount of translation perpendicular to the central axis was also allowed.

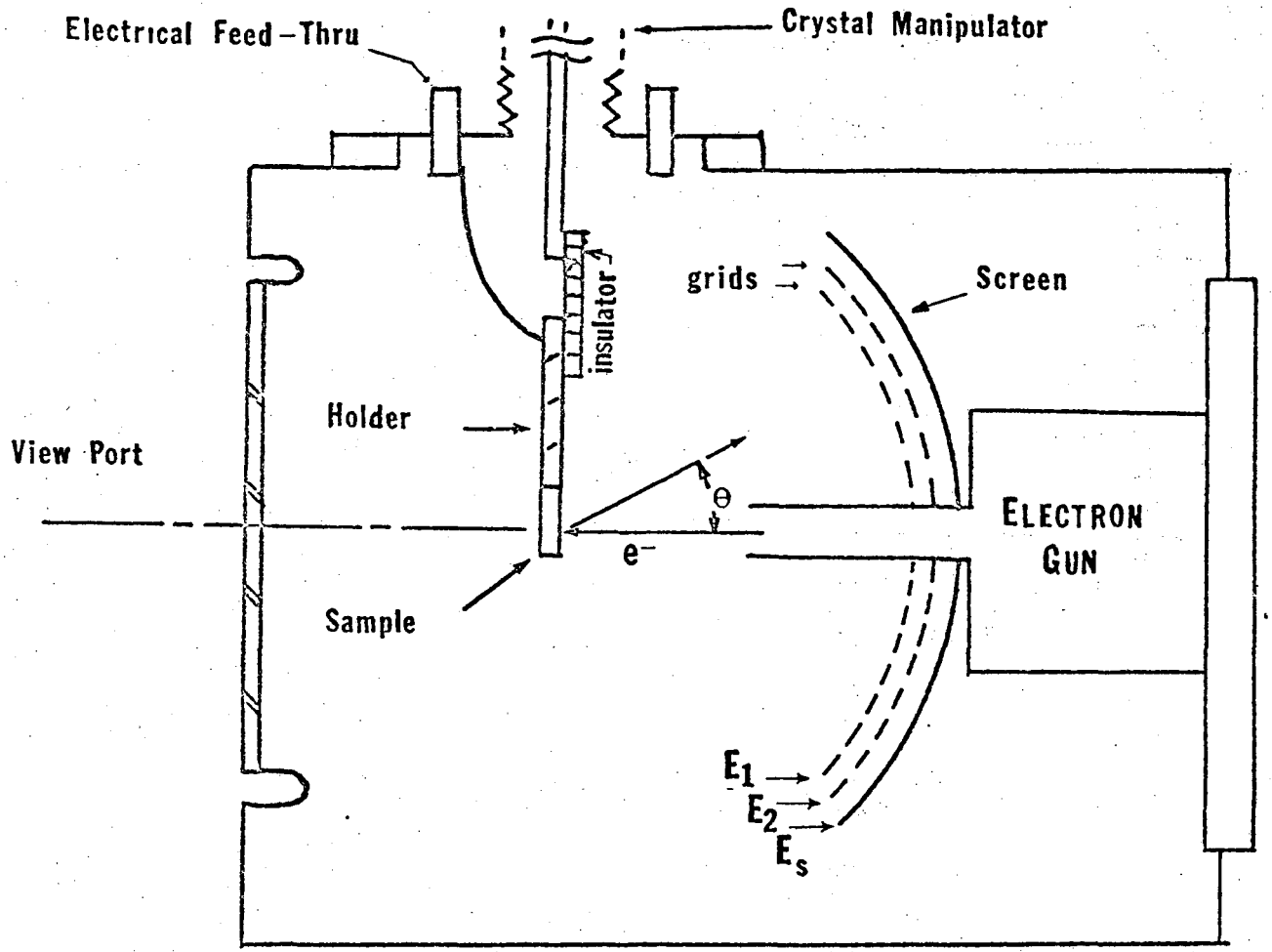

Fig. III-1. Schematic diagram of the LEED chamber.

B. General Technique

The following procedure was used to place the single crystal samples into the diffraction chamber. The electron optics were turned off at least one hour before the vacuum in the diffraction chamber was broken. This was done by admitting dry nitrogen gas slightly in excess of one atmosphere. The chamber was then opened to a dry nitrogen atmosphere by removing the sample manipulator. The resulting opening was covered to prevent dust from entering the chamber. A slight over pressure of dry nitrogen was maintained at all times. The old sample was removed from the manipulator and replaced by the new one. Then the manipulator, with a new copper gasket, was rejoined to the diffraction chamber, the system isolated and then pumped down with the cryopumps to below 5 microns. The total elapsed time from the initial admission of dry nitrogen was usually between 30 and 90 minutes. The ionization pumps were then started and the diffraction chamber was isolated from the rest of the system. The whole assembly was then baked out for 18 to 36 hours at approximately 250°C.

After the chamber had cooled enough to touch, the sample was degassed by heating to 300 or 400°C and the electron optics were turned on. In general, no diffraction patterns were observable at this point, presumably because of apparent disorder in the surface introduced by the surface preparation and because of contamination of the surface when exposed to the ambient in the loading procedure. Therefore, further steps had to be taken to clean the sample surface. Occasionally, however, a well prepared palladium sample would give a diffraction pattern of moderate quality as judged by the size and intensity of the diffraction spots with no further cleaning. Usually it was necessary to ion bombard the sample.

This was particularly so in the case of aluminum which invariably acquired a tenacious oxide coating during the loading procedure. The conditions which most frequently used ion bombard were 2×10^{-5} torr argon accelerated at 300 to 350 volts. This resulted in ion currents between 1 and 5 microamperes per square centimeter. Occasionally, xenon was used instead of argon. Ion bombardment times varied between fifteen minutes for an uncontaminated palladium sample to 36 hours for an oxidized aluminum sample. The sample was frequently ion bombarded several times during the course of an experiment. It was usually necessary to heat the samples after ion bombardment to anneal out surface damage and to desorb occluded inert gas atoms introduced in the ion sputtering process. The annealing temperature varied with the material, in general being higher for the more refractive metals than for the softer ones. For example, aluminum was usually annealed at 400 to 600°C while temperatures greater than 800°C were used for iridium.

After an acceptable diffraction pattern was obtained, intensity measurements were performed in the following manner: first, the magnetic field due to the earth and adjacent equipment was balanced with a trimming magnet so as to obtain field free conditions in the diffraction chamber. This was necessary as a net magnetic field would produce varying electron beam deflections at different beam voltages with the result that the angle of incidence would not be constant.

The intensity of the diffraction spots was monitored by focusing the telephotometer on one of the spots as it appears on the fluorescent screen. For the specularly reflected diffraction spot the scattering vector is perpendicular to the surface plane at any electron beam energy

(wavelength). Hence, its position on the fluorescent screen remains unchanged as a function of beam voltage. The telephotometer could thus be held stationary while scanning the intensity as a function of eV for this (00) reflection. However, when monitoring the intensities of the non-specularly reflected diffraction spots, it was necessary to manually track these spots with the telephotometer as their scattering angle and hence their position on the fluorescent screen changed when the beam voltage was varied. The final curves were constructed as an average of a number of trials in order to minimize any error introduced in this procedure.

C. Palladium

A single crystal of nominally 99.99% pure palladium was purchased from the Materials Research Corporation, (MRC) in Orangeburg, New York. Neutron activation analysis of the actual crystal that was used indicated that the purity was 99%. The major contaminents were found to be; Pt (5000 ppm), Cu (3000 ppm), Mn (2000 ppm); Au (180 ppm), Fe (150 ppm) and Rh (100 ppm). Also present in concentrations between 1 and 100 ppm were Ag, Al, Cd, Cr, Mo, Ni, Ru, Si, Sn, Ti, W and Ir. Sulphur was present in 2 ppm. The concentrations of oxygen and carbon were not reported.

The palladium single crystal was x-ray oriented and then spark cut to within 2° of the [100] face. The resulting samples were approximately 0.5 cm wide, 1 cm long and 0.2 cm thick. These samples were then polished either manually or mechanically with successively finer mesh abrasive down to a 5 micron alumina grit.

The samples were chemically etched at least twice before use. Once, following the polishing procedure to remove the residual mechanical damage to the surface, and once immediately before placing the sample in the LEED chamber to remove any oxide film or other surface contaminents. The etching procedure proved to be more art than science in that no consistent combination of times, temperatures and concentrations was found to be optimal for a given material and crystal face. The general procedure was as follows. A mixture of 20 parts H_2O, 5 parts HNO_3 and one part HCl was heated to 80°C. The sample was then placed in this solution with a minimum of agitation. In a short period of time, a reddish brown film formed on the sample and then sluffed off. A new film would form again and the cycle would be repeated. If the sample was removed from the solution during the period of film formation, a rough and non-reflective surface would result.

If, however, the sample was removed during a period of film deterioration, a smooth and shiny surface was more probable. Immediately after removing the sample from the etchant, it was rinsed in a dilute nitric acid solution. The sample was then rinsed in copious quantities of distilled water and finally with electronic grade methanol.

The sample was mounted by spot welding it to two tantalum strips that had previously been etched in a mixture of HNO_3, H_2SO_4 and HF. Care was taken not to mar the surface during this procedure and the sample was usually re-rinsed in dilute nitric acid followed by water and methanol to remove any copper acquired in the welding procedure. In general, the tantalum strips were placed along the long sides of the sample and the welding contacts applied to the tantalum rather than the palladium in order to minimize contamination. Once constructed in this manner, the sample could be resistively heated by applying a voltage across the tantalum strips and causing a current, either D. C. or A.C., to flow through the sample. The spot welds usually supplied the region of maximum resistance and consequently the temperature was usually highest in this region. Visual estimates of temperature gradients indicated that variations were less than 25 - 50°C across the sample. The sample temperature was monitored with a platinum-platinum 10% rhodium thermocouple spot welded either to the tantalum holder, or between the holder and the sample. Temperatures were never allowed to exceed 800°C to prevent contamination of the diffraction chamber by vaporized palladium.

1. Experimental Observation of Pd(100) Surface Structures

Several different surface structures have been observed on the (100) face of palladium. In addition to the (1×1) structure, a (2×2) structure and a C(2×2) structure have been investigated.[21,30] These structures are

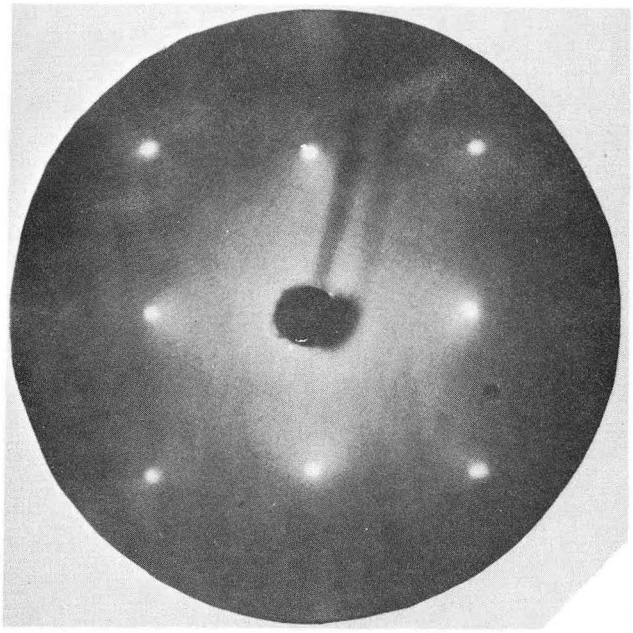

(1x1)

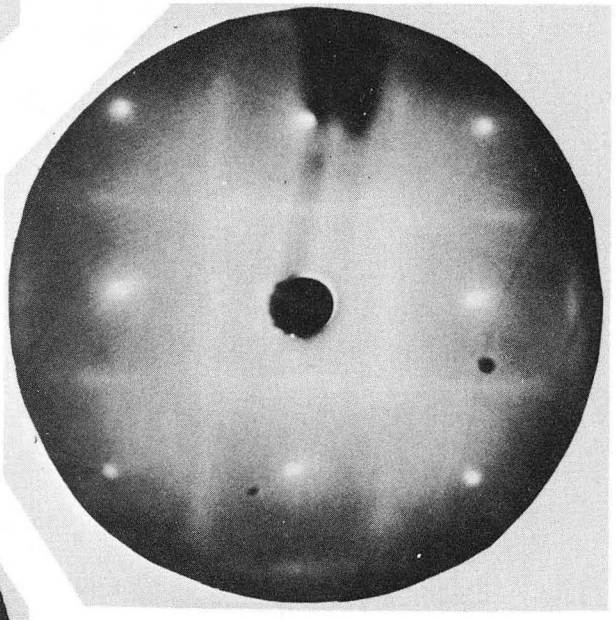

(2x2) with streaks

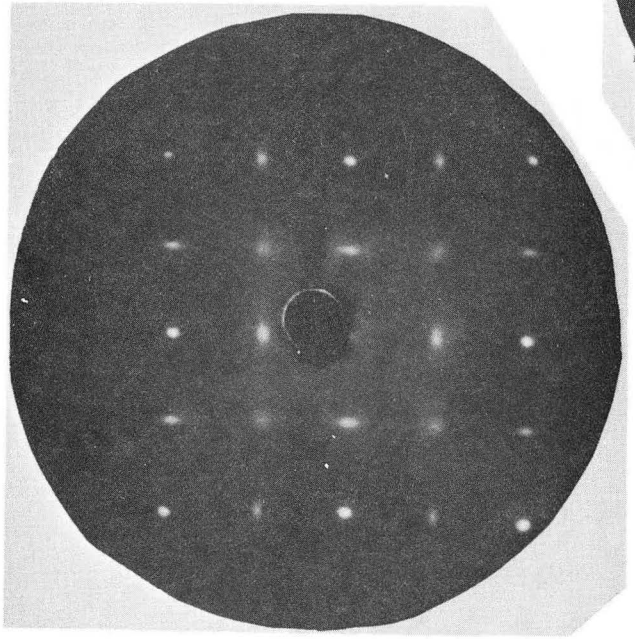

(2x2)

XBB 699-6090

Fig. III-2a. Diffraction Patterns for several different surface structures on the (100) face of palladium near 100 eV.

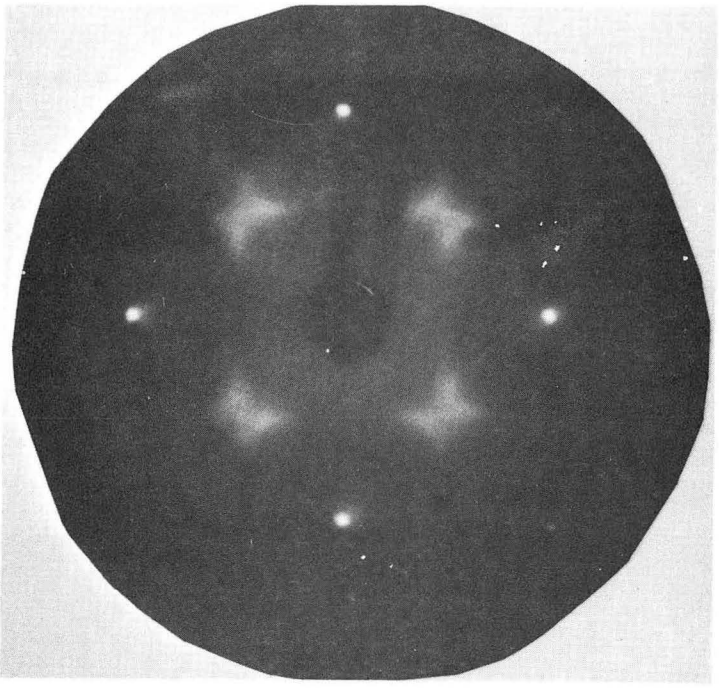

Disordered C(2×2).

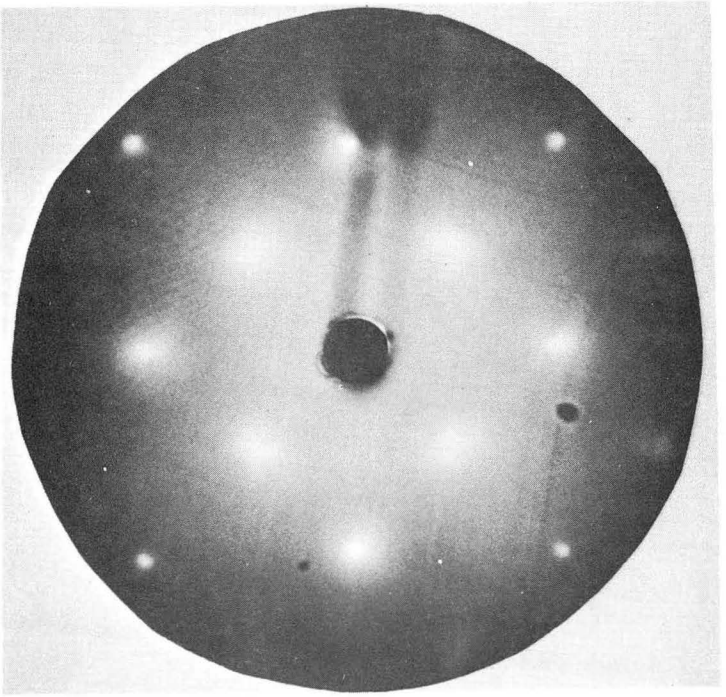

C(2×2).

XBB 699-6091

Fig. III-2a. continued

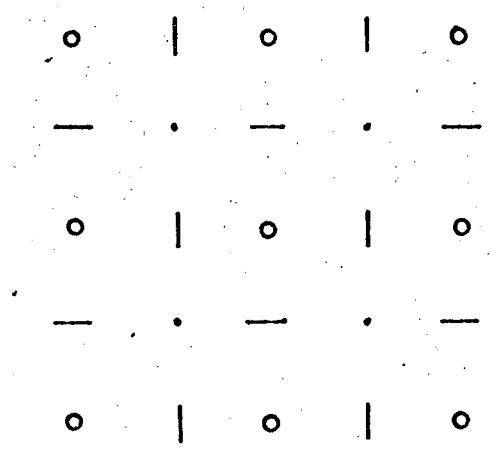

Normal (2X2) with streaks.

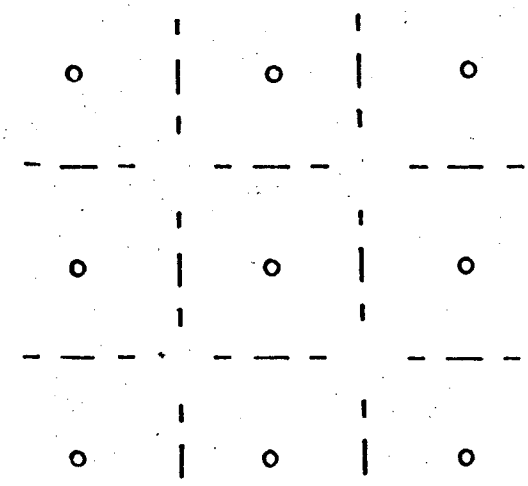

Transient (2X4).

Fig.III-2b. Schematic for the diffraction patterns from the (100) face of palladium with a normal (2X2) with streaks surface structure and with a transient (2X4) surface stucture produced by heating.

formed by heating a freshly ion bombarded Pd(100) surface to successively higher temperatures. The diffraction patterns obtained for the (1×1), (2×2) and C(2×2) surfaces are shown in Fig. III-2 along with diffraction patterns obtained from intermediate structures. The observation of a (2×2) diffraction pattern indicate that there existed some structure on the surface of the sample that had twice the periodicity of the substrate, while a C(2×2) diffraction pattern indicates that the surface structure has twice the periodicity of the substrate but is also centered. The streaking and elongation of the diffraction features that are observed for the structured surfaces indicate that a considerable amount of disorder exists along certain crystallographic directions.

The following is a description of a typical palladium experiment. A diffraction pattern was observed above 250 eV immediately after bakeout with no intermediate ion bombardment. The pattern improved upon heating to successively higher temperatures until by 500°C it was quite clear but showed a (2×2) structure with definite streaking. Repeated anneals at temperatures between room temperature and 650°C showed that, once formed, this structure was stable in this temperature range.

Upon heating the sample above 700°C, a transition to a C(2×2) structure was observed to begin. This transition was not sharp and was characterized by diffraction features that were elongated along the direction of the original streaks as shown in Fig. III-2. This gave the new diffraction features a star or butterfly shaped appearance.

After standing in a 5×10^{-10} torr ambient for 18 hours, the amount of surface area that was characterized by this disordered C(2×2) diffraction pattern had increased at the expense of that fraction of the surface area covered by the (2×2) structure. Flashing the sample did not change the

Table III-1. Several diffraction patterns observed on the (100) face of palladium.

Diffraction Pattern	Approximate Temperature Range of Stability	Comments
(1×1)	$\lesssim$ 25°C → ~ 250°C	Formed by ion bombardment
(2×2)	25°C → ~ 600°C	Initial formation between 200°C and 400°C.
C(2×2)	25 C; ~600°C → $\gtrsim$ 1000°C	Initially formed above 600°C apparently stable at room temperature, disorders when heated above 300°C.
(2×4)	~200°C	Observed as a transient when (2×2) is heated ~400°C and then cooled.

diffraction pattern. Upon standing an additional 34 hours at room temperature is an ambient of 5×10^{-10} torr, there was no longer any evidence of the (2×2) structure, and the total surface gave a definite C(2×2) diffraction pattern with broad fuzzy extra spots. Reheating the sample to 450°C initiated a transition from the pure C(2×2) back to the "butterfly" structure. The elongation of the extra spots indicated that the heating had caused some disordering along the major crystallographic directions. Further heating to around 475°C caused still further disorder and the (2×2) with streaks began to reappear. However, when the sample was allowed to stand at room temperature for 12 hours, it was found that the surface was totally covered by a well defined C(2×2) structure. The pattern remained unchanged after standing at room temperature for 12 hours, it was found that the surface was totally covered by a well defined C(2×2) structure. The pattern remained unchanged after standing at room temperature for several days. Upon flashing the sample, little evidence of gas coverage was noted. When the sample was heated to 665°C, the "butterfly" pattern was regenerated again. However, it was found that heating the sample for short periods of time (less than one minute) below 300°C did not tend to visibly disorder the pattern.

Recapitulating, it has been observed that when a Pd(100) sample was heated between 400 to 600° C, a streaked (2×2) diffraction pattern was formed. Further heating to above 700°C formed a disordered C(2×2) diffraction pattern. It was found that once the transition to the C(2×2) structure was initiated, this transformation would proceed spontaneously at room temperature over a period of several days. Heating a sample characterized by a C(2×2) surface structure caused the process to be partially reversed as first the disordered C(2×2) and then the streaked (2×2) diffraction

patterns were regenerated. No evidence for extensive gas coverage was noted.

It was usually possible to regenerate a (1×1) diffraction pattern from the C(2×2) diffraction pattern by a light ion bombardment treatment, typically 10 minutes at 240 volts and 1.4×10^{-5} $\mu A/cm^2$. However, when the C(2×2) structure had been extensively heated for long periods of time, heavier ion bombardments were found to be necessary as a light treatment would regenerate the structure characterized by a streaked (2×2) diffraction pattern rather than a (1×1) pattern.

Once a (1×1) pattern had been formed by ion bombardment, care had to be taken not to reintroduce the (2×2) structure. Heating the sample in excess of 200°C even for short periods of time often produced vague indications of the new structure. Unfortunately, the treatment necessary to anneal out ion bombardment damage was usually adequate to initiate this transition. Therefore most of the studies made on the (1×1) surface were usually performed with only a partially annealed sample.

On another sample, a careful study was made of the (2×2) with streaks structure. It was found that after this structure had been heated to less than 450 °C, transient fine structure was observed in the diffraction pattern. Approximately 5 minutes after the heating, vague detail could be seen in the streaks connecting the extra spots. These streaks had a ropy texture and these appeared to be three extra spots between the usually (1/2 1/2) positions. This structure is shown in Fig. III-2. After 10 to 12 minutes at room temperature, these transient features had coalesced into the usual streaked (2×2) diffraction pattern. This phenomena was found to be reproducible and presumably had not been noted before because of its transient nature.

3. Discussion of Pd (100) Experimental Observations

These observations are consistent with those of Mattera, Goodman and Somorjai[30] with the following exceptions. The (2×1) structure reported by these authors was not observed. Further, the fine structure noted on the (2×2) streaks has not been reported previously, presumably due to its transient nature.

The palladium (100) surface has also been studied by Park and Madden.[21] They also have observed the formation of the (2×2) and the C(2×2) surface structures and have found that the C(2×2) was stable at least up to 1000°C. However, by alternately ion bombarding and then annealing at 1000°C they were unable to regenerate these surface structures. After 20 such cycles, they found that they could no longer form the C(2×2) structure even by heating at 1000°C for 12 hours. However, they did observe distinctive changes in the intensity plots of the integral order beams that closely resembled those which accompanied the formation of the C(2×2) structure. These observations were taken as evidence of the presence of a metallic impurity that segregates out on the surface when the sample is annealed. Presumably, the successive ion bombardments and anneals exhaust the supply of this impurity at least in the neighborhood of the surface. As platinum was the major impurity in the sample, they concluded that it was possible that the surface changes reflected the formation of a platinum-palladium complex. Auger[33] studies of these structures have suggested that manganese[31] was the crucial impurity that caused these surface structures. Results from this laboratory by F. J. Zsalkowski[32] indicate that elements other than palladium are to be found on the Pd(100) surface when the (2×2) and the C(2×2) structures are formed. However, these elements have not yet been unambiguously identified. There is no clear cut evidence

in the literature that unambiguously identifies the nature of these double spaced surface structures on the palladium (100) surface. As the work function shows little change (0.03±0.02 eV) accompanying their formation,[21] it is plausible that these structures represent either reconstructions of the clean surface, or structures stabilized by metallic impurities that are similar in nature to palladium.

Carbon monoxide may in particular be ruled out as it should lead to work function changes of at least an order of magnitudes greater size. Park and Madden[21] have made a careful investigation of the adsorption of CO on palladium. They found that CO forms a distinctive $(2\times4)^{\circ}45$ surface structures on a freshly ion bombarded surface that is accompanied by a 0.69 eV increase in work function. However, the C(2×2) surface and the (1×1) surface formed by extensive ion bombardments and anneals both appeared to be completely passive to both CO and oxygen. This, with the above mentioned intensity changes indicate that the (1×1) observed by Park and Madden partakes of the nature of the C(2×2) to a great extent. The weakness or lack of the extra order spots may be ascribed equally well to either a disordered impurity or to a clean reconstructed surface that has been so damaged by the extensive ion bombardment treatments that long range surface order is badly petrubed.

The tenacity of the C(2×2) structure at high temperatures definitely rules out the possiblity that it is due to a weakly bonded or physically adsorbed species. In fact, the vapor pressure of the pure palladium is such that one monolayer per second should be leaving the surface at 1000°C. At this rate, several thousand monolayers should be removed in a typical anneal by Park and Madden. If the structure is caused by an impurity, it is interesting to note that this impurity must have vapor pressure characte-

ristics, when on a palladium surface, that are similar to those of the palladium itself. Otherwise, this impurity should either be depleted or should build up in the vicinity of the surface. If, on the other hand, the surface structure is soley the property of a clean palladium surface, then the mechanism for its formation must be self perpetuating in that the removal of many surface layers can still leave a structured surface.

In this regard, it is interesting to consider the tendancy of the slightly disordered ("butterfly") structure to convert to the more highly ordered C(2×2) structure simply upon standing at room temperature. As there is no report anywhere of a Pd (1×1) structure spontaneously converting to a C(2×2) at room temperature, the observation that the disordered structure spontaneously converts to the C(2×2) would seem to support an impurity model. If impurities had segregated out on the surface in a disordered fashion during the heating process and if the energy of diffusion was sufficiently low, less than 20 kcal, rearrangements to an ordered structure could occur at room temperature. Alternatively, one could postulate that the C(2×2) was a stable clean structure with a relatively high activation energy of formation and therefore could only be formed after extensive heating. The possibility that the conversion is associated with gas adsorbtion can be fairly well excluded on the basis of the work by Park and Madden.

The observation that the streaks associated with the (2×2) structure develop fine structure when heated and that this fine structure disappears within minutes may be taken as further evidence of the mobility of the surface atoms related to these surface structures. Here, the surface is considerably more disordered than that for the C(2×2) structure and it is possible that there are a large number of atoms on the surface in metastable equilibrium positions. However, in this case, the possibility of gas adsorption cannot be excluded with the same degree of surety as with the

C(2×2). The times and pressures involved do raise the possibility of gas adsorption. The structure is less well developed and possibly still partakes in part of the nature of the clean surface. It should be noted that this transition is from a (2×4) type structure to a (2×2) type structure upon standing in the ambient. If CO were being adsorbed upon the surface, one would expect the inverse transition, as Park and Madden[21] have observed the formation of Pd(100)-CO-(2×4) surface structure when the Pd(100)-(1×1) surface was exposed to carbon monoxide.

In either case, whether the observed surface structure represents the ordering of a clean reconstructed surface, or the ordering of some impurity, there seems to be a definite trend towards more perfect short range order with increasing time and heat treatment. The most disordered structure is characterized by the (2×2) with streaks diffraction pattern. The perfect (2×2) would represent a greater monolayer coverage. The streaks indicate that there is a considerable lack of correlation on the surface. When heated to around 450°C and then cooled, this structure seems to pass, in a transient fashion, through a partial (2×4) structure and then back to the (2×2) structure. This may be taken as an indication that some long range ordering is achieved before the shorter ordering of the (2×1) structure. Upon further heating to higher temperatures (e.g. 600-1000°C) a transition to the C(2×2) structure is initiated. This structure is characterized by a one-half monolayer coverage. In the earlier stages of the formation of this structure, some disorder will exists giving the diffraction spots the characteristic "butterfly" appearance. Finally, the ordering becomes more perfect and the diffractions spots become round in appearance. No higher transitions have been observed.

4. Pd(100) Results

The intensities of several of the low index diffraction beams as a

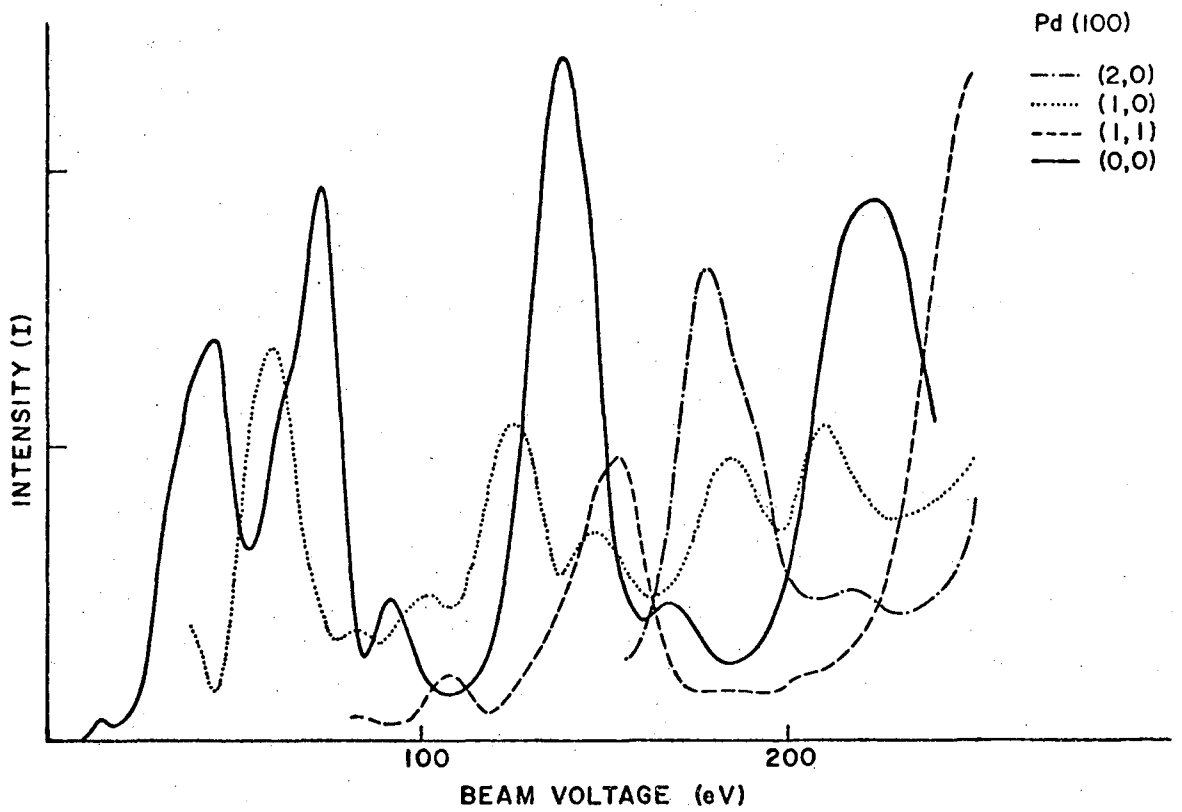

Fig. III-3. The intensities of several of the low index diffraction beams as a function of acceleration voltage near normal incidence for the (100) face of palladium with a (1×1) surface structure.

function of acceleration voltage, I_{hk} (eV) are shown in Fig. III-3 for the (100) face of palladium with a (1×1) structure. The intensities from the non-specularly reflected beams were measured within a degree of normal incidence. As it is impossible to measure the intensity of the specularly reflected beam, (00) beam, at normal incidence with a post-acceleration apparatus, because the electron gun occupies the center of the screen, these intensities were obtained at an angle of incidence of 3° with respect to the surface normal. It should be noted that the data in the experiments. That is, there have been no corrections made for the current vs voltage characteristics of the electron gun (the current increase sharply with increasing beam voltage) nor for contact potential and other errors in the measured acceleration potential or for changes in background intensity. The measurements were performed at room temperature.

Other plots taken under presumably identical conditions were quite similar though minor differences were noted. This shoulder near 70 eV has been correlated with the appearance of the (2×2) with streaks and its presence may be taken as being indicative of the incipient formation of this structure. In addition several of the weaker intensity maxima (e.g. those near 80 (eV) in I_{10} (eV) and I_{11} (eV)) were noted to be quite sensitive to small angular variations.

In Fig. III-5 are plotted the I_{00} (eV) curves for the Pd(100) - (1×1) face as a function of angle of incidence, θ, measured with respect to the surface normal. These curves have not been corrected for constant emission current or for background intensity. Interpretation of these curves is greatly simplified if one looks at their behavior within certain ranges of electron energies. I(0-30 eV), II(30-60 eV), III (600 - 120 eV), and IV(120 - 190 eV). Each region is roughly centered about an expected

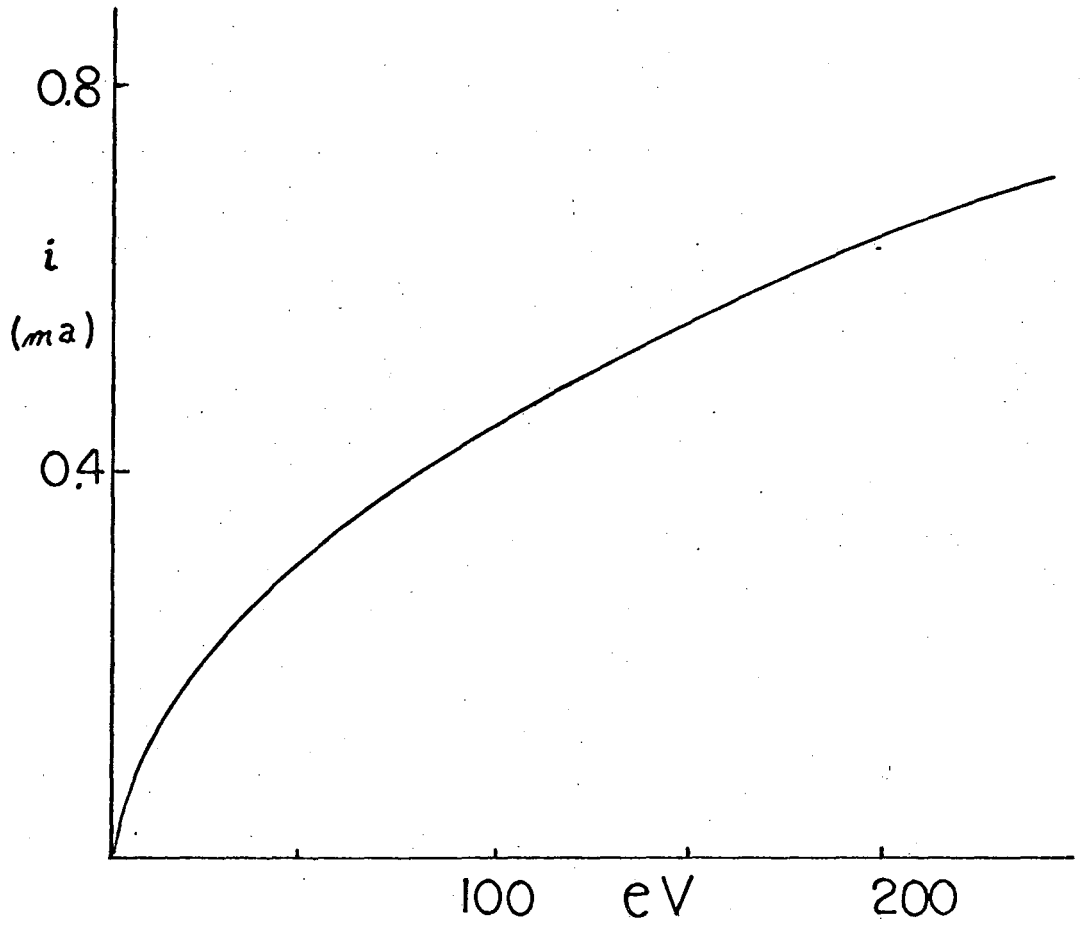

Fig. III-4. Current vs voltage characteristics for the electron gun. Current shown is that leaving the cathode, not that striking the sample.

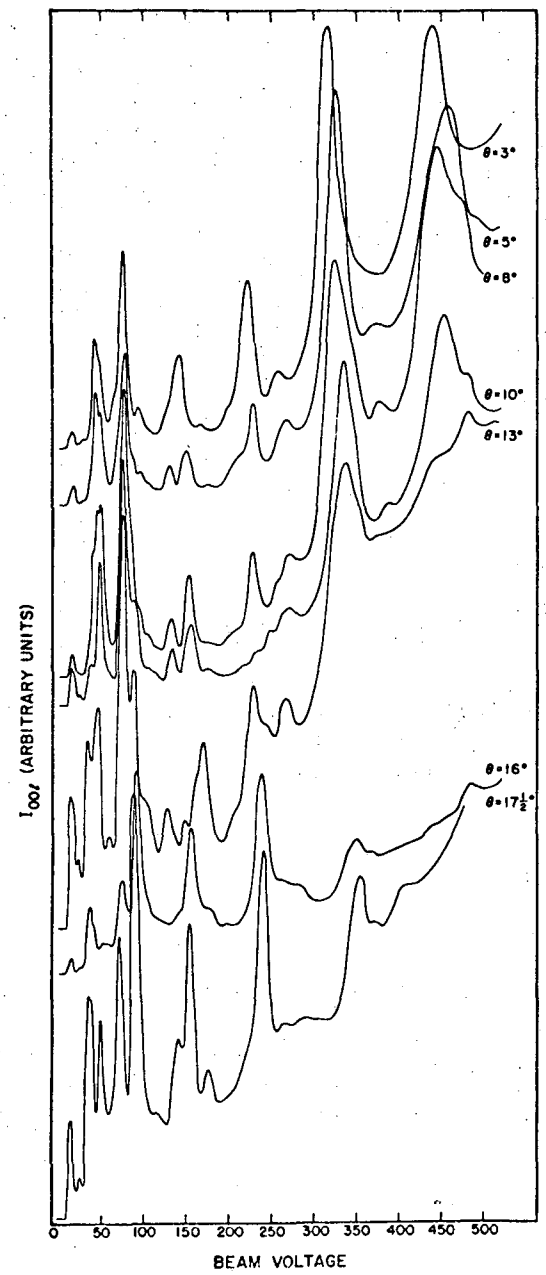

Fig. III-5. The angular dependence of the intensity vs energy of the specularly reflected beam from the (100) face of palladium with a (1 1) surface structure.

Bragg position (10, 40, 89 and 158 eV) calculated for $\theta = 0°$. Several facts are readily apparent. Some "peaks" appear to "rotate" with θ while others do not. Splitting of peaks within regions is the primary change which occurs, with some possible correlations between certain regions. For example, peaks in regions I and III appear to split at approximately the same angle, i.e., 25 eV and 91 eV peaks appear and disappear together. Also, some similarities exist between regions II and IV. In region II, the dominant peak at $\theta = 3°$ and 43 eV collapses with increasing θ, while peaks first at 50 eV and then at 37 eV grown in and in turn, dominate the region. In region IV, the dominant peak at $\theta = 3°$ and 141 eV gradually shifts slightly to higher electron energies and the shoulder separates into a separate peak at 131; the 180 eV peak maintains its position but fluctuates in intensity; at $\theta = 13°$ the peaks at 131 and 174 eV are now bigger than the central peak at 150 eV; however, by $\theta = 16°$ the curve is very similar to the one at $\theta = 3°$ but shifted by about 15 eV. The curve at $\theta = 17\,1/2°$ suggests a possible recurrence of the splittings. Regions over 190 volts seem to show definite angular effects but in no apparent correlation with the first four regions. The dominant characteristic of the curves in the high electron energy region seems to be the occurrence of severe splittings in a very narrow angular range.

In summary, the dominant effect of sample rotation on the specular intensity is the splitting and rejoining of the main peaks within regions of electron energies which center about expected Bragg peaks. The complexity of this effect is most pronounced in the lower electron energy regions. Both of these observations are qualitatively consistent with multiple scattering theory. In fact, the angular variations observed here are similar to those reported by McRae for multiple scattering calculations for a simple

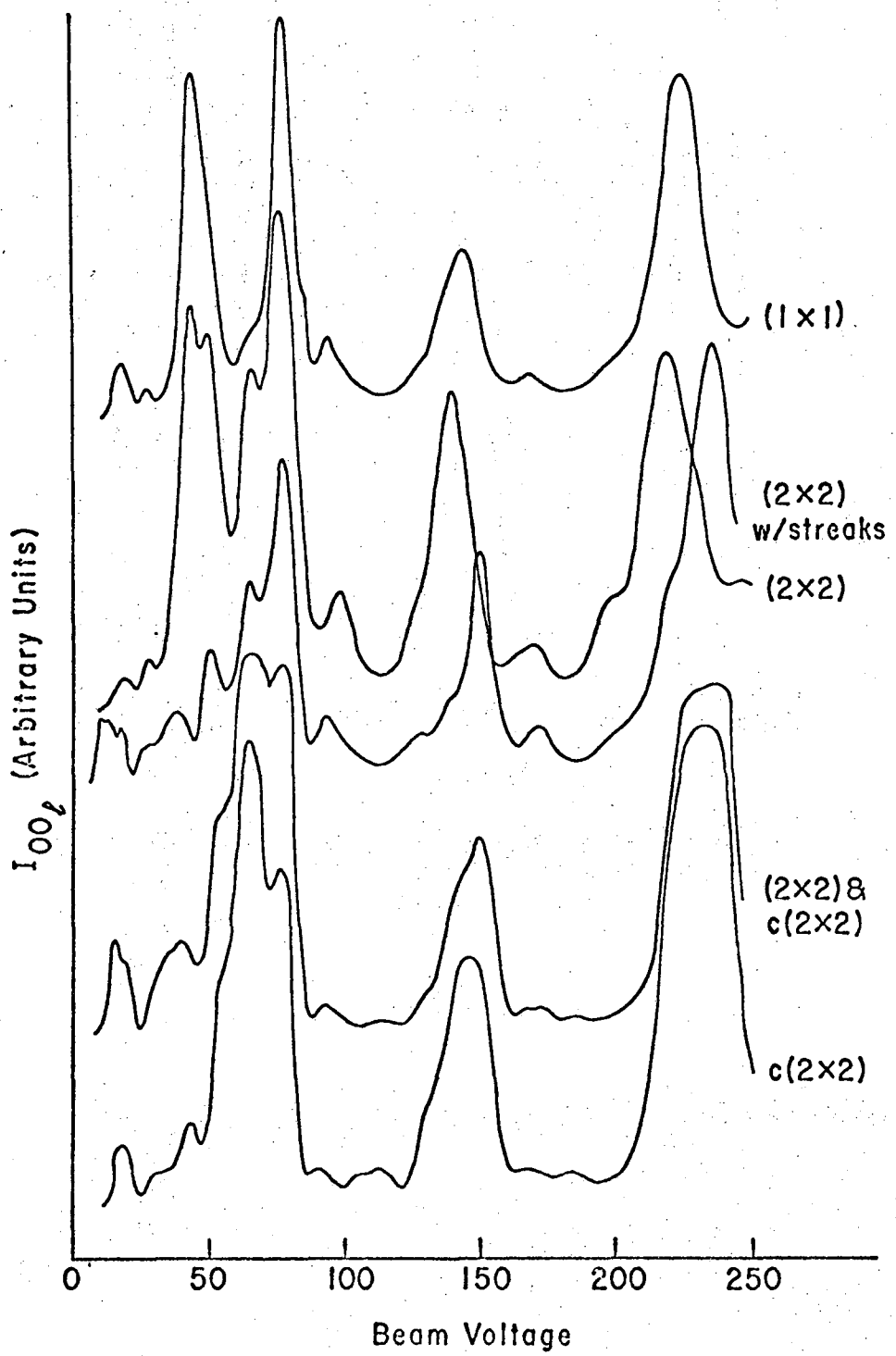

Fig. III-6. The intensity as a function of energy for the specularly reflected beam from the (100) face of palladium near normal incidence for several different surface structures.

cubic material.

Figure III-6 shows the I_{00} (eV) curves for the Pd(100) face in the presence of different surface structures at $\theta = 3°$ and $T = 300°K$. These curves are presented as obtained experimentally. The uppermost curve was taken from a surface that had been ion bombarded and then partially annealed. The next lower curve was taken after a stronger anneal and corresponds to an incipient (2×2) with streaks diffraction pattern. The corresponding new diffraction features were quite weak. The middle curve was obtained from a surface with a well developed (2×2) with streaks pattern. Here the extra diffraction features were quite prominent. The curve second from the bottom was taken from a surface displaying a disordered C(2×2) or "butterfly" diffraction pattern. Finally, the lowest curve was obtained from a well developed C(2×2) structure. It should be noted that we have investigated and determined virtually a continuum of progressive changes in the patterns as a function of heat treatment. Simultaneously with this change in diffraction pattern, the I_{00} (eV) curves undergo marked variations. In fact, the I_{00} (eV) curves so accurately "finger print" the changing surface structures that frequently changes in I_{00} (eV) foretold transitions to different structures before they were actually visible in the diffraction pattern. It should be pointed out that transition structures tend to give I_{00} (eV) curves that are to a certain extent, mixtures of those curves from the braketing structures. Note in particular the peak near 66 eV. On the "cleanest" structures this is a small shoulder. On progressing through the surface structures, the relative intensity of this peak increases until, finally, it is almost the strongest maxima for the well developed C(2×2) structure. Changes in intensity accompanying the formation of surface structures were not restricted to the specularly reflected beams. Figures III-7a and III-7b

show the intensities of several of the low index diffraction beams from the (100) face of palladium with a C(2×2) surface structure. The curves were taken from two different experiments and represent slightly different stages in the development of the C(2×2) surface structure.

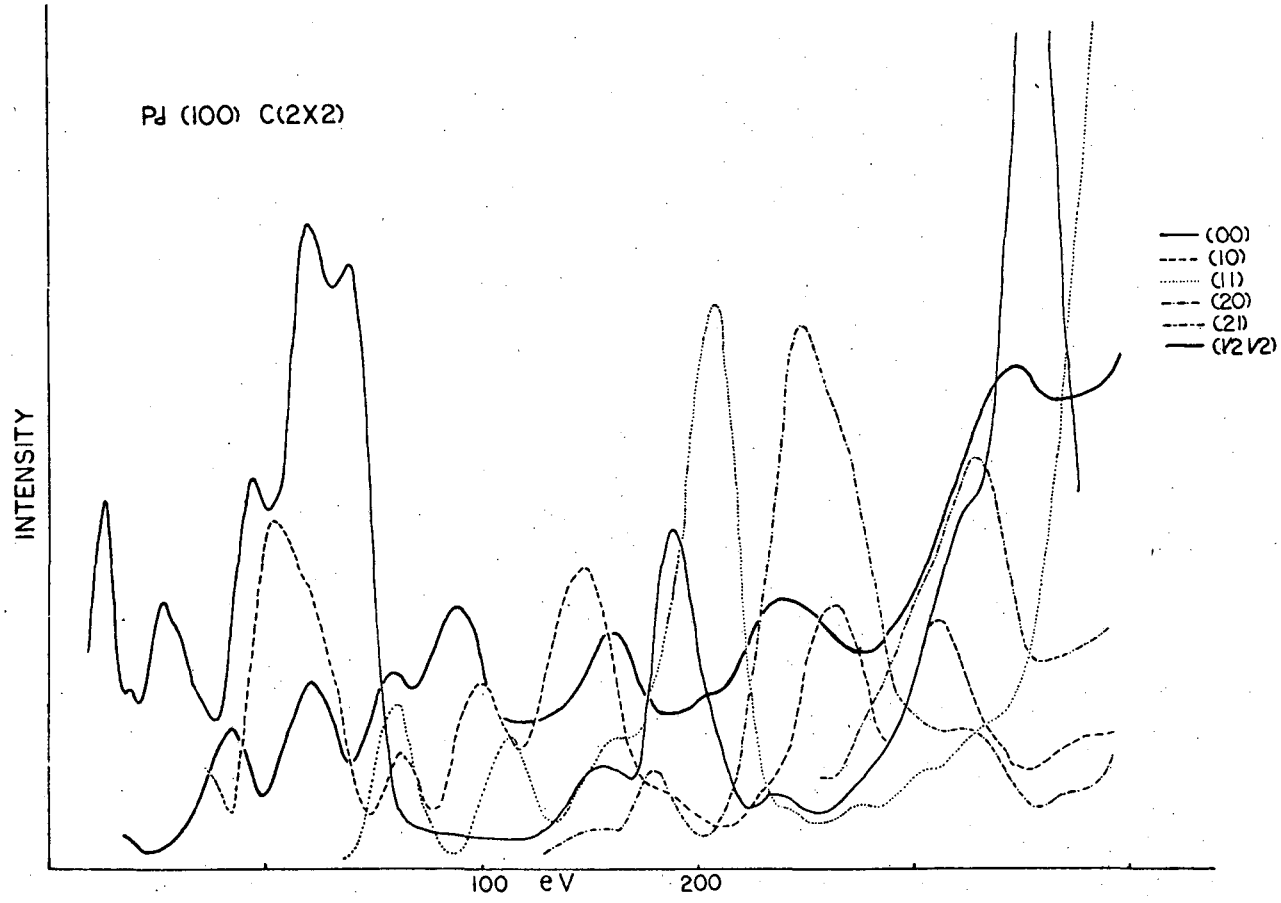

Fig. III-7a. Intensity of several of the diffraction beams from the (100) face of palladium with a C(2×2) diffraction pattern.

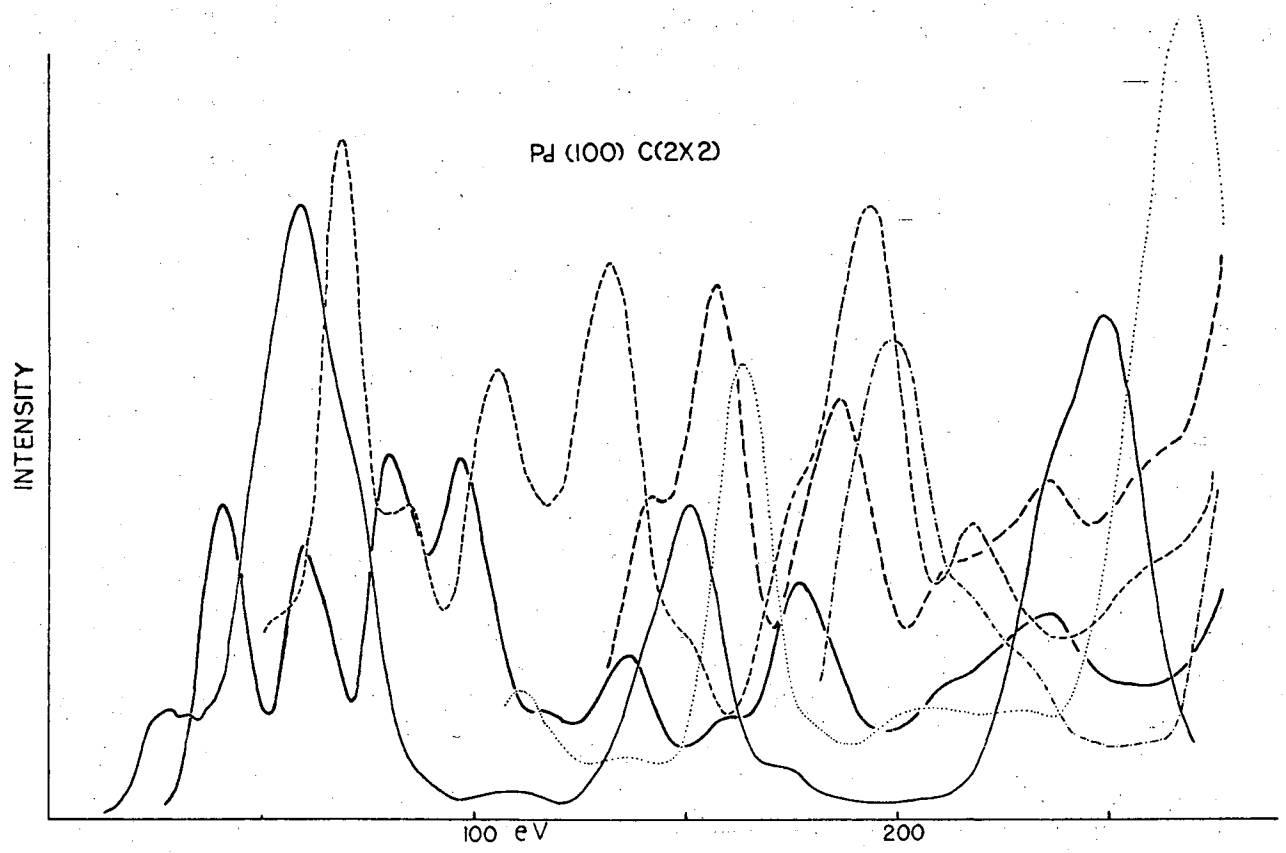

Fig. III-7b. Intensity of several diffraction beams from the (100) face of palladium with a C(2X2) diffraction pattern. Key is the same as 7a except that $I_{1/2\ 3/2}$ (eV) is represented by a heavy broken line.

D. Aluminum

A single crystal of nominally 99.997% pure aluminum was purchased from MRC. The quoted nominal analysis indicated that the major impurities were, O(15 ppm), H(12 ppm), C(10 ppm), N(5 ppm), Si(4 ppm) and Zn(1.2 ppm). The aluminum single crystal was x-ray oriented, spark cut and then mechanically polished in the same manner used for the palladium crystal. The resulting samples were chemically etched in the following manner. A mixture of 70 parts H_3PO_4, 12 parts HAc, 15 parts H_2O and 3 parts HNO_3 by volume was heated to between 60°C and 80°C. A small piece of high purity Al_2O_3 had been previously dissolved in the mixture. This procedure was found to produce a smooth aluminum surface. The sample was then placed in this mixture and the temperature adjusted in the range 60 - 80°C to maintain a mild evolution of hydrogen. After several minutes, the sample was removed from the etchant, rinsed in a basic solution and then rinsed with large quantities of distilled water and finally with electronic grade methanol.

Several problems were encountered in mounting the sample. Aluminum has notoriously poor spot welding properties. Several attempts at utilizing aluminum samples which were spot welded to aluminum holders indicated that the mechanical properties of this contact are poor. Consequently, most of the aluminum samples were held in place by pressure contacts rather than by being spot welded. Care should be exercised in choosing an appropriate holder material. Virtually all metals, with the exception of the alkali metals, have a high solid solubility in aluminum. The optimum combination of low vapor pressure, structural strength and reasonable solubility was found in the refractory b.c.c. metals such as

tantalum or niobium. All of the work reported here was carried out using a tantalum holder. In order to minimize the diffusion of tantalum impurities in the aluminum sample, the holder was lined with a high purity aluminum boat. The aluminum sample was then placed in this boat and both the holder and the boat were then bent around the sample in order to obtain good mechanical and thermal contact. Temperatures were measured by a platinum/platinum 10% rhodium thermocouple spot welded to the outside of the tantalum holder. It was found that thermocouples in direct contact with the aluminum sample have reacted with it and have frequently disintegrated.

1. Al(100) Experimental Observations

A diffraction pattern was never visible on an aluminum single crystal sample immediately after bake out without additional cleaning procedure. Several different methods were used to prepare an ordered aluminum surface in situ. The simplest cleaning procedure that was used was extensive argon ion bombardment e.g. 350 volts at 2×10^{-5} $\mu A/cm^2$ for 36 hours. The unusually long time necessary to obtain a diffraction pattern with this technique may be ascribed to a very low efficiency of ion sputtering in the early stages of ion bombardment. The surface oxide is an insulator and the surface of the crystal acquires a positive charge which repels the inert gas ions. It should be possible to reduce the ion bombardment time by using higher acceleration potentials and/or pulsing techniques developed in this laboratory by T. M. French[34] for insulating materials.

A second technique employed was one reported by F. Jona[35] for cleaning aluminum surfaces. In this method, short ion bombardments (30 minutes) were interspersed with high temperature anneals (400-450°C).

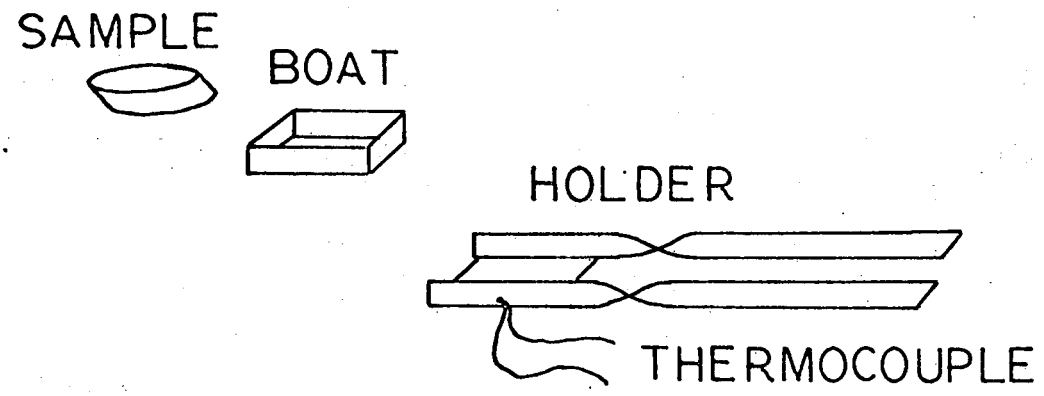

Fig. III-8. Schematic for aluminum sample holder showing sample, aluminum boat used to line tantalum, tantalum holders and thermocouple.

An Al(100) - (1 x 1) diffraction pattern could be generated after several of these cycles. Also recommended by Jona was a simultaneous hydrogen ion bombardment and annealing treatment. Simply heating the sample in hydrogen is thermodynamically inadequate to effect the reduction of the oxide coverage. However, when the hydrogen had previously been dissociated in the ion bombardment unit, some improvement in the removal of the oxide was found. There was some question as to whether the treatments that involved heating to produce an Al(100) diffraction pattern were successful due to migration of the oxygen into the lattice. Therefore an attempt was made to clean an aluminum sample by heating alone without ion bombardment. It was found that a fair diffraction pattern could be formed by heating a freshly prepared sample to 600°C for several hours with no ion bombardment. However, the quality of the pattern was somewhat poorer than those prepared with ion bombardment. Thus, it appears that the surface impurities (most likely oxygen) diffuse into the bulk during heat treatments and an ordered Al(100) surface is produced.

When ordering was effected with heat treatment only, it was found that the diffraction spots were sharp, even when there was a fairly high background intensity. When only ion bombardment was used to clean the surface, the resulting diffraction features tended to be broad and fuzzy, reflecting the surface disorder introduced by this sputtering technique. Therefore, the samples were annealed after ion bombardment at temperatures between 400° and 600°C to remove surface damage.

No surface structures other than the ordered (1 x 1) substrate structure, were observed to be formed by heating the (100) face of aluminum at any temperature between room temperature and the melting

point (659°C) in a 10^{-10} - 10^{-9} torr ambient. In addition, no surface structures were observed to be formed when a "clean" surface exhibiting a sharp (1 x 1) diffraction pattern was allowed to stand in a 10^{-10} - 10^{-9} torr ambient for several days. However, some increase in the background intensity was noted. Mass spectrometric determinations of the ambient composition in similar systems indicate that the major contaminents are CO, H_2O, CO_2H_2 and perhaps N_2, O_2 and the lighter hydrocarbons.[28] Though a detailed investigation was not made, no evidence was found for the formation of surface structures due to the adsorption of hydrogen during the hydrogen treatments.

As was found by Jona,[35] oxygen was absorbed on the (100) face of aluminum as amorphous layers at room temperature. No new diffraction features were observed, only a general increase in the background intensity accompanied by a deterioration of the diffraction pattern. The intensity of the specularly reflected beam was monitored as a function of oxygen coverage. It was found that the peak heights diminished and that their shapes became less distinguishable.

A sharp diffraction pattern could be regenerated by any of the procedures used to clean a freshly prepared surface.

When an aluminum (100) sample was extensively exposed to oxygen while at temperatures near 600°C, it was found that the usual (1 x 1) diffraction pattern of a good quality was observed when the oxygen was pumped out of the chamber and the sample cooled to room temperature. This was taken as further evidence of the diffusion and marked solubility of oxygen in aluminum at elevated temperatures. No investigation was made of the oxygen surface structure formed at intermediate temperatures and reported by Bedair.[9]

2. Discussion

The basic experimental behavior observed for the (100) face of aluminum is consistent with that observed by F. Jona.[8] The diffraction pattern was essentially obliterated after being exposed to approximately 700 Langmuirs (10^{-6} torr-seconds) of oxygen. Jona estimated that the oxygen sticking coefficient, α, was between 10^{-3} and 10^{-2}. At room temperature oxygen is adsorbed onto the aluminum surface in a disordered manner and results in an amorphous layer. Further, the aluminum sample could be cleaned after exposure to oxygen by annealing at 450°C. The most probable mechanism explaining this effect involves the diffusion of the adsorbed oxygen atoms into the aluminum lattice.

Among others, Jona has suggested that the mechanism for the adsorption of oxygen onto aluminum surfaces involves oxygen assimilation into the metal lattice or place exchanges at the metal-oxygen interface. The other investigations of the early stages of the oxidation of aluminum have employed work function measurements. Huber and Kirk[37, 38] have found a decrease of 0.05 eV in the work function of aluminum when it is exposed to oxygen at room temperature. This had been taken as evidence for an alternating dipole model where half of the oxygen atoms are above aluminum atoms and half are below. The initial decrease in the work function is followed by a gradual increase with continuing oxygen exposure, presumably corresponding to more than a monolayer coverage. Roberts and Wells[39] have also investigated the oxidation of aluminum films using work function measurements. One aspect of their work is particularly interesting. They investigated the temperature dependence of the work function of an oxygen covered film. At -195°C, the work

function increased to 0.8eV at 10^{-4} torr oxygen exposure. Upon evacuating and warming the sample, the work function decreased until it was slightly below the clean metal values and had attained a value similar to that reported by Huber and Kirk. Again, further oxygen exposure caused the work function to increase. They concluded that the decay in the work function when the sample was heated reflected a surface rearrangement of the chemisorbed oxygen that involved incorporation into the subsurface region. They further concluded that chemisorbed oxygen is somewhat unstable on aluminum even at -195°C and that the activation energy for the oxygen incorporation is very small.

This is particularly interesting in that it implies that the oxygen may be positioned above the aluminum at temperatures near or below -195°C. It might, therefore, be fruitful to investigate the LEED pattern of aluminum at low temperatures after exposure to oxygen as it is possible that an ordered structure may be formed under these conditions. If this were so, an investigation of the temperature dependence of the LEED pattern might shed further light on the oxidation mechanism.

3. Measurements of Diffraction Peak Intensities on the Al(100) Surface

a. Clean Surface, Normal Incidence. The intensities of several of the low index diffraction beams as a function of acceleration voltage are shown in Figure III-9 for the (100) face of aluminum. The intensities of the non-specularly reflected beams were measured at normal incidence (plus or minus one degree). The intensity of the specularly reflected beam was obtained at an angle of incidence of 3° with respect to the surface normal. The data is given as obtained in the experiment. The measurements were performed at room temperature. Consequently, above

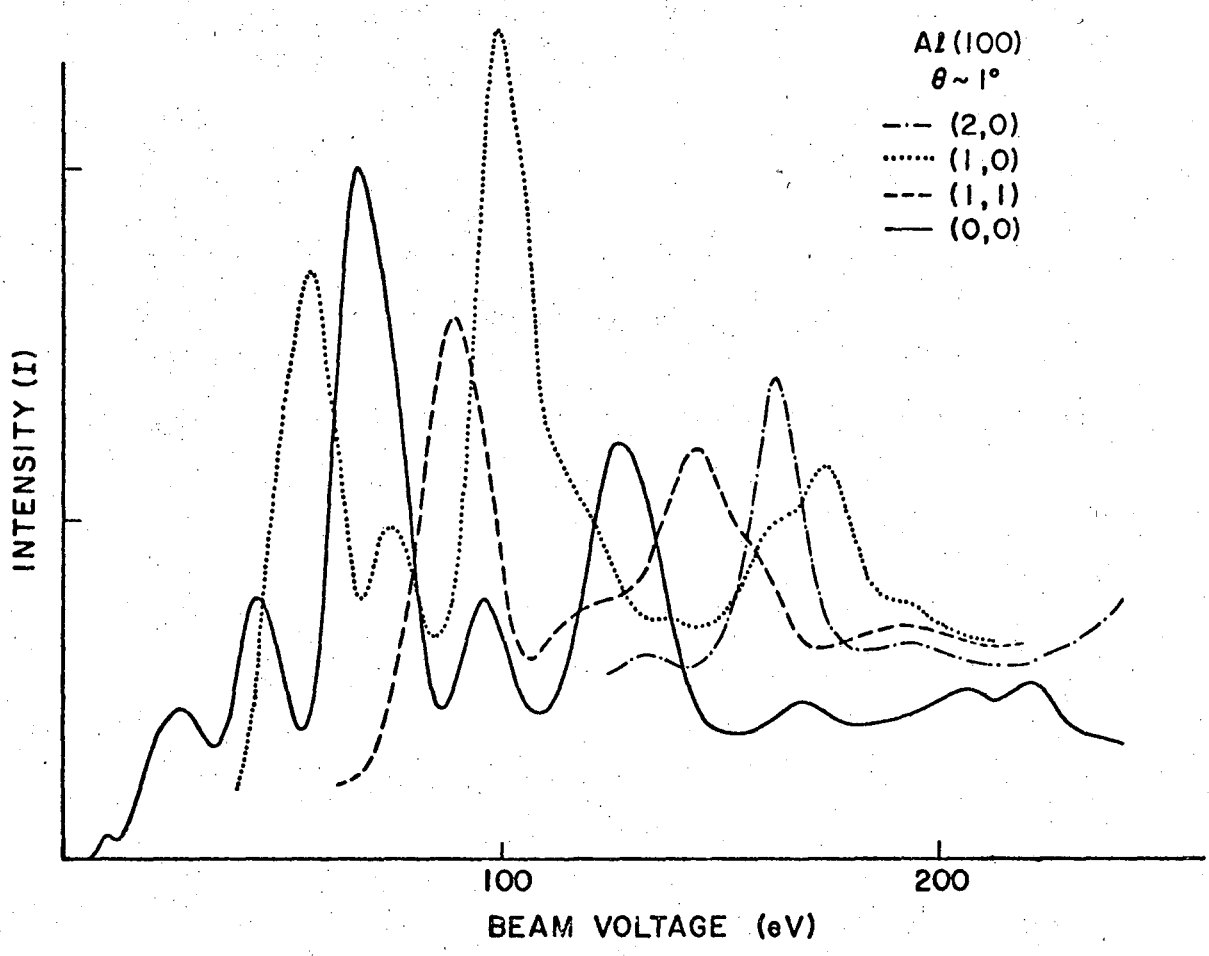

Fig. III-9. The intensities of several of the low index diffraction beams as a function of energy for the (100) face of aluminum near normal incidence.

150eV, much of the elastically scattered intensity for aluminum is obscured by the Debye-Waller effect and multi-phonon processes which are responsible for most of the background intensity.

As will be discussed below, the positions of the non-specularly reflected intensity maxima are very sensitive to slight variations in the angle of incidence. It is estimated that the deviations in the positions of the peaks shown here are less than 5eV at 100eV primary voltage and 20eV at 200eV primary voltage. Further, there are some changes in peak shape that were noted in different plots all nominally taken at normal incidence. For example, the peak in the $I_{10}(eV)$ curve just above 70eV frequently appeared as a massive shoulder on the peak near 55eV rather than as a distinct entity. In addition, the shoulder just below the maxima near 180eV in the $I_{10}(eV)$ curve readily became more intense than that maxima with angular variations of less than one degree.

b. Clean Surface, Non-Normal Incidence. Figures III-10a, III-10b and III-10c show the angular dependence of $I_{00}(eV)$ for the aluminum (100) face for several different azimuthal angles. The angle of incidence, θ, is measured with respect to the surface normal. The azimuthal angle, ϕ, is measured with respect to the (100) crystallographic direction. The data are presented in an uncorrected form as obtained in the experiment. Note the general decrease in intensity with increasing angle.

Comments similar to those made about the angular variations of the palladium $I_{00}(eV)$ curves could be restated here with an important difference. While the intensity curves for palladium display severe fluctuations when the angle of incidence is varied, those for aluminum appear to retain their gross structures and show only subtle variations

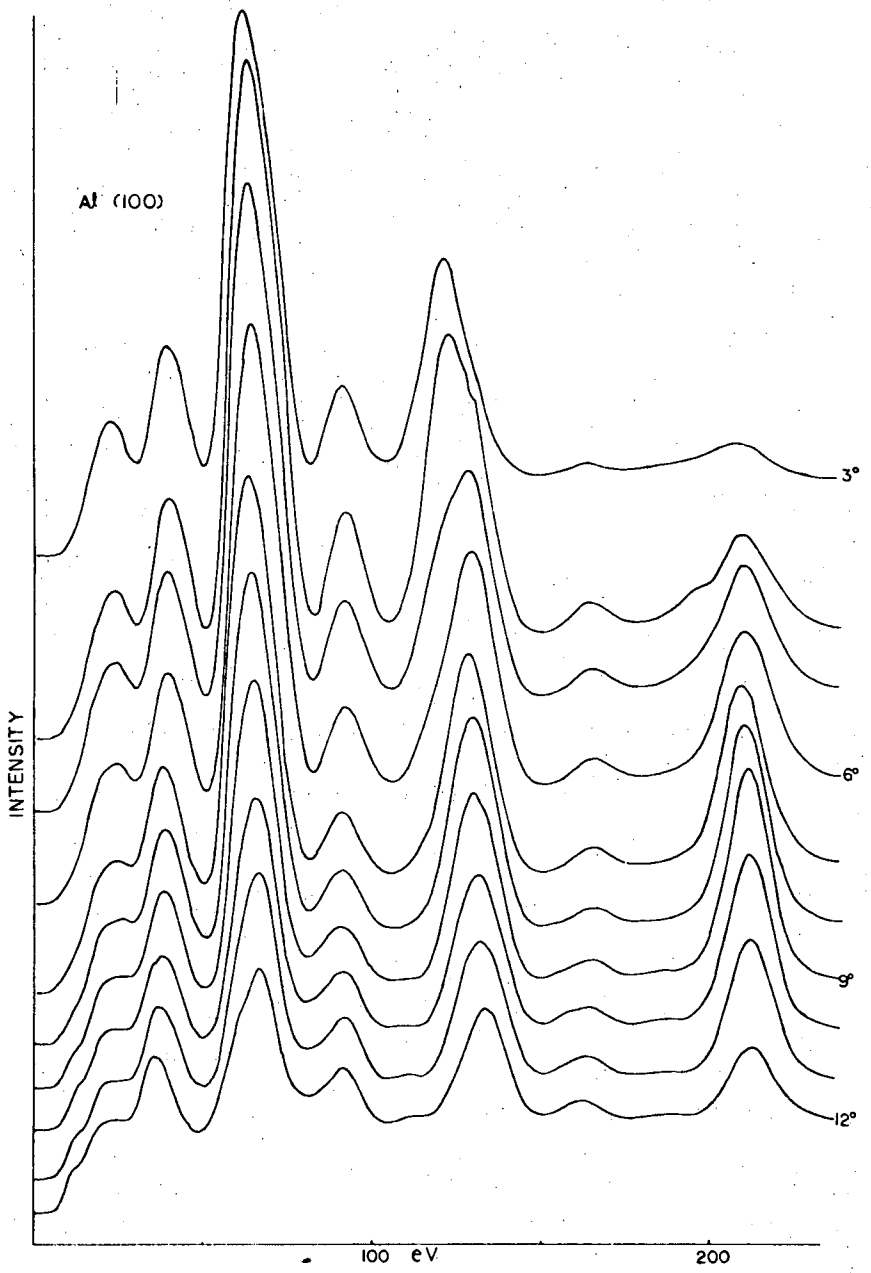

Fig. III-10a. The intensity as a function of voltage for the specularly reflected electron beam from the (100) face of aluminum for several different angles of incidence.

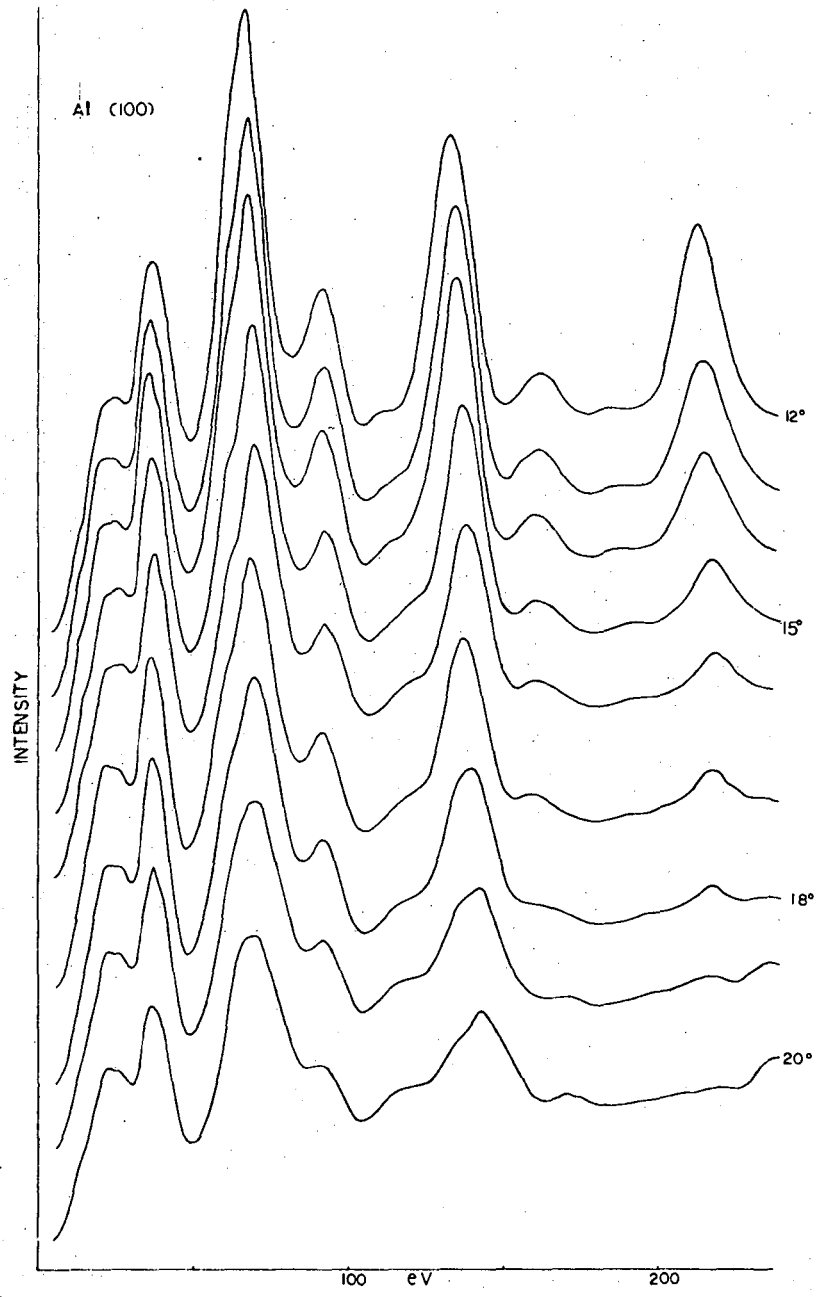

Fig. III-10a. continued

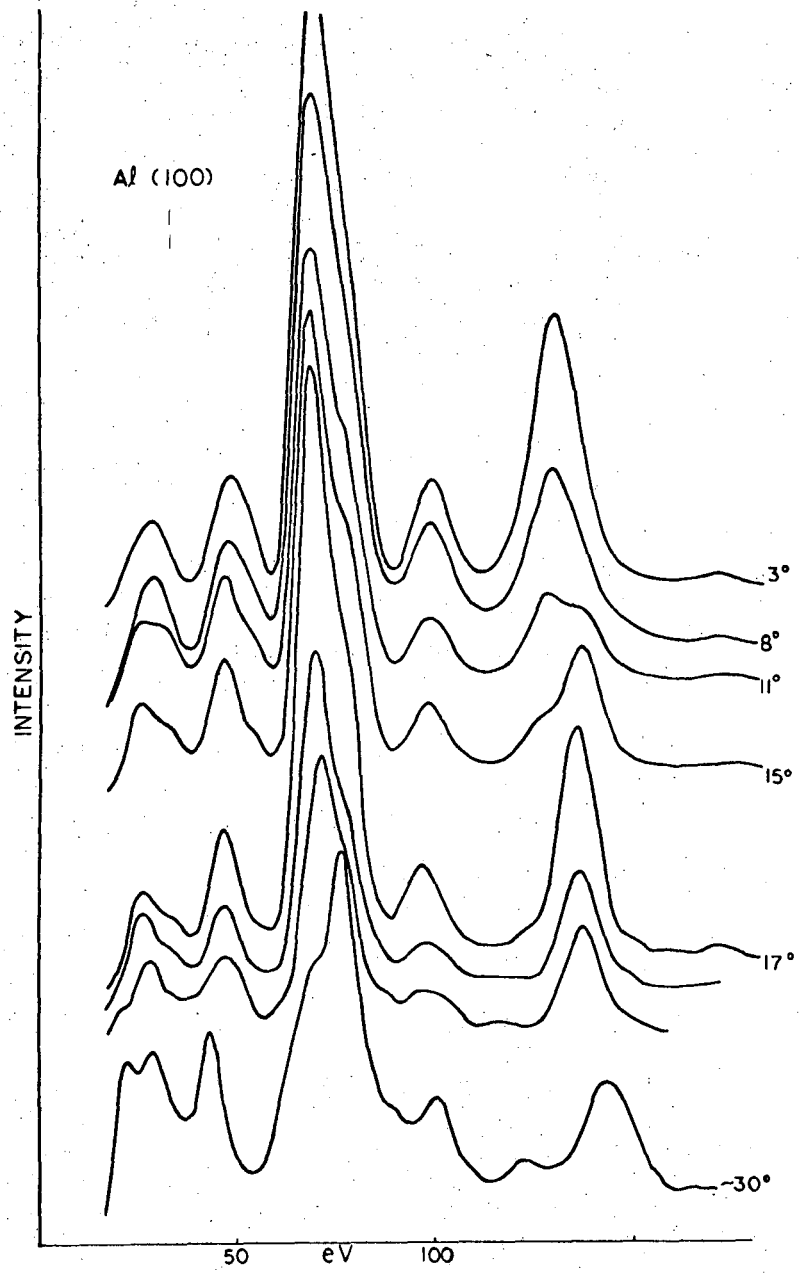

Fig. III-10b.

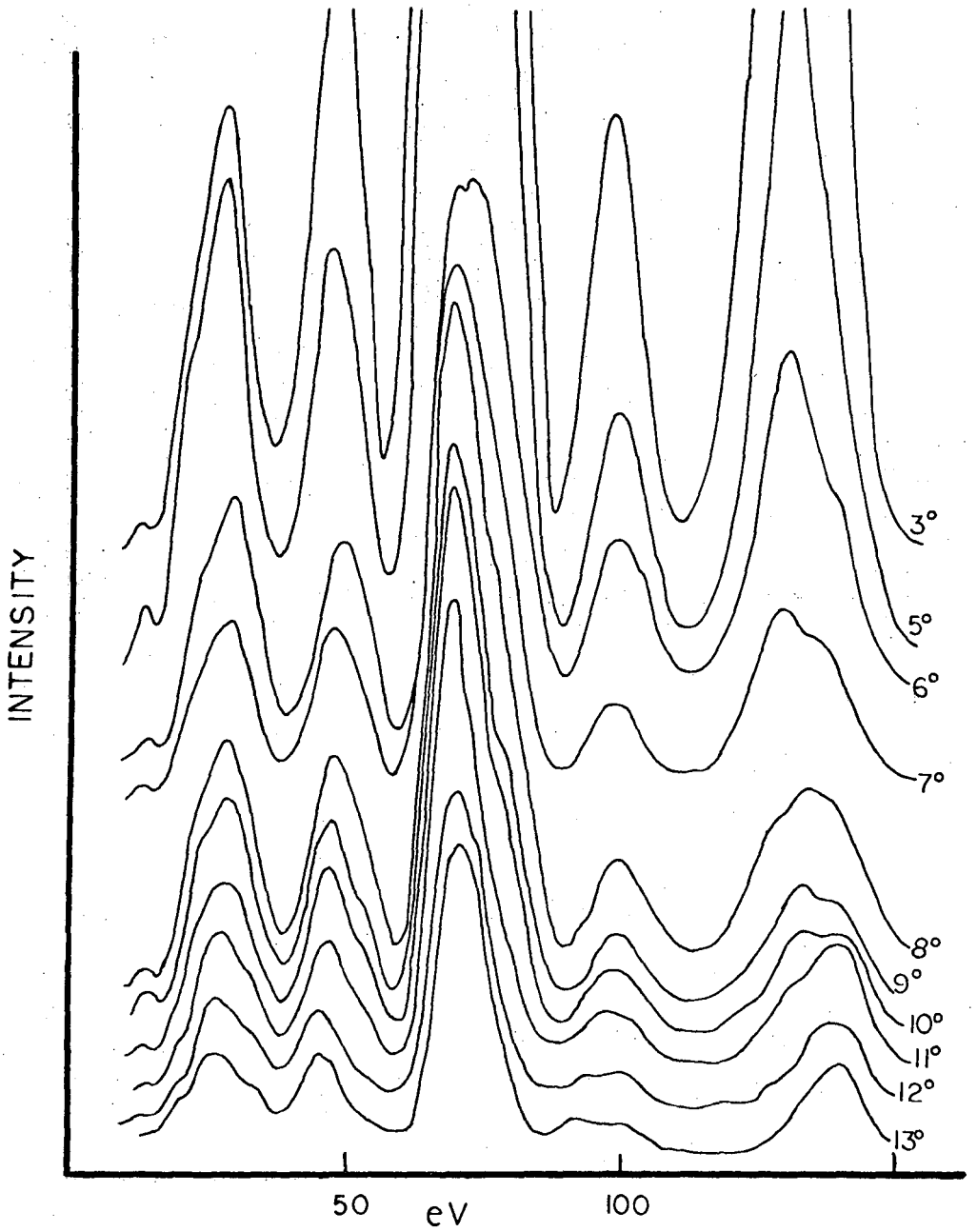

Fig. III-10c

particularly near normal incidence. This is so to such an extent that the curves for different azimuthal angles appear quite similar until closely scrutinized. For example, at an angle of incidence near 16°, the curves in Figures III-9a and III-9b both show peaks near 25, 45, 70, 100 and 130 eV in approximately the same intensity ratios. However, there are certain minor but definite differences such as the shoulder on the maxima near 70eV. In Figure III-9a, there is a shoulder on the low eV side of this peak, while in Figure III-9b, there is a shoulder on the high eV side. In addition, the shape of the peak near 25 eV is distinctly different in these two curves. There exist many other small differences in the data for the different azimuthal angles.

This apparent insensitivity of the aluminum data, relative to the palladium data, to angular variations could possibly be ascribed to one of several causes. The effective band structure of aluminum near the surface could contain larger band gaps that were less sensitive to angular changes. Alternatively, the strong fine structure observed on the palladium intensity curves could be strongly masked by the relatively greater Debye-Waller effect in aluminum (see Appendix III).

Observation of the angular dependence of the first order diffraction beams tend to support the latter possibility. Figure III-11 shows the intensities of the four first order diffraction beams measured at $\phi \cong 45°$ and $\theta \cong 2° \pm 1°$. Note that even near normal incidence, there are definite variations in peak shape and position in the non-specularly reflected electron beams when the angle is varied. This may be contrasted with the relative insensitivity of the specularly reflected beam to small angular variations in this region. Experimentally, the specularly

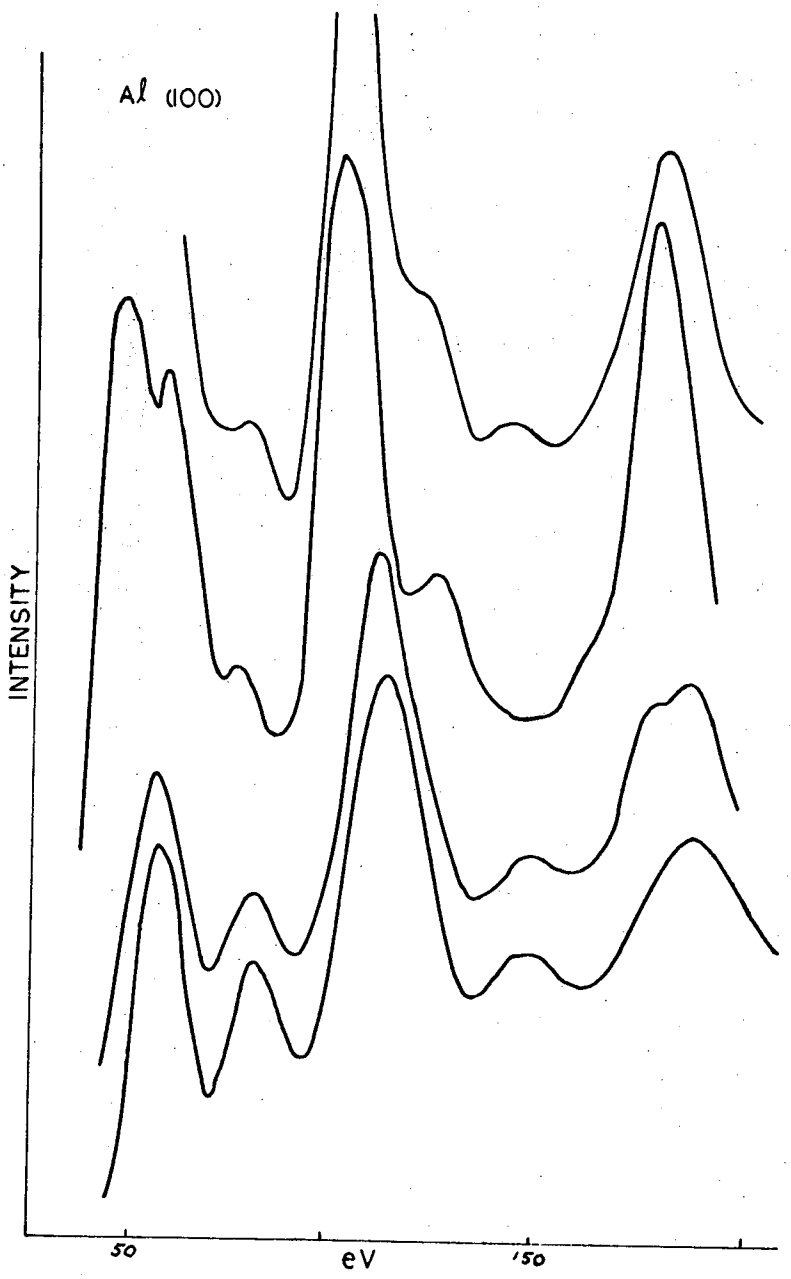

Fig.III-11. The intensities of the $(\bar{1}0)$, $(0\bar{1})$, (10) and (10) diffraction beams from the (100) face of aluminum at $\theta \cong 2°$ and $\phi \cong 45°$.

reflected spot was moved towards the (11) diffraction spot. Therefore, the (10) and the (01) diffraction features were identical and the $(\bar{1}0)$ and the $(0\bar{1})$ diffraction features were identical. Consequently, at any given eV, the component of the wave vector perpendicular to the surface of the sample that characterized the (10) and (01) beams was smaller than that characterizing the $(\bar{1}0)$ and the $(0\bar{1})$ beams. Commensurately, the intensity maxima for the (10) and the (01) beams tended to fall at higher electron energies than did those for the $(\bar{1}0)$ and the $(0\bar{1})$. This is as one would expect on the basis of both kinematic and double scattering diffraction mechanisms.

c. Oxygen Exposed Surface. Figure III-12 shows the effect of oxygen exposure on $I_{00}(eV)$ for the (100) face of aluminum. The angle of incidence was approximately 3°. The data are presented as obtained in the experiment. The oxygen exposure and the intensity measurements were performed at room temperature. After about 500 Langmuirs exposure, the intensity had dropped by about an order of magnitude and the resolution had seriously deteriorated. Further exposure resulted in a still greater loss in intensity accompanied by a further decrease in resolution. Note the change in peak positions after several thousand Langmuirs exposure. The general decrease in intensity, deterioration of resolution and lack of appearance of new diffraction features was taken as evidence for a fairly amorphous combination of oxygen with aluminum under these conditions. However, the almost indiscernible change in the structure of the $I_{00}(eV)$ curve after extensive exposure indicate that some new ordering is beginning to dominate, in however feeble a form, in the neighborhood of the surface.

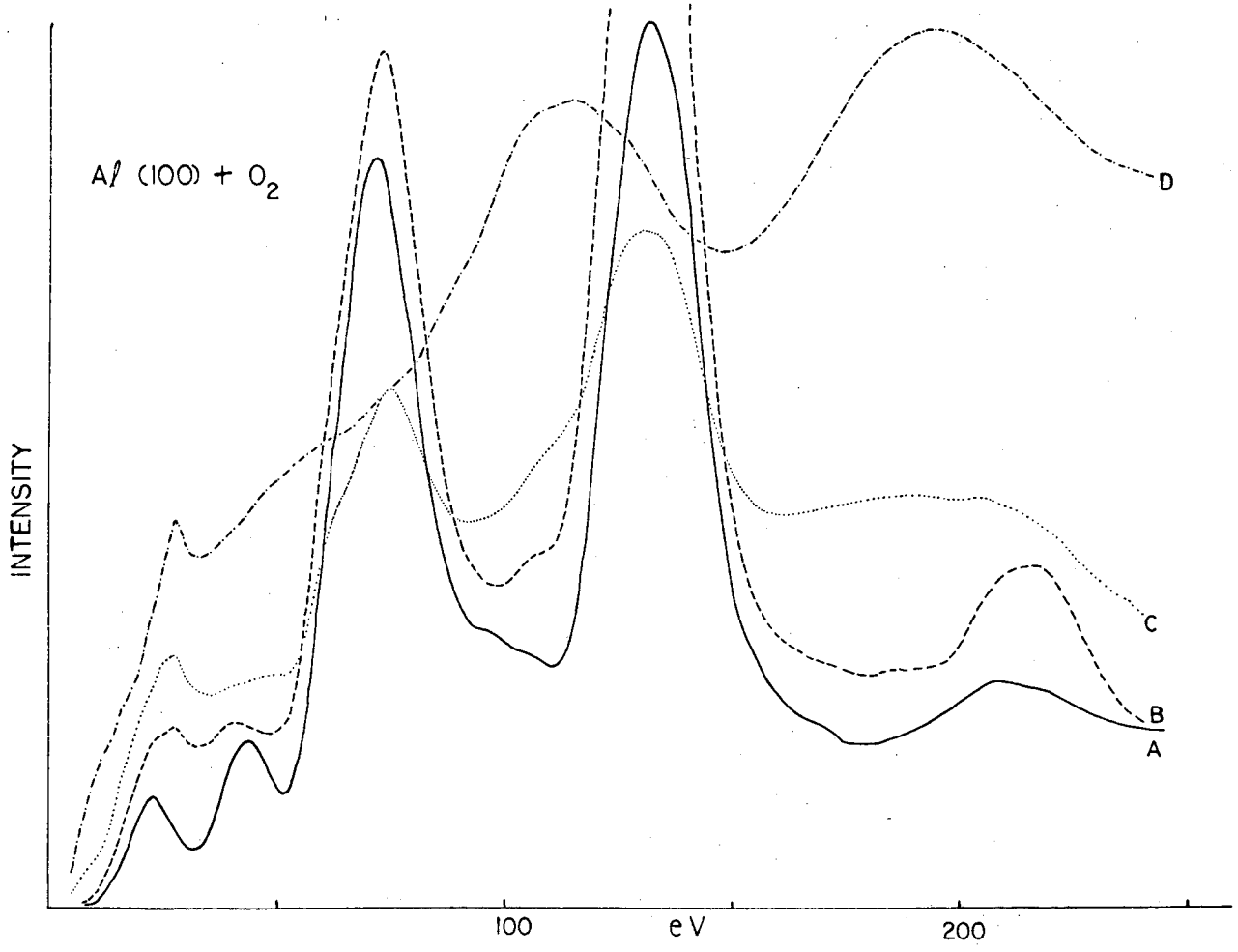

Fig. III-12. The intensity of the (00) beam vs energy from the (100) face of aluminum as a function of oxygen coverage. A - "clean surface". B - after 10,000 Langmuirs of oxygen at ~600°C, intensity scale comparable with A. C-after 500 Langmuirs of oxygen at room temperature, intensity scale has been magnified 3 times. D. - after 1500 Langmuirs of oxygen at room temperature, intensity scale has been multiplied 10 times.

E. Platinum, Iridium and Bismuth

The properties of the non-specularly reflected diffraction beams from platinum, iridium and bismuth were also studied. The crystal preparations of both iridium and platinum are quite similar to that of palladium with the exception that different chemical etches were used. The iridium sample was etched in hot concentrated nitric acid prior to loading. The platinum sample that was used was etched in a dilute aqua regia solution.[28] The preparation of the bismuth sample has been described in some detail by R. M. Goodman.[40]

1. Platinum (100) - (5 x 1)

The formation of the (5 x 1) surface structure on the platinum (100) may be effected by a heat treatment of the freshly bombarded surface or by a combination heat and oxygen treatment. This process has been extensively described elsewhere.[28] Figure III-13 shows the intensities of several of the electron diffraction beams from this surface structure plotted as a function of electron energy. The intensities of the non-specularly reflected beams were measured at normal incidence. The intensity of the specularly reflected beam was measured at $\theta = 3°$. The data are presented as obtained in the experiment. Only the intensities of the first two partial order spots, [(0 1/5), (0 2/5)], are shown. The intensities of all of the fractional order spots tended to decrease with increasing beam voltage. This may be taken as an indication that the electron beam samples more of the bulk structure rather than the surface structure at higher energies. The intensity of the (0 3/5) spot not shown here has a maximum near or below 30eV and then a broad minimum between about 50 and 70eV. At 85eV, $I_{0,3/5}$ is greater than $I_{0,1/5}$ or

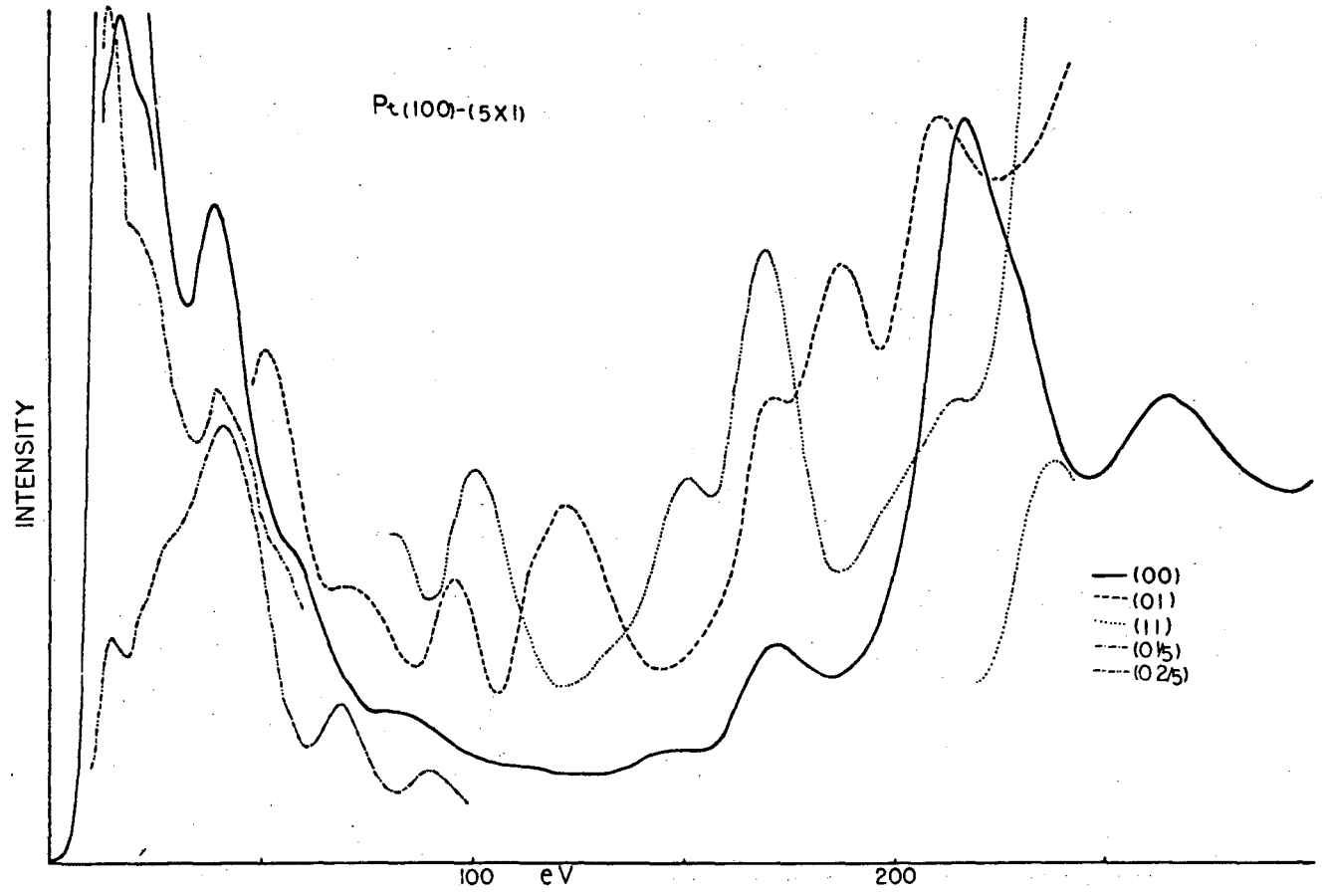

Fig. III-13. The energy dependence of the intensities of several of the low index beams from the (100) face of platinum with a (5×1) diffraction pattern.

$I_{0,2/5}$. The intensity of the (0 4/5) beam shows a broad maxima of medium to weak intensity in the region between 50 and 70eV. The exact fine structure was not determined.

2. Iridium

The intensities of several of the diffraction beams from the (100) face of iridium are shown in Figure III-14. The non-specularly reflected diffraction beams were measured at normal incidence. The intensity of the specularly reflected diffraction beam was measured at $\theta = 3°$. The data is presented as obtained in the experiment. The reproducibility of these curves was not checked.

One of the outstanding features of these curves is the continued increase in peak height with increasing beam voltage. This may be contrasted with the behavior of the intensity of the beams back diffracted from aluminum were there is a very pronounced decrease in intensity above approximately 100eV. As the Debye-Waller factor, 2W, is an order of magnitude less for iridium than for aluminum, this difference may be ascribed to thermal effects.

Figure III-15 shows the angular dependence of I_{10}(eV) near normal incidence in the region between 300 and 400eV. There the azimuthal angle was approximately 45° so that the (10) and the (01) beams were equivalent and the $(\bar{1}0)$ and the $(0\bar{1})$ beams were equivalent. As with aluminum, small changes in the angle of incidence produce significant changes in the intensities of the non-specularly reflected beam. It is interesting to note there is considerable fine structure even in this relatively high energy range. This may be taken as an indication of the importance of multiple scattering in the region above 100eV at least for iridium.

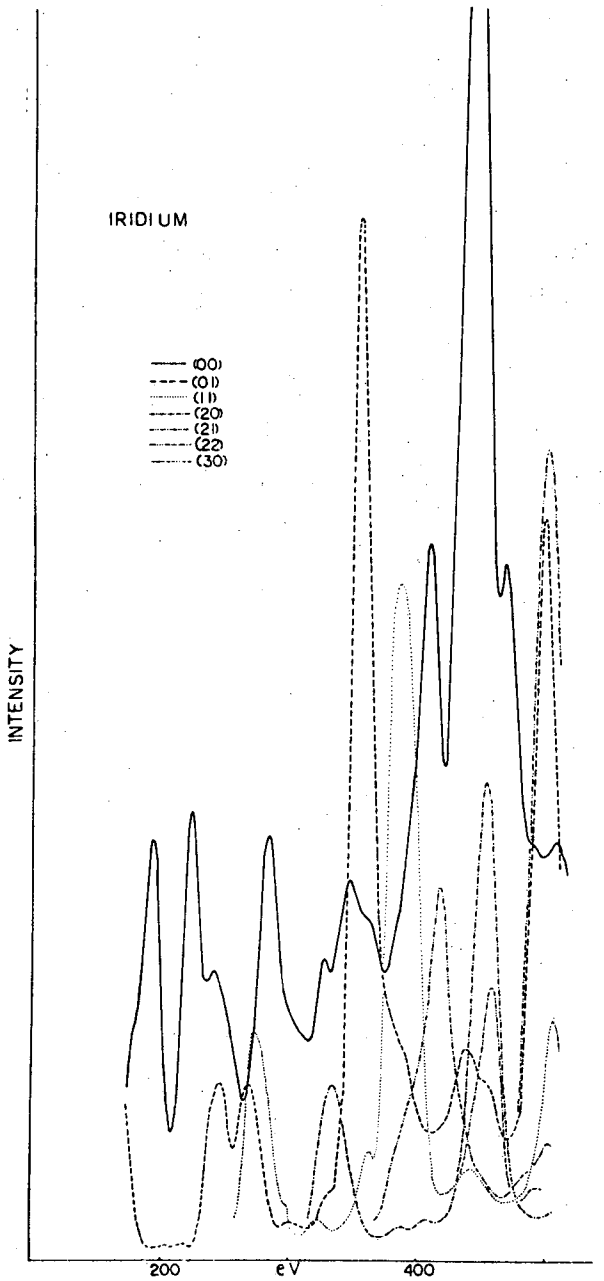

Fig. III-14. The energy dependence of the intensities of several of the diffraction beams from the (100) face of iridium.

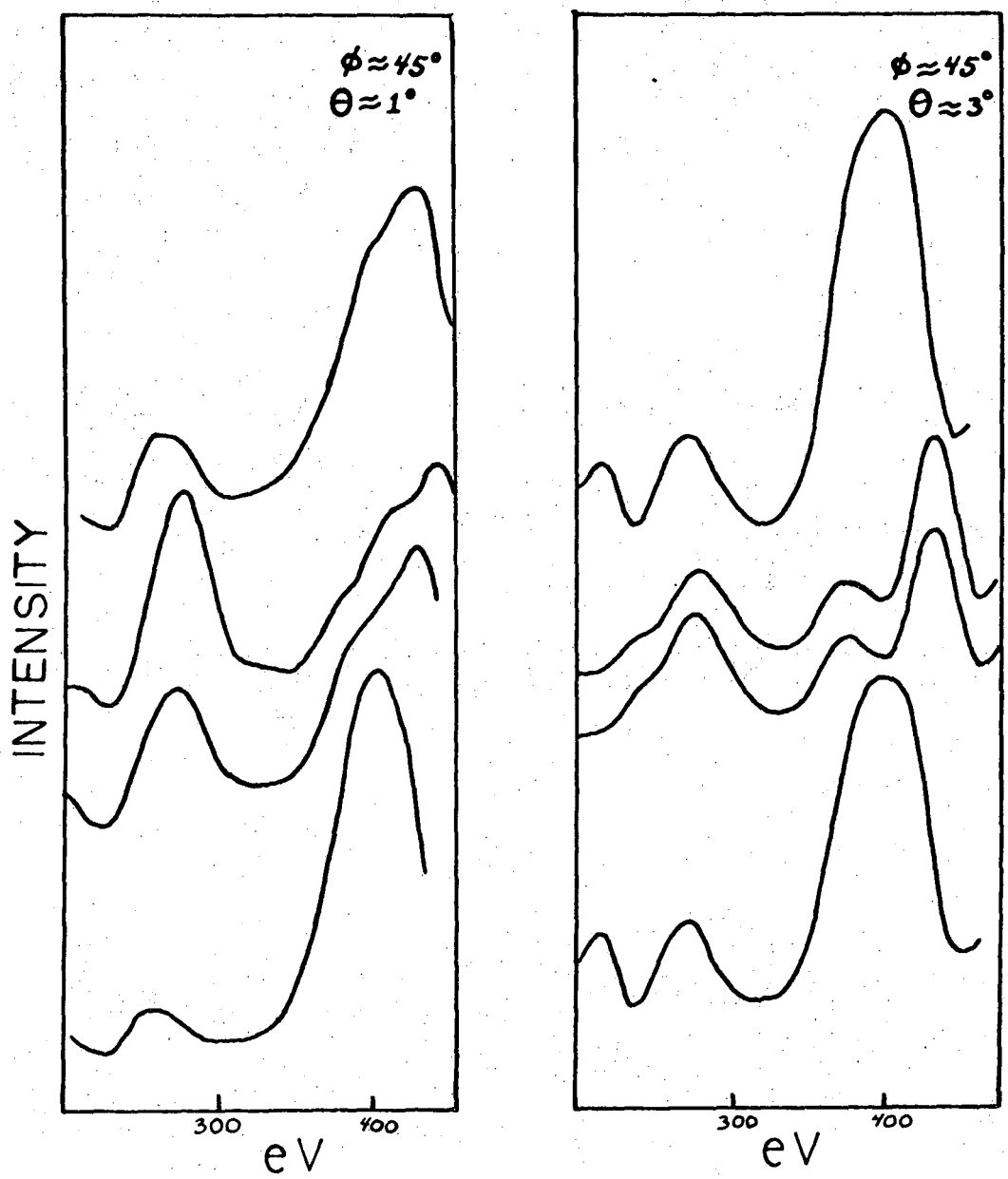

Fig. III-15. The intensities of the $(\bar{1}0)$ (10) (01) $(0\bar{1})$ diffractions beams for the (100) face of iridium at non-normal incidence.

3. Bismuth

The intensities for the (10) and the ($\bar{1}$0) electron beams diffracted from the hexagonal face of bismuth are shown in Figure III-16. The maximum expected shift in peak position due to angular deviation from normal incidence is 4eV. The curves are shown as obtained in the experiment without any correction for background and intensity, contact potential, etc. The reproducibility of these curves has not been changed. Both curves show some fine structure, though, as with aluminum, this is not very pronounced and the peaks tend to be fairly broad (10-20eV). There is a strong fall off in peak intensity with increasing electron energy that is primarily due to the large Debye-Waller effect in bismuth.

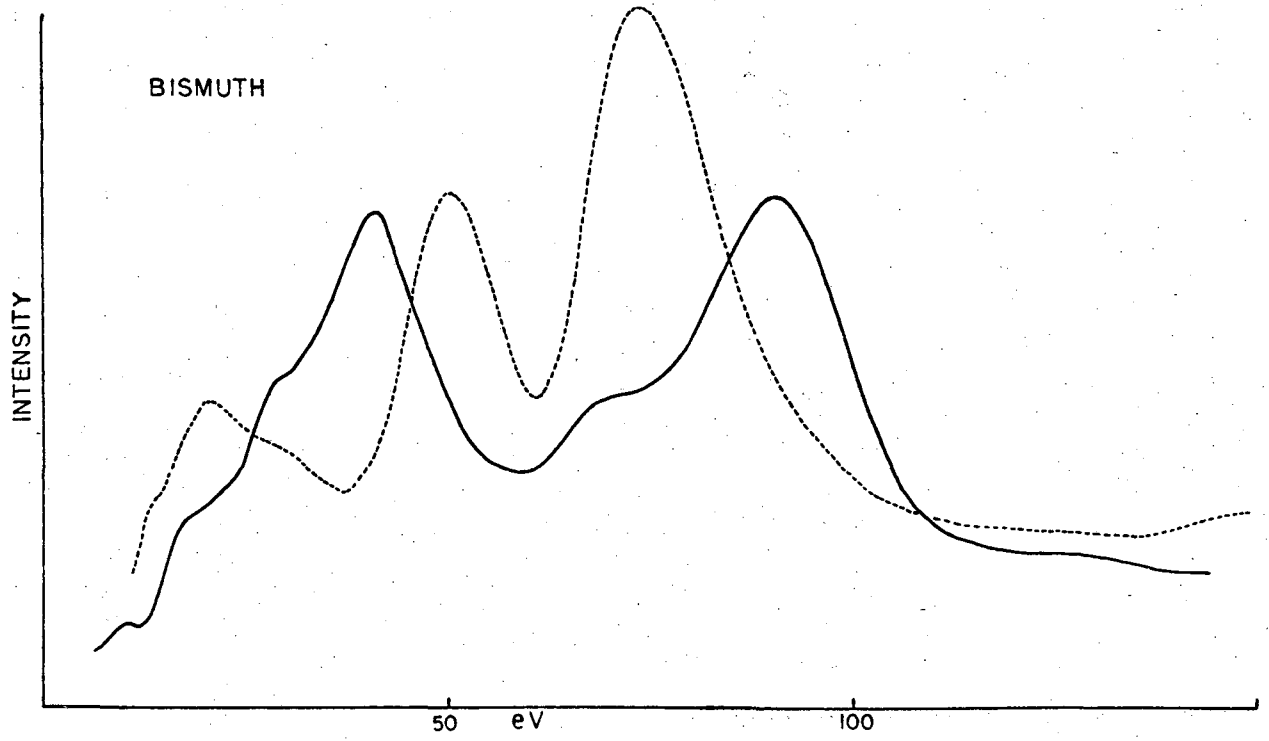

Fig. III-16. The energy dependence of the intensities of the first order diffraction spots from the hexagonal face of bismuth.

IV. DISCUSSION

One of the ultimate goals of low energy electron diffraction is to be able to elucidate the precise structure of clean surfaces and surfaces that have been reconstructed or have been contaminated by the diffusion of an impurity. In addition, it is of great importance to determine the structure of adsorbed gases which have condensed in an ordered manner on single crystal surfaces. As with other branches of science, an understanding of a complex problem is often achieved by the successive solution of related but relatively more elementary problems.

Proceeding in this spirit, we will attempt to take a step towards the understanding of complicated surface structures by first trying to determine the relationship between the structure of simple clean surfaces and to analyze the intensities scattered by these surfaces in low energy electron diffraction.

The simplest surfaces are presumably the clean surfaces of monatomic materials that have not undergone any surface reconstruction. Here, it is known that the surface has the same symmetry and dimensions parallel to the surface that characterize the bulk material. Deviations from bulk values in the dimensions of the lattice parameters perpendicular to the surface are, hopefully, not large.[41] It may therefore be assumed that one has an approximate knowledge of the geometry and the chemical nature of these surfaces.

The first phase of the problem then is to develop a computational procedure which will reproduce the experimentally observed features of the LEED beams from these known surface structures using trial atomic potentials. Ultimately, one would like a computational procedure that

would generate potentials and positions from experimentally observed intensities. The problem is sufficiently complex however, that this preferred method will have to wait for a better understanding of the physics of low energy electron scattering.

This first phase may be subdivided further into two steps: the calculation of the positions of the experimentally observed intensity maxima and the calculation of their relative intensity ratios. There are several advantages to calculating the peak positions first. This step serves as a check on several basic assumptions such as the importance of multiple scattering in low energy electron diffraction. If there is no correlation between calculated and observed peak positions, then there is little point in attempting to calculate intensity with the same mechanisms that failed to reproduce peak positions. Further, by comparing calculated and observed peak positions, it should be possible to determine which scattering mechanisms are dominant. This information would be of considerable importance in the choice of a potential and the determination of an appropriate computational model for the calculation of intensity ratios.

A. Clean (100) Surfaces of fcc Metals

1. Positions of Intensity Maxima

As discussed earlier, there are a number of papers in the literature concerned with the theory of low energy electron diffraction.[2-14] However, much of this work has been concerned with either general theoretical considerations or with model calculations for the hypothetical case of the simple cubic crystal with isotropic scatterers.[2,11,13] The work that does relate to scattering from a real crystal surface has been primarily concerned with the theoretical interpretation of the properties of the specularly reflected beam.[2c,16]

A great deal of information could be obtained on the nature of low energy electron diffraction from the properties of the nonspecular electron beams. In the following section, the experimental data obtained in this laboratory for the nonspecularly reflected beams from the (100) face of aluminum and palladium will be investigated and correlated with data already in existence in the literature for several other face centered cubic materials.

There are several advantages to working with more than one material in a comparison between calculated and observed peak positions. First of all, there is the possibility of checking an implicit assumption in multiple scattering theory that peak positions are determined basically by geometry while the peak intensities are determined by the detailed nature of the atomic potential as has been found in x-ray diffraction. Further, a peak or set of peaks that may be strong for one material may be missing or weak for another material. Therefore, considering several materials allows one a greater opportunity for the experimental observation of any given calculated position. Finally, the consideration of a number

TABLE IV. Experimentally observed positions (in electron volts) of intensity maxima in nonspecularly diffracted beams for the (100) faces of several fcc crystals at normal incidence.

Al (100) (eV)	Pd (100) (eV)	Ag (100) (eV)	Au (100) (eV)	Cu (100) (eV)	Ni (100) (eV)
First-order (0 1) diffraction beams					
59	57	20	27.0	26.5	29
72	78	27	32.0	37.3	35
110	98	34.0	55.0	69.7	47
135	120	56.0	64.0	87.0	55
170	141	62.0	117.0	127.5	62
180	173	115.0		146.0	70
29	203	168.3		220.0	92
40		175.5		243.0	132
					145
					187
Second-order (1 1) diffraction beams					
60	81	46.1	58.0	60.3	65
88	106	55	101.5	72.5	78
118	150	75.7	136.0	115.5	100
150	202	93.5	247.0	128.5	120
190	235	141.0		191.5	153
237	625	229.5		210.5	190
		335.5		296.5	
				310.5	
Third-order (0 2) diffraction beams					
130	174	77.5	70.0	99.0	
168	215	112.5	78.5	111.0	
200		158.5	120.0	138.0	
		173.5	163.0	154.5	
		250.5	256.0	206.0	
				215.0	
				320.0	
Fifth-order (2 2) diffraction beams					
		152.5	171.0	200.5	
		206.5	191.0	260.5	
		280.5	303.0	277.0	

of different materials opens the possibility of studying trends in various intensity ratios that could be correlated with atomic number or position in the periodic table. Any such trend could lead to a better understanding of the scattering potentials involved.

The intensity data for aluminum and palladium which were measured as a function of electron energy (I vs eV) were obtained in this laboratory by the author. Supplementary data for aluminum and palladium were drawn respectively from Bedair et al[36] and Park and Madden.[21] The data for gold, silver and copper were taken from the work of Farnsworth.[42,43] The data for nickel were drawn from papers by Park,[44] Farnsworth et al.[45] and Onchi and Farnsworth.[46] The position of the diffraction peaks (the electron energy at which the intensity is a maximum) for all of these materials are tabulated in Table IV-1.

A more detailed comparison is made for the (10) and (11) beams in Figs. IV-1 and IV-2. The convection used in indexing these beams is shown in Fig. IV-3. Here, the energy scale has been "normalized" to compensate for variations in the lattice parameter among the metals ($I_{h,k}$ vs. e $Vd^2 \cos\theta$). All of the data were taken at normal incidence, $\theta = 0°$. Note that all of the data are for the (100) face of fcc metals. Therefore, peaks corresponding to the same diffraction mechanism should fall at the same corrected electron energies.

As was also found for the specularly reflected beams[24] from different materials, the peak positions do seem to come at the same modified electron energies when plotted on this "normalized" scale. However, the intensity of these peaks vary considerably from material to material, presumably reflecting variations in the characteristics of the atomic potentials. Certain trends have been noted, and will be discussed in more detail below.

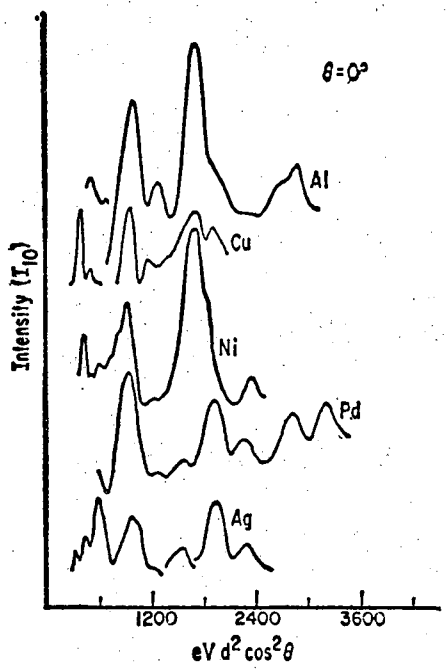

Fig. IV-1

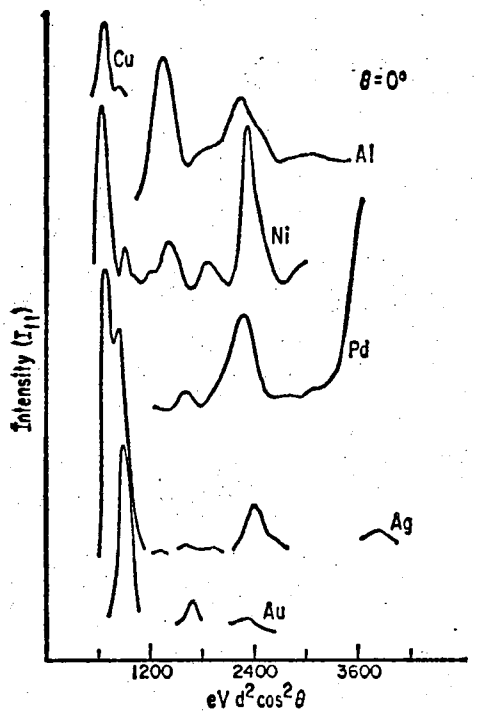

Fig. IV-2

Fig. IV-1. I_{10} vs $eVd^2 \cos^2\theta$ for aluminum, copper, nickel, palladium and silver. Note that abscissa has been adjusted to compensate for variations in the various lattice parameters. Therefore, maxima associated with the same diffraction condition should appear at the same "normalized" electron energy.

Fig. IV-2. I_{11} vs $eVd^2 \cos^2\theta$ for aluminum, copper, nickel, palladium, silver, and gold. Abscissa has been normalized as in Fig. IV-1.

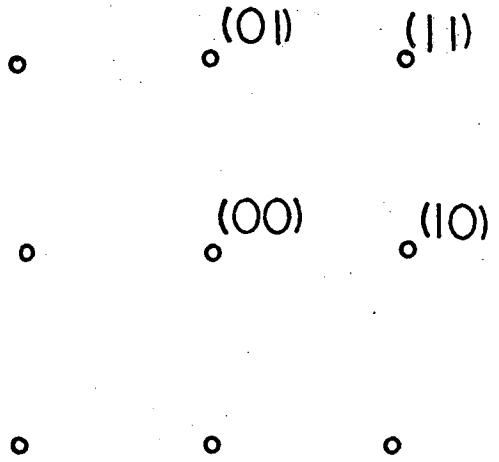

Fig. IV-3. Schematic of diffraction pattern showing convention used in indexing several of the low energy electron diffraction beams.

In Tables IV-1 to IV-4 I have tabulated the calculated and experimentally observed peak positions. Equation 5 was used to determine the theoretical values. The various observed peaks are tentatively assigned to the different single and double diffraction mechanisms.

It should be emphasized that all of these assignments are tentative and have been made on the basis of the best fit between the calculated and the observed peak positions. Two important parameters were neglected in arriving at these assignments. The first was inner potential, and the second was that due to likely experimental inaccuracies.

All of the data which were reported from other laboratories were obtained via Faraday-cup detectors.[42,46] These published data were generally accompanied by detailed correlations between the angle at which a diffraction feature was observed and that calculated from the plane grating formula using the experimental beam voltage. It may be seen that in the low eV region, (below approximately 50 or perhaps even 100 eV), as noted by Farnsworth,[43] the agreement was quite good. This agreement between data and calculations for the diffraction angle seemed to indicate that small inner potential corrections of the order of 5 eV or less were appropriate in this region. Cursory studies in this laboratory gave similar results for palladium surfaces.

We have observed that in using the commercial display instruments fitted with Phillips cathodes,[27] serious discrepancies may exist between the measured electron energy and the actual energy of the electrons striking the crystal. This difference increased with increasing beam voltage and was a function of the temperature of the cathode. This discrepancy resulted in an uncertainty (as much as 5-20eV) in determining the electron energy at which diffraction peaks appeared. Significant shifts in the I_{hk} (eV) curves may occur along the voltage scale as a result of minor changes

TABLE IV-2. Calculated and experimentally observed positions of intensity maxima from the (100) face of several fcc metals.

FIRST ORDER (10) DIFFRACTION BEAMS

hk	h'k'	Pd(100) cal.	Pd(100) obs.	Al(100) cal.	Al(100) obs.	Ag(100) cal.	Ag(100) obs.	Au(100) cal.	Au(100) obs.	Cu(100) cal.	Cu(100) obs.	Ni(100) cal.	Ni(100) obs.
01	01	20		18.4		18.1		18.1		23.0		24.3	
00	01	22.5		21		20	20	20		26	26.5	28	29
01	01	30		28	29	27	27	27	27.5	35	37.5	36	35
00	01	33+		31		30	34.0	30	32.0	39		41	47
01	11	42.5		39	40	38		38		49		52	55
01	11	53.5		49		48		48		62		65	62
01	01	60	57	55	59	54	56.0	54	55.0	69	69.7	73	70
00	01	73	78	67	72	66	62.0	66	64.0	84	87.0	89	92
01	02	82.5		76		75		75		95		100	
01	11	92.5	98	85		84		84		107		112	
01	11												
01	12	110		101		100		100		127	127.5	134	132
01	02	115.5	120	106	110	104		104		133		140	145
00	01	130		119	115	117	115.0	117	117.0	149	146.0	158	
01	02	142.5	141	131	135	129		129		164		173	
01	12	155		143		140		140		179		188	187

TABLE IV-3. Calculated and experimentally observed positions of intensity maxima from the (100) face of several fcc metals.

		SECOND ORDER (11) DIFFRACTION BEAMS											
		Pd(100)		Al(100)		Ag(100)		Au(100)		Cu(100)		Ni(100)	
hk	h'k'	cal.	obs.	cal.	obs.	cal.	obs.	cal.	obs.	cal.	obs.	cal.	obs.
00	11	40		37		36		36		46		49	
11	11												
01	11	42.5		39		38		38		49		52	
11	11	50		46		45	46.1	45		58	60.3	61	
01	11	53.5		49		48		48		62		65	65
00	11	62.5	62.5	58	60	57	55	57	58.0	72	72.5	76	78
11	11	80	81	74		72	75.7	72		92		92	100
11	02												
01	11	92.5		85	88	84		84		107		112	
11	02	102.5	106	94		93	93.2	93		118	115.5	125	120
11	12												
00	11	111.5		103		101		101	101.5	128	128.5	135	
11	11	130		120	118	118		118		150		158	153
11	12	133		122		120		120		153		162	
11	02	152	150	141		137	141	137	136	180		188	190

TABLE IV-4. Calculated and experimentally observed positions of intensity maxima from the (100) face of several fcc metals

hk	hk'	THIRD ORDER (02) DIFFRACTION BEAMS							
		Al(100)		Ag(100)		Au(100)		Cu(100)	
		cal.	obs.	cal.	obs.	cal.	obs.	cal.	obs.
11	02	74		72		72	70.0	92	
02	02								
01	02	76		75		75		95	
00	02	83		81	77.5	81	78.5	104	99.0
02	02								
11	02	94		93		93		118	111.0
02	12								
02	12	104		102		102		130	
01	02	106		104		104		133	
02	02	110		109	112.5	109		138	138.0
00	02	120		119		119	120.0	151	154.5
01	02	131	130	129		129		164	

in the cathode characteristics. It was not verified if this same effect existed for the instruments used in the previously published data, but the good agreement between the calculated and the observed angles would seem to indicate that at least it could not have been significant in the low electron-energy region.

Another possible source of experimental error was small uncertainties in the angle of incidence. It was found that slight deviations from normal incidence resulted in noticeable shifts in peak positions and changes in peak shape. These variations become more pronounced with increasing beam voltage.

All of these effects tend to make the assignments at the higher beam voltages less reliable than those at the lower beam voltages. It should be noted however, that most of the beams which contain significant information about the surface structure appear in the lower more reliable voltage range 0 - 140 eV. In order to discuss the properties of the different non-specular beams separately and to correlate them to single- and double-diffraction events, it is useful to arbitrarily divide the electron-energy range in which they were studied into four ranges; (I) 0-20 eV, (II) 20-40 eV, (III) 40-80 eV, and (IV) > 80 eV. The voltage limits given correspond to palladium. Those for aluminum, silver and gold are approximately 10% lower, and those for copper and nickel are approximately 20% higher. In units of ev d^2 cos θ, range I covers 0-300; II, 300-600 and III, 600 to 1200.

a. Beam Voltage Range ~ 0-20 eV

In this region, below the appearance voltage of the first order diffraction beams, only the specularly reflected beam [(00) reflection] is directly observable. There is only one elastic scattering phenomenon expected in this region. That is the appearance of a Bragg peak ($2K^{\circ}_{z} = G_z$), pre-

dicted by both the single (kinematic) and the multiple-scattering theories.

In the experimentally observed specularly reflected (00) beam intensities from the (100) face of aluminum and palladium, only one maxima is observed in this region at energies around 10 and 14 eV, respectively. These values are slightly higher than those expected for the appearance of the Bragg maxima. It should be noted that the quality of the data is relatively poor in this low voltage region because of the low current levels of the electron gun. A more detailed investigation in this region with a constant current electron source and using more sensitive detection techniques would be useful.

b. Beam Voltage Range ~ 20-40 eV

The second region starts at the appearance voltage of the first order diffraction (10) beams and ends just below the appearance voltage of the second order diffraction (11) beams. It is more complex than the first region because of the increase in the number of beams that are present[(00) and (10)]. At the emergence voltage, a diffraction condition of the form $K_z^{10} \pm K_z^{10} = G_z$ is met, where G_z is the perpendicular component of the reciprocal lattice vector with zero magnitude. This condition is similar to that for the surface wave resonance predicted by McRae[2] for the simple cubic case. There is no experimental data in this energy region for the (10), diffraction beam for any of the materials investigated here.

The second phenomena in this region, which should occur at a slightly higher beam voltage, is characterized by a diffraction condition of the form $K_z^{00} + K_z^{10} = G_z$. Here, $|G_z| = \frac{2\pi}{2a_z}$ where a_z is the interplanar spacing perpendicular to the surface. This maximum is predicted by the kinematic theory and, if single scattering predominates, this diffraction process would produce an intensity maximum only in the first order (10) diffraction

beam. Multiple-scattering considerations indicate that there may be a maximum in the specularly reflected beam as well.

The available experimental data for the first order diffraction beams from aluminum and palladium do not extend into this low-voltage range. However, for silver, copper and nickel intensity maxima are reported in the (1 0) beams within about 1 eV of the respective calculated values for the single scattering process ($K_z^{00} + K_z^{10} = G_z$). No equivalent peak has been reported for gold, but it may have been outside of the range of experimental observation.

The next predicted maximum involves a diffraction condition of the form $2K_z^{10} = G_z$. This is strictly a multiple scattering effect as it formally necessitates at least double diffraction. This region is still outside of the experimentally observed range for palladium, but maxima have been observed for aluminum, nickel, copper, gold and silver within 3 eV of the respective calculated theoretical values. The maximum for nickel is distinct but weak in the curves reported by Park and appears only as a shoulder in the curves reported by Farnsworth. This is an example of the sensitivity of peak shape and position to slight variations in the experimental arrangement.

This peak is of particular interest for several reasons. First, it is forbidden in the kinematic limit of diffraction and therefore may be taken as evidence of multiple scattering. Secondly, it is the first of a general class of dominant peaks (ignoring surface wave resonance) that are characterized by the equation $2K_z = G_z$. Here the diffraction interaction involves beams differing primarily in the sign but not the magnitude of that component of their wave vector (or momentum) that is perpendicular to the surface.

At a slightly higher beam voltage, there is a diffraction condition of the form $K_z^{00} + K_z^{10} = G_z$ where $|G_z| = 3\frac{2\pi}{2a_z}$. In the kinematic limit, a peak should appear only in the (10) beam. In the case where there is considerable multiple scattering, a secondary Bragg maxima may also appear in the specularly reflected beam. In the first order diffraction beams from the (100) face of Au and Ag and possibly from Ni and Cu there appear intensity maxima in this voltage region. It should be noted that all of these maxima appear at uniformly higher voltages than those predicted.

The relative intensity of this maxima generally increases with increasing atomic number. That is, it is not observed on aluminum, is weak or questionable on nickel and copper, but is quite prominent for gold and silver. This region for palladium was outside of the range of experimental observation. Regardless of the assignment of this diffraction peak, this trend in intensities is a manifestation of the effect of varying the potential at the scattering centers by varying the atomic number.

There are no further maxima in the first order diffraction beams below the emergence voltage of the (1,1) diffraction beams. All of the preceding phenomena may contribute to the intensity of the specularly reflected beam in this region. Comparisons with experiment are complicated by the fact that the intensities of the specularly reflected beam cannot be obtained at normal incidence. Aluminum shows a rather featureless hump in this region at $\theta \sim 3°$. Palladium shows a gradual increase in intensity throughout the region. More structure is observable on copper where there are two distinct maxima in this region. It is probable that all of the phenomena contribute to the intensity of the (00) beam in this range. Careful angular studies should allow one to distinguish among the various components.

c. Beam Voltage Range ~ 40-80 eV

This is the region between the appearance of the second-order diffraction beams (1 1) and the third order diffraction beams (2 0). For the (100) face of fcc metals at normal incidence, the appearance of the (1 1) beams coincides with the second Bragg maxima in the specularly reflected beam. McRae has concluded that there should be a zero in the reflectivity curve for the (h k) beam when the following two conditions are met simultaneously; $K_{h\,k} = n2\pi/d$ and $K_{h'k'} = 0$. In this case the first condition corresponds to the Bragg maxima in the (0 0) beam and the second to the surface wave resonance in the (1 1) beams. Consequently, at normal incidence, there should be a minimum in the specularly reflected beam in this region in the fully elastic multiple scattering model. Such a minimum is observed for aluminum, and possibly for copper. Data for gold, silver, and nickel were not investigated. No such minimum is observed in the specular (0 0) beam, for palladium. As all of the data for the specularly reflected beam were taken at non-normal incidence, it is difficult to conclude anything about the magnitude of this effect for these materials. It is possible that the intensity of this diffraction feature becomes more pronounced with decreasing atomic number.

The first diffraction condition that is met after the appearance of the (1 1) beams is between the (1 1) beams and the (1 0) beams and is characterized by a diffraction condition of the form $K_z^{10} + K_z^{11} = G_z$. This may produce observable maxima in either set of beams. No intensity maxima have been reported in this region for the (1 1) beam, possibly because of the experimental difficulties inherent in investigating a beam this close to its emergence voltage. The (1 0) beam represents a different case, however. Here the experimental data are reliable, and an intensity

maximum is definitely observed in this region for both aluminum and nickel within 2 eV of the calculated values. In addition, there is a definite shoulder for silver, just below 40 eV (calculated value 38.6 eV). No maxima have been reported in this region for the (1 0) beams from gold and copper, but it is possible that they may be present as shoulders or veryweak peaks masked by adjacent phenomena. The data for palladium do not extend into this region. At higher energies, there are two diffraction conditions that are met almost simultaneously. The first is of the form $2K_z^{11} = G_z$ and several eV higher, there is another of the form $K_z^{10} + K_z^{11} = G_z$. Except perhaps for nickel, there is a uniform absence of significant intensity maxima in the (10) beam in this range [~ 45 - 55 eV for Pd (100)]. However, for the (11) beams definite maxima are observed for silver, copper and nickel within several eV of the positions calculated from $2 K_z^{11} = G_z$. Similarly, there appears to be a shoulder in this region for gold. The curves for aluminum do not extend into this range.

Proceeding to still higher energies, we encounter strong maxima in the (1 0) beams diffracted from all of the materials under investigation. All of the positions are within 3 eV of those calculated from the diffraction condition $2K_z^{10} = G_z$ and there are no other diffraction conditions involving this beam within approximately a 7 V range. These maxima are generally quite strong and represent one of the more notable and consistent correlations between materials made in this study. As these peaks are relatively strong, they tend to dominate a fairly large energy range. As a result, weaker peaks may be obscured making interpretation in adjacent regions somewhat difficult.

On the high energy side of these intensity maxima in the (1 0) beam, there is some indication of a shoulder for several materials, and definite maxima for both gold and silver. The higher peaks on silver and gold are

within 5 and 3 eV, respectively of the positions calculated from the kinematic condition $K_z^{00} + K_z^{10} = G_z$. Further, the shoulder on aluminum was occassionally resolved as a separate peak also within several eV of the calculated position. In the specularly reflected beam, both aluminum and palladium have strong maxima in this region that are most probably related to this diffraction condition.

At slightly lower energies (@.5 eV for palladium), there are definite intensity maxima in the (1 1) beams for all of the materials investigated in this region. Furthermore, all of these maxima are within 1 eV of the positions calculated from the diffraction condition $K_z^{00} + K_z^{11} = G_z$ with the exception of that for silver which is within 3 eV of the calculated position. These maxima presumably are a manifestation of a diffraction condition that is allowed in the limit of kinematic scattering.

d. Beam Voltage Range > 80 eV

The next diffraction process of interest is the appearance of the (2 0) diffraction beams and, at approximately 20 eV higher, the (2 1) beams. It becomes excessively tedious to enumerate in detail all of the possible diffraction conditions as the number of possible types of interactions increases rapidly with the number of beams present even at normal incidence. Away from normal incidence, the situation should be considerably more complicated. Furthermore as the band structure becomes more complex, bands overlap and the interpretation becomes more difficult. Fewer of the diffraction conditions are met "purely" i.e., without any mixing, and not all of the allowed conditions will be observed as multiple scattering may become less pronounced. Comparisons with experimental data also become less reliable at higher beam voltages unless extreme care was exercised in obtaining those data. In general, however, the analysis can be carried out in the

same manner as above. The results of such an analysis are tabulated. There are several points of interest. At normal incidence, the appearance of the (2,0) beams coincides exactly with a diffraction condition of the form $2K_z^{11} = G_z$ for the (1 1) beam. Therefore, a diffraction condition of the form $K_z^{11} + K_z^{20} = G_z$ is automatically met. Accordingly, there should be a resonance minima in the back reflected (1 1) beam intensity.[2] In fact no strong maxima are observed or reported for the (1 1) beams in this region for any of the materials under consideration. This may be taken as an indication of the significance of the resonance effect in this region for these materials. It should be noted that there are very weak maxima observed in this general region for the (1 1) beams of several of these materials. However, on palladium it has been noted that this beam is very sensitive to position, and that its appearance is probably due to small deviations from perfectly normal incidence.

As with the n = 2 Bragg peak there is a similar coincidence for the n = 4 Bragg peak. In fact, it may be shown that all of the even-integral-order Bragg peaks from the (100) face of fcc materials at $\vartheta = 0°$ coincide with the appearance of some set of (h,h) beams. Consequently, there should be a resonance minimum rather than a Bragg maximum at these voltages in fully elastic multiple scattering treatment developed by McRae.[2] On Al, Pd, Pt, and Cu a minimum is observed in the specular reflected beam at the appropriate voltage. However, on all of these materials, a strong maximum is observed approximately 20 eV lower. It is tempting to assign this to a Bragg peak with a reasonable inner potential and say that the resonance minimum is not observed. The former may be correct, but the latter is not necessarily so as all the observations were carried out at $\theta = 0°$. McRae[2] has shown that for slight deviations from normal incidence, the Bragg peak may appear and that its shape structure may still be

strongly influenced by the coupling with the surface wave resonance that accompany the emergence of the new diffraction beams. There is another interesting feature in this region that may be associated with simultaneous diffraction conditions. On aluminum, very strong intensity maxima in the (1 0) beam occur at approximately 100 eV. There are at least four diffraction conditions which may be met; $2K^{10} = G_z$, $K_z^{10} + K_z^{21} = G_z$, $2K_z^{21} = G_z$, and $K_z^{10} - K_z^{21} = G_z$.. On the high energy side of this maxima for aluminum, a definite shoulder is observable. Going to the corresponding region on nickel one finds that the relative intensity of the shoulder is comparable to that of the main beam. Continuing to the noble metals, it may be seen that the peak that was so intense for aluminum has essentially vanished, and that the region is dominated by what was the shoulder. It would be interesting to investigate the behavior of the (2,1) beams in this range in order to observe whether or not they manifest the inverse trend in intensities. If so, this would provide an interesting correlation between scattering amplitudes and potentials for the different metals

e. Inner Potential Considerations

The preceding assignments have been made with the assumption of zero inner potential correction. As there are a large number of calculated peak positions, it is possible to make alternate assignments by assuming various inner potentials. As noted before, the assignments given above are based upon the best fit between the experimental and the calculated values with a zero inner potential correction. If small non-zero values of the inner potential are assumed, the agreement in the region below 100 eV primary beam voltage becomes progressively worse out to a value of about -5 or -6 eV (inner potential correction). Then, however, the fit becomes gradually better as the magnitude of the inner potential is increased. At corrections of about -10 or -11 eV, the fit between the

experimental and the calculated peak positions has improved to the point where it is comparable to the fit with no inner potential correction. The assignments, however, are entirely different. In this manner, it is possible to generate several sets of alternative assignments and the question naturally arises as to which is correct. It is therefore necessary to investigate further the validity of the neglect of inner potential corrections.

To do this, it is of value to first inquire into the nature of the inner potential. It is well known that metals have work functions on the order of several electron volts, that is, energy must be supplied to electrons in order to leave a metal surface and to be able to escape into free space. Similarly, energy is gained by an electron when it enters a metal crystal as it is then in a state of lower potential energy than in free space. Consequently, the wavelength associated with an electron becomes somewhat shortened when the electron penetrates into a crystal and the diffraction conditions given in Eq. 5 are met at lower acceleration energies than those calculated with the assumption of a zero inner potential. Therefore, the calculated values should be modified by the subtraction of an inner potential correction.

The basic question then revolves around how large an inner potential should be used. Heine[47] has shown that this inner potential is essentially V_{00}, the matrix element along the diagonal of the secular determinent given in Eq. 31. When the matrix is properly diagonalized, this term will be modified by the addition and/or subtraction of other matrix elements, V_G but as these terms are usually about an order of magnitude smaller than V_{00} they may be neglected to a first approximation. This matrix element V_{00}, is simply the zeroth order coefficient in the Fourier expansion of the potential. Alternatively it is essentially the amplitude of the trans-

mitted beam in the kinematic or Born approximation.

Using pseudopotentials,[48] Pendry[49] has calculated the inner potential for several materials. He finds that this quantity is voltage dependent in the region below 100 eV. The inner potential has some minimum absolute value in the primary voltage range somewhat above the Fermi energy. Upon going to higher primary energies, the absolute value of the inner potential increases, finally becoming fairly constant somewhere in the vicinity of 50 eV to 100 eV. For nickel, Pendry calculated that the inner potential was about 4 eV at 25 eV, 6 eV at 50 eV and 10 eV at 100 eV. No calculations were performed for the other metals considered in this study.

These values are reasonably consistent with the experimentally observed behavior of the diffraction angle discussed earlier. Considering both the experimental diffraction angle data and the pseudopotential calcuations, the following conclusions may be drawn. In the region above 100 eV, considerable inner potential correction may be necessary. Consequently, the previously tabulated assignments in this region which were made using zero inner potential are questionable. On the other hand, in the region between approximately 20 and 50 eV, corrections of the order of several electron volts, definitely less than 10, are reasonable. It may then be necessary to reassign some features in this region, but the majority of the assignments are most probably correct.

It is necessary to inquire into the assignments between 50 and 100 eV. One assignment in particular begs justification. In the (10) diffraction beams for all of the materials studied, there is a very strong maximum that has been assigned to a diffraction condition of the form $2K_z^{10} = G_z$.

Not far above this condition is another of the form $K_z^{00} + K_z^{10} = G_z$. Except for silver, only relatively weak maxima have been assigned to this second condition. As the first condition is purely a multiple scattering mechanism, while the second is allowed even in the kinematic limit, it is at first thought inconsistent to assign a strong peak to a multiple scattering mechanism and a weak peak to a kinematic mechanism when a not unreasonable alternative assignment could be made. For nickel, this intense maximum is observed at approximately 70 eV. In the absence of inner potential corrections, the $2K_z^{10} = G_z$ multiple scattering peak is predicted at 73 eV and the $K_z^{00} + K_z^{10} = G_z$ kinematic peak at 87 eV. Thus, an inner potential correction of 3 eV is needed to assign this maxima to the multiple scattering mechanism while an inner potential correction of 17 eV is necessary for the kinematic assignment. As the calculated value is 7 eV and as that estimated from the data on the angle of diffraction is definitely less than 10 eV, the multiple scattering assignment appears to definitely be the more reasonable one on the basis of existing evidence.

It is of some interest to inquire as to why a multiple scattering intensity should be so much stronger than an adjacent kinematic maximum. The higher correlation observed among all of the materials studied seems to argue against this being due to a fluctuation in the form factor. An alternate suggestion may be made from a consideration of the band structure in this neighborhood. Immediately above the $2K_z^{10} = G_z$ condition, there is a $K_z^{00} + K_z^{11} = G_z$ condition. However, there are no diffraction conditions in the neighborhood of the $K_z^{00} + K_z^{10} = G_z$ condition. Thus, if the band gaps are only several eV wide, there is a "complete" band gap in the first case, but only an incomplete gap in the second. Therefore, in the first case, there are no allowed states within which the electron can travel into the crystal. Consequently, in the absence of inelastic scattering,

it must be scattered out of the crystal and the intensity in one or more of the back-scattered beam may be expected to be high. However, in the second case, the (11) beam is allowed in the crystal, and perfect back diffraction is not required in the elastic limit. A similar case is discussed in more detail in Appendix I.

f. Angular Dependence

The advantages of studying the intensities of the electron beams at normal electron beam incidence are obvious. Under these conditions, all of the diffraction beams with the same indices and the same sign of K'_z are degenerate. Consequently, considerably fewer diffraction conditions of the form given in Eq. 5 need be considered. For example, in the region between approximately 20 and 40 eV, in addition to the transmitted and the specularly reflected beams, there exist only the first order diffraction beams, four directed into and four scattered out of the crystal. At normal incidence, the four beams in these two sets are degenerate. Therefore, there are only four unique beams in this energy range, and we need only consider three equations of the form of Eq. 5. However, away from normal incidence, there may be 10 unique beams in this same energy range, and it may be necessary to consider up to 45 diffraction conditions. The situation becomes increasingly complex as one goes to higher voltage ranges.

When multiple scattering is dominant, then it is to be expected that one will experimentally observe the gradual resolution of an intensity maximum into several distinct components as the degeneracy is lifted by slowly varying the angle of incidence away from the normal. This may be contrasted with the case where only single scattering is dominant. In this kinematic limit, only a gradual shift in peak position with no development

of fine structure is to be expected when the angle of incidence is varied.

The basic diffraction condition, Eq. 5,

$$\vec{K}'_z - \vec{K}''_z = \vec{G}_z,$$

may be combined with Eqs. 4 and 6 to give,

$$\sqrt{|\vec{K}^\circ|^2 - |\vec{K}^\circ_{xy} + \vec{G}'_{xy}|^2} \pm \sqrt{|\vec{K}^\circ|^2 - |\vec{K}^\circ_{xy} + \vec{G}''_{xy}|^2} = |\vec{G}_z| \tag{56a}$$

or

$$\sqrt{|\vec{K}^\circ_z|^2 - |\vec{G}'_{xy}|^2 - 2\vec{K}^\circ_{xy} \cdot \vec{G}'_{xy}} \pm \sqrt{|\vec{K}^\circ_z|^2 - |\vec{G}''_{xy}|^2 - 2\vec{K}^\circ_{xy} \cdot \vec{G}''_{xy}} = |\vec{G}_z|. \tag{56b}$$

Noting that $|\vec{K}^\circ_z| = |\vec{K}^\circ| \cos\theta$ and $|\vec{K}^\circ_{xy}| = |\vec{K}^\circ| \sin\theta$, and that $|\vec{K}^\circ| = 2\pi$ eV/150.4 Å^{-1}, it may be seen that the energy at which Eq. 5 is met is dependent upon θ, the angle of incidence. Furthermore, as this equation contains a dot product between $\vec{K}^\circ_{xy}$ and $\vec{G}_{xy}$, the angle between the parallel component of the incident wave vector and the parallel reciprocal lattice vectors is also important. This, of course, is the azimuthal angle, ϕ.

As noted before, variations in the azimuthal angle produce subtle but definite differences in the shapes of the intensity maxima in the specularly reflected electron beam from the (100) face of aluminum. As is to be expected, these difference become more pronounced at larger angles of incidence.

The dependence of the intensity of the first order diffraction beams is even more strongly affected by variations in the azimuthal when at non-normal incidence. The data for the (10) beams from both aluminum and iridium taken at non-normal incidence and shown in Figs. III-11 and III-15 were obtained at an azimuthal angle of approximately 45°. As it is difficult to measure the azimuthal angle to better than 4° with the present

experimental equipment, there is some uncertainty in these measurements. Note, however, the slight differences between curves that should be identical at $\phi = 45°$. Other data taken at several different azimuthal angles showed marked dependence upon ϕ.[50]

The expected resolution of intensity maxima into several different components when the angle of incidence is increased is definitely observed for the specularly reflected beam from the (100) face of palladium. The maxima near 40 eV shows two components even at $\theta = 5°$ and three at 8°. When $\theta = 17\text{-}1/2°$, this peak has been completely split into two strong components. The corresponding peak on aluminum does not display this drastic splitting to the same extent. It does, however, show some sign of fine structure and actually appears to move to lower voltages when the angle of incidence is increased. For both aluminum and palladium, the strong peak near 70 eV also shows considerable dependence upon the angle of incidence, not only in position but also in line shape. Again, the resolution into sub-components is far more marked for palladium. This peak has been assigned to a diffraction condition of the form $K_z^{00} + K_z^{10} = G_z$. The alternate assignment would be to a kinematic Bragg peak with a 15-20 eV inner potential shift. The development of several components when θ is increased definitely supports a multiple scattering assignment in preference to a kinematic assignment. Similar comments could be made about practically all of the observed maxima.

Even for aluminum, the intensity maxima in the first order diffraction beams show a much stronger dependence upon the angle of incidence than do those in the specularly reflected beam. The data from both aluminum and iridium show the same trend. Those beams for which K'_{xy} is parallel to K°_{xy}, or $\vec{K}'_{xy} \cdot \vec{K}^\circ_{xy} > 0$, have their maxima shifted to higher energies

when θ is increased. Conversely, those beams for which K'_{xy} is anti-parallel to K°_{xy} or $\vec{K}'_{xy} \cdot \vec{K}^{\circ}_{xy} < 0$, have their maxima shifted to lower energies. This is reasonable, as K'_z is greater in the anti-parallel case than in the parallel case. Consequently, Eq. 5 will be met at lower energies for $\vec{K}'_{xy} \cdot \vec{K}^{\circ}_{xy} < 0$ than for $\vec{K}'_{xy} \cdot \vec{K}^{\circ}_{xy} > 0$.

In Fig. III-11 for the (10) beams diffracted from the (100) face of aluminum, note that the peaks near 55 eV appear to shift more when the angle of incidence is varied than do the peaks near 70 eV. This would be expected if the former were assigned to a multiple scattering condition, and the latter to a kinematic condition. These observations also support the earlier assignment of the 55 eV peak to a $2K_z^{10} = G_z$ condition.

g. Conclusions

The position of the intensity maxima of the nonspecular low-energy-electron beam seem to verify the importance of multiple scattering in LEED. This is consistent with earlier observations on the specularly reflected beam.[24] The number of observed diffraction maxima is too large to allow for their assignment solely on the basis of kinematic considerations. The coincidence of observed intensity maxima positions with those calculated on the basis of a double diffraction mechanism would seem to substantiate the validity of the double diffraction approach in predicting possible peak positions.

The double diffraction condition, $2K'_z = G_z$ appears to be particularly dominant in the electron energy just above the appearance energy of the beam under consideration. There also appears to be a general tendency for diffraction conditions with relatively small magnitudes of G to dominate. As most atomic potentials would favor forward scattering this is physically reasonable. This generalization, of course, is not meant to preclude oscillatory behavior in the form factors with increasing values of G, the scatter-

ing vector.

Assuming that the preceding assignments are at least partially correct, inner potential corrections appear to be considerably less than 10 eV and probably less than 5 eV in the very low-energy range. Finally, it may be seen that the atomic potential plays a significant role in determining peak shape and intensity.

2. Intensity Maxima Ratios

A computational method was developed to calculate the intensities of the low energy electron beams back diffracted from single crystal surfaces. The method is described in detail in Appendix II.

Initially, a simple screened coulombic potential of the form

$$V(r) = \frac{ze^2}{r} \exp[-\lambda r]$$

was used for the atomic potentials. Here, z is the atomic number and λ is the screening parameter. This potential resulted in Fourier coefficients

$$V_G = \frac{D}{\lambda^2 + G^2}$$

where $\vec{G}$ is the scattering vector, and the D is the normalization coefficients. Later, it was found to be advantageous to use a potential whose Fourier coefficients had the form

$$V_G = \frac{D}{\lambda^2 + G^2 + \nu G_{\|}^2}$$

where $G_{\|}$ is that component of the scattering vector that is parallel to the surface and ν is a second parameter.

Inelastic scattering was introduced in the form of atomic excitations. The fraction of the intensity that was scattered elastically in a single scattering event by each atomic scattering center was given by α^2 where α is a computational parameter usually assigned the value of 0.9. The thermal motion of the lattice was simulated through the use of the Debye-Waller factor where the mass was taken as 27 amu, the absolute temperature as 300°K and the Debye temperature as 400°K in the bulk and 200°K at the surface (see Appendix III).

a. Four Beam Case In this case, in addition to the transmitted and the specularly reflected beam, there are two diffracted beams, one directed into, and one directed out of the crystal. There is no identical situation

in the real case of a (100) face f.c.c. material at normal incidence. However, there is an approximately equivalent case between about 20 and 40 eV. Here, the first order diffraction beams are allowed and are the highest order present. The one beam directed out of the crystal then represents a set of four beams directed away from the surface. Similarly assumptions were made for the inward directed beams. The computational case is approximate in that it neglects the interactions among beams in a given set and between beams in different sets that do not have the same parallel reciprocal lattice vector. As these neglected interactions are all characterized by relatively large scattering vectors, $|\vec{G}|$, this approximation is not unreasonably in the case of the screened Coulombic potential where V_G is inversely proportional to $\lambda^2 + G^2$.

Figure IV-4 shows the calculated intensity of the specularly reflected beam and the first order diffraction beam for the (100) face of aluminum at normal incidence between 19 and 36 eV. The beam intensity was attenuated by the inclusion of inelastic and thermal scattering. Several values of the screening parameter, λ, were used to simulate different diffraction conditions. When $\lambda = 0.1\ \mathring{A}^{-1}$, the calculation is essentially in the kinematic limit, as V_0 is inversely proportional to λ^2. For the specularly reflected or (00) beam, only one peak is visible. This is the Bragg peak at 37 eV. For the first order or (10) diffraction beam, there are two maxima; one at 31 eV corresponding to the kinematic condition $K_z^{00} + K_z^{10} = G_z$ and one just below 19 eV corresponding to a diffraction condition of the form $2K_z^{10} = G_z$. This type of multiple scattering condition would ordinarily be forbidden for such a small value of the screening parameter except that the cross sections are extremely large at the appearance voltage due to their inverse dependence upon K'_z. This may be an artifact of the model, as the $1/K'_z$ term arises as a direct consequence of the imposition of

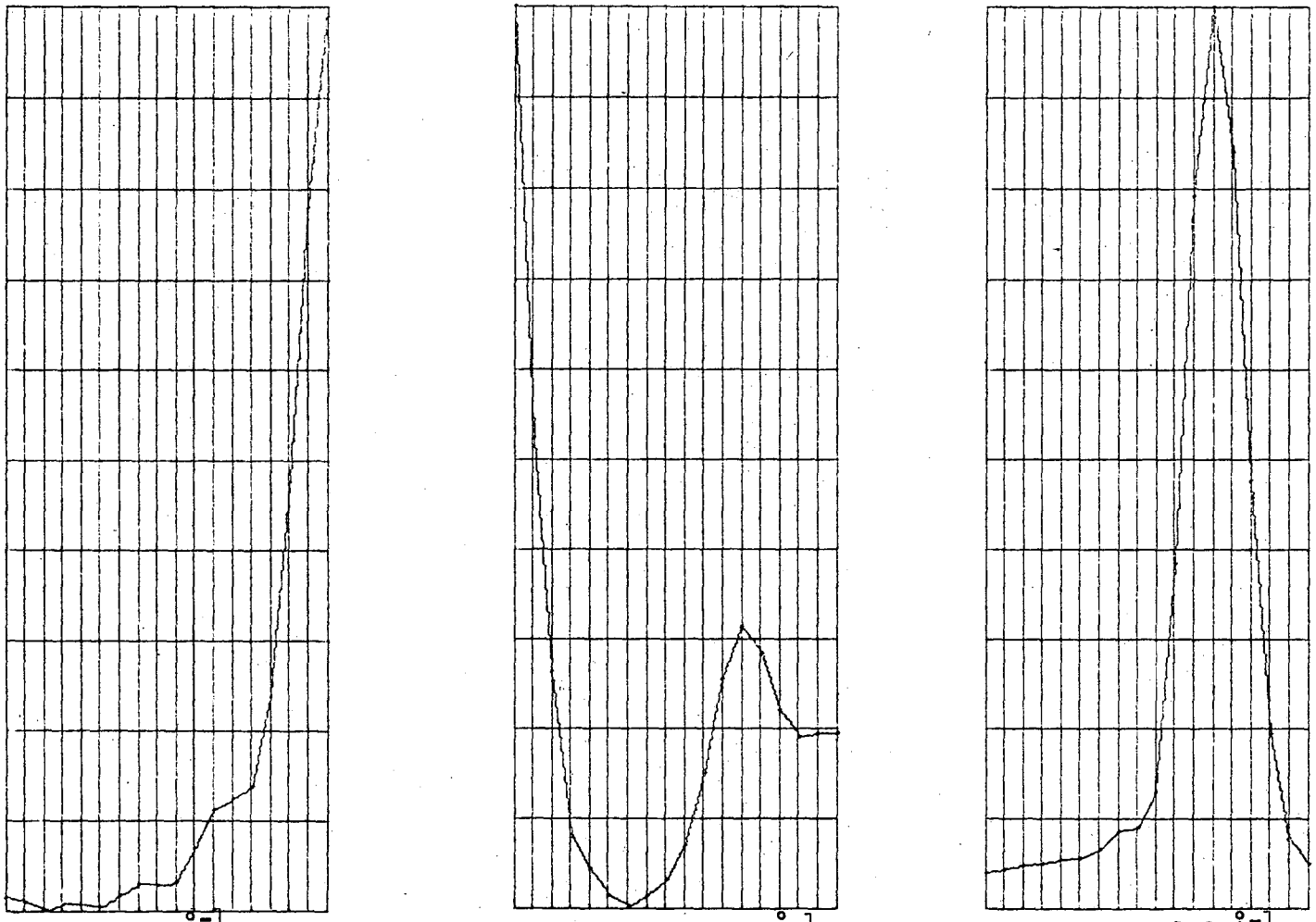

Fig. IV-4a. I_{00} vs eV for Al(100) between 19 and 36 eV at $\theta = 0°$ for several values of the screening parameter λ and with $\nu = 0$, $\alpha = 0.9$, $T = 300°K$, $\theta_B = 400°K$ and $\theta_S = 400°K$. Fifteen scattering events were used and the four beam approximation was made.

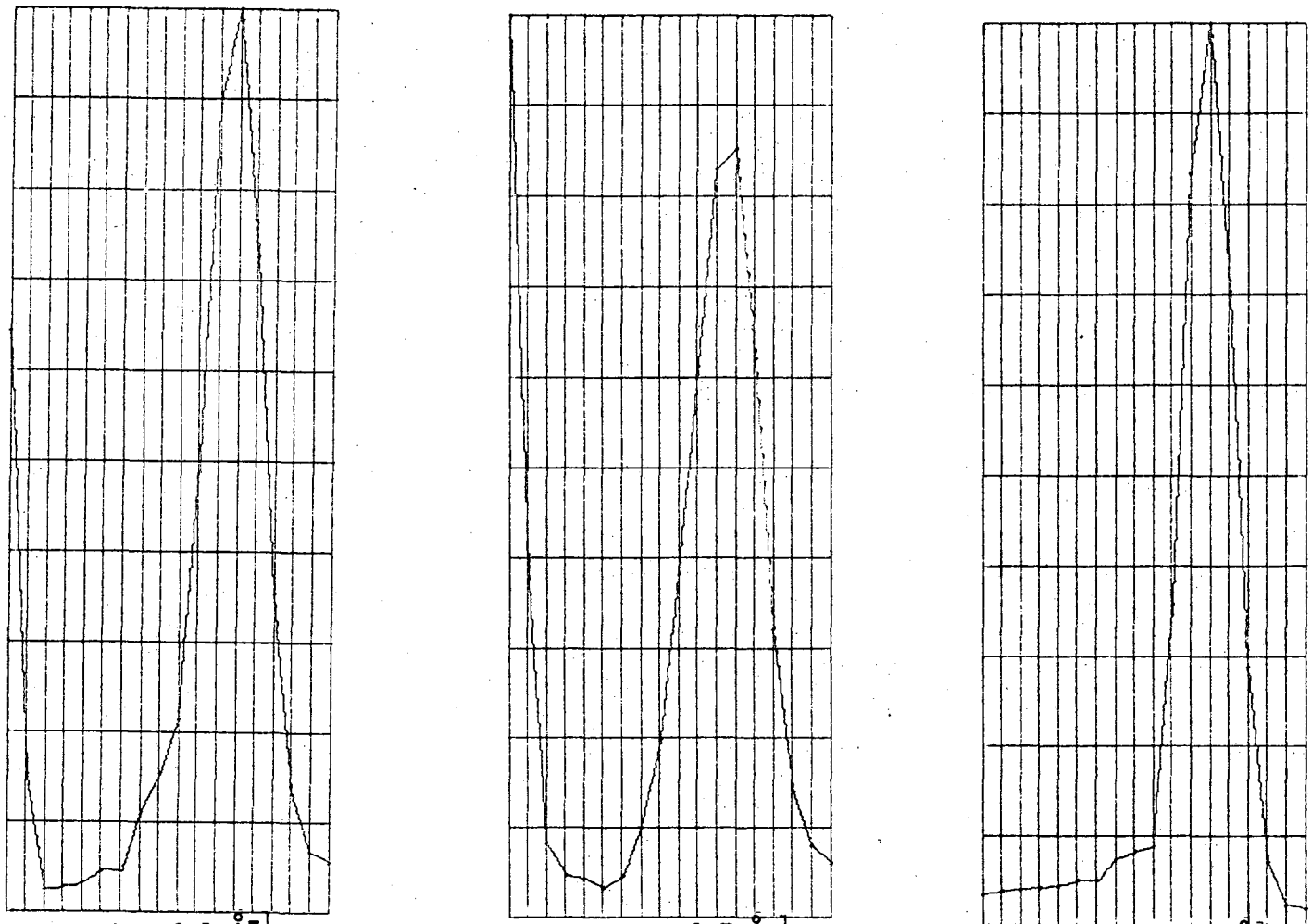

Fig. IV-4b. I_{10} vs eV for Al(100) between 19 and 36 eV at $\theta = 0°$ for several valuesof the screening parameter λ and with $\nu = 0$, $\alpha = 0.9$, T = 300°K, θ_B = 400°K and θ_S = 400°K. Fifteen scattering events were used and the four beam approximation was made.

of strict two dimensional symmetry upon the Greens function (see section II-B-2). A similar condition at 28 eV does not result in a maxima for $\lambda = 0.1$ Å^{-1}. The kinematic diffraction condition near 21 eV does not give maxima in this calculation. The reason for this is not known, but it is possibly that the intervals at which the intensity is calculated are too far apart to show these maxima. It is likely that the (10) beam does not penetrate very deeply at this voltage and consequently is rather insensitive to this condition.

When the screening parameter is increased to 0.5 and then 1.0 Å^{-1}, there is a definite shift in the peak position in the (00) beam. For the larger cross section, multiple scattering becomes dominant, and the condition $K_z^{00} + K_z^{10} = G_z$ at 31 eV is met more strongly than the Bragg condition $2K_z^{00} = G_z$ at 37 eV.

Figure IV-5 shows a comparison among calculations done for this region with an isotropic potential, Gaffners potential and the isotropic scattering potential with $\lambda = 1$ Å^{-1}. Note the similarities between the calculations which were carried out with the two forward scattering potentials. On the other hand, the calculations performed with the isotropic potential result in high background and broad peaks that are shifted to slightly lower voltages.

In none of these curves, however, is there much indication of the intensity maxima at 28 eV corresponding to the $2K_z^{10} = G_z$ diffraction condition. As this peak is observed for several materials, it is of some importance to be able to generate it in model calculations. This was done by the introduction of the parameter ν described above. The use of this parameter enhances diffraction conditions that involve no change in the component of the wave vector parallel to the surface. Figures IV-6 shows the result of using various values of ν. When $\nu = 5$, there is a shoulder

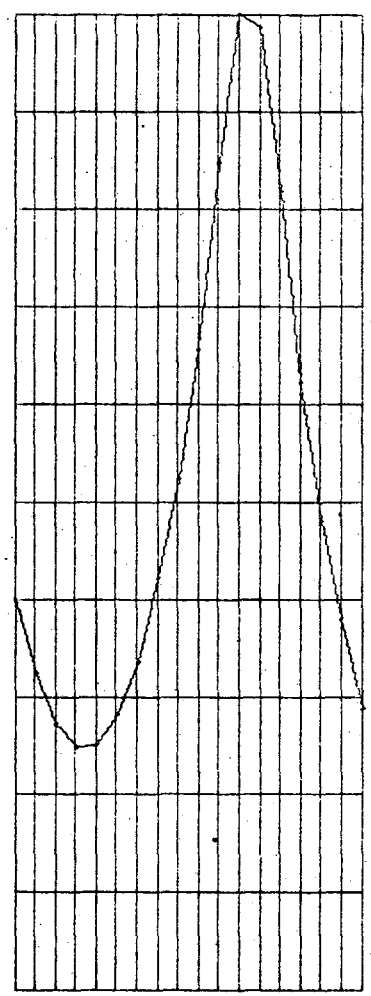

Gafners Potential

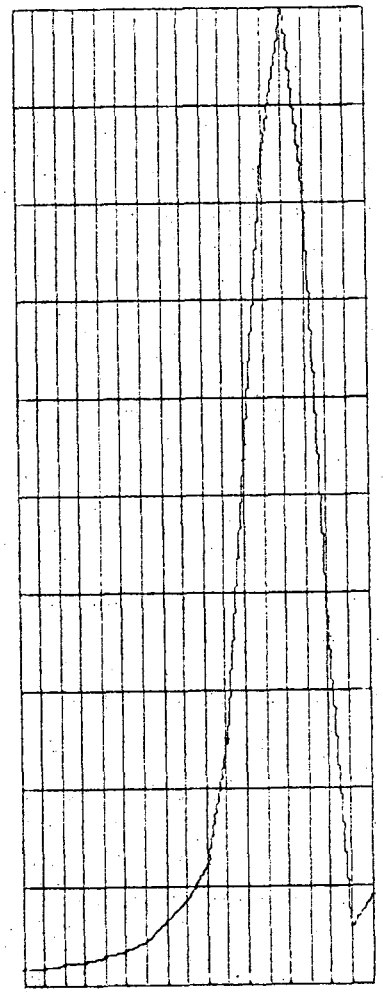

Isotropic Scattering Potential

Fig. IV-5a. I_{00} vs eV for Al (100) between 19 and 36 eV at $\theta = 0°$ for Gafners potential and the isotropic scattering potential with $\alpha = 0.9$, $T = 300°K$, $\theta_B = 400°K$ and $\theta_S = 200°K$. Fifteen scattering events were employed, and the four beam approximation was made.

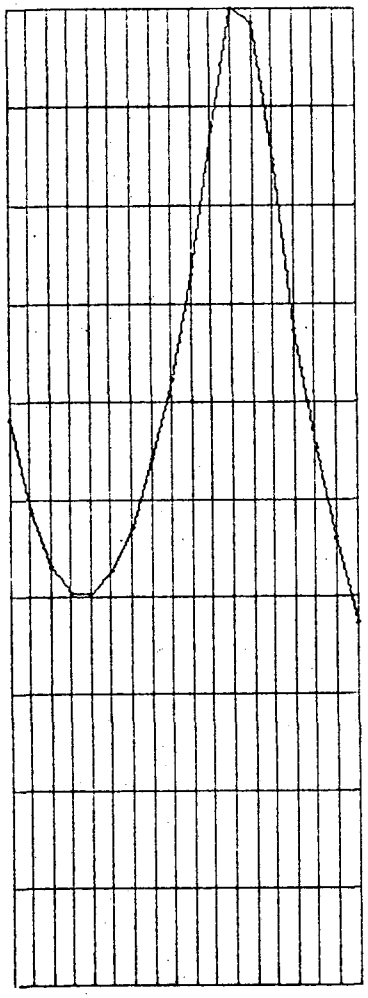

Gafners Potential

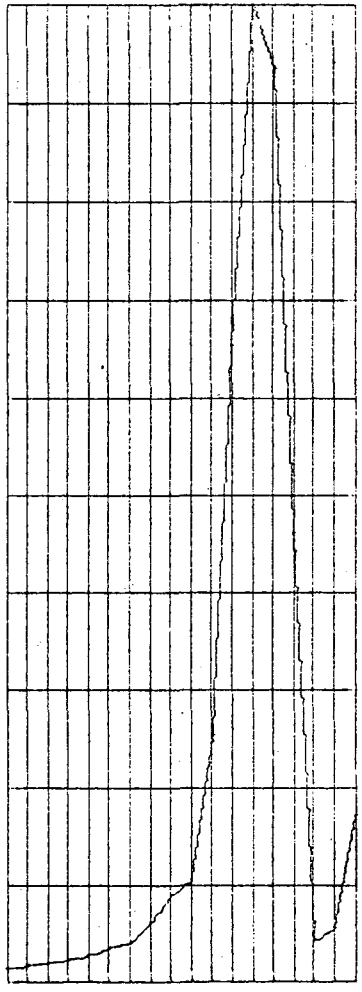

Isotropic Scattering Potential

Fig. IV-5b. I_{10} vs eV for Al (100) between 19 and 36 eV at $\theta = 0°$ for Gafners potential and the isotropic scattering potential with $\alpha = 0.9$, T = 300°K, θ_B = 400°K and θ_S = 200°K. Fifteen scattering events were employed, and the four beam approximation was made.

on the low eV side of the 31 eV maximum for the (10) beam. At $\nu = 20$, this shoulder has become a maximum in its own right, and the 31 eV maximum has been reduced to a shoulder. These changes are also reflected in the (00) beam. Note, however, that the higher energy peak remains more dominent for the (00) beam than for the (01) beam. This is reasonable as the $2K_z^{10} = G_z$ condition does not involve the (00) beam. Therefore, any intensity in this beam is a result of a third order multiple scattering situation where intensity is scattered out of the (10) beam into the (00) beam in the absence of any strict diffraction condition.

The intensity ratios for the 31 and 28 eV maxima in the 10 beam correlate very well with the real diffraction features of many face centered cubic solids. Both of these peaks are experimentally observed for several materials. As noted before, the relative intensities of these peaks show a definite trend with increasing atomic number. For the lighter materials, (e.g., Al, Cu and Ni), the peak corresponding to $2K_z^{10} = G_z$ is strong while that for $K_z^{10} + K_z^{00} = G_z$ is either absent or weak. Upon proceeding to the heavier materials, (e.g. Ag and Au) the situation is reversed and the higher energy maxima becomes dominant. Thus, aluminum might correspond to values of ν on the order of 30 to 50. Nickel and copper might better be fit with values like $\nu = 20$ or 30. Silver and gold are most closely reproduced with values of $\nu = 5$, or 10.

The broad peak observed in the specularly reflected beam from the (100) face of aluminum could easily correspond to either of the calculated maxima, or, more probably, to an unresolved combination of both. It should also be noted that there is a minimum in the Al (100) I_{00} (eV) curve at about 36 eV. Note that these calculations also indicate the existance of relatively little intensity at this energy except in the kinematic limit. As there is a Bragg peak predicted at this position, this may be taken as

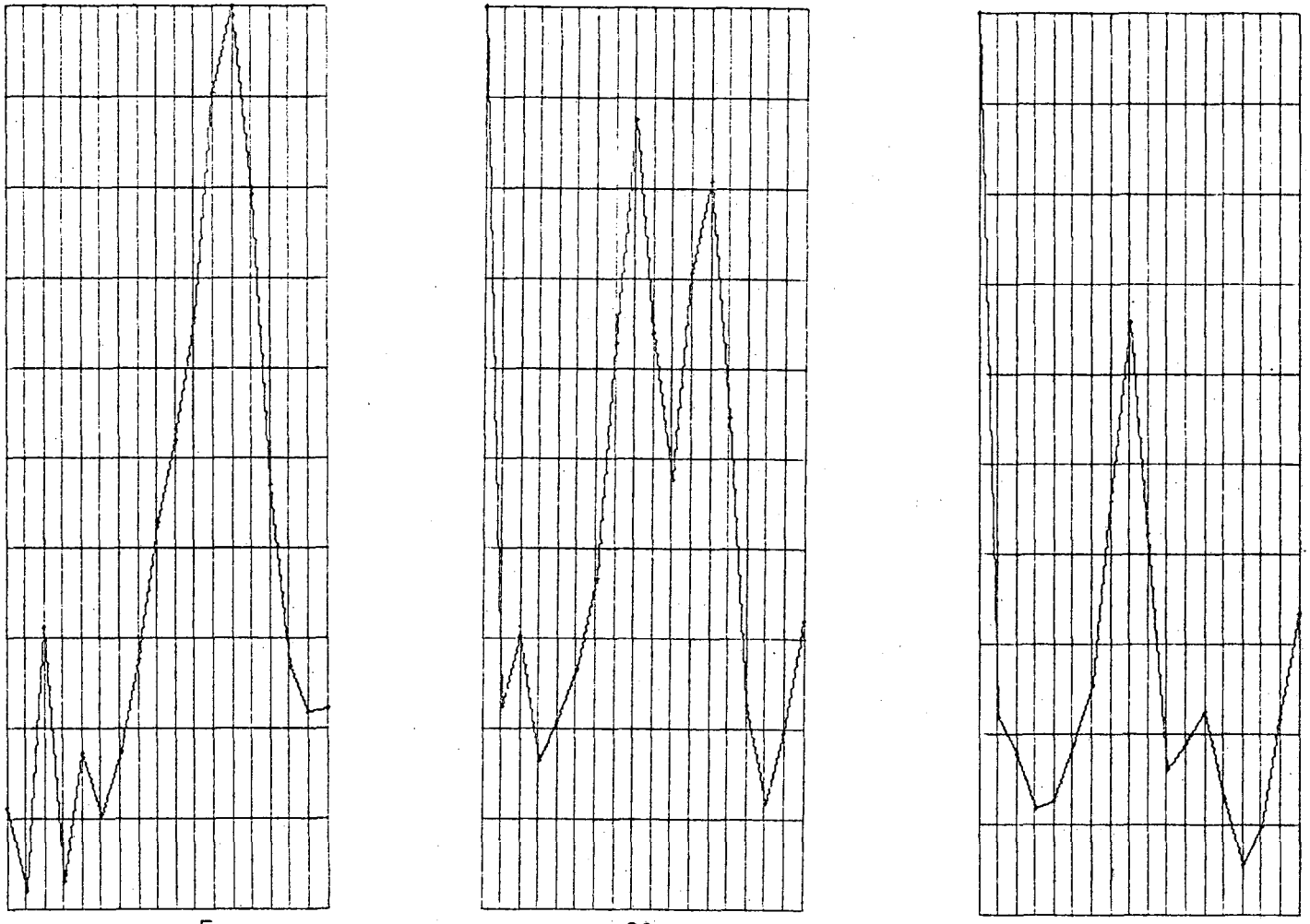

Fig. IV-6a. I_{00} vs eV for Al (100) between 19 and 36 eV at $\theta = 0°$ calculated with $\lambda = 1.0\text{Å}^{-1}$ $\alpha = 0.9$, T = 300°K, $\theta_B = 400°K$, $\theta_S = 200°K$ for several values of the parameter v. Fifteen scattering events were employed and the four beam approximation was made.

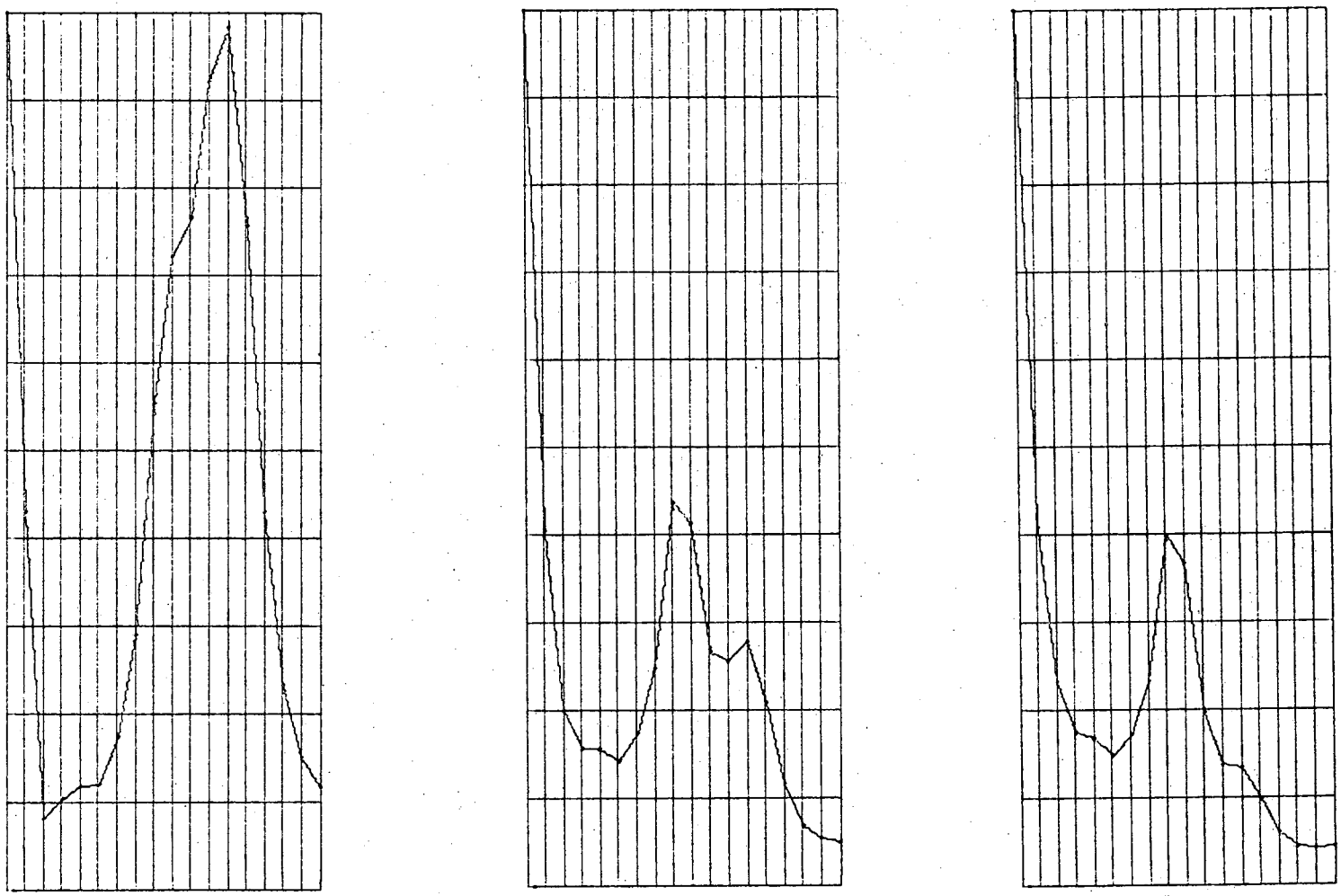

Fig. IV-6b. I_{10} vs eV for Al (100) between 19 and 36 eV at $\theta = 0°$ calculated with $\lambda = 1.0 Å^{-1}$ $\alpha = 0.9$, $T = 300°K$, $\theta_B = 400°K$, $\theta_S = 200°K$ for several values of the parameter v. Fifteen scattering events were employed and the four beam approximation was made.

a proof of the dominance of multiple scattering in low energy electron diffraction.

b. Six Beam Case As with the four beam case, there is no exact analogue to this case for the (100) face of fcc materials. There is, however, an approximate correspondence in the energy range between 40 and 80 eV where there exists six separate sets of beams. As before, arguements may be made about the validity and applicability of this model.

The calculations for the (100) face of aluminum in this region were started at 40 eV rather than 37 eV. This is because the maximum in the (11) beam at 37 eV was so intense that it dwarfed all of the other peaks. Consequently, the behavior of the intensity near 39 eV where the $K_z^{10} + K_z^{11} = G_z$ condition is met has not been studied. As the (11) beam is not observable in this range, this is not too great a loss.

When the scattering approaches the kinematic limit, as for $\lambda = 0.1\text{Å}^{-1}$, only three maxima are observable. The one below 40 eV for the (00) diffraction beam is presumably the Bragg maxima located at 37 eV. The maximum in the (01) beam at 67 eV and that in the (11) beam at 57 eV are both kinematic. When the cross sections are increased by raising λ to 0.5Å^{-1}, there are definite indications that multiple scattering phenomena are becoming important. A peak appears in the (00) beam at 67 eV that corresponds to the diffraction condition $K_z^{00} + K_z^{10} = G_z$. In the (11) beam, there is evidence of the appearance of two peaks at 46 and 49 eV. These are due to conditions of the form $2K_z^{11} = G_z$ and $K_z^{10} + K_z^{11} = G_z$ respectively. When the cross sections are increased still further by raising λ to 1.0Å^{-1} the multiple scattering features become dominent. Note also that some shifts in peak position have appeared. This was commonly observed for large cross sections. It seems to be related to the tendency for the peaks to coales as all conditions become more coupled at larger

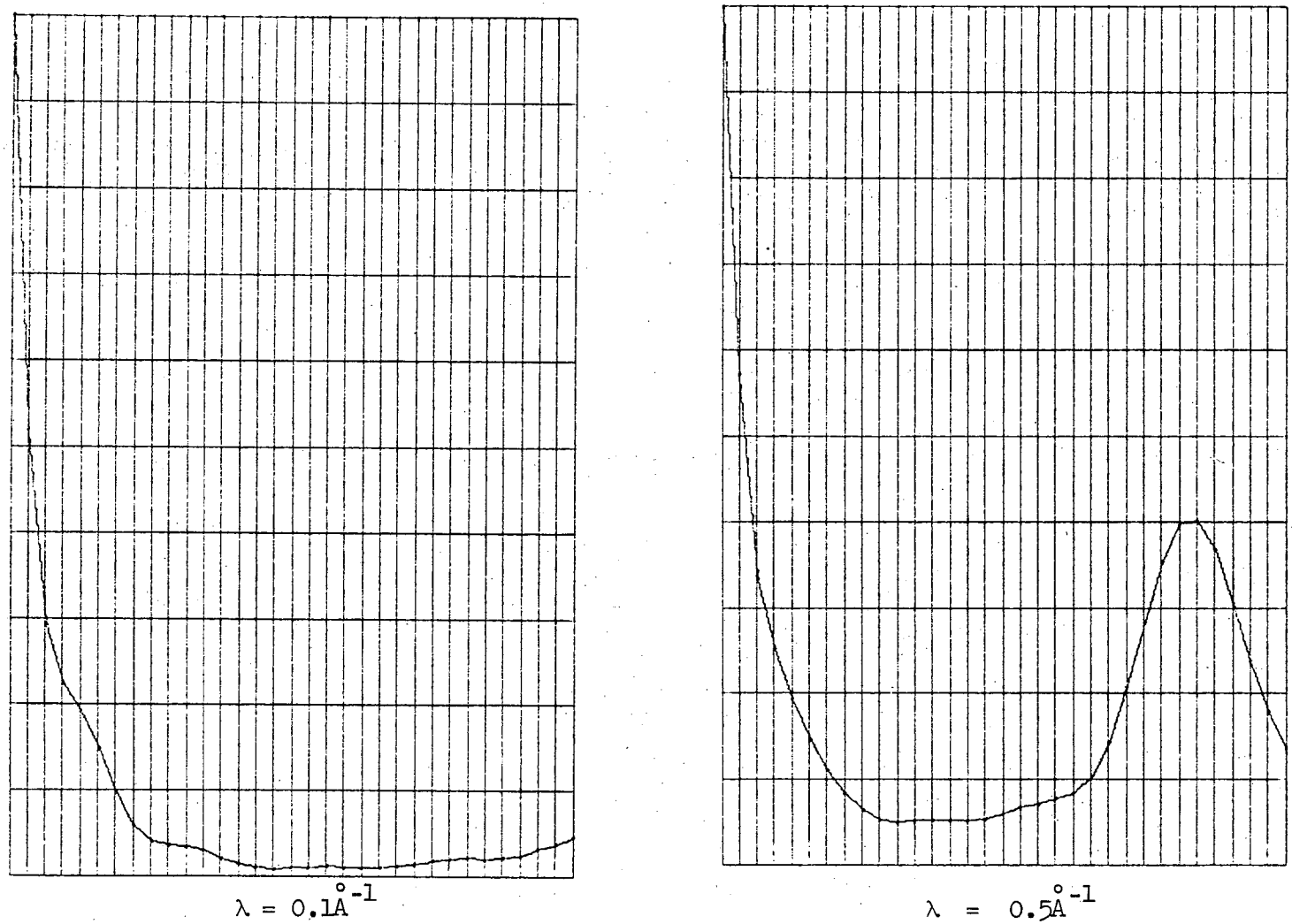

Fig. IV-7a. I_{00} vs eV for Al(100) between 40 and 72 eV at $\theta = 0°$ calculated for several values of λ and with $\alpha = 0.9$, $v = 0$, T = 300°K, θ_B = 400°K and θ_S = 200°K. Fifteen scattering events were used and the six beam approximation was made.

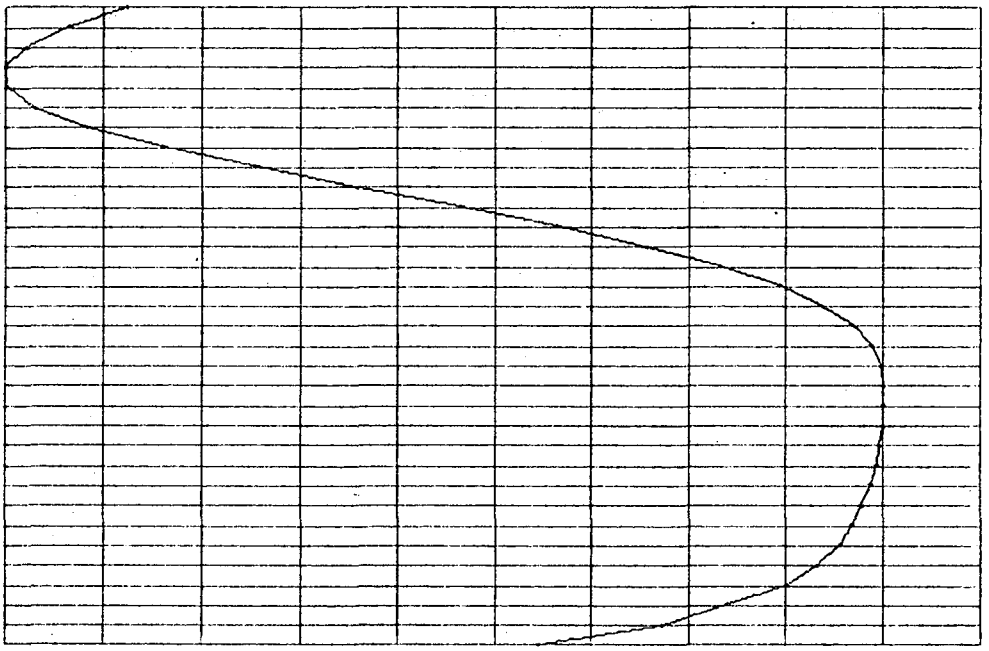

Fig. IV-7a. continued

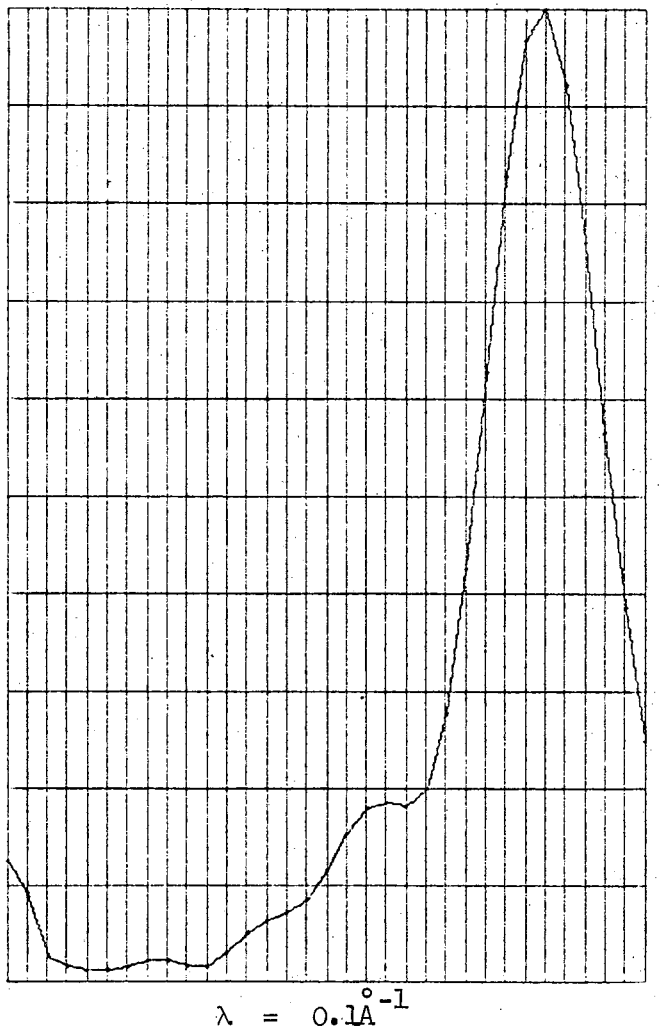

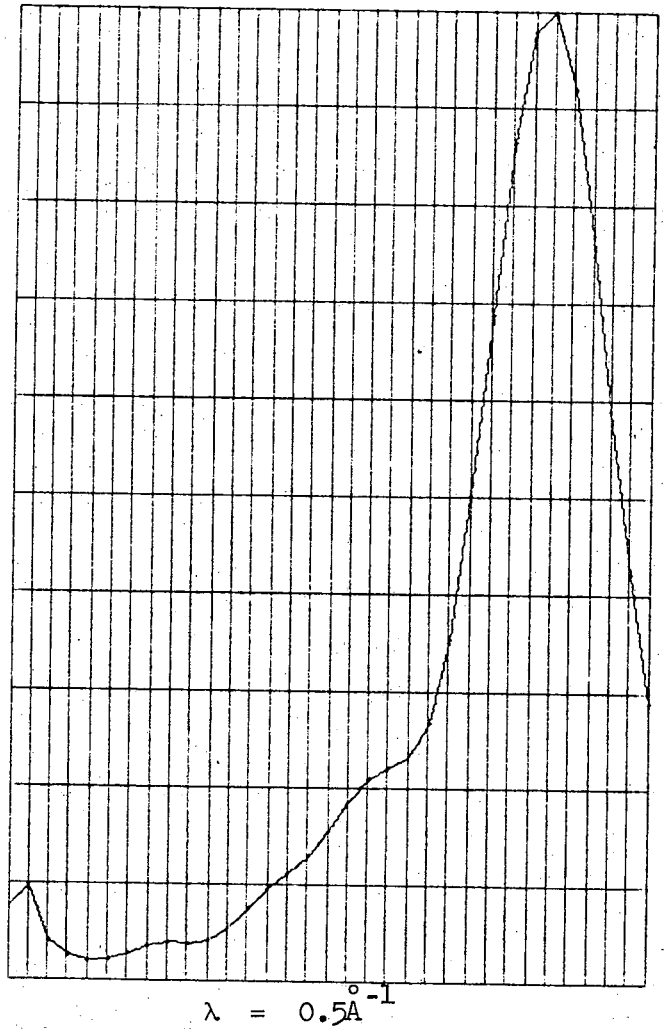

Fig. IV-7b. I_{10} vs eV for Al(100) between 40 and 72 eV at $\theta = 0°$ calculated for several values of λ and with $\alpha = 0.9$, $\nu = 0$, $T = 300°K$, $\theta_B = 400°K$ and $\theta_S = 200°K$. Fifteen scattering events were used and the six beam approximation was made.

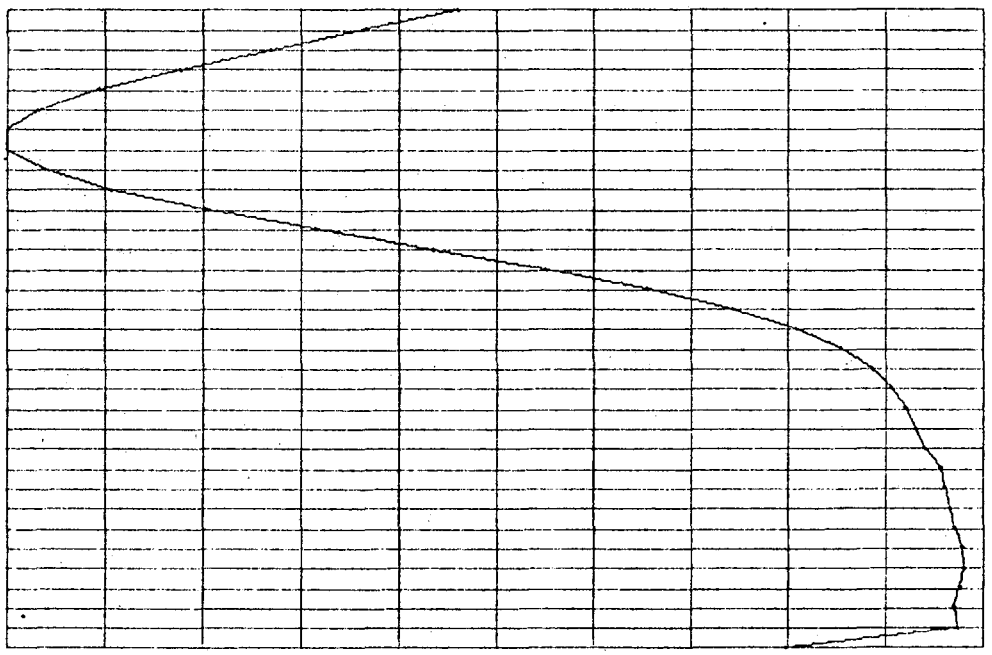

Fig. IV-7b. continued

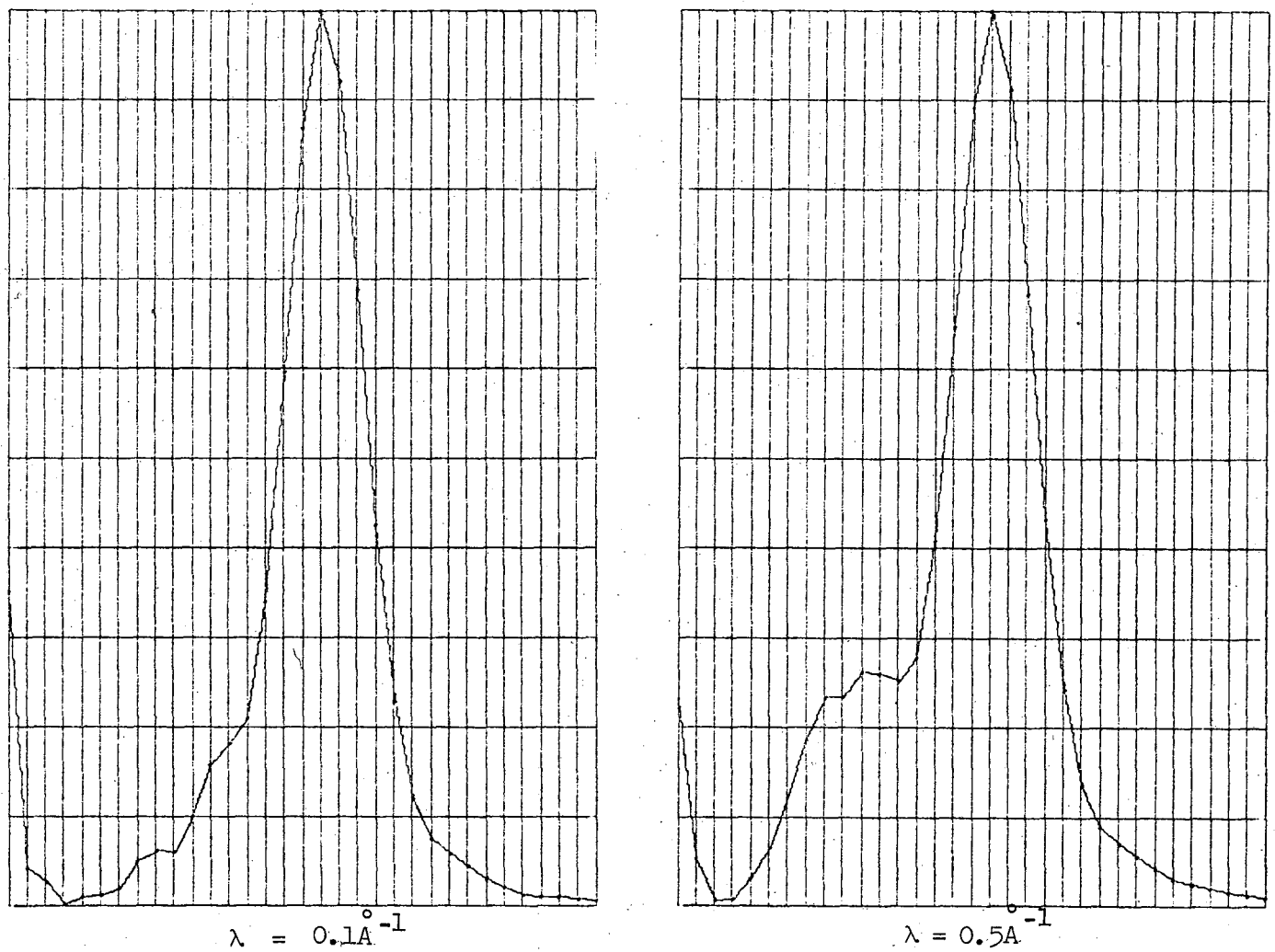

Fig. IV-7c. I_{11} vs eV for Al(100) between 40 and 72 eV at $\theta = 0°$ calculated for several values of λ and with $\alpha = 0.9$, $\nu = 0$, $T = 300°K$, $\theta_B = 400°K$ and $\theta_S = 200°K$. Fifteen scattering events were used and the six beam approximation was made.

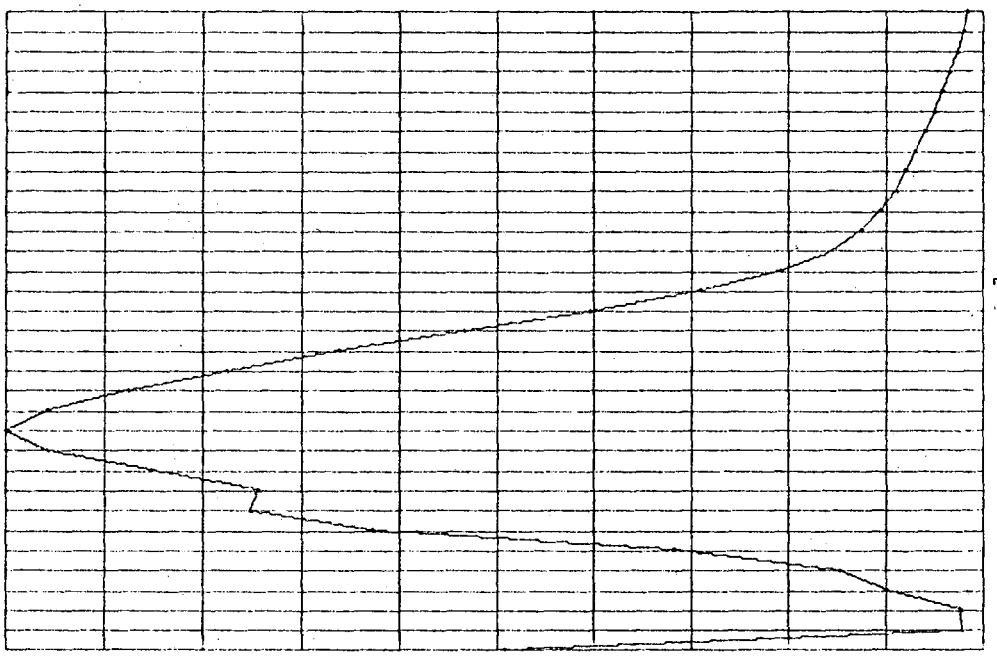

Fig. IV-7c. continued

cross sections.

Increasing the amount of inelastic scattering tended to broaden the peaks somewhat and to discriminate against the multiple scattering features. For example, when α was decreased stepwise to 0.5, the kinematic peak below 40 eV in the (00) beam gradually became more intense than the double diffraction peak at 67 eV.

As in the four beam case, an intensity maximum is not observed that was predicted by a diffraction condition of the form $2K_z^{10} = G_z$. To investigate this peak, the parameter ν was again introduce, as before, the introduction of this parameter generates this type of intensity maximum. When ν is 5, a peak appears in the (10) beam at 54 to 55 eV. In addition, there is an improvement in the resolution of the (11) beam. As ν is increased to 20 and then to 50, the intensity ratios in the (10) beam of the $2K_z^{10} = G_z$ peak at 55 eV and the $K_z^{00} + K_z^{10} = G_z$ peak at 67 eV are reversed. At the same time the $2K_z^{11} = G_z$ peak at 46 eV in the (11) beam becomes a dominent feature.

This $2K_z^{10} = G_z$ peak at 55 eV is of particular interest as it has been experimentally observed and indeed is the strongest intensity maximum present in this energy range for all of the materials studied. For aluminum, it is more intense than the neighboring kinematic peak at 67 eV by at least a factor of 2. This intensity ratio may diminish somewhat with increasing atomic number as it is fairly close to 1 for silver.

It is of some interest to note that the use of the parameter, ν, has generated intensities for the (11) beam that are also similar to those observed experimentally. The use of relatively large values of ν, 20 to 50, has caused the $2K_z^{11} = G_z$ peak at 46 eV to become considerably more intense than the kinematic $K_z^{00} + K_z^{11} = G_z$ peak at 57 eV. This region is one of the considerable experimental difficulty, but for the three

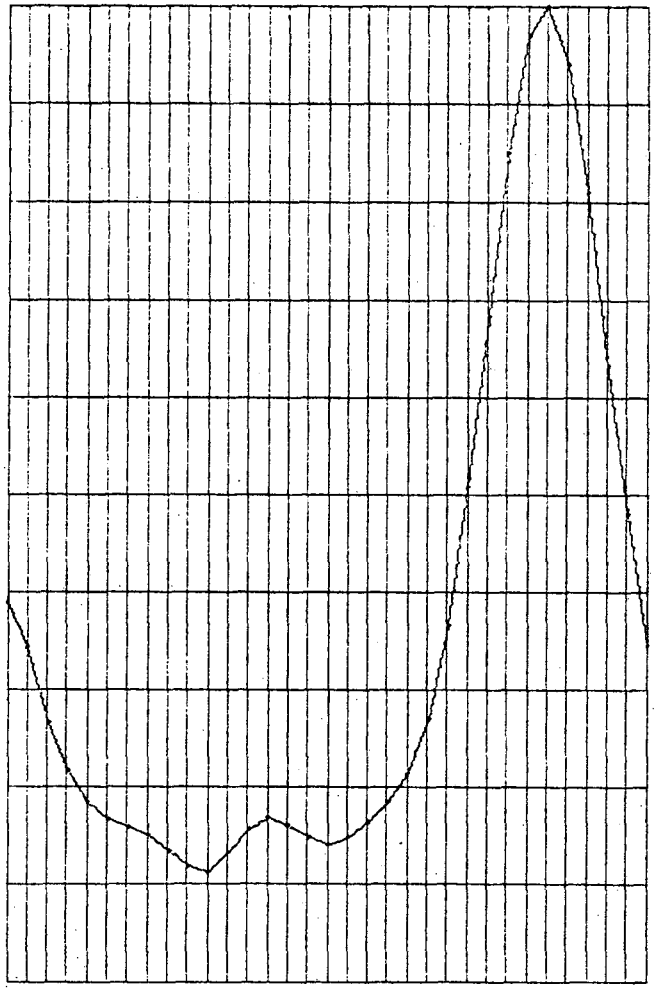

$\nu = 5$

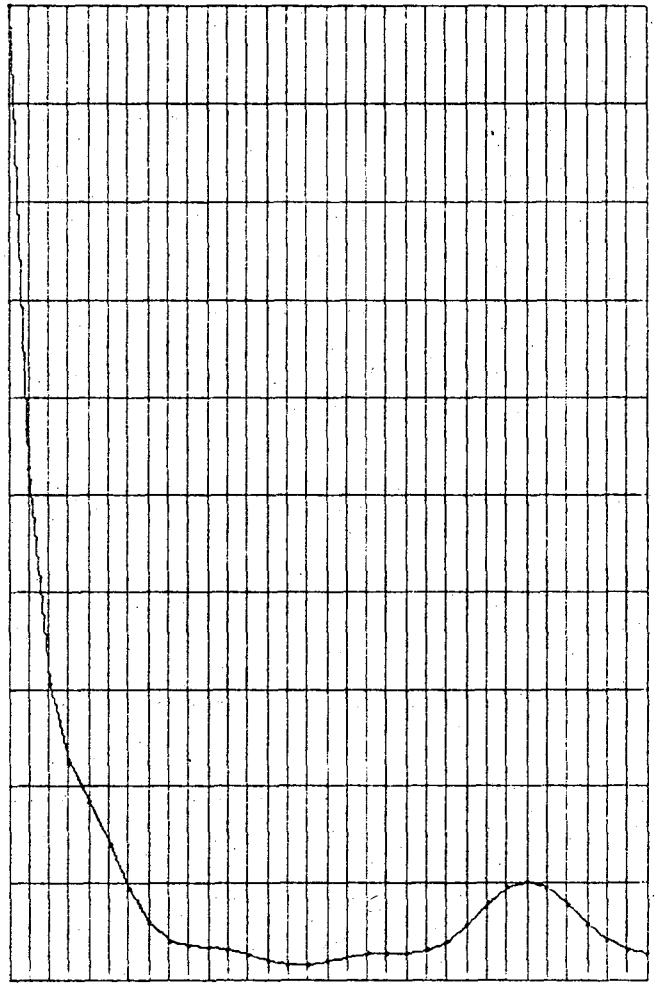

$\nu = 10$

Fig. IV-8a

I_{00} vs eV for Al(100) between 40 and 22 eV at $\theta = 0°$ calculated with $\lambda = 1.0\text{Å}^{-1}$, $\alpha = 0.9$, $T = 300°K$, $\theta_B = 400°K$, and $\theta_S = 200°K$ for several values of the parameter ν. Fifteen scattering events have been employed and the 6 beam approximation was made.

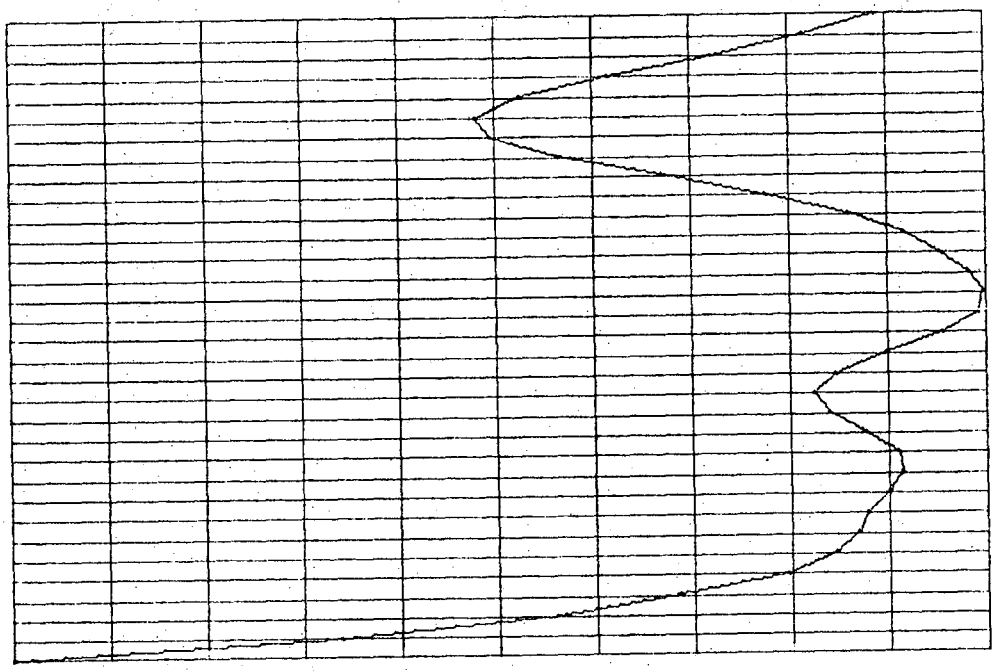

$\nu = 50$

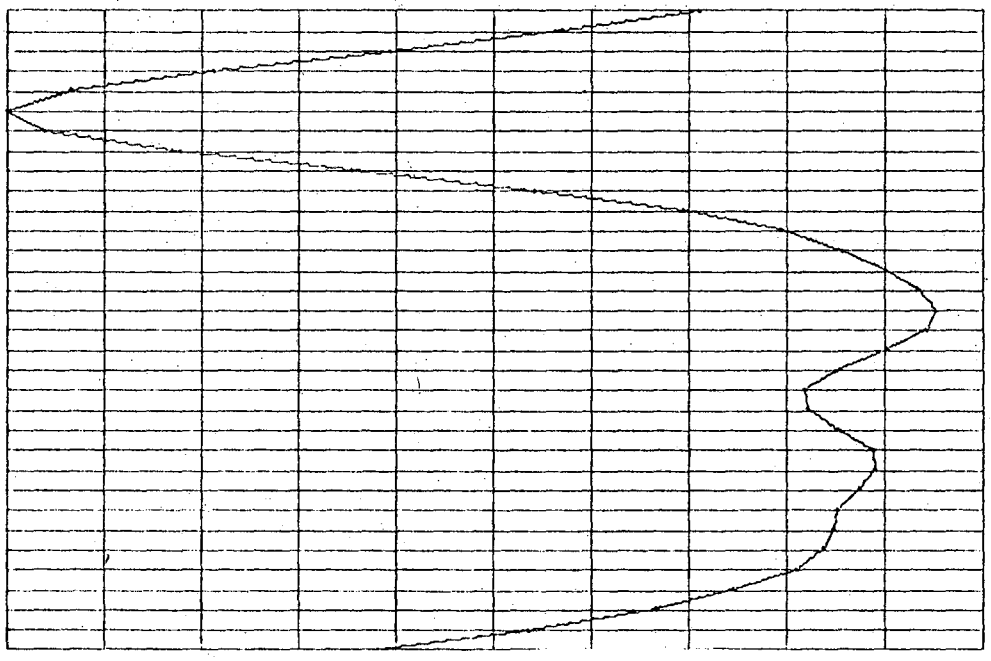

$\nu = 20$

Fig. IV-8a continued

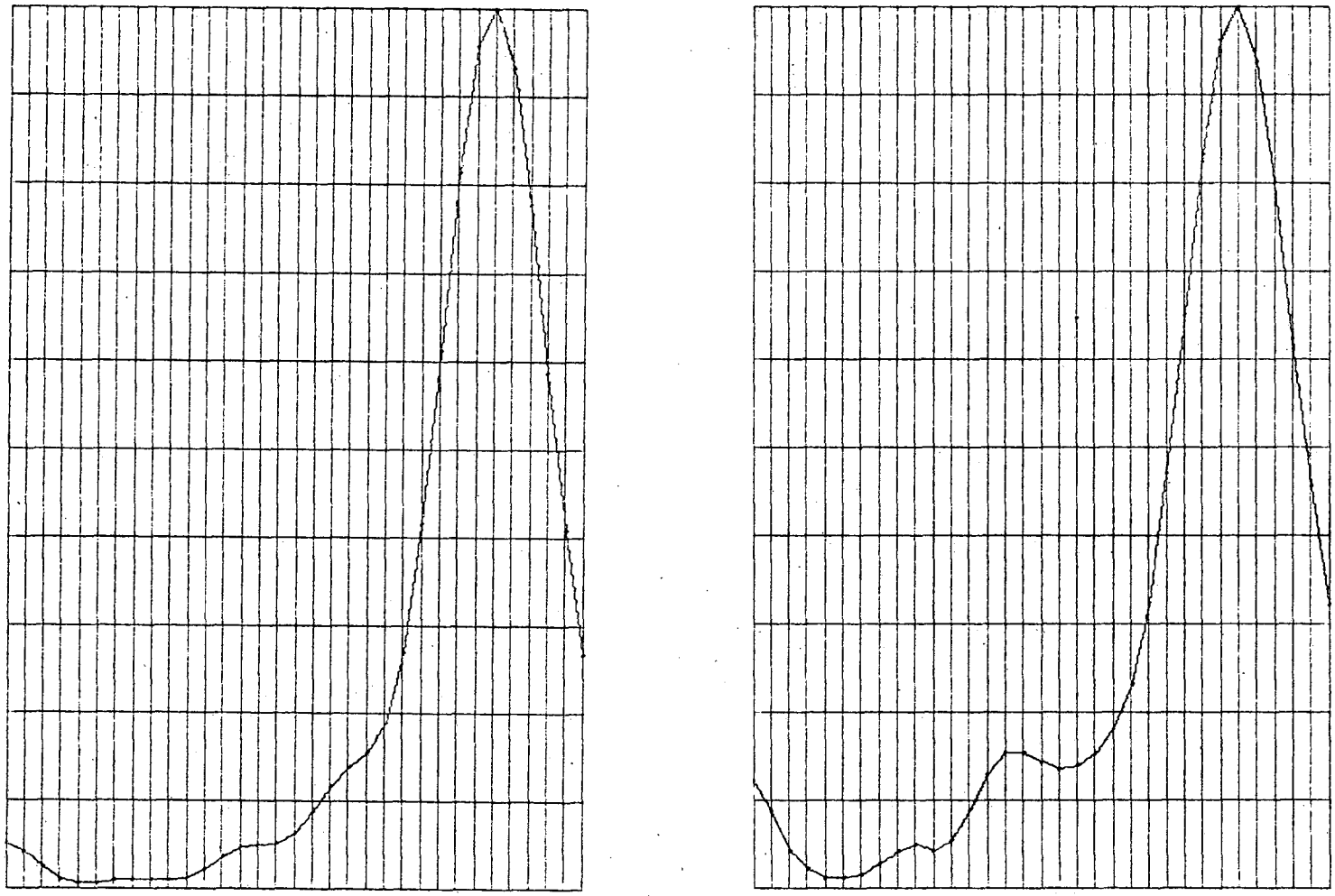

$\nu = 5$ $\nu = 10$

Fig. IV-8b. I_{10} vs eV for Al(100) between 40 and 22 eV at $\theta = 0°$ calculated with $\lambda = 1.0\text{Å}^{-1}$, $\alpha = 0.9$, $T = 300°K$, $\theta_B = 400°K$, and $\theta_S = 200°K$ for several values of the parameter ν. Fifteen scattering events have been employed and the 6 beam approximation was made.

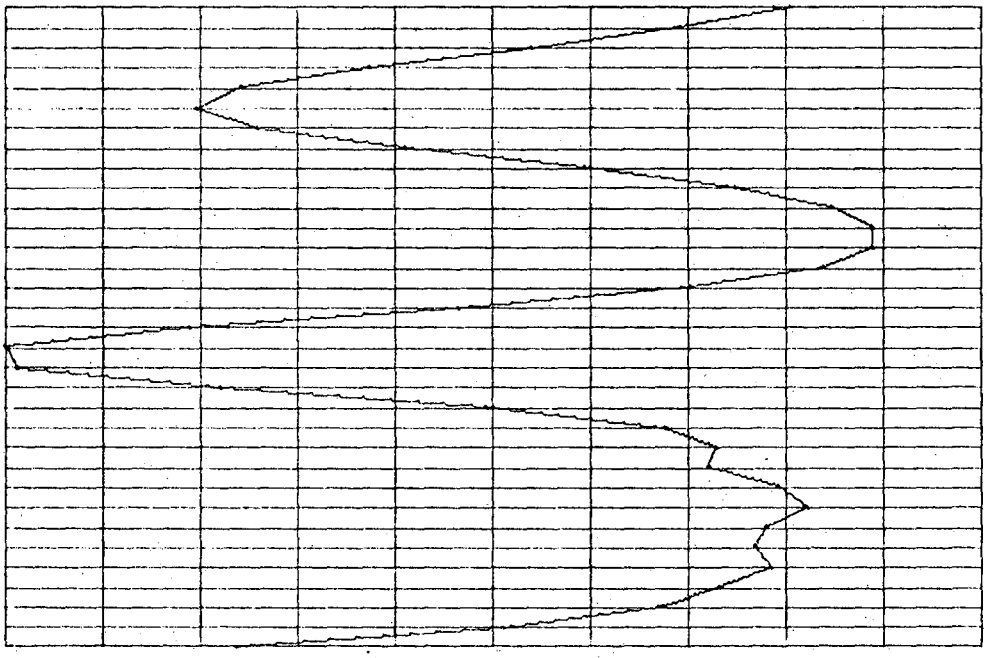

$\nu = 50$

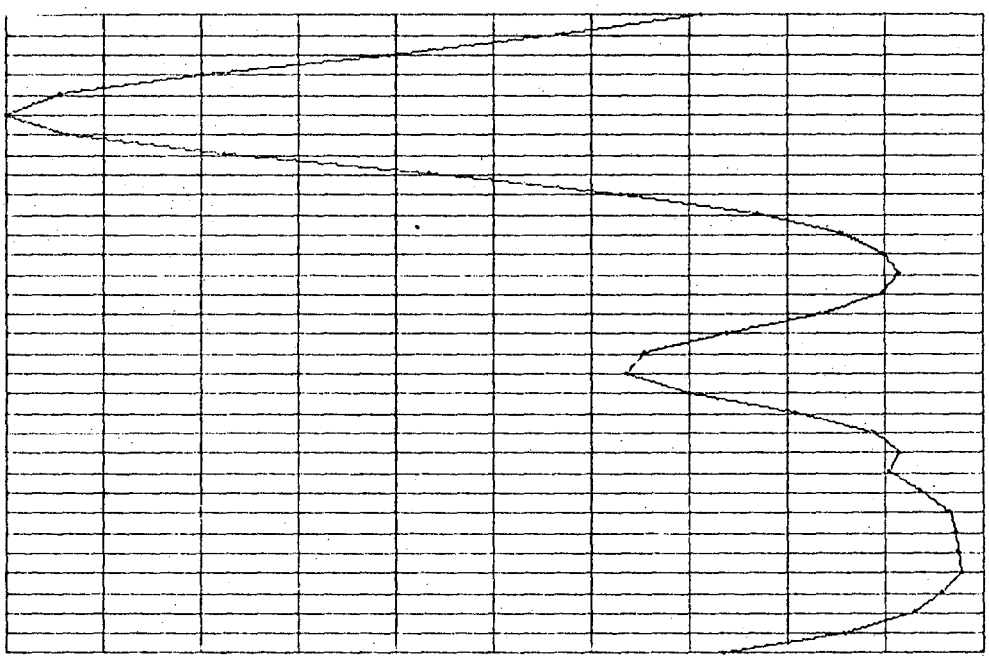

$\nu = 20$

Fig. 8b. continued

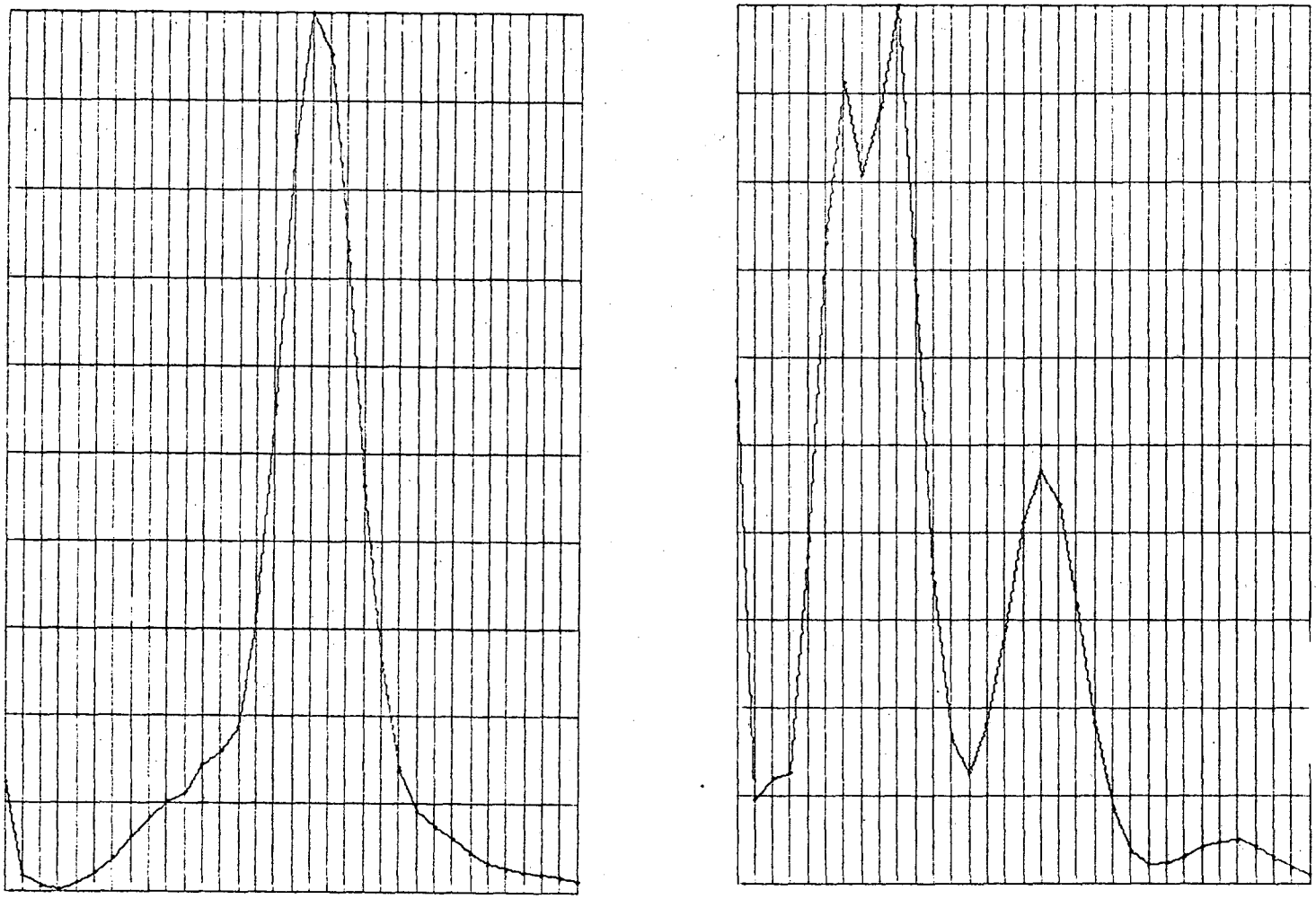

$\nu = 5$ $\nu = 10$

Fig. IV-8c. I_{11} vs eV for Al(100) between 40 and 22 eV at $\theta = 0+$ calculated with $\lambda = 1.0\text{Å}^{-1}$, $\alpha = 0.9$ $T = 300°K$, $\theta_B = 400°K$, and $\theta_S = 200°K$ for several values of the parameter ν. Fifteen scattering events have been employed and the 6 beam approximation was made.

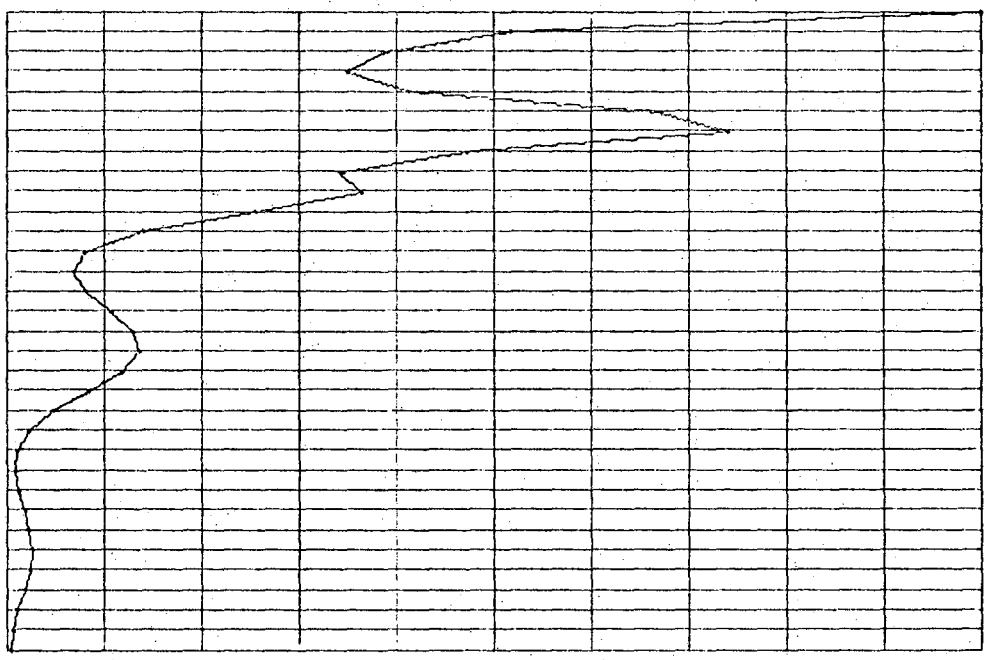

$\nu = 50$

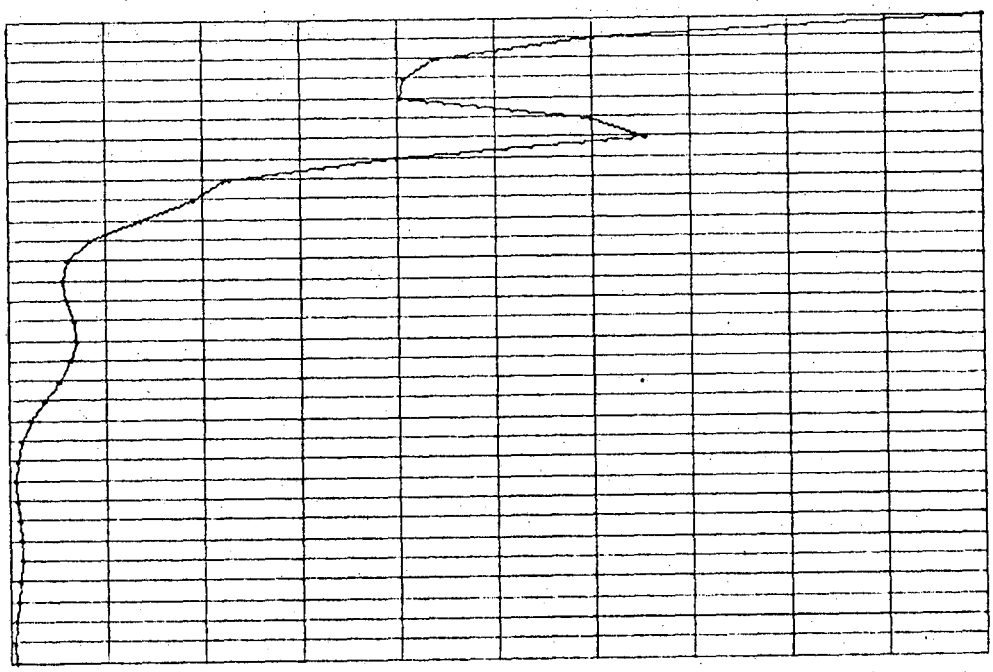

$\nu = 20$

Fig. IV-8c. continued

materials, Cu, Ag and Ni, where both of these peaks have been observed, the multiple scattering peak was more intense than the kinematic peak in good agreement with the model calculations.

c. The Ten Beam Case

There exists an exact analogy for this case for the (100) face of face centered materials. In the region between approximately 20 and 40 eV, in addition to the transmitted and the specularly reflected beams, there are four first order diffraction beams scattered back from the crystal and four scattered into it. The treatment of the four beam case was an approximate solution to this situation. There, it was necessary to introduce a variable parameter, v, to force the calculations to reproduce the observed intensity maxima. When this energy region was considered in a more exact manner with a full compliment of beams, it was found that the experimentally observed intensity maxima could be generated by a simple forward scattering potential without the use of the parameter v. It would therefore appear that the use of this parameter simulates the interactions of the degenerate beams neglected in the approximate case.

Calculations were performed for aluminum in the energy region between 19 and 36 eV. Fifteen scattering events were used and it was assumed that 19% of the intensity of each scattering event was lost to inelastic processes. A pure screened Coulombic potential $\frac{ze^2}{r} e^{-\lambda r}$ was employed with a variable screening parameter λ. Figure IV-9 shows the intensities of the (10) and the (00) beam calculated at normal incidence for values of λ, the screening parameter, between 0.1Å^{-1} and 1.5Å^{-1}.

As in the four beam case, when $\lambda = 0.1 \text{Å}^{-1}$, we are fairly close to the kinematic limit. The only peak that is observed in the (10) beam is the kinematic $\vec{K}_z^{00} + \vec{K}_z^{10} = \vec{G}_z$ peak at 31 eV. In the (00) beam, the Bragg peak at 37 eV is quite strong, and there is some evidence of the

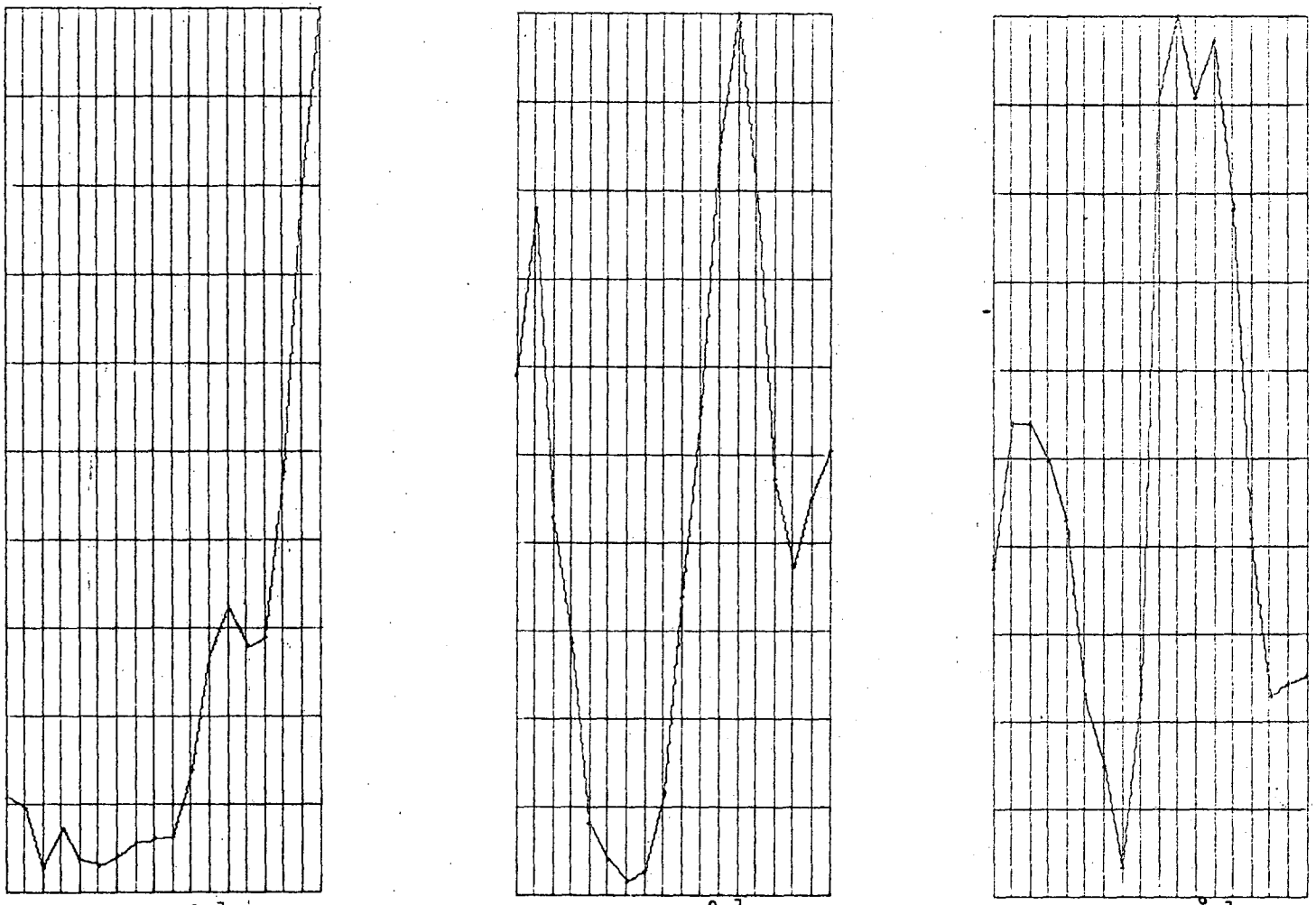

Fig. IV-9a. I_{00} vs eV for Al(100) at $\theta = 0°$ between 19 and 36 eV calculated for several values of the screening parameter λ with $\nu = 0$, $\alpha = 0.9$, $T = 300°K$, $\theta_B = 400°K$ and $\theta_S = 200°K$. Fifteen scattering events and ten beams were employed.

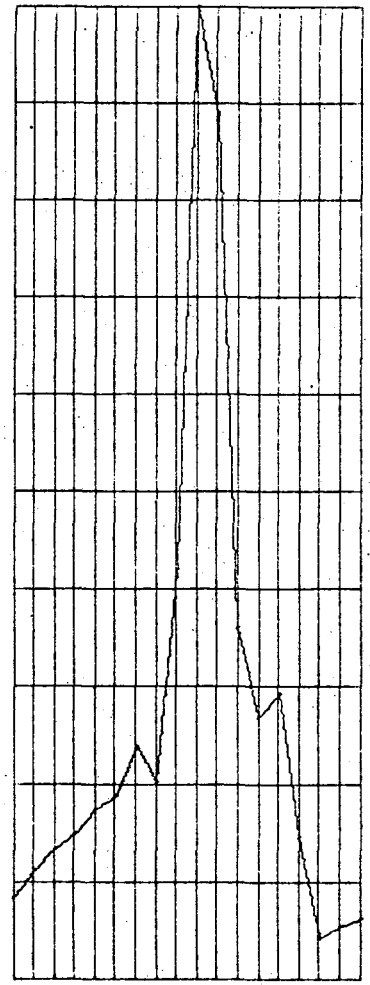

$\lambda = 1.0 \text{Å}^{-1}$

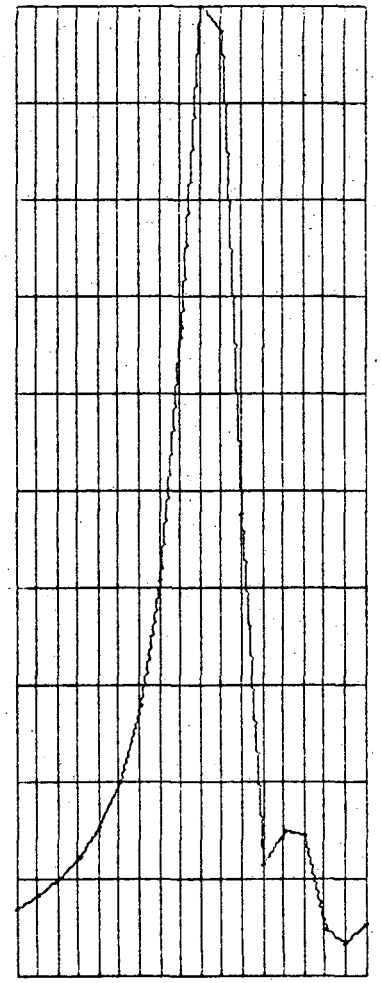

$\lambda = 1.5 \text{Å}^{-1}$

Fig. IV-9b. Same as caption Fig. IV-9a.

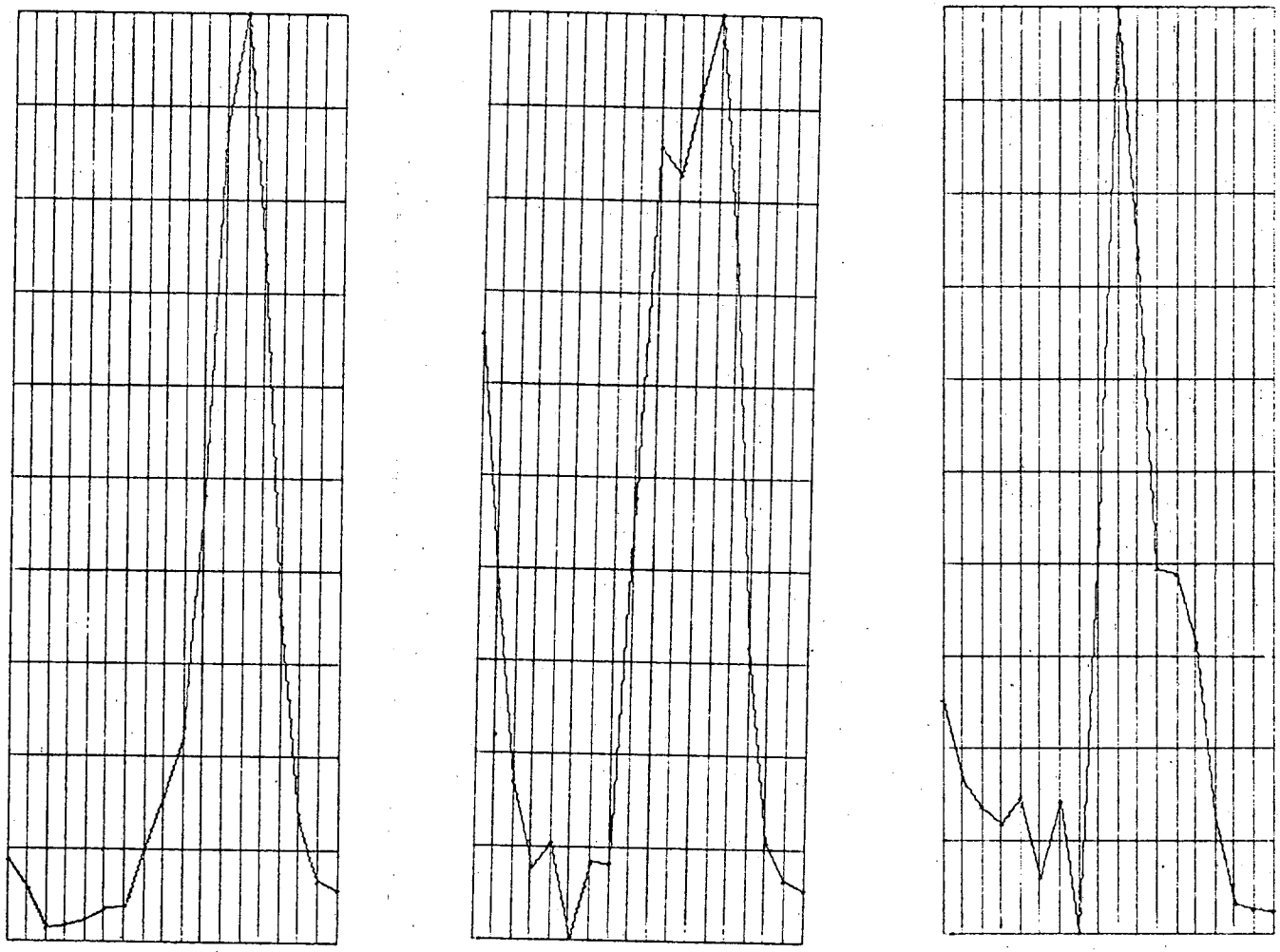

$\lambda = 0.1$ $\lambda = 0.5$ $\lambda = 0.75$

Fig. IV-9c. I_{10} vs eV for Al(100) at $\theta = 0°$ between 19 and 36 eV calculated for several values of the screening parameter λ with = 0, $\alpha = 0.9$, T = 300°K, θ_B = 400°K and θ_S = 200° K. Fifteen scattering events and ten beams were employed.

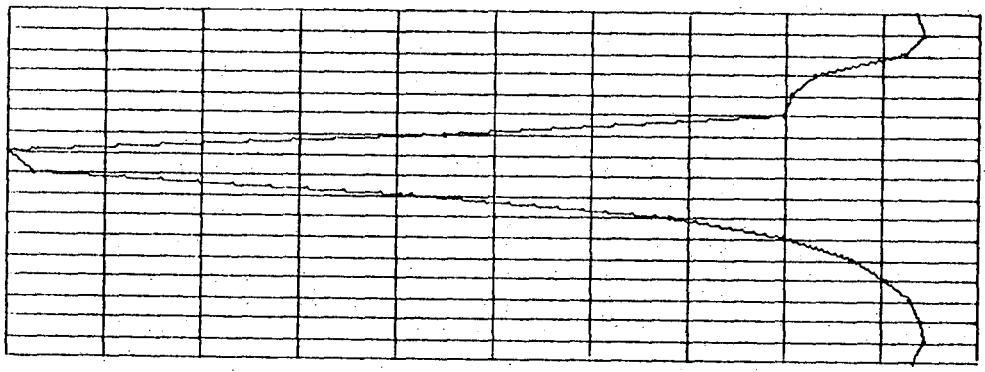

$\lambda = 1.5\text{Å}^{-1}$

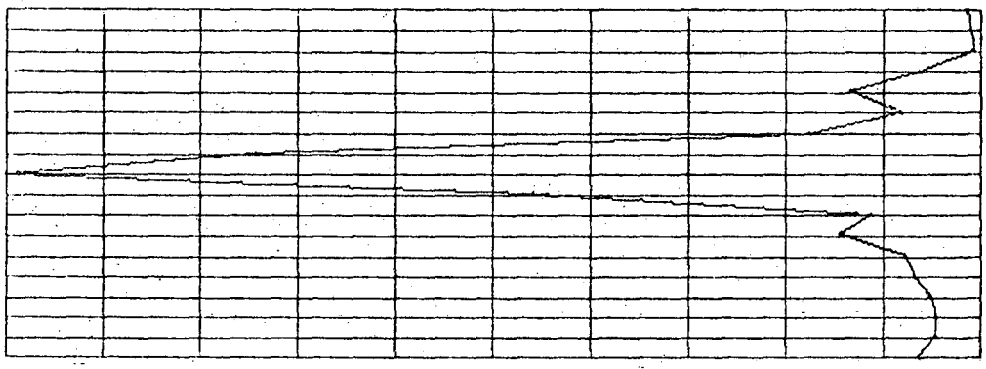

$\lambda = 1.0\text{Å}^{-1}$

Fig. IV-9d. Same as caption Fig. IV-9c.

double diffraction $K_z^{00} + K_z^{10} = G_z$ peak at 31 eV.

When λ is increased to 0.5 $\mathring{A}^{-1}$, this double diffraction peak at 31 eV in the (00) beam is the dominant feature in this region and the 37 eV Bragg peak is reduced in relative intensity. The 31 eV peak in the (01) beam is still quite strong, but the pure multiple scattering $2K_z^{10} = G_z$ peak at 28 eV has become apparent.

As λ is increased further to 0.75 $\mathring{A}^{-1}$, this 28 eV multiple scattering peak in the (10) beam has become the dominent feature and the kinematic 31 eV peak is reduced in relative intensity. In the (00) beam, the Bragg maximum is quite reduced. The double diffraction 31 eV peak is still quite strong, but a new feature at 28-29 eV has become apparent. This is a tertiary multiple scattering feature and represents an increase in the intensity of the (00) beam reflecting the $2K_z^{10} = G_z$ intensity maxima in the (10) beam.

When λ is increased still further to 1.0 and 1.5 $\mathring{A}^{-1}$ the 28 eV peak becomes the strongest feature for both beams. The 31 eV peak is still apparent as a shoulder. Note that the peaks have a greater width for $\lambda = 1.5$ $\mathring{A}$ than for $\lambda = 1.0$ $\mathring{A}^{-1}$. In this limit, all of the beams are strongly coupled and one major maximum is found.

The peak near 21 eV in the (00) beam for $\lambda = 0.5$ $\mathring{A}^{-1}$ and 0.75 $\mathring{A}^{-1}$ may be related to the double diffraction condition $\vec{K}^{00} + \vec{K}^{10} = \vec{G}$. There could be several reaons why there is no corresponding peak in the (10) beams. As mentioned before, it may be because the (10) beam does not penetrate very deeply in this region. Alternatively, it could be because it is masked by the $2K_z^{10} = G_z$ maximum at 18-19 eV that occurs at these values. Note that there is some "rippling" occuring in the intensities. This is due to the use of a finite size model crystal.

As in the four beam case, a correlation may be made between the value of λ and the fit between the calculated and the observed intensity ratios. It would appear that for lighter materials, such as aluminum, there is better agreement for larger values of λ, say between 0.75 $\mathring{A}^{-1}$ and 1.0 $\mathring{A}^{-1}$, while the heavier materials, such as silver, need a stronger forward scattering potential such as one approximated by $\lambda = 0.5\ \mathring{A}^{-1}$.

d. The Eighteen Beam Case

As with the ten beam case, the eighteen beam case has a direct analogy in the diffracted beams from the (100) face of face centered cubic crystals. In the region between approximately 40 and 80 eV, there are eight (11) beams, eight (10) beams and two (00) beams. One half of each set is directed into, and one half of each set is directed out of the crystal. This energy range was treated in an approximate manner in the six beam case. Again, there it was necessary to introduce the parameter ν to reproduce the experimentally observed maxima. Here, however, when this situation is treated with a full compliment of diffraction beams, the observed intensity maxima may be reproduced again with a pure screened Coulombic potential using suitable screening parameters.

Calculations were performed for the (100) face of aluminum for fifteen scattering events. It was assumed that 19% of the intensity of each individual scattering event was lost to inelastic processes. The best fit between the observed and the calculated intensity vs energy plots was obtained with a value of the screening parameter of 0.75 $\mathring{A}^{-1}$. Smaller values of λ emphasized the kinematic processes while larger values, such as $\lambda = 1.5\mathring{A}^{-1}$, over emphasized the multiple scattering processes to such an extent that all of the beams became very strongly coupled and only one maxima was observed in all of the beams near 50 eV.

Figure IV-10 shows the intensities of the (11), (10) and (00) beams between 40 and 70 eV for $\lambda = 0.75$ $\mathring{A}^{-1}$. For the (11) beam, three strong maxima are produced in this region. The first, at 46 eV, corresponds to a multiple scattering condition of the form $2K_z^{11} = G_z$ and the second, at 49 eV, corresponds to another multiple scattering condition between the (10) and the (11) beams of the form $K_z^{10} + K_z^{11} = G_z$. The third peak at 58 eV exists in the kinematic diffraction limit and is described by $K_z^{00} + K_z^{11} = G$. The exact intensity ratios are not in good agreement with those observed experimentally. In general, the $K_z^{11} + K_z^{10} = G_z$ peak is missing while the $2K_z^{11} = G_z$ peak has a significantly greater intensity than the kinematic $K_z^{00} + K_z^{11} = G_z$ maximum.

The strongest feature in the (10) beam is the intensity maximum at 55 eV which is related to the $2K_z^{10} = G_z$ diffraction condition. It is followed by a weaker intensity maxima at 67 eV of the kinematic $K_z^{00} + K_z^{10} = G_z$ form. The calculated relative intensities of these two peaks are pleasing as the 55 eV peak is generally found to be the strongest intensity maximum in this region for the experimentally observed data from all materials considered. The calculated intensity maximum at 49 eV is a $K_z^{10} + K_z^{11} = G_z$ multiple scattering feature. With the possible exception of nickel, this maximum is generally not observed experimentally. Note the peaks at 47 and 57 eV. These are tertiary multiple scattering phenomena and reflect intensity maxima in the (11) beam.

The two peaks at 57 and 67 calculated for the (00) beam are related to double diffraction conditions of the form $K_z^{00} + K_z^{11} = G$ and $K_z^{00} + K_z^{10} = G_z$ respectively. The calculated intensity ratio for these two peaks is in poor agreement with experimental data. For aluminum and palladium, the $K_z^{00} + K_z^{10} = G_z$ peak is observed to be the dominant feature in this

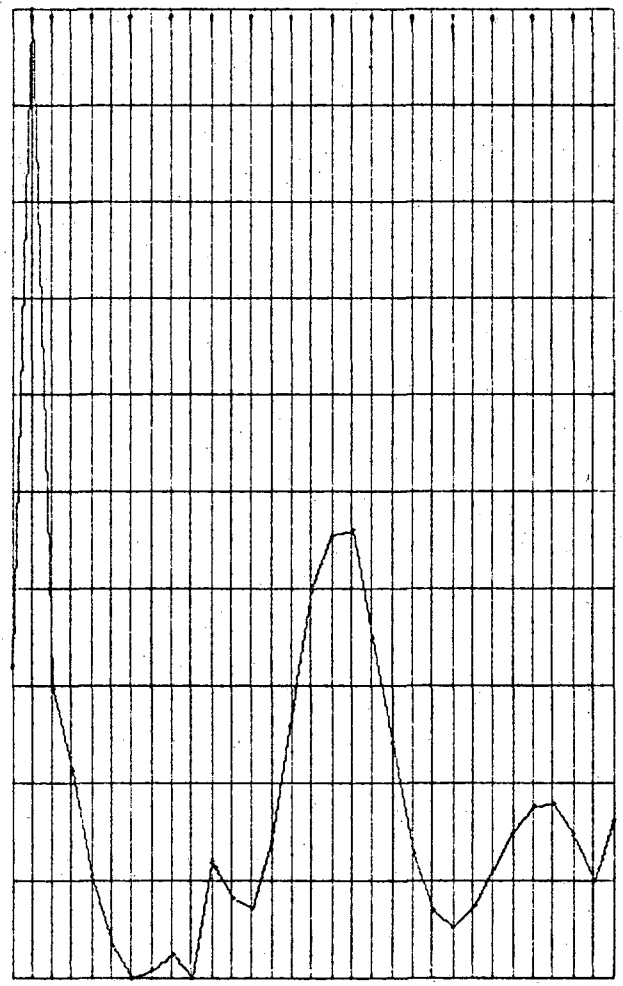

Fig. IV-10a. I_{00} vs eV for Al(100) at $\theta = 0°$ between 40 and 60 eV calculated with $\lambda = 0.75\text{Å}^{-1}$, $v = 0$, $\alpha = 0.9$, T = 300°K, $\theta_B = 400°K$ and $\theta_S = 200°K$. Fifteen scattering events and eighteen beams were employed.

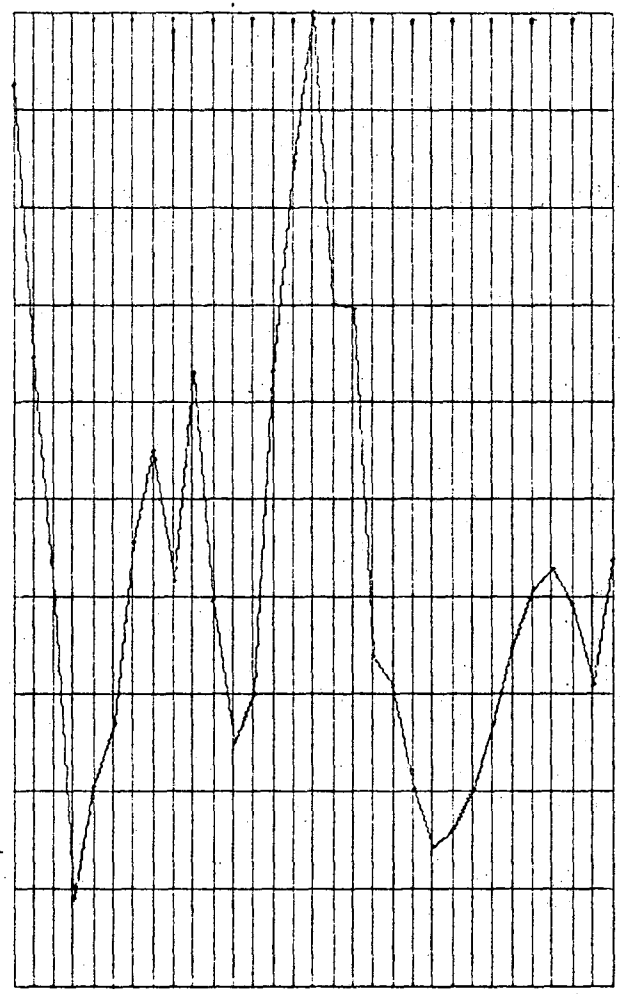

Fig. IV-10b. I_{10} vs eV for Al(100) at $\theta = 0°$ between 40 and 60 eV calculated with $\lambda = 0.75A^{-1}$, $v = 0$, $\alpha = 0.9$, T = 300°K, $\theta_B = 400°K$ and $\theta_S = 200°K$. Fifteen scattering events and eighteen beams were employed.

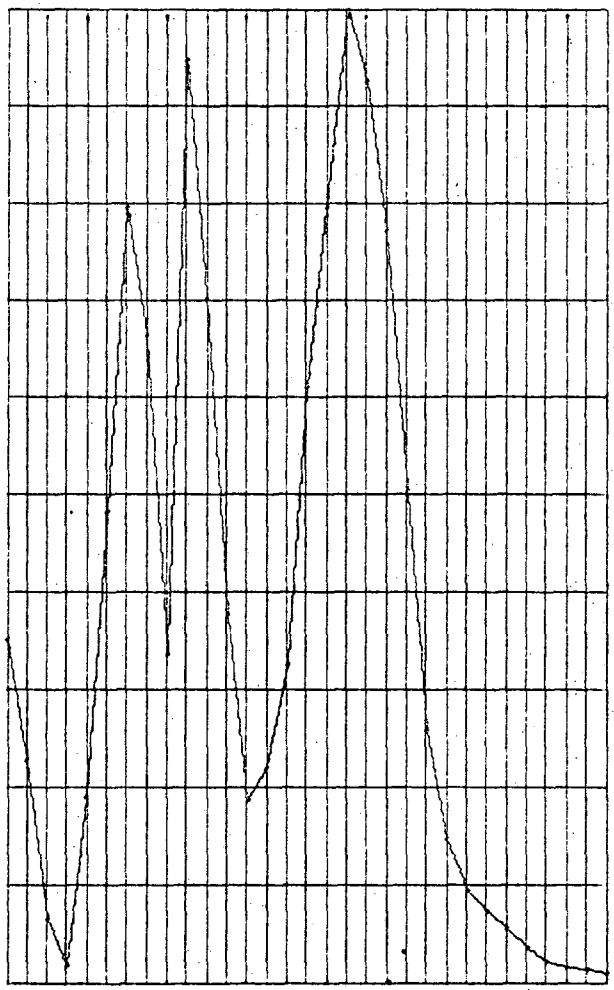

Fig. IV-10c. I_{11} vs eV for Al(100) at $\theta = 0°$ between 40 and 60 eV calculated with $\lambda = 0.75\text{Å}^{-1}$ $\nu = 0$, $\alpha = 0.9$, T = 300°K, θ_B = 400°K and θ_S = 200°K. Fifteen scattering events and eighteen beams were employed.

region while the $K_z^{00} + K_z^{11} = G_z$ peak is either not observed or appears as a small shoulder on the $K_z^{00} + K_z^{10} = G_z$ peak for palladium. The region below 50 eV is also poorly reproduced for the (00) beam in these calculations. For both aluminum and palladium, a strong maximum is observed in this region that may be related to the 49 eV peak calculated with $\lambda = 1.5$ Å^{-1}.

When the agreement between the calculated and the experimentally observed intensities for all of the beams in this region is considered, it may be seen that there is a fairly good correlation. However, even though most of the observed intensity maxima may be generated with this computational procedure, the calculated intensity ratios are less than optimal.

e. Summary

A computational procedure has been developed that will reproduce most of the features observed in the intensities of the low energy electron diffraction beams from the (100) face of face centered cubic crystals in the energy range 1-80 eV. Two forms of this method have been employed. In the shorter form at normal incidence, only one beam in a degenerate set of beams is considered in an actual calculation. It has been found that the neglect of the other beams may be partially compensated for with the use of a parameter, v, that enhances scattering events that do not involve a change in that component of the scattering vector that is parallel to the surface. This method has the advantage that it uses a significantly smaller amount of computer time than does the full treatment where all diffraction beams are considered. There is a six fold saving in time when the four beam case is used instead of the ten beam case, and an eight fold saving in time when the six beam case is used rather than the full eighteen beam case.

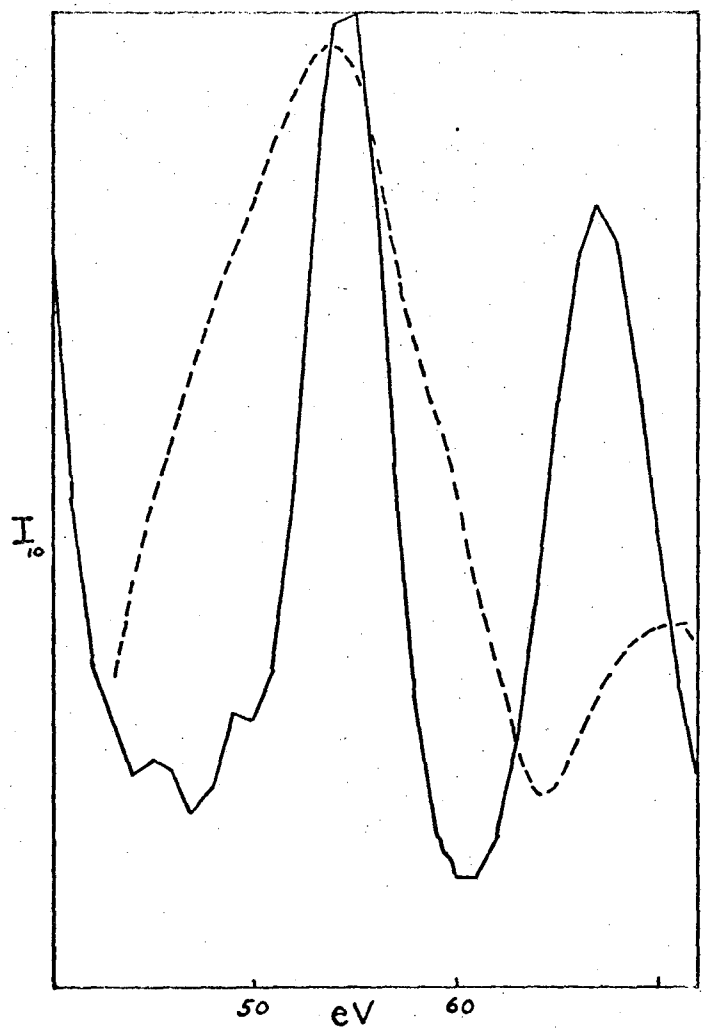

Fig. IV-11. Comparison between experimental (dashed curve) and calculated I_{10} vs eV curve for Al(100) at $\theta = 0°$ for the six beam approximation.

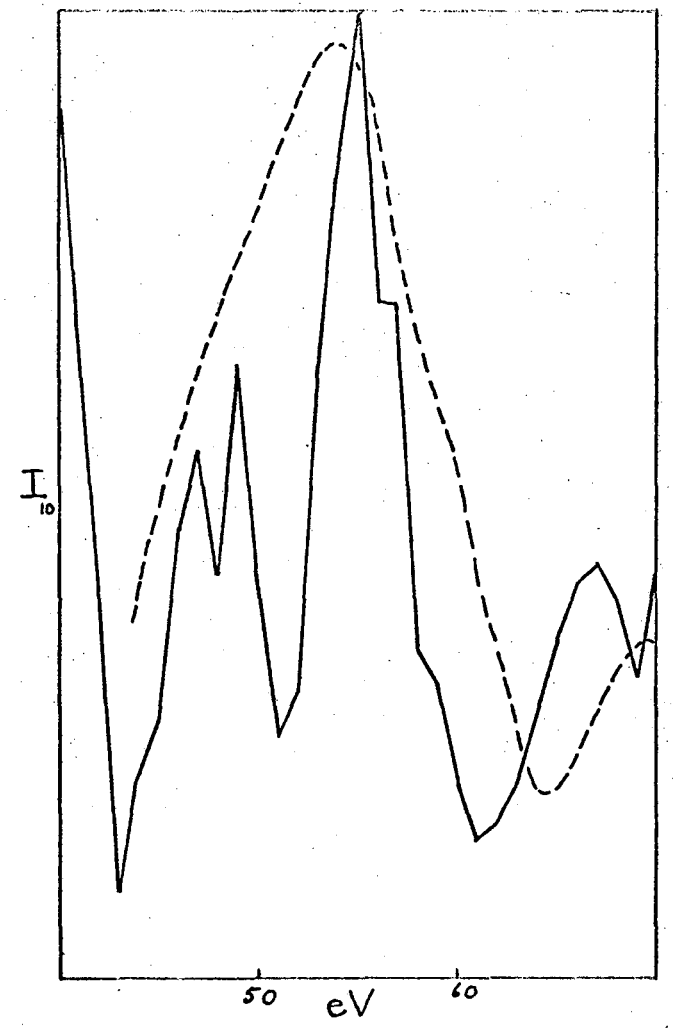

Fig. IV-12. Comparison between experimental (dashed curve) and calculated I_{10} vs eV for Al(100) at $\theta = 0°$ for the full eighteen beam case.

The longer form of this computational procedure, though more expensive, has the advantage that it does not employ the artifical parameter ν. Thus, it should be more applicable to calculations performed on actual surface structures.

Both methods suffer from the unavailability of good scattering potentials. Though the observed diffraction features can usually be reproduced with either method, the calculated intensity ratios only rarely reproduce those which were measured experimentally. It is to be hoped that adequate scattering potentials will soon be available. Work is proceedingon this problem, notably by Pendry and Heine[49,47] among others.

Although the (100) face of fcc materials was studied here, this approach could easily be applied to the (110) face or the bcc materials. The choice of the (100) face of fcc materials was made on the basis of the availability of existing experimental data, and the simplicity that this case affords. Though this particular method resembles that of several different authors in some aspect, it is unique in its total construction. The basic equations used were derived from an integral equation approach similar to that of McRae and Kambe. However, a plane wave of Fourier expansion of the eigenfunctions and potential were employed rather than a spherical harmonic expansion. In this aspect, the method resembles that used by Carpart and others in the differential equation approach. The scattering is considered as a stepwise process though, rather than all together as in most solid states like approaches. In this stepwise procedure, this method is perhaps closest to that of Gaffner. However, here again there are significant differences. The intensities or probabilities are normalized rather than the amplitudes as in Gaffners' approach. Further, the stepwise process is allowed to proceed into the crystal as well as between layers. In Gaffner's method, the scattering

is restrained to occur between layers until exhausted whereupon events between the next layers are then considered.

Of greater importance is the use of a more realistic potential than the isotropic scattering potential. Though not nearly so sophisticated as a good pseudo-potential, the screened Coulombic potential bears some relationship to reality as in the Thomas-Fermi-Dirac model. Further, the Debye-Waller effect has been taken into account in the approach developed here. As e^{-2W} may be considerably less than unity for many scattering events, a consideration of this effect is important, when attempting to reproduce experimentally observed phenomena.

Finally, these computations were performed for actual, not hypothetical, situations and the calculated intensities were compared with experimentally observed intensities for several different materials over a wide range of electron energies.

B. Structured Surfaces

1. fcc(100)

a. Pt(100) (5 × 1)

The study of the (5 × 1) surface structure on the (100) face of platinum presents an interesting confirmation of McRae's[4] hypothesis that the intensities of fractional order beams will "reflect" the intensities of the integral order beam. It may be seen from Fig. III-13 that the intensity of the (0 1/5) fractional order beam mimics very closely the behavior of the specularly reflected or (00) beam. The intensity of the (0 2/5) beam also shows similar behavior, thought to a less marked extent. The (0 3/5) and the (0 4/5) beams appear to be less strongly coupled to the specularly reflected beam but the (0 4/5) beam does follow the intensity of the (0 1) beam to a certain extent as they both have a maxima just above 50 eV and just above 75 eV. It would seem then that these fractional order beams show a tendency to vary with beam voltage in the same way as the intensity of that integral order beam to which they are the closest. This is reasonable as one would expect that in general the scattering amplitudes should be the largest when there is the least change in the electron momentum (i.e. when scattering vector is smallest). Note the marked decrease in intensity with increasing energy. This is to be expected as the higher energy electrons would tend to penetrate more deeply and would "sample" less of the surface.

b. Pd(100) - C(2 × 2)

The intensity for the specularly reflected beam from the Pd(100) face has been discussed in some detail earlier. As noted then, there is a marked progression of changes in the shape of the I_{00} (eV) curve upon going from the (1 × 1) to the c(2 × 2) surface structure. The intensities

of the other beams will now be discussed. It is convenient to consider the region above 100 eV and the region below 100 eV separately.

In the region above 100 eV, there is a great similarity in the intensities of all of the integral order beams for both the (1 × 1) and the C(2 × 2) surface structures. There are some changes in the intensity ratios, but not much more than might be expected from small variations in the angle of incidence. The most notable change is the slight increase in the energy at which the intensity maxima occur in the specularly reflected beam.

As with the Pt(100) - (5 × 1), there is tendency for the fractional order beams to have the same behavior as a function of electron beam energy as the integral order beams. For example, the maxima at 130 and 153 eV in the (11) beam may have their counterparts in the (1/2 1/2) beam. Though intensity ratios vary, there is a much stronger correlation in the peak positions between the (1/2 1/2) and the (1/2 3/2) beams. Unlike the (5 × 1) structure, the C(2 × 2) structure gives fractional order spots whose intensities tend to increase with increasing energy. This may indicate that the surface structure is not confined solely to the first layer, but either extends several layers into the crystal, or perturbs these underlying layers in a significant fashion. Alternatively, it could indicate that the (5 × 1) structure was more loosely bound than the C(2 × 2) structure. This would result in a larger Debye-Waller factor for the atoms on the (5 × 1) surface than on the C(2 × 2) surface with the consequent more rapid extinction of intensity with increasing energy.

In the region below 100 eV, the intensities of the integral order beams are quite different for the C(2 × 2) surface structure than for the (1 × 1) surface. In the (00) beam, the peak near 13 eV is much more intense in the C(2 × 2) case. This, presumably, is the first Bragg peak which

occurs coincidently with the appearance of the (1/2 1/2) beams for the C(2 × 2) surface structure. There is also some indication of a maximum in the (1/2 1/2) beams in this region, though the intensity at the appearance voltage is outside of experimental detection for the experimental arrangement used.

For the (1 × 1) surface, there is a gradual increase in intensity in the (00) beam near 40 eV. For the C(2 × 2) surface, however, there is a definite minimum in this region. Just above 40 eV, there is a maximum in the (1/2 1/2) beams. This may be a "reflection" of the predicted maximum in the (11) beams at their appearance energy.

In the (10) beams, the maximum near 60 eV for the (1 × 1) surface has shifted down to around 52 eV for the C(2 × 2) surface. There is still a shoulder near 60 eV. This new peak is possibly due to a diffraction condition of the form $K_z^{10} + K_z^{11} = G_z$. This assignment is supported by the observation of the shift of the kinematic 62.5 eV peak in the (11) beam to approximately 54 eV observed by Park.[21] This energy shift was observed when a (1 × 1) surface was annealed after many ion bombardment and annealing cycles. As no fractional order beams were observed, Park has suggested that this shift is due to an increase in the effective inner potential as ledges and other low inner potential protrusions on the surface are annealed out. It is, however, equally likely that this shift is due to the incipient formation of a surface structure that was too perturbed to give strong fractional order diffraction beams.

Near 60 eV, in addition to the shoulder in the (10) beams, there is a maximum in the (1/2 1/2) beams and a new maximum in the (00) beam for the C(2 × 2) surface structure. These maxima occur very near to where the $2K_z^{10} = G_z$ and the $K_z^{00} + K_z^{11} = G_z$ diffraction conditions are met. It is

probable that intensity is scattered into the (00) beam from both the (10) and the (11) beams via the (1/2 1/2) beams.

In the (00) beam, the peak near 70 eV remains unshifted while that near 90 eV has vanished when the C(2 × 2) surface structure is formed. The (1/2 1/2), (10) and (11) diffraction beams all exhibit maxima near 80 eV. This is the energy at which the (20) beams should appear. The (11) beams should be strongly coupled to the (20) beams at this energy. It appears that the fractional order beams redistribute the back reflected intensity in this region into several of the integral order beams.

In summary, the formation of a C(2 × 2) surface structure on the (100) face of palladium would seem to have relatively little effect upon the intensities of the integral order beams at higher energies. However, for energies below 100 eV, there is a marked effect upon the intensities. It would appear that the primary result was to redistribute the back reflected intensity into the integral order and the fractional order beams.

c. Ni (100) - C(2 × 2) As the intensity in the (1/2 1/2) beams from the Pd (100) - C(2 × 2) to a certain extent varies in the same way with electron energy as the intensities of the integral order beams, it is of interest to inquire as to whether or not all C(2 × 2) structures will result in similar intensity vs voltage plots. If this were the case, it would be difficult to distinguish between essentially different surface structures that happened to have the same two dimensional symmetry parallel to the surface.

Several C(2 × 2) structures are known for the (100) face of nickel. Carbon monoxide is absorbed on Ni(100) to form a C(2 × 2) structure. Oxygen also forms a C(2× 2) structure as in intermediate phase in the formation of a NiO rock salt structure. Both the oxygen and the carbon

monoxide C(2 ×2) structures have been studied by Park and Farnsworth[51] among others. These two structures are presumably quite different though they both possess the same two dimensional symmetry. Infrared evidence indicates that the CO is above the surface and is attached to the nickel through the carbon while LEED studies would seem to support the hypothesis that the oxygen is involved in a reconstructed three dimensional oxygen nickel structure where at least some of the oxygen is below the surface.[21]

The Ni (100) - C(2 × 2) - CO structure has a fairly strong peak near 21 eV in the (1/2 1/2) beams that may be associated with the appearance of the (10) beams. At about 33 eV there is a strong maximum. This is somewhat low to correlate with the $2K_z^{10} = G_z$ diffraction condition, but it is definitely too high for the $K_z^{00} + K_z^{10} = G_z$ condition. Above these, there is a fairly weak peak at 46 eV that is most probably a reflection of the appearance of the (11) beams. Near 60 eV, there is a doublet with components at 57 and 65 eV. These have been assigned to the $K_z^{10} + K_z^{11} = G_z$ and the $2K_z^{11} = G_z$ diffraction conditions respectively.

When the Ni(100) - C(2×2) CO structure is heated in oxygen, it can be replaced by the Ni(100) - C(2 × 2) - O structure.[21] During this transformation, the intensity maximum at 21 eV in the (1/2 1/2) beams disappears and a new peak at approximately 26 eV appears. This peak at 26 eV is most probably associated with the $K_z^{00} + K_z^{10} = G_z$ diffraction condition. Further, the peak at 33 eV and the doublet near 60 eV also vanish. New peaks near 38, 44 and 50 eV appear as a weak and poorly resolved triplet. A new peak near 68 eV also appears. The peak at 38 eV is fairly well assigned to the $2K_z^{10} = G_z$ diffraction condition. The peaks at 44 and 68 eV are difficult to assign. The peak near 50 eV may be related to the appearance of the (11) beams. If so, it is the only peak that is observed for both the Ni(100) - C(2 × 2) - CO surface structure and

the Ni(100)-C(2×2)-O surface structure. Further, it is the only peak that has the same assignment as any of those given the peaks in the (1/2 1/2) beam from the Pd-C(2×2) surface structure.

As these three surface structures, the Ni(100)-C(2×2)-CO, the Ni(100)-C(2×2)-O and the Pd(100)-C(2×2), may be safely assumed to have three essentially distinct atomic arrangements despite the superficial similarity of their two dimensional periodicity, it is comforting to find that they give three distinctly different $I_{1/2\ 1/2}$ vs eV curves. This implies that it should be possible to apply computational methods to distinguish among alternative models for given surface structures.

2. bcc(100)

a. bcc(100)-(1×1)-O

Nickel is not the only metal where the oxidation process has been studied in detail. Perhaps the most extensive set of data has been published for the body centered cubic metals.

The (111) face of the metal oxides have been observed to form on the (110) face of both tantalum and iron with extensive oxygen exposure and some heat treatment.[52,53] Prior to the formation of the full oxide, several intermediate phases were observed for iron. When exposed to oxygen, the Fe(100) face first formed a C(2×2)-O structure with a quarter monolayer coverage and then a C(3×1)-O structure with two thirds monolayer coverage. Further exposure led to a full monolayer coverage which was unstable when heated and passed through several presumably reconstructed structures before the full oxide structure was developed.

The (110) face of molybdenum exhibited somewhat similar behavior.[54,55] Initial exposure to oxygen gave a C(2×2)-O structure with one quarter monolayer coverage. Further exposure resulted in a full monolayer coverage (1×1)-O, that was accompanied by an increase in work function. However, when this surface was heated the inverse sequence was noted and a MoO(111)

structure was not observed. Similar results have been observed for the (110) face of tungsten.[56]

The (100) faces of several bcc metals have also been studied as a function of oxygen exposure, and a (1 × 1)-O structure has also been observed on several of these. At room temperature Cr (100) appears to absorb oxygen in an amorphous fashion with no decomposition.[57] It was reported that the oxygen was removed by heating the sample to 300°C. Unfortunately, the published data were insufficient to determine whether or not a (1 × 1)-O structure existed in addition to the amorphously adsorbed oxygen.

The (100) face of iron first forms a C(2 × 2)-O structure upon exposure to oxygen.[58] Further exposure results in the disappearance of the (1/2 1/2) beams and definite changes in the intensity of the (10) beam. These, presumably, indicate the formation of a (1 × 1) -O structure. When this structure is heated and exposed to more oxygen, a FeO structure results.

The (100) face of vanadium has been observed to form a (1 × 1)-O structure at room temperature.[59] Upon heating this structure to 1100°C, it is converted to a (2 × 2)-O structure. Further heating to 1400°C resulting in the regeneration of a (1 × 1) structure, presumably because the oxygen diffused into the bulk. The specularly reflected intersites for the clean V(100) face and the V(100) - (1 × 1) -O face were similar, but with two important differences. Two peaks, one near 20 eV and one near 70 eV, in the I_{00} vs eV curve for the clean surface were not present in the I_{00} vs eV curve for the (1× 1)-O surface. These peaks may be assigned to the kinematical Bragg condition $2K_z^{00} = G_z$. Note, however that this condition is strongly coupled with the appearance conditions for the (10) and (20) beams near 17 and 67 eV respectively. Unfortunately

the results of this study were not completely unambiguous as there was some question of contamination from the tantalum holders.

Possibly one of the most detailed studies of the interaction of oxygen with a (100) bcc surface is that for molybdenum by Hayek, Farnsworth and Park.[55] When the Mo(100) face was exposed to oxygen between 10^{-9} to 10^{-7} torr at room temperature, a (1×1)-O structure was formed. No new beams were observed, but definite changes in the I vs eV curves were noted. In addition, an increase of about 1.4 eV in the work function was measured. Both the I vs eV curves and the work function indicated that further exposure to oxygen resulted only in a secondary amorphous coverage. When this (1×1)-O surface was heated to 350°C, a disordered surface resulted and the work function dropped below the clean metal value. Further heating to 500°C caused the formation of a $C(2 \times 2)$ structure. This was interpreted with an atomic displacement model where at least one half of the oxygen atoms had exchanged places with molybdenum atoms resulting in a surface layer composed of equal numbers of molybdenum and oxygen atoms. When this structure was heated to 1000°C, (1/3, 1/3) spots appeared. It was suggested that this structure had a one-third monolayer oxygen coverage on the surface with displaced molybdenum atoms positioned above oxygen atoms. Further heating to 1100°C resulted in a clean regeneration of a clean surface, again presumably due to the diffusion of the oxygen into the bulk of the crystal.

It was concluded that the existing evidence for the Mo (100) surface favored the exchange process in the two structures requiring heat treatment. Further, because of the activation energies involved, it was deemed probable that the one-half and one-third monolayer structure were formed with atomic oxygen, while the initial monolayer formed at room temperature

consisted of molecular oxygen above the molybdenum substrate.

This conclusion is consistent with all of the available information. The changes in work function and disordering of the surface upon heating the (1 × 1)-O structure particularly seem to support a model where oxygen above the metal surface becomes engaged in a place exchange process. Further, this model is supported by the fact that nearly all of the (1 × 1)-O surfaces were stable at room temperature, but converted to structures with fractional monolayer coverages upon heating. The exception was the Ta(110) face which spontaneously oxidized at room temperature. Though the data are incomplete, it appears that the lighter bcc transition metals are more resistant to place exchange than the heavier metals. Similarly, the (100) faces appear to be more stable towards place exchange than the (110) faces.

The (1 × 1)-O surface structure presents an interesting case for structural analysis. The experimental data indicate that the oxygen is above the surface, possibly in the molecular form. Therefore, these are a limited number of ways in which the oxygen can be arranged in a manner which is consistent with chemical intuition. It would be extremely unusual if the oxygen were in a highly unsymmetrical position. It is therefore most probably in one of the three symmetrical positions; 1) the bridged position where the oxygen is bonded to two adjacent metal atoms, 2) the face centered position where the oxygen is equidistant from the four metal atoms forming the corners of a face of an x-ray unit cell, 3) the linear position where an oxygen is placed directly above a metal atom in the surface layer.

As the sides of the two dimensional unit cell are approximately 3Å for most of the bcc metals, and as the oxygen-oxygen bond varies between 1.2 for O_2 to 1.5 for H_2O_2, the most probable configuration for molecular

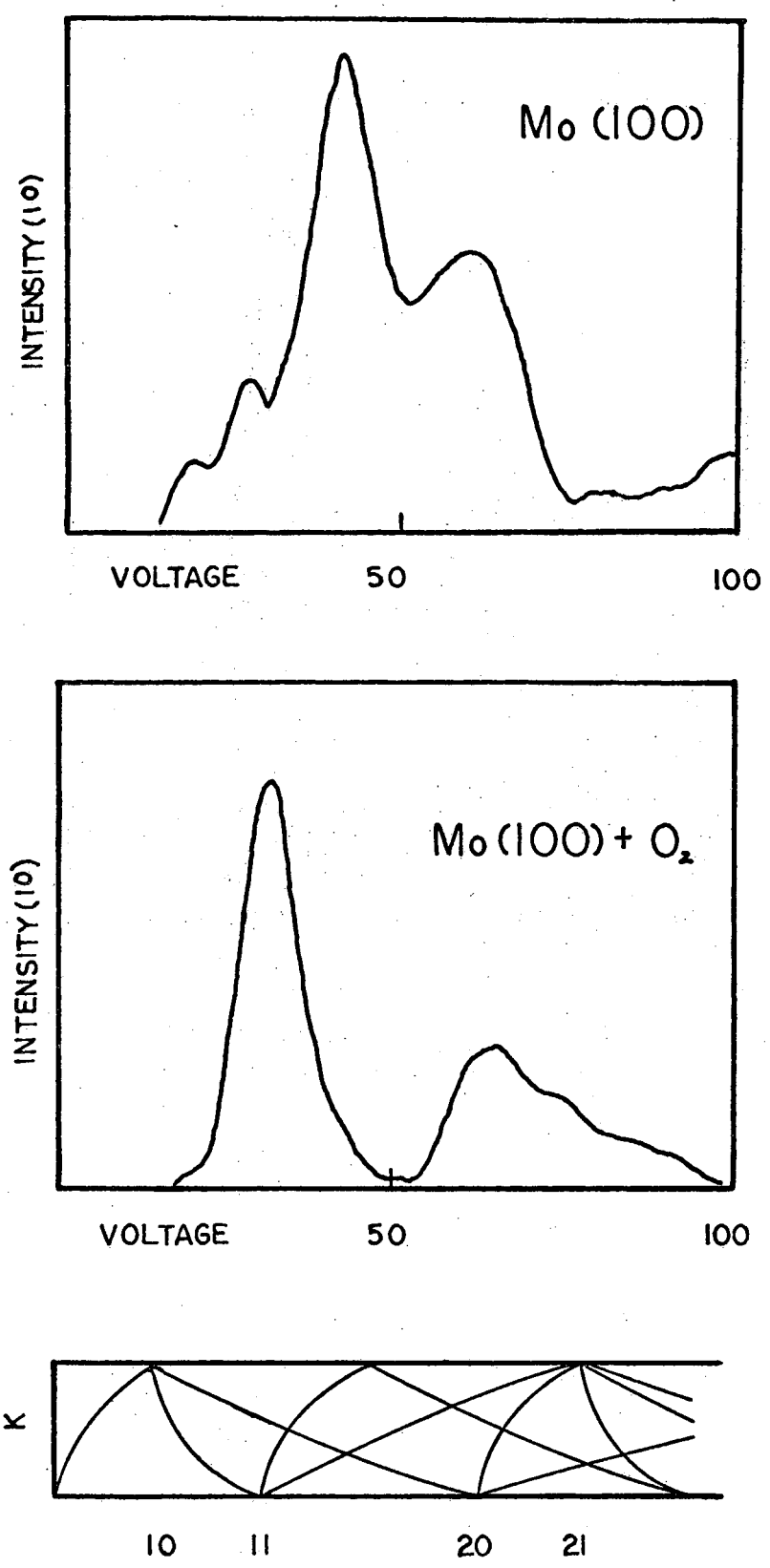

Fig. IV-13. Experimentally observed[55] I_{10} vs eV for clean and oxygen covered Mo (100). Band structure is shown for comparison.

oxygen adsorbed in a (1×1) structure would be with the molecular axis normal to the surface. It is difficult to form an isotropic (1×1) coverage with the molecular axis parallel to the surface without extensive distortion to the point where the oxygen may better be regarded as atomic or perhaps ionic.

It should be possible to distinguish among these alternative models by analyzing the intensities of the back diffracted electron beams. As noted before, the formation of the (1×1)-O structure on vanadium extinguishes two peaks in the specularly reflected beam. Further, on molybdenum the presence of the (1×1)-O structure removes the strongest intensity maximum in the I_{10} vs eV curve for the first order diffraction beam. This maximum occurs at approximately 41 eV and may be assigned to a diffraction condition of the form $K_{\perp}^{00} + K_{\perp}^{10} = G$. This peak is also observed on chromium. Data for the (10) beam of the other metals were not available.

Model calculations reproduce this maximum for the clean surface reasonably well with a screening parameter of $\lambda = 1\text{Å}$. Several different models for the (1×1)-O structure were studied. It was first assumed that the oxygen had been adsorbed in an atomic fashion at a normal face centered position on the lattice. The geometry was the same as for the clean surface. The screening parameters, λ, were varied to simulate the effect of placing a chemically different atom at this position. When λ was increased above 1Å^{-1}, this peak became more pronounced. When λ was less than 1Å^{-1} the intensity decreased. As λ should be larger for oxygen than for molybdenum, this model was discarded.

The effect of varying the geometry with a constant screening parameter was next studied. The top layer was gradually relaxed inwards towards the bulk of the crystal. It was found that the intensity of the 41 eV

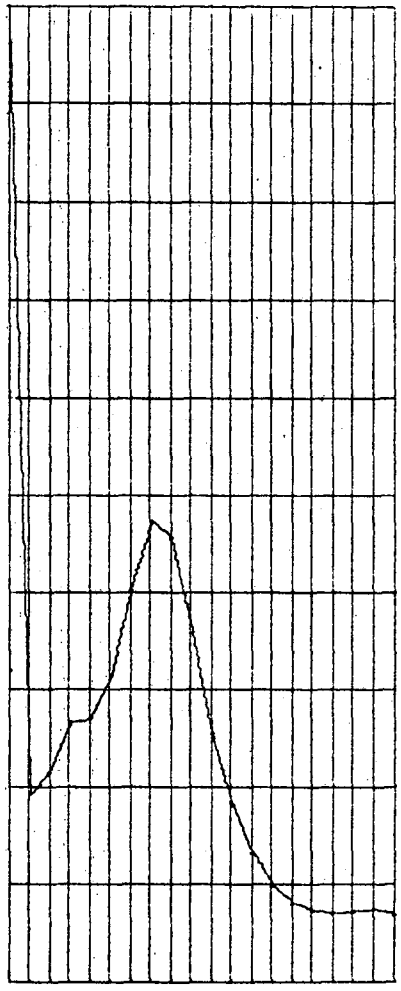

$\lambda_S = \lambda_B = 1.0\text{Å}^{-1}$

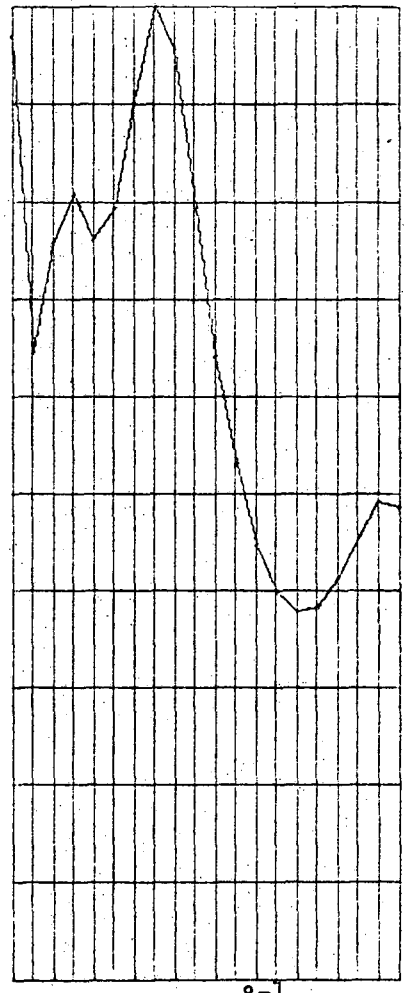

$\lambda_S = 2.0\text{Å}^{-1}$
$\lambda_B = 1.0\text{Å}^{-1}$

Fig. IV-14a. Calculated I_{10} vs eV for Mo(100) between 31 and 62 eV. Curve at left is for "clean structure with $\lambda = 1.0\text{Å}^{-1}$, $\alpha = 0.9$, $v = 0$, $T = 300°K$. Curve at right is identical except that $\lambda = 2.0\text{Å}^{-1}$ for surface atoms.

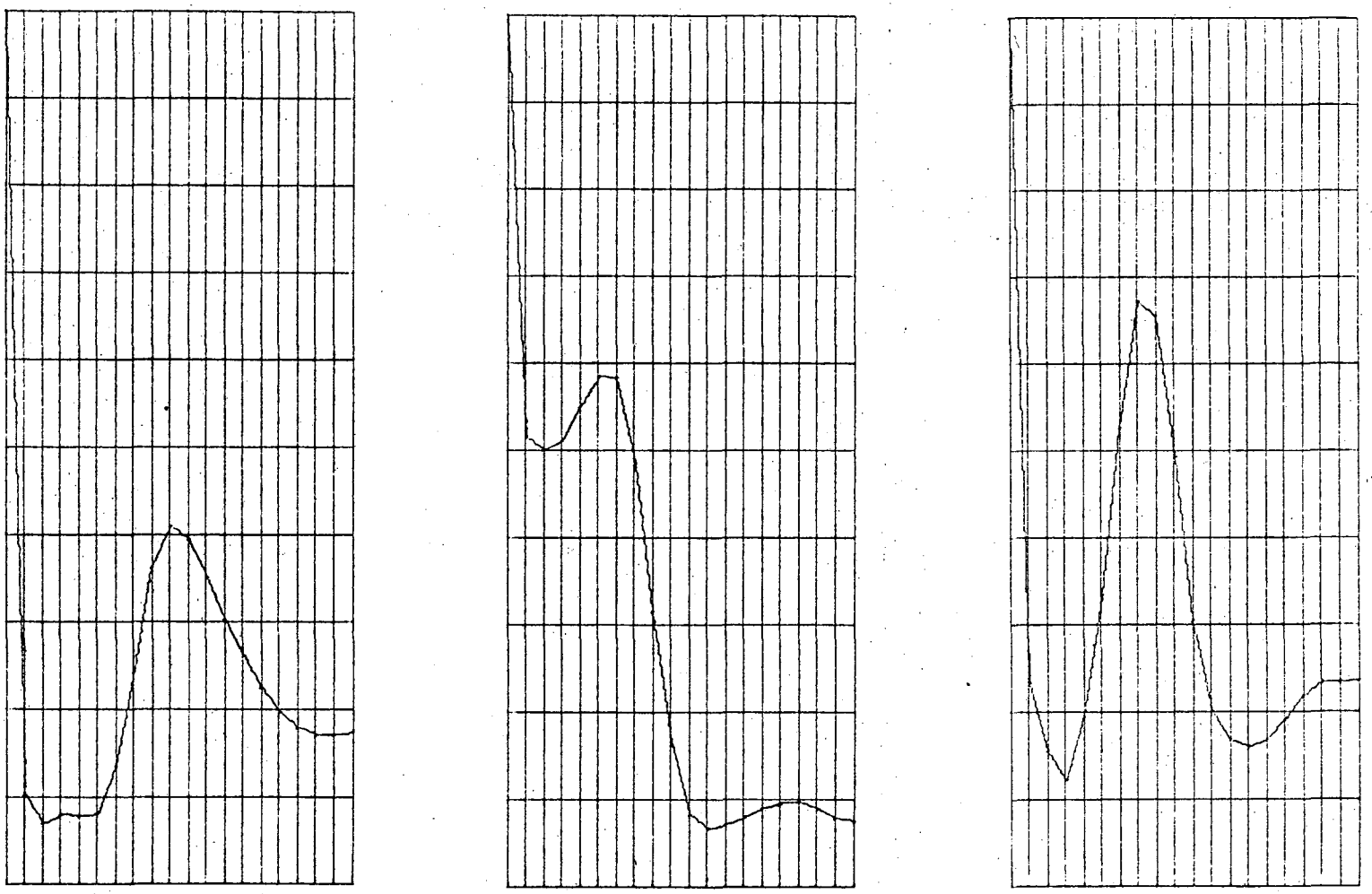

Fig. IV-14b. Calculated I_{10} vs eV for Mo(100) between 31 and 62 eV with $\lambda = 1.0\text{Å}^{-1}$, $\nu = 0$, $\alpha = 0.9$ and $T = 300^{\circ}K$. From the left, the surface layer has been relaxed in 1680, 3370 and 5090 respectively. The second layer has been relaxed in one half of the respective values for the first layer.

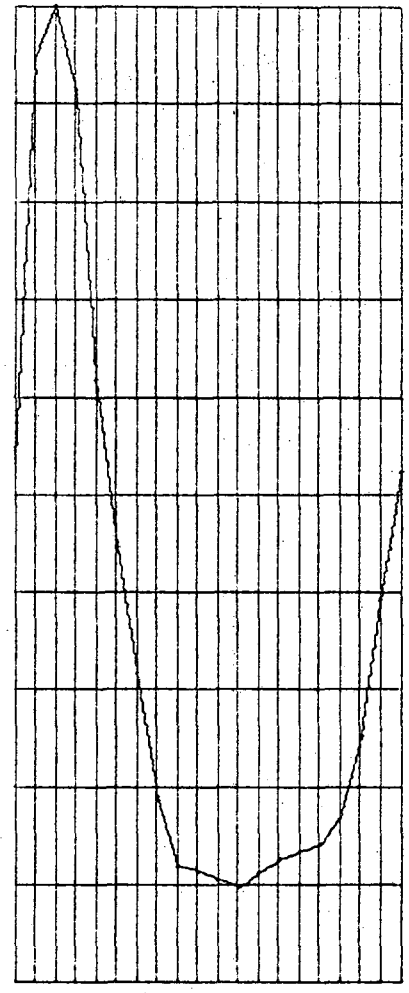

Fig. IV-14c. Calculated I_{10} vs eV for Mo(100) between 31 and 62 eV with $\lambda = 1.0A^{-1}$, $\nu = 0$, $\alpha = 0.9$, and $T = 300$ K. This calculation corresponds to the situation where either an oxygen atom is placed above a Mo atom with the normal interplanar spacing, or, an oxygen molecule is adsorbed into a normal face centered position.

peak underwent a minimum near relaxations of approximately 33%. The oxygen-metal distance would be only 1.6Å however for this structure. As the effect of varying the potential was not studied for this structure, it is possible that a relaxed monolayer of oxygen atoms in face centered positions does present a viable model for the real surface structure.

The bridged structure was also studied. This model has the disadvantage that it is anisotropic. It was found that the intensity was of the 41 eV peak was enhanced in the (10) beams parallel to the bridging and that it was extinguished in the (10) beams perpendicular to the bridging. As there is no report in the literature of anisotropy in the (10) beams, thus structure could only occur as small domains randomly rotated at 90° to one another. This however would result in the observed intensities of the (10) beams being averaged over both directions. Consequently, the 41 eV maximum would not be so strongly extinguished as is observed experimentally. This model may then be regarded as rather unlikely.

The linear structure, where an oxygen atom is placed directly above a metal atom in the surface layer, has also been considered. Calculations on this model gave the best agreement with experimental results. The 41 eV intensity maximum was completely extinguished. Further, there was a peak generated near 30 eV in good agreement with experimental results. Most satisfactory was the fact that the Bragg peak near 60 eV in the (00) beam was diminished most for this of all of the model calculations in good agreement with the data from the vanadium surface.

However, this model is geometrically almost identical with one that is more acceptable and in good agreement with the available experimental data. This is the model where an oxygen molecule is adsorbed into a face centered position with its axis perpendicular to the surface. If it is assumed that the oxygen is only weakly bonded to the four nearest

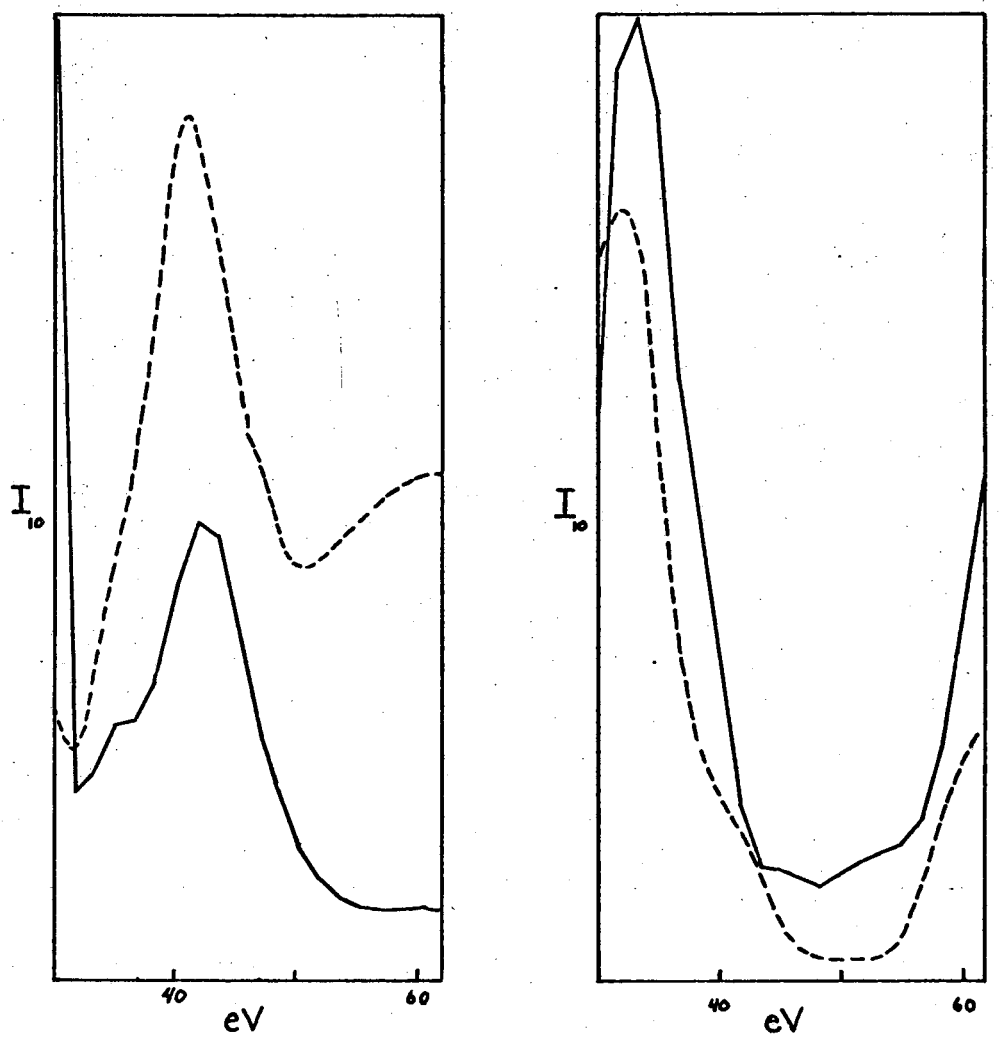

Fig. IV-15. Comparison between the calculated (solid line) and observed I_{10} vs eV from the clean (left) and the oxygen covered Mo(100) face.

molybdenum atoms, then a metal-oxygen distance of about 2.4Å is not unreasonable. Allowing the oxygen-oxygen bond to relax out to about 1.3 to 1.5Å is consistent with known oxygen-oxygen bond lengths. In this arrangement, the upper oxygens form a plane that will scatter exactly out of phase with the rest of the atoms for this $K_z^{00} + K_z^{10} = G_z$ 41 eV intensity maximum.

This model is the most prefered of all of those studied on several points. However, the assignment of the Mo (100) - (1 × 1)-O surface structure to this model is not at all unambiguous. The alternate assignment to a relaxed surface layer of oxygen atoms has some merits. Furthermore, by varying potentials and positions, exchange models could be forced to result in the weakening of this 41 eV peak. Calculations performed on only a limited voltage region and primarily for only one diffraction beam may be regarded at best as indicative rather than conclusive. Unfortunately, a complete set of experimental data has not been reported in the literature.

Experimental data can, however, be obtained. The greatest obstacle at this point to the structural analysis of surfaces through the investigation of the intensities of LEED beams is the lack of good potentials or, more concisely, good form factors. Particularly when multiple scattering is important, the precise nature of the form factors can greatly alter the shape of the I vs eV curves. Approximate form factors for, say, molybdenum can be obtained by parametrically fitting experimental data from clean surfaces. Information about substances such as oxygen is more difficult to obtain, particularly when it is not known whether or not it is in an atomic, molecular or ionic state. Hopefully, continued experimental investigations coupled with accurate potential calculations will lead to a resolution of this problem.

V. CONCLUSION

The primary purpose of this work was to investigate the relationship between the theory describing the intensities of low energy electron beams back diffracted from single crystal surfaces and the actual experimentally measured intensities. To that end, the intensities of several of the low index diffraction beams from the (100) face of aluminum and palladium have been measured and correlated with data for several other face centered cubic metals. When the variations in the lattice parameters among these different metals were taken into account a high degree of correlation for the positions of the intensity maxima were found. Further, it was possible to assign those maxima in the low energy region to various diffraction mechanisms predicted from multiple scattering conditions. It was found that maxima occurred not only at those positions predicted by kinematic or single scattering mechanisms, but also at those positions predicted by double scattering mechanisms. These correlations substantiate a basic assumption in multiple scattering theory that the position of intensity maxima are determined primarily by the geometry and dimensions of the scattering centers while the intensity ratios are determined by the detailed nature of the atomic potentials.

Significant variations in intensity ratios were observed for the different materials, presumably reflecting variations in the types of atoms composing the crystal. For several different maxima, definite trends in intensity ratios with atomic number were noted. There appeared to be a tendency for diffraction conditions with scattering vectors of relatively small magnitude to dominate.

It was found that inner potential corrections tend to be small in the very low energy region. In the range between approximately 20 and 50 eV

the correction is most certainly less than 10 eV and possibly less than 5 eV for the materials studied here. This is consistent with recent pseudo-potential calculations and earlier studies of the diffraction angle.

The intensities of several of the low index integral and fractional order diffraction beams from the Pd (100) - C(2×2) and Pt(100-(5×1) surface structures were measured. It was found that the intensities of the functional order beams from these surfaces tended to mimic the behavior of neighboring integral order beams in good agreement with a prediction of multiple scattering theory. The intensity maxima in the fractional order beams occurred near positions where diffraction conditions for the integral order beams were met. For palladium, the intensity of specularly reflected beam was monitored as a function of the development of the surface structure. It was found that changes could frequently be observed in the intensity vs voltage plots before new diffraction spots were observed. At least for this surface structure, the intensity vs voltage plots provide a very sensitive and reproducible indication of the state of the surface. The intensities for the integral order beams were compared for a (1×1) and a C(2×2) surface. The development of this surface structure had a pronounced effect of the shape of the intensity vs voltage curves in the region below 100 eV. This indicates that the very low energy region should be the most valuable in determining the structure of surfaces through an analysis of electron beam intensities. A comparison was made of the intensities of the (1/2 1/2) diffraction beam for several C(2×2) surface structures of presumably different constructions. It was found that the intensities were significantly different for the different structures indicating that it is possible to discriminate among surface structures that have the superficial similarity of the same two

dimensional symmetry i.e. have the same diffraction pattern.

Model calculations were performed to compute the intensities of electron beams back diffracted from the (100) face of the clean face centered cubic metals. It was found that many of the experimentally observed intensity features could be reproduced using a simple multiple scattering approach. However, good intensity ratios were not obtained with the use of simple model potentials. A better fit with the experimental data was obtained by parameterizing the model potential. However, the use of the more sophisticated and meaningful potentials, such as the pseudo-potential, should eventually lead to reasonable calculations.

There was some indication that the metals with higher atomic numbers were better fit by more forward scattering potentials. This is reasonable on the basis of very simple models as the nuclei of atoms with a high atomic number are not as well shielded, charge for charge, as are those with a low atomic number. This of course, is a generalization as it neglects the details of electronic arrangement.

Model calculations were also performed for several arrangements of oxygen on the (100) face of body centered cubic metals. The effect of potential was ignored and variations in geometry were considered primarily. The model where an oxygen molecule was adsorbed into the normal face centered position with the molecular axis perpendiuclar to the surface gave the best agreement with the experimental data for molybdenum in the initial stage of oxidation. However, the neglect of the effect of potential and the limited amount of available data severely restrict the validity of this model. These calculations were performed as an indication of general approach to the problem of determining the structure of adsorbed gases on surfaces from LEED intensities rather than as a definitive solution for a particular structure.

In conclusion, it was found that a multiple scattering approach is valid in the interpretation of the intensities of low energy electron beams back diffracted from single crystal surfaces. The position of intensity maxima may be predicted with fair accuracy by this method, particularly in the very low energy region and when inner potential corrections are properly taken into account. It may be predicted with a reasonable degree of certainty that accurate intensity ratios will also be predictable for both simple and structured surfaces when good model potentials become available and when inelastic processes are properly taken into account.

APPENDIX I

Several authors have performed extensive model calculations for the (100) face of a simple cubic lattice containing identical, spherically symmetric scatterers.[2,11,13] While this case does not correspond to any known physical situation, because of its simplicity and because of the number of detailed calculations that have been performed, it is informative to consider it in some detail. The qualitative results may be generalized to more complicated situations in a fairly straight forward manner.

In the simple cubic lattice, all of the primative translations have the same magnitude and, consequently, all of the primative reciprocal lattice vectors have the same magnitude. Therefore, we may write

$$|\vec{G}_x| = 2\pi\, h/a, \quad |\vec{G}_y| = 2\pi\, k/a; \quad |\vec{G}_{\|}| = 2\pi\,(h^2 + k^2)^{1/2}/a$$

and $|\vec{G}_{\perp}| = 2\pi\, M_z/a$ where a is the lattice constant. From the simple considerations outlined earlier, we would expect intensity maxima to occur in the diffraction beams when

$$K'_{\perp} - K''_{\perp} = G_{\perp} \tag{57}$$

When the scattering amplitudes are sufficiently large (as is the case with isotropic scatterers), we must consider this diffraction condition not only between the incident beam and a diffracted beam as in the kinematic case but also between the various diffracted beams. At normal incidence, this condition may be written as

$$\left[\frac{K^2a^2}{(2\pi)^2} - [(h')^2 + (k')^2]\right]^{1/2} \pm \left[\frac{K^2a^2}{(2\pi)^2} - [(h'')^2 + (k'')^2]\right]^{1/2} = M_z \tag{58}$$

where we have divided through by $(a/2\pi)^2$.

TABLE A-1. Calculated positions of intensity maxima in the free electron limit for a simple cubic crystal at normal incidence.

h k	h' k'	K^2 / a^2	COMMENT
0 0	0 0	0.00	Kinematic Position
0 0	0 0	0.25	Kinematic Position
0 0	0 0	1.00	Kinematic Position
0 0	0 1		Kinematic Position
0 1	0 1		Double Diffraction Position
0 1	0 1	1.25	Double Diffraction Position
0 0	0 1	1.56	Kenematic Position
0 1	0 1	2.00	Double Diffraction Position
0 1	1 1		Double Diffraction Position
1 1	1 1		Double Diffraction Position
0 0	0 0	2.25	Kinematic Position
0 0	1 1		Kinematic Position
1 1	1 1		Double Diffraction Position
0 1	1 1	2.56	Double Diffraction Position
0 0	0 1	2.79	Kinematic Position
1 1	1 1	3.00	Double diffraction Position

The values of the energies in units of $K^2a^2/(2\pi)^2$ where this equation is satisfied are given in Table A-1. The assumptions made in calculating the intensity maxima positions given in Table A-1 are essentially the same as those in the free electron model, e.g. that there are no band gaps. Note the large number of cases where different diffraction conditions correspond to the same energy. These coincidences are due to the high symmetry of the (100) face of the simple cubic crystal at normal incidence. It is to be expected that the different diffracted beams under consideration would be strongly coupled at these points of coincidence and that as a consequence the positions of their intensity maxima may be perturbed from those values given in Table A-1. When the cross sections are large, the coupling between beams should be strong and larger perturbations may be noted than in those situations where the cross section is relatively small.

The results of the calculations of McRae,[3] Carpart,[13] and Marcus and Jepsen[11] are given in Fig. A-1. All of these calculations were performed in the absence of inelastic scattering. Those of McRae and of Carpart were performed at normal incidence, while that of Marcus and Jepsen was performed slightly off of normal incidence. McRae and Carpart used isotropic scatterers while Marcus and Jepsen used point ions with unit charge surrounded by a uniform negative charge. The first thing to note is the remarkable similarity of these results. The deviation from normal incidence introduces fine structure into the calculations of Marcus and Jepson because the first order diffraction beams are no longer degenerate, but the qualitative results are similar. The similarity among the three curves is even more striking when one considers that three quite dissimilar computational techniques and two non-identical potentials were used. Therefore, it is to be hoped that these results are physically reasonable within the limit of the model.

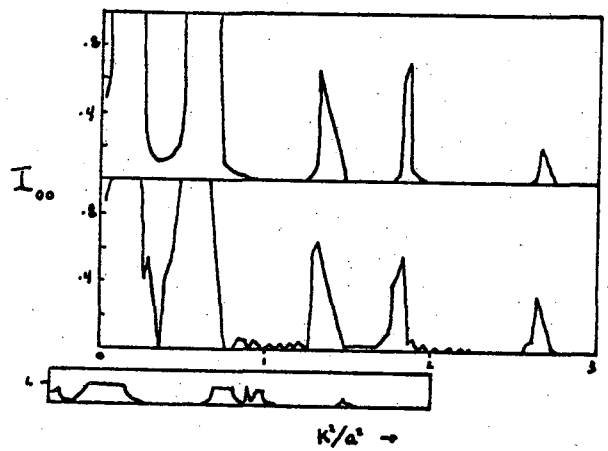

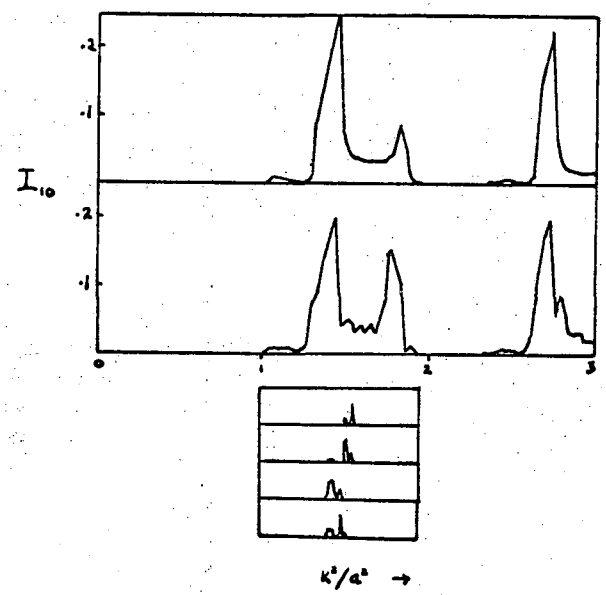

Fig. A-1. Calculated I_{00} and I_{10} vs eV for the simple cubic case. Carpart (top) and McRae (middle) performed the calculation for isotropic scatterers at normal incidence. Jepson and Marcus (bottom) considered a non-normally incident situation. Note the differences in the four non degenerate first order diffraction beams for the non-normal calculations.

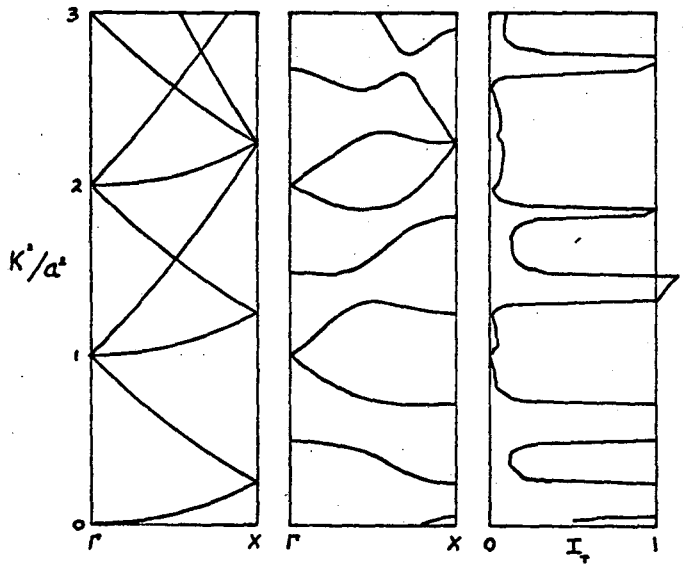

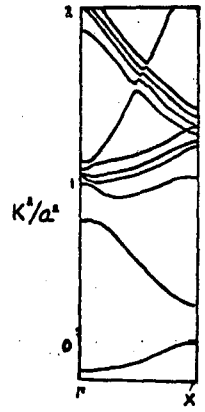

Fig. A-2. Band structures calculated by Carpart for the free electron model far left, and for the isotropic scatterer model (middle left) are shown with the calculated total back scattered intensity. Band structure calculated by Marcay and Jepson (far right) is shown for comparison.

As expected, in addition to the maxima predicted in the kinematic limit, a number of other peaks appear in these intensity curves. However, not all of the peaks that are predicted in Table A1 occur. Furthermore, the positions of those peaks that do occur are shifted downward to considerably lower energies (e.g., the third Bragg peak in the specularly reflected beam is displaced by greater than 0.4 units). The shifts may be taken as an indication of the existance of strong coupling between the various beams.

It is informative to consider the relationship between these results and the corresponding energy band structure in the solid. In Fig. A-2 are shown the bands structures calculated by Carpart for the free electron model and for the isotopic scatterer model and by Marcus and Jepsen for the model of point ions in a sea of electrons. Despite the multiplicity of lines that are due to the lack of degeneracy in Marcus' and Jepsen's model, it may be seen that this case is somewhat closer to the free electron situation than is that corresponding to the isotropic scatter model. For the latter model, the band structure is considerably distorted from that of the free electron case. This of course is due to the strong interaction between the electrons and the lattice that results in the large scattering factors. Further, this strong interaction has the consequence that the peak positions are significantly perturbed from those predicted by the free electron model. For example, consider the situation where $K^2a^2/4\pi^2 = 1$. At this energy there should be the $n_z = 2$ Bragg peak in the specularly reflected beam and the simultaneous appearance of the first order diffraction beams. Inspection of the band structure shows that considerable interaction between these two states has occurred with the result that the position of the corresponding band gap has been significantly decreased in energy. Proceeding to higher energies, according to Table A-1, the next

diffraction condition to be met is of the form $2K_{\perp}^{10} = 1(2\pi/a)$ at $K^2/a^2 4\pi^2 = 1.25$. However, only a very small intensity maxima may be seen in the first order diffraction beam (01 beam) at this energy. Inspection of the band structure, shows that there is no complete band gap at this energy. Consequently, there are at least two travelling waves allowed in the crystal (specifically, the transmitted beam and the specularly reflected beam) that the electron can be scattered into. This traveling wave permits the electron to penetrate into the crystal with the result that total back reflection is not required as in the case when there is a complete band gap. Consequently, the back scattered amplitude may be considerably less than unity.

The next diffraction condition encountered upon increasing the energy is of the form $K_{\perp}^{00} + K_{\perp}^{10} = 2(2\pi/a)$. In the kinematic limit, there should be a maxima only in (01) beam. However when multiple scattering is strong, maxima may appear in both beams. Maxima of this type have been experimentally observed in the specularly reflected beam. They are frequently called secondary Bragg peaks or fractional order Bragg peaks because they follow equations of the form[20]

$$2K_{\perp}^{00} = (n + m^2/n) \; 2\pi/a_z \qquad (59)$$

As there is a complete band gap corresponding to the condition $K_{\perp}^{00} + K_{\perp}^{10} = 2(2\pi/a)$, we know that the total of all of the back reflected intensities from all of the beams must be unity. The manner in which this intensity is distributed among the various beams depends upon the detailed nature of the potential. For both of the potentials considered here, it may be seen that initially most of the intensity is scattered into the (00) beam and that at a slightly higher energy, the (00) beam "dims" and the intensity is scattered almost entirely into the (01) beams. This gives the effect that the peak position in the specularly

reflected beam is at a lower energy than those in the (01) beams.

In the energy region around the appearance of the (11) beams the band structure has become very distorted. Looking at Table A-1, we see that even in the free electron model, the (01) and the (11) beams are coupled at $K^2a^2/4\pi = 2.0$ and that the (00) and the (11) beams are coupled at $K^2a^2/4\pi^2 = 2.25$. Upon going to the isotropic scatterer model, these two adjacent regions of coupling become further coupled with each other. There is then one complete energy gap corresponding to these interactions. As a result, the n = 3 Bragg peak in the specularly reflected beam falls significantly lower than expected. There is a complimentary peak in the (10) beam that would correspond to a diffraction condition of the form $2K_{\perp}^{10} = 2.(2\pi/a)$ in the free electron limit. This diffraction event is coupled with the emergence of the second order diffraction beams in a manner entirely analogous to the interaction of the specularly reflected beam and the first order diffraction beams at the emergence energy of the latter. The strong intensity of the (10) beams at this energy is to be contrasted with that at $a^2K^2/4\pi^2 = 1.25$ where an identical diffraction condition is met, but where there is no complete band gap.

The weak and broad maxima that occurs in the (11) beam between $K^2a^2/4\pi^2 = 2.0 \rightarrow 2.5$ presumably corresponds to the diffraction conditions $2K_{\perp}^{11} = 2\pi/a$ and $K_{\perp}^{10} + K_{\perp}^{11} = 2(2\pi/a)$ but in the absence of a complete band gap. A weak maxima occurs in the (10) that presumably also corresponds to the $K_{\perp}^{10} + K_{\perp}^{11} = 2.(2\pi/a)$ condition. The highest energy gap considered here appears to be a mixture of the conditions $2\,K_{\perp}^{11} = 2\,(2\pi/a)$ and $K_{\perp}^{00} + K_{\perp}^{10} = 3\,(2\pi/a)$. Maxima occur in this energy range in all of the allowed diffraction beams. The maximum in the specularly reflected beam is another example of a fractional order Bragg peak.

APPENDIX II

A computer program was written to calculate the intensities of low energy electron diffraction beams. The integral form of the Schroedinger equation was used with the spectral representation of the Green function. It was assumed that the potential could be expressed as a sum of individual potentials centered at the various lattice positions. The two dimensional periodicity was employed to expand both the potential and the eigenfunctions in Fourier series. The basic eignefunction could then be written as

$$\psi(\vec{r},\vec{K}) = \psi^{\circ}(\vec{r},\vec{K}) + \sum_{G,G'} \int_{\vec{K}'} \int_{\vec{r}'} d^3K' \; \frac{e^{i\vec{K}'\cdot(\vec{r}-\vec{r}')}}{|\vec{K}'|^2 - |\vec{K}^{\circ}|^2} \; V_G \, e^{i\vec{G}\cdot(\vec{r}'-\vec{R}_s)} \times A_{G'} \, e^{i(\vec{K}^{\circ}+\vec{G}')\cdot\vec{r}'} \, d^3r'$$

The assumptions enumerated in Section II have been used here. The meaning of the symbols are the same as described above. The summations over G and G' implicitly include the integrations over γ and γ', the continuously varying components of G and G' that are perpendicular to the surface. Here, the structure factor terms, $e^{-i\vec{G}\cdot\vec{R}_s}$, have been shown explicitly and are not included in V_G. The indicated integrations are then performed as described in Section II-B. Equation 46 then becomes

$$\psi(\vec{r},\vec{K}) = \psi^{\circ}(\vec{r},\vec{K}) + \sum_{G,G'} e^{-i\vec{G}\cdot\vec{R}_s} \; \frac{V_G A_{G'}}{\pm 2i k_g} \; e^{i(\vec{K}^{\circ}_{\parallel} + \vec{g} + \vec{g}' \pm \vec{k}_g)\cdot\vec{r}} \times \delta(K^{\circ}_z + \gamma + \gamma' \pm k_g)$$

where the total eigenfunction is described as a sum of the incident or primary beam, $\psi^{\circ}(r,K)$, plus all of the diffracted beams. These diffracted beams have wave functions that contain a travelling wave component, $e^{i(\vec{K}^{\circ}_{\parallel} + \vec{g} + \vec{g}' \pm \vec{k}_g)}$, where the positive sign is used when k_g is directed out of the crystal, and the negative sign is used when it is directed into

the crystal. The eigenfunctions of the diffracted beams also contain structure factor terms of the form $e^{i\vec{G}\cdot\vec{R}_s}$ which may be interpreted as describing a scattering event at the center or atom located at $\vec{R}_s$ where the wave vector was changed by a factor $\vec{G} = \vec{g} + \vec{\gamma}$. The amplitudes of these diffracted beams contain, in addition to the structure factor terms, a component of the form $V_G A_{g'}/\pm 2 k_g$ where the factor i has been dropped as it adds only an arbitrary phase factor to all terms. V_G is, of course, the G^{th} coefficient in a Fourier transform of the potential. The term $A_{G'}$ is the coefficient of the diffraction beam whose wave vector differs from that of the incident beam by a scattering vector $\vec{G}'$. It is this set of quantities, $\{A_G\}$, that must be determined as the intensities of the different diffraction beams are proportional to the square of the absolute values of the amplitudes. As discussed above, there are several ways to solve for these amplitudes. The method chosen for computation was a stepwise procedure. It was assumed that the total scattering situation could be regarded is a sum of individual scattering events. The first step involved allowing a primary beam with unit amplitude to be diffracted off of the first layer of the crystal. In this manner, an elementary set of diffracted beams was generated. Their amplitudes were taken to be $(V_G/ 2 kg)\ e^{-i\vec{G}\cdot\vec{R}_1}$ where $\vec{R}_1$ is the coordinate of the surface layer to within a translational vector. Note that this term does not include an $A_{G'}$. This is because it was assumed that the initial beam had unit amplitude and that this amplitude was divided up among all of the new diffracted beams (including the forward diffracted beam) in a manner that was dependent upon the V_G's. Half of the diffracted beams that were generated in this first step were directed back out of the crystal. Their amplitude was stored to be later added to the amplitudes scattered from other layers. The other half was

directed into the crystal. The second step in the scattering process was to allow those beams directed into the crystal to be scattered from the second layer. This resulted in new sets of diffracted beams, half of which were directed back up toward the first layer, and half down towards the third layer. The amplitudes of these beams were given by

$$\frac{V_{G'}}{2\,k_g}\; e^{-i\vec{G}\cdot\vec{R}_1}\quad \frac{V_{G'-G}}{2k_{g'-g}}\quad e^{-i\,(\vec{G}'-\vec{G})\cdot\vec{R}_2}.$$

The first part of the amplitude, $\left(V_G/2\,k_g\right)e^{-i\,\vec{G}\cdot\vec{R}_1}$, came from scattering the incident electron with wave vector K° into a diffracted beam with wave vector $K^\circ + G$ at the first layer. The second part of the amplitude came from scattering this diffracted beam into another with wave vector $\vec{K}^\circ + \vec{G}'$ at the second layer. The third step in this scattering procedure involved two parts. The first was the scattering at the first layer of those beams that had been back diffracted from the second layer. In this step, some beams were re-diffracted back towards the second layer and some were scattered out of the crystal. The amplitude of these beams that had left the crystal were then added to those that had been scattered away from the crystal in the initial scattering step. The second part of the third scattering step involved the diffraction off of the third layer of those beams which had been scattered into the crystal from the second layer.

This procedure was repeated 15 or 20 times. In a 20 step process the electron would have penetrated into the 20^{th} layer and amplitude scattered from as deep as the tenth layer would have escaped from the crystal.

Normalization was performed to ensure that the total probability was still unity after any given number of scattering steps. The intensities, or electron densities were normalized rather than the amplitudes. In this

fashion, it is only the relative values of the amplitudes that determine the electron beam intensities. Therefore, for convenience, only relative values of V_G were employed. The terms, $V_G/2\ k_g$, were determined for a single scattering event, and then these are normalized prior to their usage in the stepwise scattering calculations. Inelastic scattering is considered in the form of atomic excitations. The amplitude of each diffracted beam is multipled by a factor α (which is less than or equal to one) at each scattering event. When $\alpha = 1$, there is only elastic scattering, when $\alpha < 1$, then $(1 - \alpha^2)$ is the fraction of the intensity which is scattered inelastically at each event. The inelastically scattered intensity is stored separately and is used in the final normalization.

Dynamical thermal motion of the crystal is considered by multiplying the amplitude of each diffracted beam by a factor e^{-W} at each event. 2W is the Debye-Waller factor. It is inversely proportional to the square of the Debye temperature and the atomic weight, and is directly proportional to the absolute temperature and the square of the scattering vector $\vec{G}$. As with the inelastic intensity, the thermally scattered intensity is stored and is used in the final normalization. The relationship between the Debye-Waller factor and multiple scattering is considered in greater detail in Appendix III.

Several different model potentials have been used. They are the isotropic potential, the screened Coulombic potential and Gaffners potential. All of the V_G's are equal for the isotropic scattering potential. This is commonly called the S-wave scattering potential.

The screened Coulombic potential is a forward scattering potential. The form factors, V_G, are inversely proportional to the square of the scattering vector, $\vec{G}$, plus the square of the screening parameter, λ. A modification of this potential that favored scattering events that did

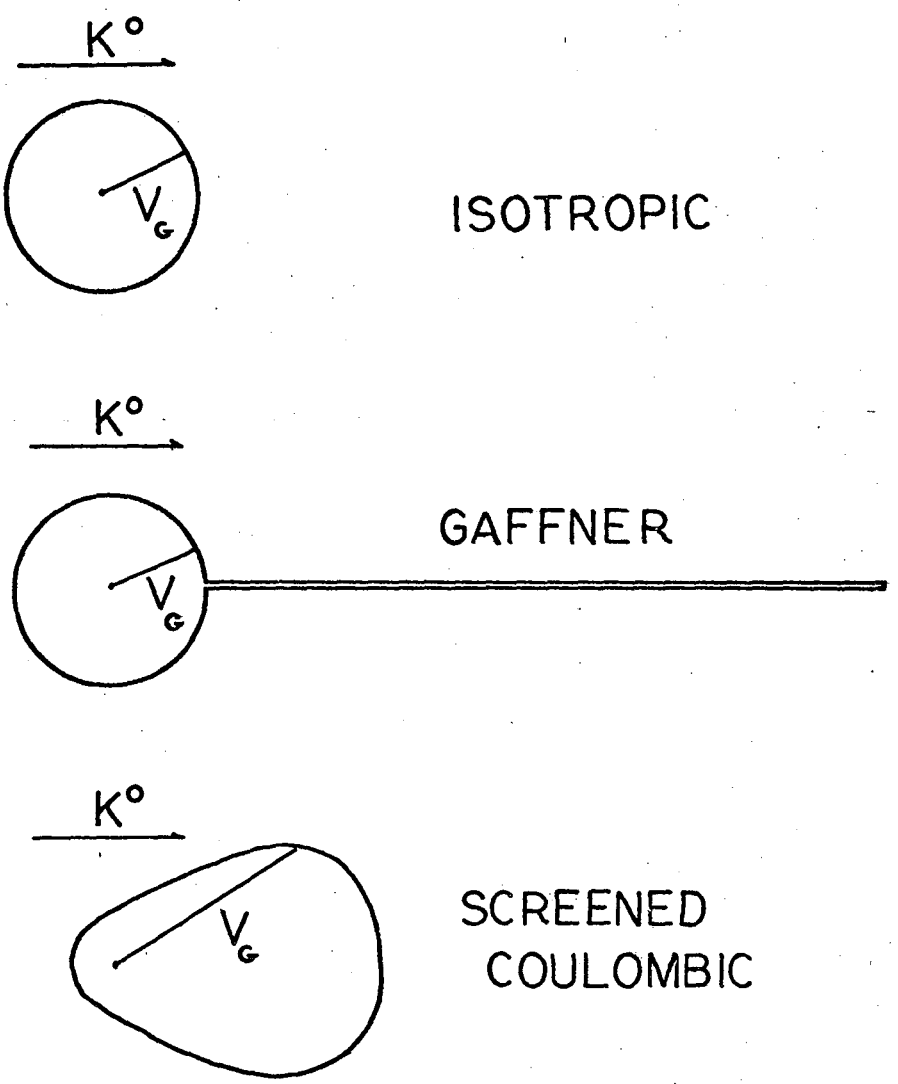

Fig. A-3. Form factors, V_G, for several different model potentials.

not involve a change in the component of G parallel to the surface was also used. In this modification, V_G was inversely proportional to $\lambda^2 + G^2 + \nu G_{\|}^2$ where ν was a variable parameter.

"Gaffners potential" is also a forward scattering potential. It was used by G. Gaffner to calculate LEED intensities for the (111) face of nickel. For this potential, the forward scattering form factor, V_0, is 9 times as large as all of the other V_G's. This is a very simple model potential which simulates the gross features of many real potentials.

Two Beam Case

In this case there are only the transmitted and the back reflected beams. For the (100) face of face centered cubic crystals, this is true in the voltage range below approximately 20 volts. There should be only one Bragg peak in this region located at approximately 9 eV for aluminum. Figure A-4 shows model calculations in the region 1-18 eV. For the (100) face of aluminum a screened Coulombic potential with $\lambda = 3\text{Å}^{-1}$ was used. No inelastic scattering or thermal scattering was employed. These calculations were performed for 4, 8, 12, and 16 scattering events. Contributions from the 2^{nd}, 4^{th}, 6^{th} and 8^{th} layers respectively would have reached the surface of the crystal and contributed to the back scattered intensity. It may be seen that increasing the number of layers utilized in the calculation results in an increase in the intensity in the region between 9 and 10 eV when the first Bragg peak should occur. The presence of the subsidiary maxima, or "ripples" is a direct result of the use of a finite lattice. Increasing the number of layers also has the effect of narrowing the peak width and reducing both the intensity of the ripples and the interval between their maxima. The situation is similar to one where a delta function is approximated by sin NX/NX for finite values of N.

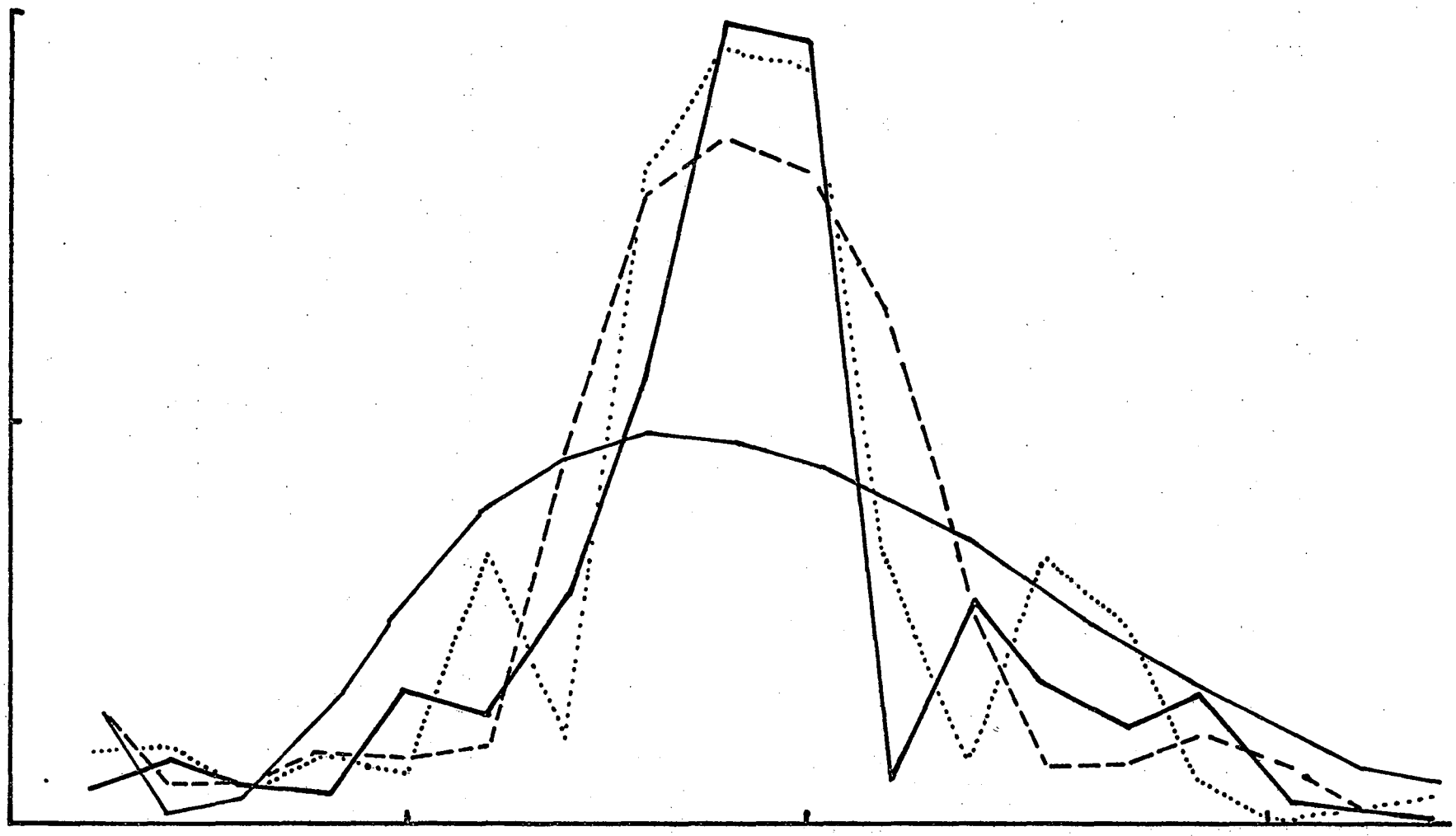

Fig. A-4. I_{00} vs eV for Al(100) at $\theta = 0°$ between 1 and 18 eV calculated with T = 0°K, $\alpha = 1.0$ and $\lambda = 3.0$Å^{-1} for 4, 8, 12 and 16 scattering events.

In a typical situation, the intensity maxima reaches better than 90% of its height after contributions from 5 layers have reached the surface, i.e. often 10 scattering evens. Twelve and fourteen scattering events results in intensities that are 96 and 98% respectively of their final height. Lower value are observed in the case where the potential is very strongly forward scattering in nature.

In Figs. A-5 and A-7, the range of the two beam case has artificially been extended by decreasing the lattice parameters parallel to the surface to one tenth of their natural value. The interplanar distance perpendicular to the surface has been maintained at 2.02Å. Consequently, there are three maxima in the region between 1 and 100 eV. These are pure Bragg maxima and should come at 9, 37 and 83 eV. These graphs were produced with a Cal-Comp plotting routine.[60] They have been normalized to the tallest peak. The intensities have been modulated by an $(eV)^2$ factor to mimic the current vs voltage characteristics of the electron gun.

These curves were calculated for three potentials; the isotropic potential, Gaffners' potential and a screened Coulombic potential with $\lambda = 1\ Å^{-1}$. The effects of inelastic and thermal scattering have been considered. As predicted, three peaks appear in all curves, though with widely differing intensities.

A number of interesting conclusionsmay be drawn from an inspection of these curves. One of the most obvious effects is the decrease in intensity with increasing beam voltage when thermal scattering is considered. This is to be expected as the Debye-Waller factor is proportional to the electron energy for the specularly reflected beam. It may also be seen that the intensity of the voltage dependent screened Coulombic potential decreases with increasing beam voltage relative to the intensities of the

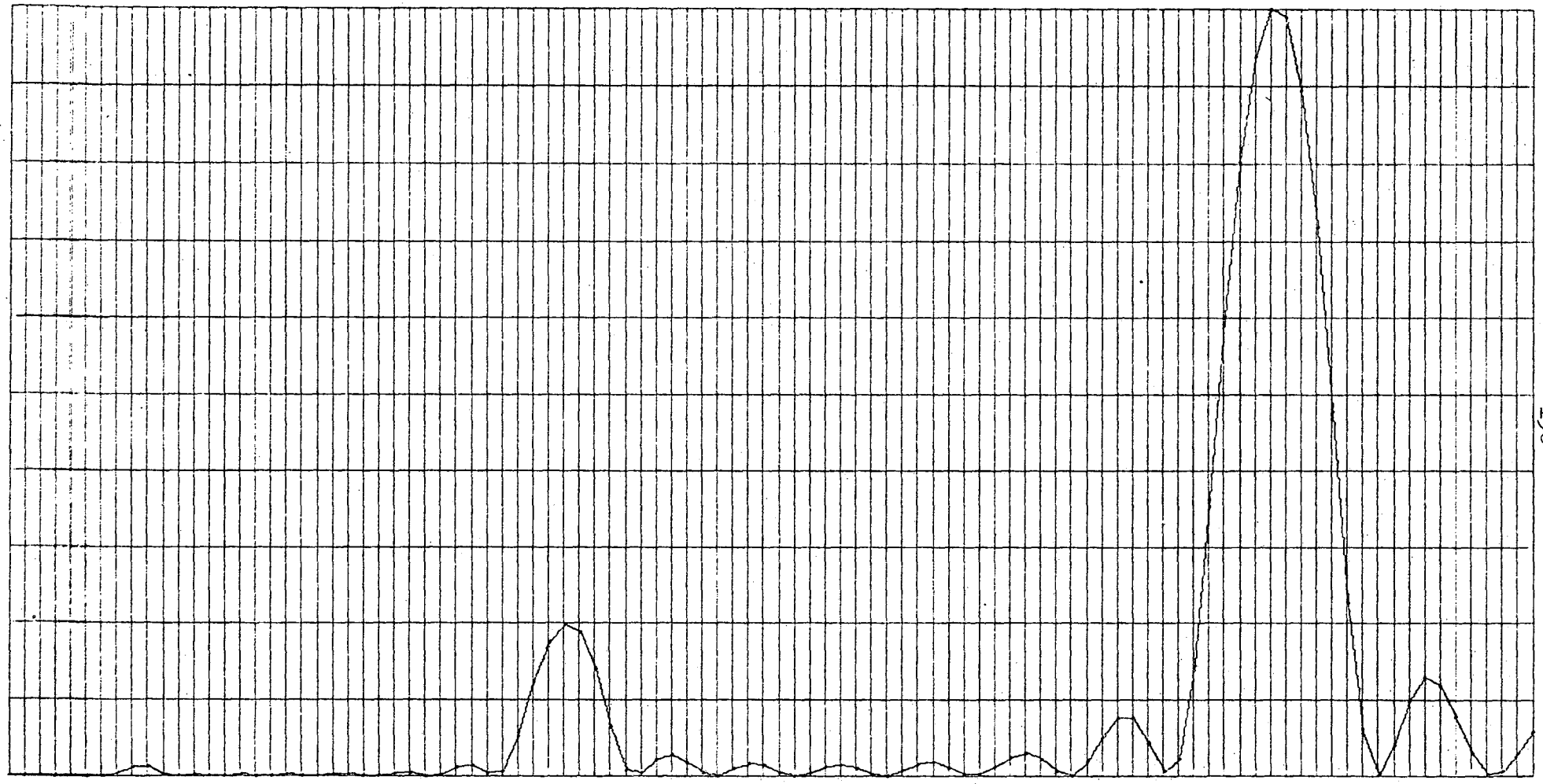

Fig. A-5a. Calculated I_{00} vs eV for Al(100) at $\theta = 0°$ between 1 and 100 eV in the 2 beam approximation. Isotropic scattering potential, $\alpha = 1.0$, $T = 0°K$.

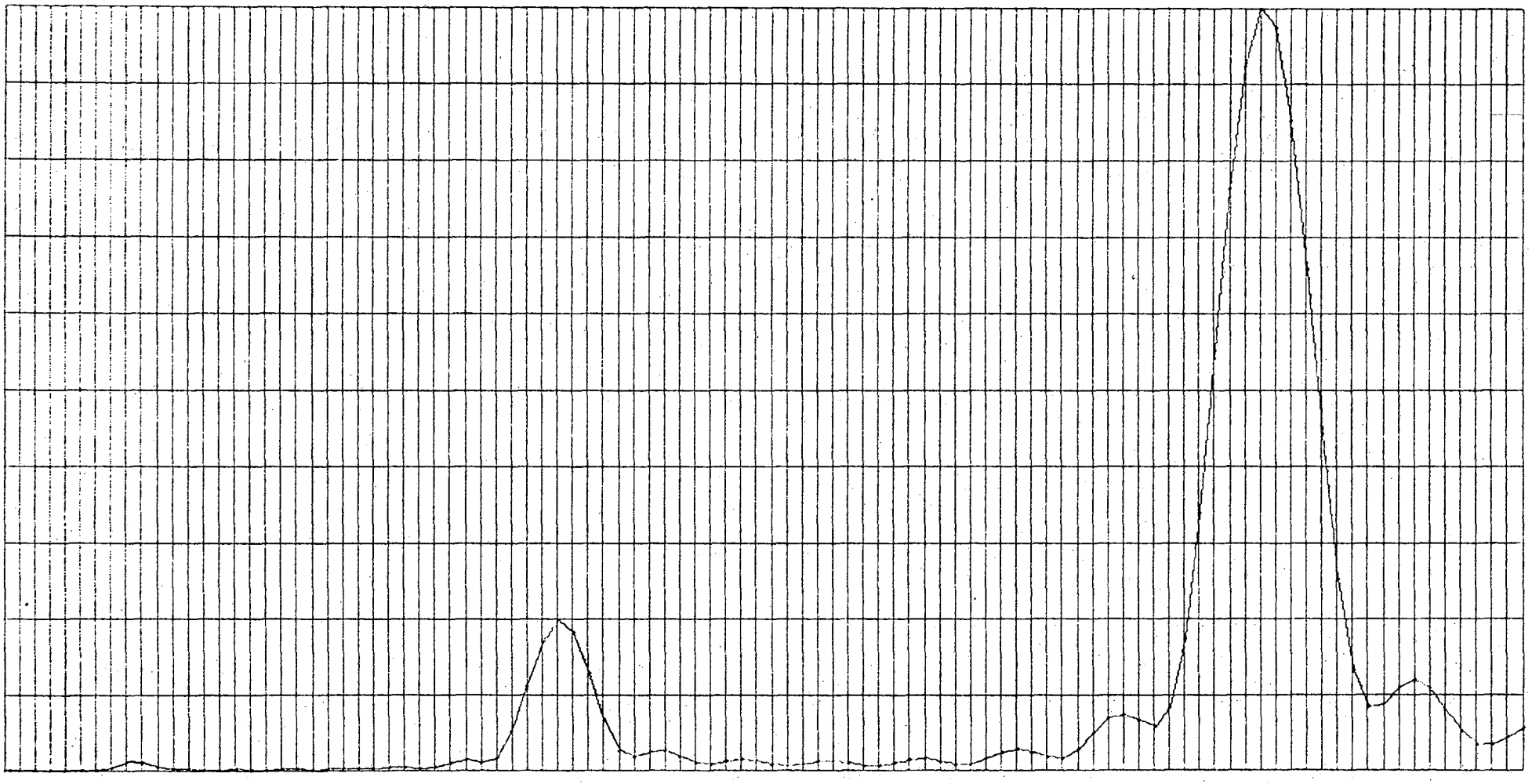

Fig. A-5b. Calculated I_{00} vs eV for Al(100) at $\theta = 0°$ between 1 and 100 eV in the 2 beam approximation. Isotropic scattering potential $\alpha = 0.9$, $T = 0°K$.

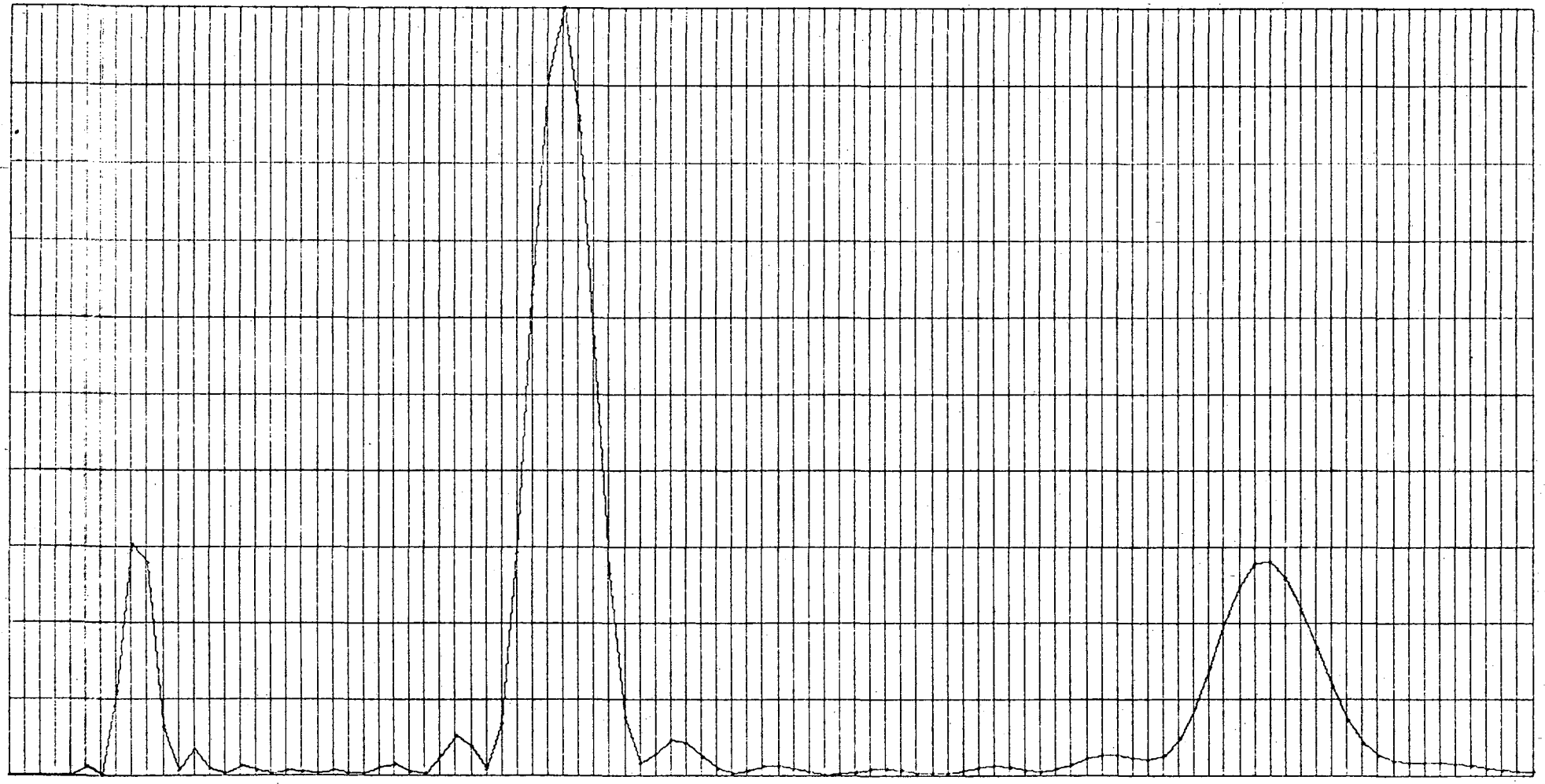

Fig. A-5c. Calculated I_{00} vs eV for Al(100) at $\theta = 0°$ between 1 and 100 eV in the 2 beam approximation. Isotropic scattering potential, $\alpha = 1.0$, $T = 300°K$.

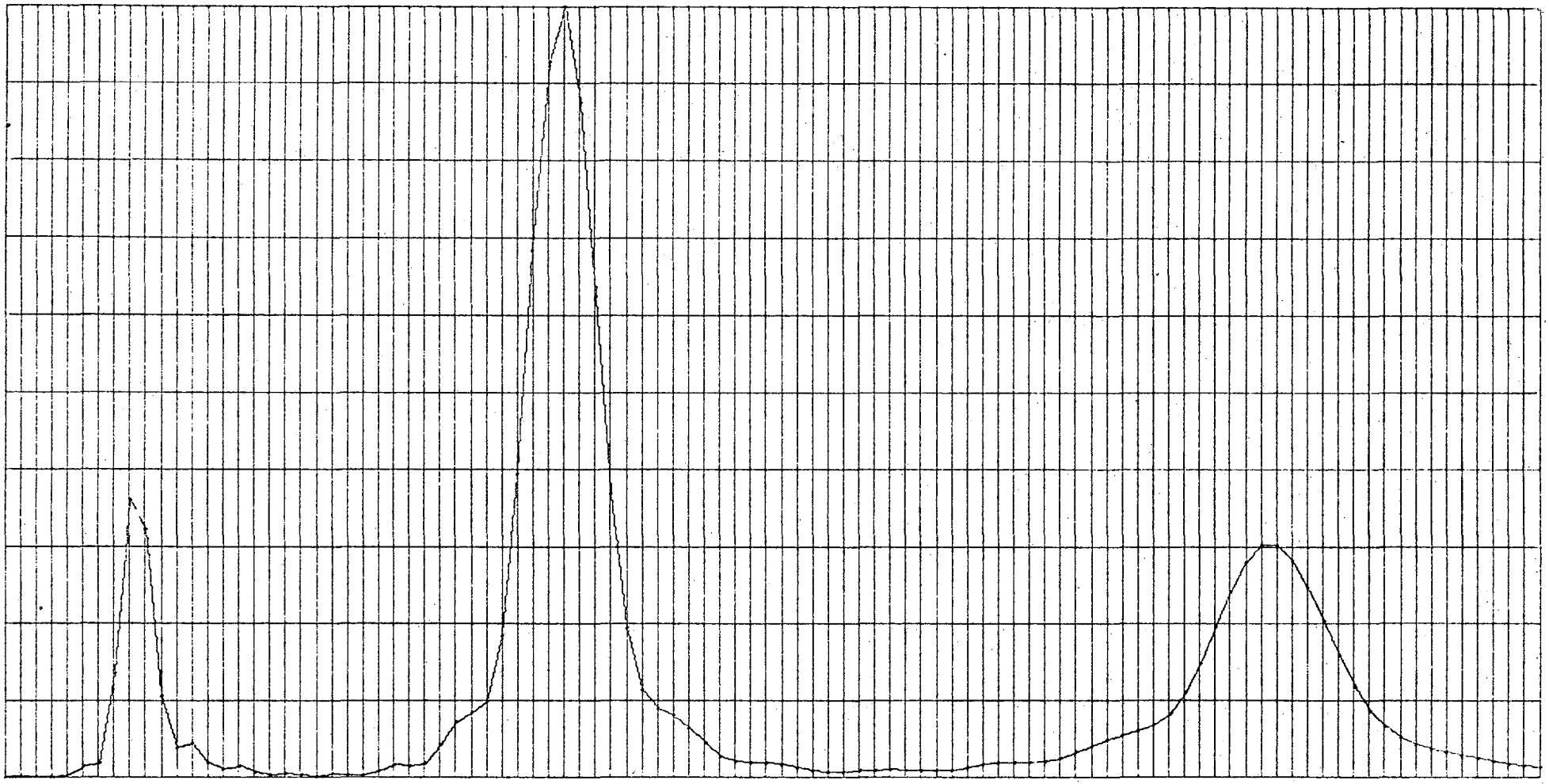

Fig. A-5d. Calculated I_{00} vs eV for Al(100) at $\theta = 0°$ between 1 and 100 eV in the 2 beam approximation. Isotropic scattering potential, $\alpha = 0.9$, T = 300°K.

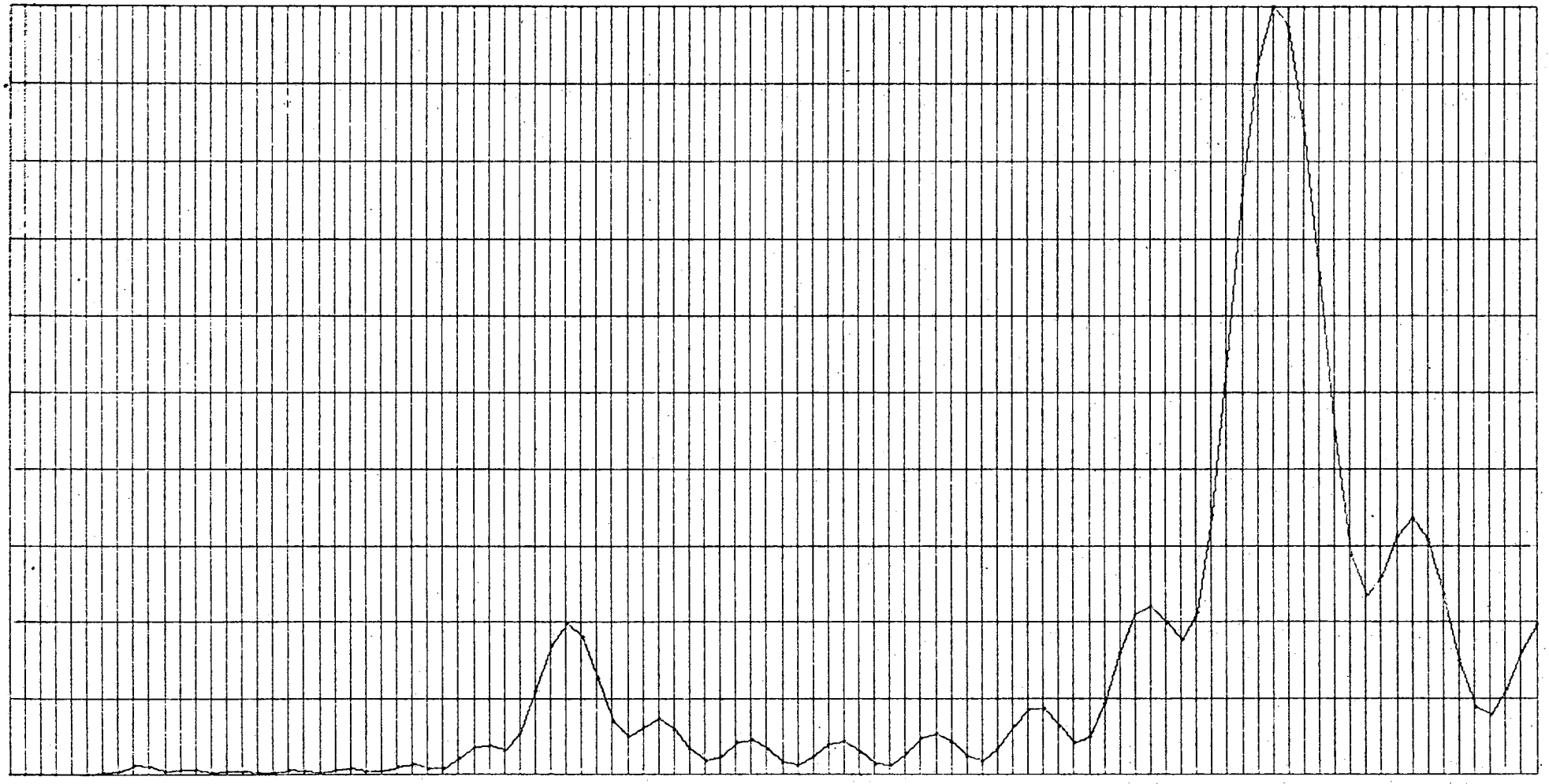

Fig. A-5e. Calculated I_{00} vs eV for Al(100) at $\theta = 0°$ between 1 and 100 eV in the 2 beam approximation. Gafner's potential $\alpha = 1.0$, $T = 0°K$.

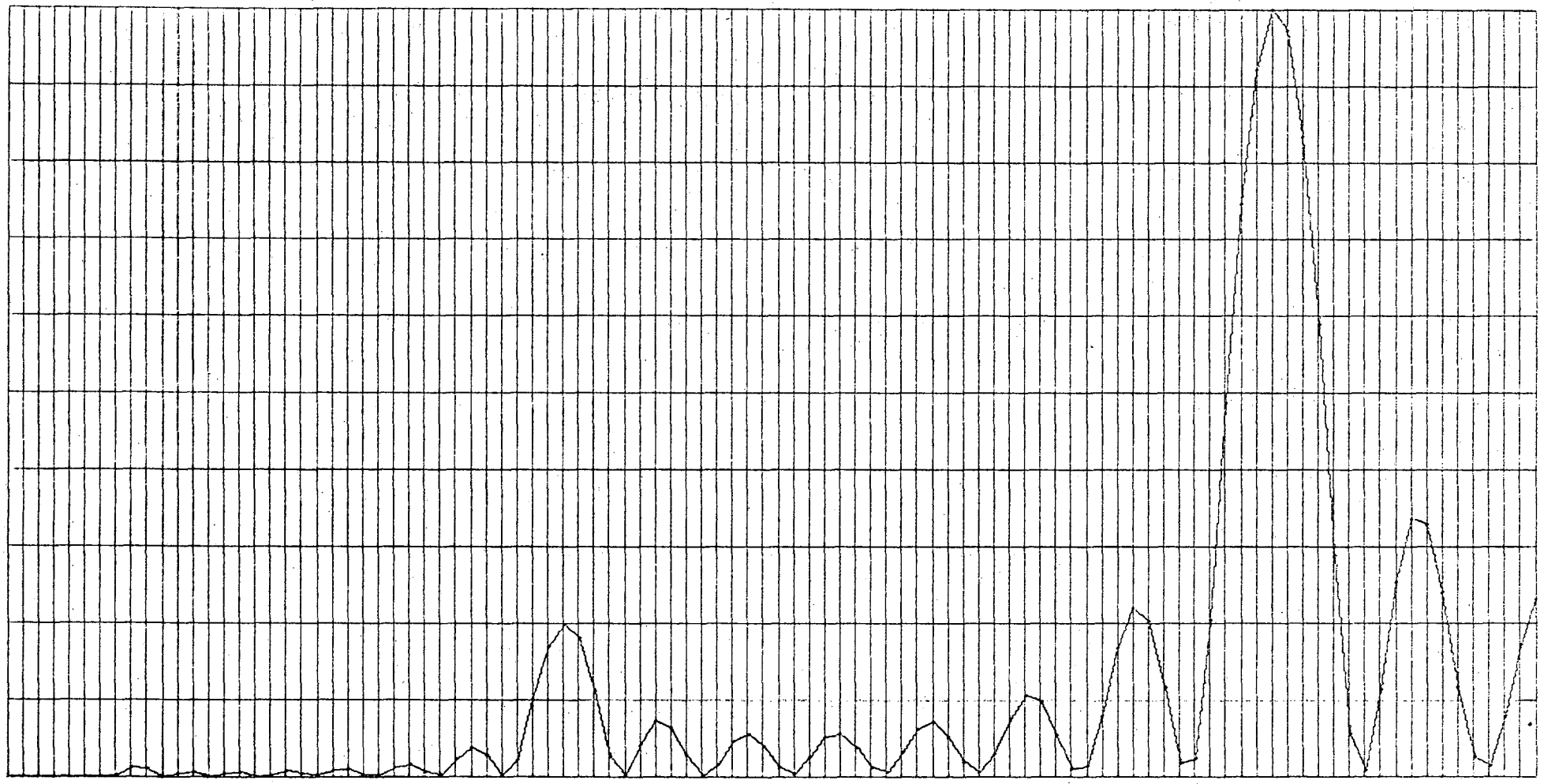

Fig. A-5f. Calculated I_{00} vs eV for Al(100) at $\theta = 0^{\circ}$ between 1 and 100 eV in the 2 beam approximation. Gafner's potential $\alpha = 0.9$, $T = 0^{\circ}K$.

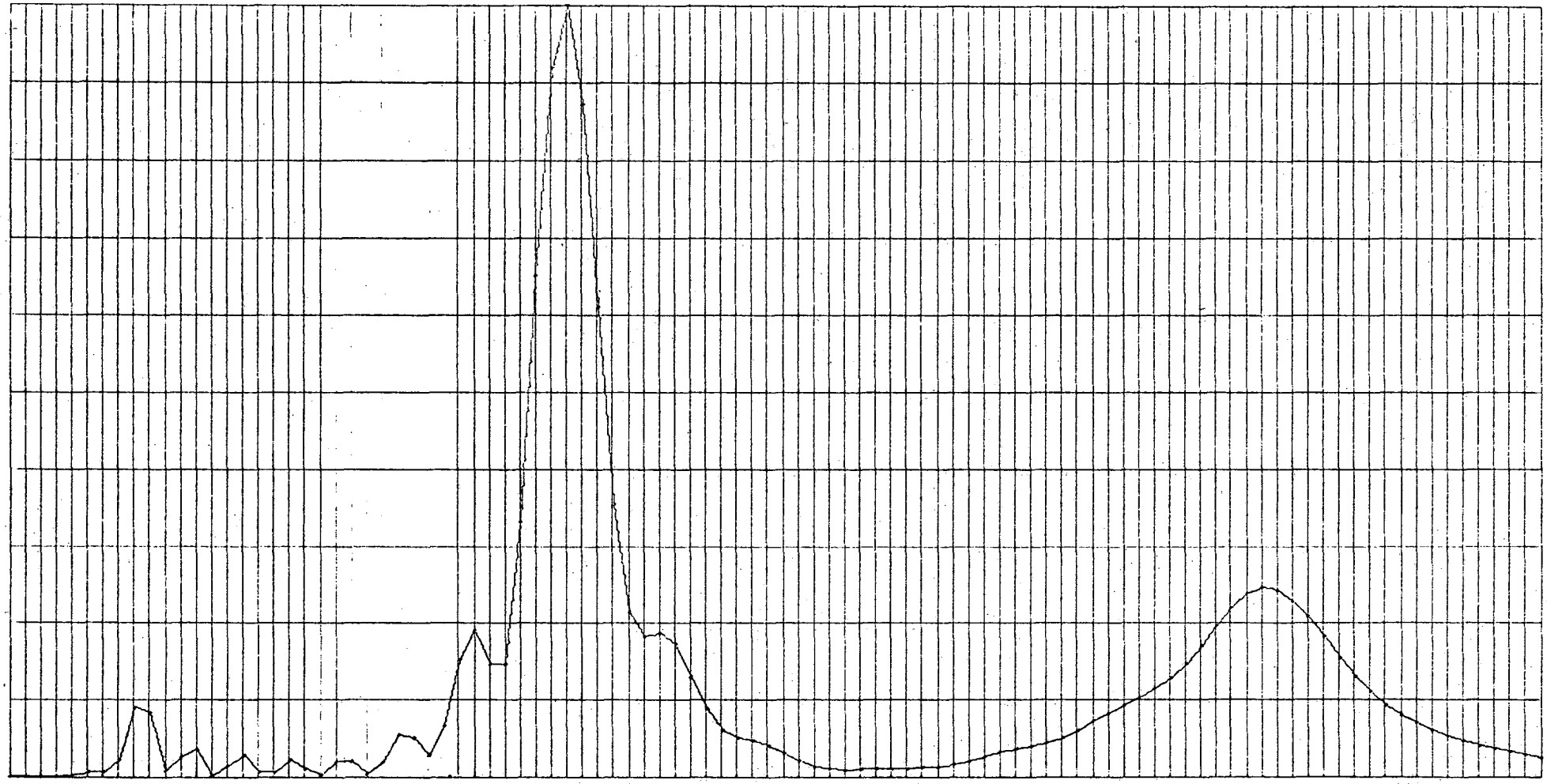

Fig. A-5g. Calculated I_{00} vs eV for Al(100) at $\theta = 0°$ between 1 and 100 eV in the 2 beam approximation. Gafner s potential $\alpha = 1.0$, T = 300°K.

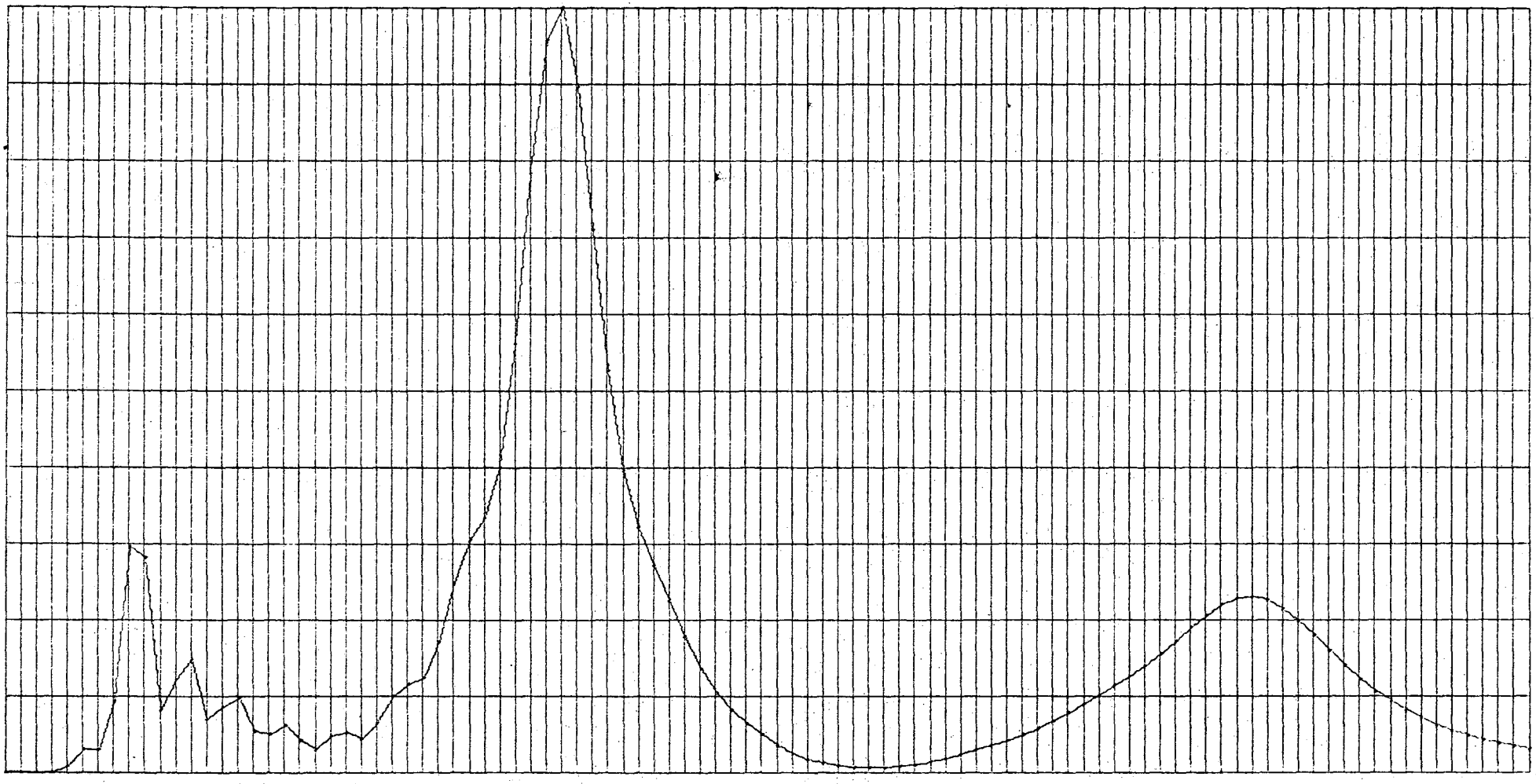

Fig. A-5h. Calculated I_{00} vs eV for Al(100) at $\theta = 0°$ between 1 and 100 eV in the 2 beam approximation. Gafner's potential $\alpha = 0.9$, T = 300°K.

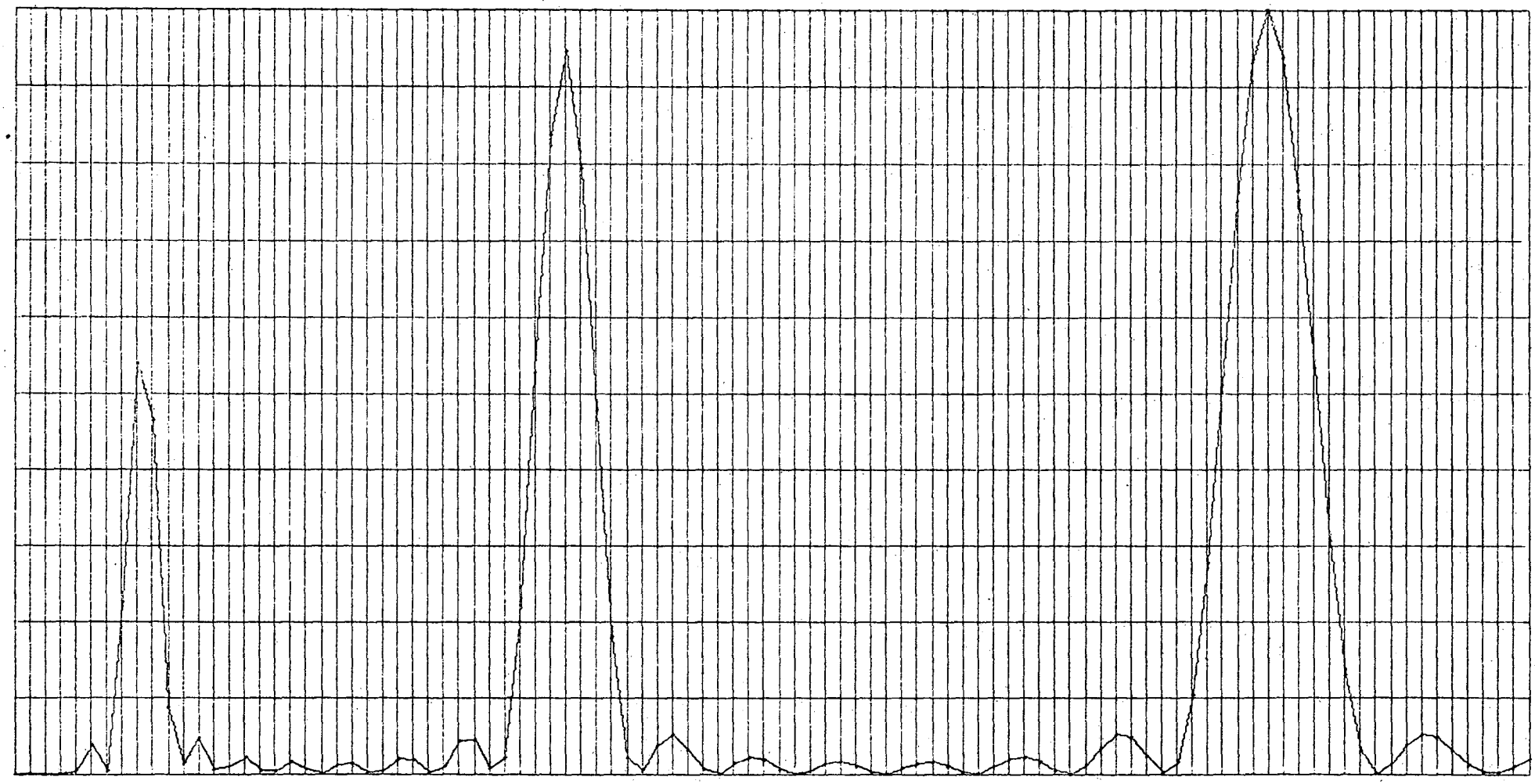

Fig. A-5i. Calculated I_{00} vs eV for Al(100) at θ = 0°between 1 and 100 eV in the 2 beam approximation. Sareened Coulombic potential, α = 1Å^{-1}, α = 1.0 T = 0°K.

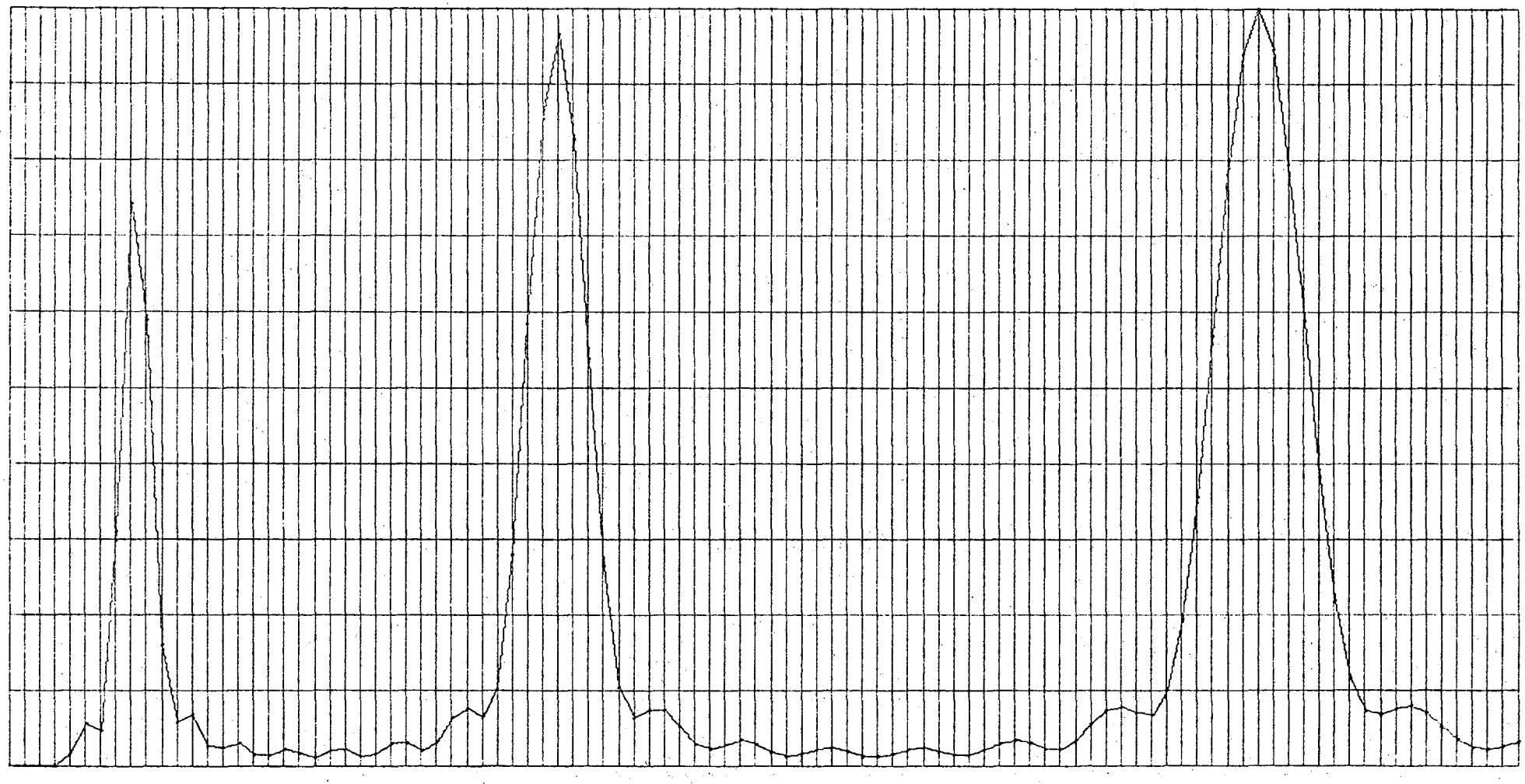

Fig. A-5j. Calculated I_{00} vs eV for Al(100) at $\theta = 0°$ between 1 and 100 eV in the 2 beam approximation. Screened Coulombic potential $\lambda = 1\text{Å}^{-1}$, $\alpha = 0.9$, $T = 0°K$.

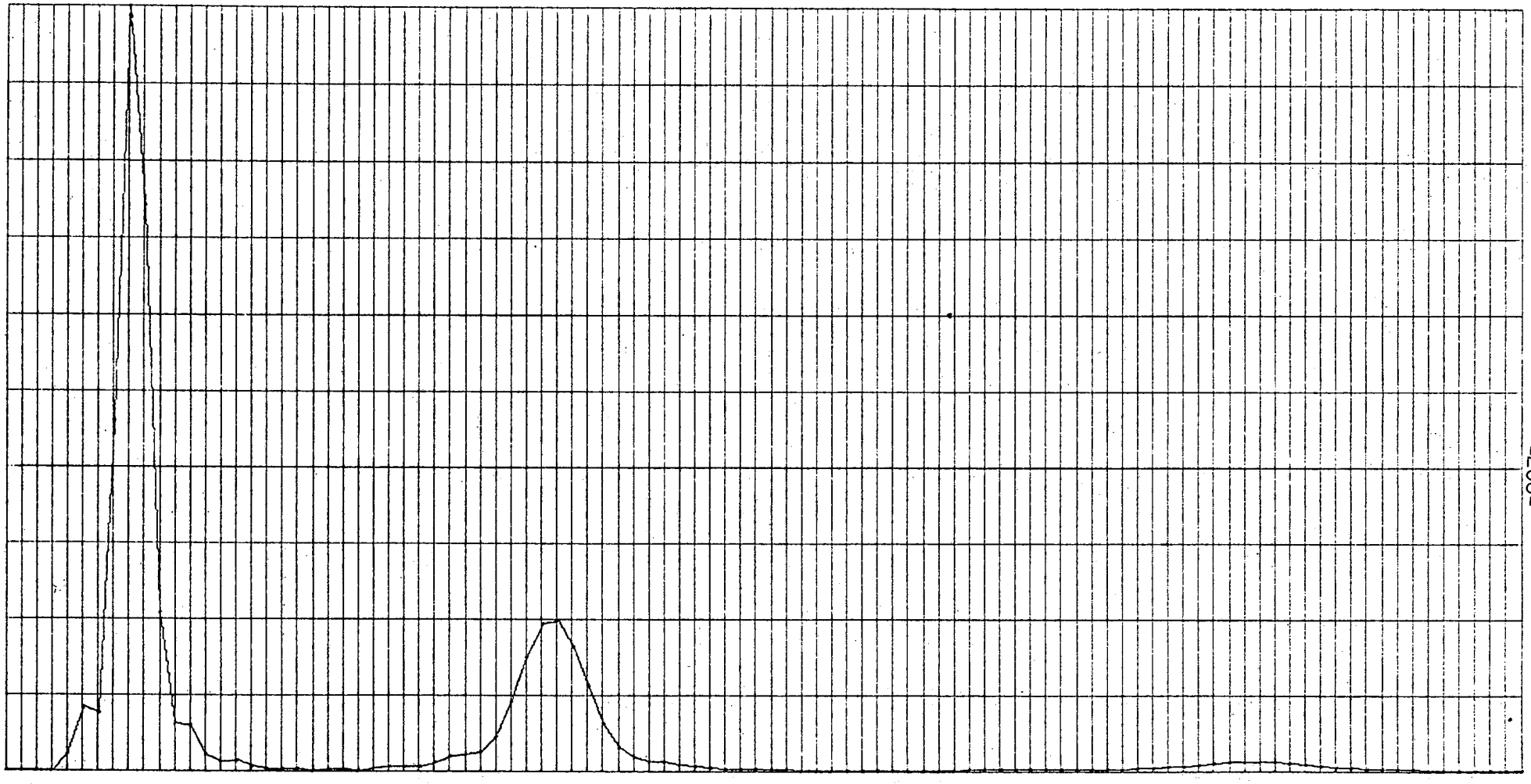

Fig. A-5k. Calculated I_{00} vs eV for Al(100) at $\theta = 0°$ between 1 and 100 eV in the 2 beam approximation. Screened Coulombic potential $\lambda = 1\text{Å}^{-1}$, $\alpha = 1.0$, $T = 300°K$.

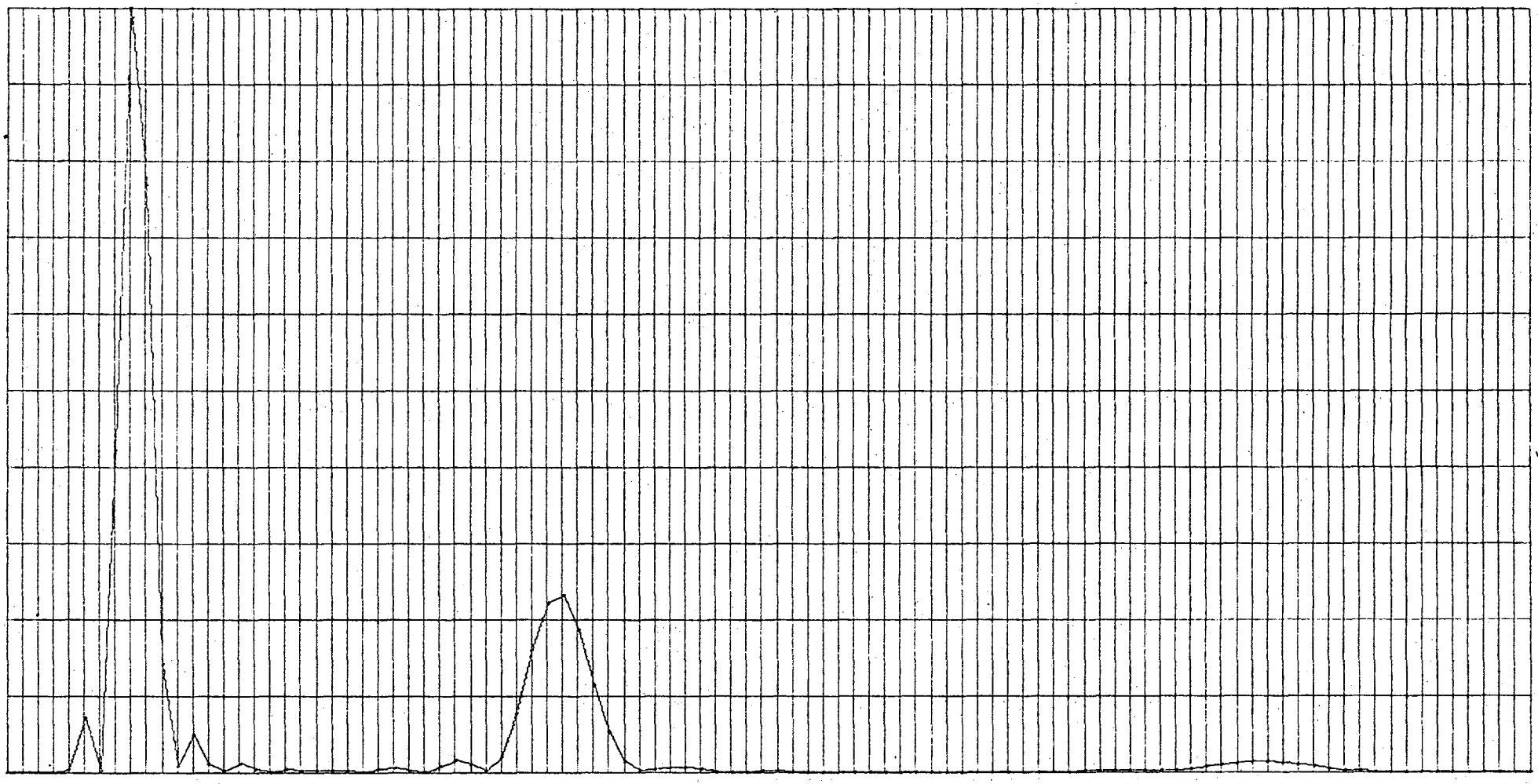

Fig. A-51. Calculated I_{00} vs eV for Al(100) at $\theta = 0°$ between 1 and 100 eV in the 2 beam approximation. Screened Coulombic potential, $\lambda = 1\text{Å}^{-1}$, $\alpha = 0.9$, $T = 300°K$.

voltage independent Gaffner and isotropic potentials. This reflects the fact that the screened Coulombic potential becomes more forward scattering at higher energies.

Both the screened Coulombic and Gaffners potential favor forward scattering. Note that the intensity maxima for these potentials tend to be more narrow than for the isotropic potential. In addition, the "ripples" due to the use of a finite lattice are less pronounced for these forward scattering potentials. This is because the isotropic scatterers tend to allow even less penetration. Further, the base line between intensity maxima is higher for the isotropic potential than for the other two for the same reason.

The introduction of attenuation either through the use of inelastic or thermal scattering, or both tends to decrease the peak height. It also tends to broaden the beams and diminish the "rippling." In the form used in this model, inelastic scattering causes a constant attrition throughout the voltage range while thermal scattering attenuates more at higher energies than at lower energies. The use of a voltage dependent parameter to describe the inelastic processes would undoubtably be more realistic, but, as a precise analytical form was not available, a voltage independent parameter was used.

APPENDIX III

If an electron is scattered from a state characterized by a wave vector $\vec{K}^\circ$ to a state characterized by a wave vector $\vec{K}$, and if this scattering takes place at some position $\vec{r}_s$, then the eigenfunction of the scattered wave will contain a phase factor $e^{i \vec{G}\cdot\vec{r}_s}$ where $\vec{G} = \vec{K}' - \vec{K}^\circ$. At temperatures other than $0^\circ K$, the position vector $\vec{r}_s$ will not be a constant but will contain a small oscillatory contribution due to the thermal motion of the atoms in the solid. One may then express $\vec{r}_s$ as

$$\vec{r}_s = \vec{r}_s^\circ + \vec{v}_s$$
$$= \vec{r}_s^\circ + \Sigma_g \left[\vec{U}_g e^{i \vec{g}\cdot\vec{r}_s^\circ} + \vec{U}_g^* e^{-\vec{g}\cdot\vec{r}_s^\circ}\right]$$

where $\vec{r}_s^\circ$ is the equilibrium position, $\vec{g}$ is the wave vector of the mode of vibration under consideration and $\vec{U}_g$ is the associated vector amplitude. The phase factor may now be expressed as

$$e^{i \vec{G}\cdot\vec{r}_s} = e^{i\vec{G}\cdot(\vec{r}_s^\circ + \Sigma_g[\vec{U}_g e^{i\vec{g}\cdot\vec{r}_s^\circ} + \vec{U}_g^* e^{-\vec{g}\cdot\vec{r}_s^\circ}])}$$
$$= e^{i \vec{G}\cdot\vec{r}_s^\circ} \pi_g e^{i \vec{G}\cdot(\vec{U}_g e^{i\vec{g}\cdot\vec{r}_s^\circ} + \vec{U}_g^* e^{-i \vec{g}\cdot\vec{r}_s^\circ})}$$

For small displacements, we may make the expansion

$$e^{i\vec{G}\cdot(\vec{U}_g e^{i \vec{g}\cdot\vec{r}_s^\circ} + \vec{U}_g^* e^{-i\vec{g}\cdot\vec{r}_s^\circ})} = 1 - i \vec{G}\cdot(\vec{U}_g e^{i \vec{g}\cdot\vec{r}_s^\circ} + \vec{U}_g^* e^{-i \vec{g}\cdot\vec{r}_s^\circ})$$
$$- 1/2 \left|\vec{G}\cdot\vec{U}_g\right|^2 + \ldots$$

The leading term, 1, will contribute to the static crystal diffraction pattern. The second term that is linear in $\vec{G}$ will contribute to the thermal diffuse scattering. The effect of this term is to increase the background intensity, particularly in the neghborhood of the diffraction spots. This phenomenon has been considered in detail elsewhere.[40]

The third term, $-1/2 \left|\vec{G}\cdot\vec{U}_g\right|^2$ will contribute to the Debye Waller effect. As we are actually dealing with a product of these terms, it is

conventional to make the definition

$$e^{-W} = \pi_g \{1 - 1/2 |\vec{G}\cdot\vec{U}_g|^2\}$$

where $2W$ is commonly called the Debye Waller factor. This term modifies the amplitudes of the diffracted beams. As the lattice vibrational amplitudes increase with increasing temperature, it may easily be seen that there will be a corresponding decrease in the amplitude of the diffracted electron beams.

As shown by Ziman[61] for example in the simple harmonic oscillator limit, W may be evaluated in the following manner for one atom per unit cell. The energy associated with the lattice vibrations may be written as

$$E = \Sigma_g N m \omega_g^2 |\vec{U}_g|^2$$

and

$$E = \Sigma_g (n_g + 1/2) \hbar \omega_g$$

where N is Avagadro's number, $\hbar$ is Plancks constant divided by 2π, m is the mass of the atom and n_g and ω_g are the vibrational frequency and the quantum number of the gth lattice model respectively. Assuming a Debye frequency distribution and evaluating in the high temperature limit, it may be shown that[61]

$$W = \frac{3}{2} \frac{\hbar^2 T}{mk} \left(\sum_{i=1}^{3} [\,|\vec{G}_i|^2/\theta_i^2]\right)$$

where, for cubic systems

$$\sum_{i=1}^{3} |G_i|^2/\theta_i^2 = \frac{G_x^2}{\theta_x^2} + \frac{G_y^2}{\theta_y^2} + \frac{G_z^2}{\theta_z^2}$$

Here, $\vec{G} = \vec{G}_x + \vec{G}_y + \vec{G}_z$ is the scattering vector between the initial and the final states, T is the absolute temperature, k is Boltzman's constant and θ_x, θ_y and θ_z are the effective Debye temperatures in the x,y and z directions respectively.

Each time an electron is scattered, it will acquired a term like e^{-W}. In the kinematic limit, the intensity of a diffraction beam will be proportional to e^{-2W}. It is therefore customary to evaluate w from the temperature dependence of the intensity as

$$W = T/2 \left[d/dT \ln I_{hk} (T,K)\right]$$

Some interesting complications arise when this approach is applied to the intensities of low energy electron diffraction beams. These involve the unique nature of the surface and the existence of multiple scattering. As the surface layer is in an asymmetric environment, having no atoms above it, there is no reason to assume that the root mean square vibrational amplitudes for the surface atoms will be the same as those in the bulk of the crystal, particularly for those modes with vibrations perpendicular to the surface. The temperature dependence of the specularly reflected intensity has been measured as a function of electron energy for several materials.[62-64] It has been found in all cases that W increases when the electron energy is decreased in the very low electron energy region. Within the kinematic model, this would correspond to an increase in the effective r m s vibrational amplitudes or to a decrease in the effective Debye temperature that is measured at lower beam energies. The argument is usually made that the electron beam is scattered more from the neighborhood of the surface at lower beam voltages than at high beam voltages. Consequently, the voltage dependence of W has been interpreted as reflecting the fact that the atoms in the surface layer experience larger r m s vibrational amplitudes than do those in the bulk of the crystal. This type of measurement provides one of the few technqiues for investigating the lattice dynamics of the surface. Consequently, it is of some interest to investigate the assumptions that are contained in this model.

One of the basic assumptions of this simple model is that the scattering is kinematic in nature. As there is ample evidence that multiple scattering is non-negligible, particularly in the low energy region where one presumably is measuring surface effects, it is of importance to consider the effect of multiple scattering upon the temperature dependence of the intensities of the low energy electron diffraction beams.

Using an approach similar to that of Beeby[9] and McRae,[4] one may express the total eigenfunction for a diffraction beam in a Born type expansion as

$$\psi_n(\vec{r},\vec{K}) = \psi_0(\vec{r},\vec{K}) + \psi_1(\vec{r},\vec{K}) + \psi_2(\vec{r},\vec{K}) + \ldots$$

where

$$\psi_n(\vec{r},\vec{K}) = -1/4\pi \int G(\vec{r},\vec{r}')\, V(\vec{r}')\, \psi_{n-1}(\vec{r}')\, d^3\vec{r}'.$$

Here, $\psi_0(\vec{r},\vec{K})$ is the eigenfunction of the incident beam. The term $\psi_1(\vec{r},\vec{K})$ corresponds to that portion of the total eigenfunction that has been kinematically or singly scattered. Double scattering events would be contained $\psi_2(r,K)$ and higher order events would be represented by the other terms in the expansion. As in Eq. 46, it may be shown that

$$\psi_1(\vec{r},\vec{K}') = \left(1/2K'_z\right) e^{i(\vec{K}^\circ+\vec{G})\cdot\vec{r}} \sum_s e^{i\vec{G}\cdot\vec{r}_s} V_{s,G}$$

or

$$\psi_1(\vec{r},\vec{K}) = \left(1/2K'_z\right) e^{i(\vec{K}^\circ+\vec{G})\cdot r} \sum_s e^{i\cdot\vec{G}\cdot\vec{r}_s^\circ} e^{-W_s} V_{s,G}$$

If one makes the assumption that all of the layers are identical, then

$$\psi_1(\vec{r},\vec{K}') = A_G\, e^{i(\vec{K}^\circ+\vec{G})\cdot\vec{r}}$$

where

$$A_G = e^{-W} \frac{V_G}{2K'_z} \sum_s e^{i\vec{G}\cdot\vec{r}_s^\circ}$$

In a similar manner, it may be shown that the double diffraction term is given as

$$\psi_1(\vec{r},\vec{K}) = \Sigma_{G_i}' A_{G-G_i}' A_{G_i}' e^{i(\vec{K}^\circ+\vec{G})\cdot\vec{r}}.$$

In general,

$$\psi_n(\vec{K};\vec{r}) = [\pi_{i=1}^{n} (\Sigma_{G_i} A_{G_i} e^{i\vec{G}_i\cdot\vec{r}})] e^{i\vec{K}^\circ\cdot\vec{r}}.$$

The intensities of the various beams characterized by G are given by

$$I = \int_{\vec{r}} \psi_T^*(\vec{r},\vec{K}^\circ+\vec{G}) \psi_T(\vec{r},\vec{K}^\circ+\vec{G}) d^3 r$$

$$= \int_{\vec{r}} (\Sigma_n \psi_n^*(\vec{r},\vec{K}')) (\Sigma_m \psi_m(\vec{r},\vec{K}')) d^3 r$$

$$= \Sigma_{n,m} \int_{\vec{r}} \psi_n^*(\vec{r},\vec{K}') \psi_m(\vec{r},\vec{K}') d^3 r$$

where the eigenfunctions have been expanded in the Born type series. On the basis of this expansion, the intensity itself may be expressed as a series as

$$I_T = \Sigma_n I_n ,$$

Here, the first term

$$I_1 = |A_G|^2$$

is the kinematic term and would contribute to the intensity even in the absence of multiple scattering. This term, of course, carries the kinematic temperature dependence as

$$I_1 = I_1^\circ e^{-2W}$$

where W is a linear function of temperature in the Debye approximation. I_1 arises as the product of the amplitudes for single scattering events.

The second term, I_2 is generated as the product of the amplitude for single scattering events with the amplitude for double scattering events and may be written as

$$I_2 = \Sigma_{G_i}' |A_G^* A_{G-G_i}' A_{G_i}'|.$$

This term will be referred to as the double diffraction contribution to the total intensity. It has the temperature dependent form

$$I_2 = I_2^{\circ} \; e^{-W_1} \, e^{-W_{12}} \, e^{-W_2}$$

where W_1 is proportional to $|\vec{G}|^2$, W_{12} to $|\vec{G}' \; \vec{G}|^2$ and W_2 to $|\vec{G}'|^2$ in the approximation that the crystal is isotropic and that all of the layers are identical.

There will be two contributions to the third term in the expansion of the intensity. The first will arise as a product of the single scattering amplitude and the triple scattering amplitude. The second term comes from a product of the double scattering amplitudes. Consequently, this intensity term will have the form

$$I_3 = \sum_{G_1 G_2} |A_G^* \, A_{G-G_1-G_2} \, A_{G_1}| + \sum_{G_1, G_2} |A_{G-G_1} \, A_{G_1}^* \, A_{G-G_2} \, A_{G_2}|.$$

Its temperature dependence may be determined in a manner similar to that for I_2. Higher order scattering contributions to the intensity will have increasingly complex forms and will bring correspondingly more complicated temperature dependent terms into the total intensity. As A_G must be less than or equal to unity, these higher order terms should be generally less important. However, there do exist cases where a term may be more important than the preceding lower order terms. For example, there are observed "secondary" Bragg peaks in the specularly reflected intensity that do not correspond to kinematic diffraction conditions. When multiple scattering is reasonably strong, diffraction conditions of the form

$$K_z^{00} + K_z^{hk} = G_z$$

can lead to intensity maxima in the (00) beam. Note that, even though this condition is kinematic for the (h k) beam, it must involve at least

double diffraction to produce an intensity maximum in the (00) beam. Consequently, the double diffraction contribution to the total intensity, I_2, may be expected to be larger than the kinematic contribution, I_1. Higher order contributions may also be significant. Therefore, it may be expected that the experimentally determined quantity, $-T\, d/dT \ln I$, will more closely resemble $W_1+W_{12}+W_2$ rather than the kinematic $2W$, assumed in the simple model. As one might expect terms like $W_1+W_{12}+W_2$ to be larger than $2W$, it would seem at first glance that multiple scattering alone could lead to the apparent determination of lower "effective" Debye temperatures or higher "effective" r m s displacements for the surface. This is however not necessarily true in all cases. For simplicity, let us retain the assumption that the crystal is isotropic and that all of the layers are identical. We may then write

$$W = 3/2 \frac{\hbar^2 T}{mk} \left[\frac{G_x^2}{\theta_x^2} + \frac{G_y^2}{\theta_y^2} + \frac{G_z^2}{\theta_z^2}\right]$$

as

$$W = B \left|\vec{G}\right|^2$$

Within this approximation

$$2W_1 = 2B \left|G\right|^2$$

and

$$W_1 + W_{12} + W_2 = B \left(\left|\vec{G}_1\right|^2 + \left|\vec{G}_1 - \vec{G}_2\right|^2 \left|\vec{G}_2\right|^2\right)$$

It may easily be seen that three cases arise. When

$$\left|\vec{G}_1\right|^2 - \vec{G}_1 \cdot \vec{G}_2 < \left|\vec{G}_1\right|^2,$$

then $W_1 + W_{12} + W_2$ will be less than $2 W_1$. In this case the experimentally determined effective Debye temperature derived from the simple model would be less than the actual effective Debye temperature. Alternatively, the apparent r m s displacements would be greater than those actually contri-

buting to the temperature dependence of the intensity.

In the second case, $|\vec{G}_2|^2 - \vec{G}_1 \cdot \vec{G}_2 > |\vec{G}_1|^2$ and $W_1 + W_{12} + W_2$ is greater than $2W_1$. Here, the experimentally determined value for the r m s displacements would be less than the real value.

In the third case $|\vec{G}_2|^2 - \vec{G}_1 \cdot \vec{G}_2 = |\vec{G}_1|^2$ and $W_1 + W_{12} + W_2$ is equal to $2W_1$. In this case, the use of the simple kinematic model to determine the effective Debye temperature and the atomic displacements would lead to the same results as the use of a more complicated kinematic model.

At normal incidence, double diffraction contributions to the specularly reflected beam fall in the last case. Thus, if one neglects any possible asymmetry of the surface, one would expect that the contributions from this type of mechanism would give results that were experimentally indistinguishable from those arising from kinematic scattering. Away from normal incidence, double diffraction contributions will no longer fall into the third case, but will give rise to contributions of both the first and the second type. Whether the experimentally determined r m s displacements will be greater than or smaller than the actual displacements will depend upon the detailed nature of the scattering potential. For simple forward scattering potentials, such as the screened Coulombic potential, one would expect those terms giving smaller apparent r m s displacements to dominate.

Higher order scattering events can also lead to apparent displacements that are either greater than or less than the real displacements. In the limit of an isotropic crystal with identical layers, the relationship between $\Sigma_i W_i$ and $2W$ may be determined in a manner similar to that for the double diffraction situation. Again, one would expect that those terms leading to smaller apparent r m s displacements would dominate when

the scattering potential was of a smooth, forward scattering type. Similar arguments may be made concerning the effect of multiple scattering on the temperature dependence of the intensity of the higher order diffraction beams.

The assumption that all of the layers of the crystal are identical is unrealistic, particularly in the presence of a surface structure.

Let us then consider the case where the first layer is different from all of the other layers. For simplicity, the factors $V_G/2K'_z$ will be taken to be unity. The kinematic contribution to the eigenfunction for a given diffraction beam may then be written as

$$\psi_1(\vec{r},\vec{K}') = e^{i(\vec{K}^\circ+\vec{G})\cdot\vec{r}} \sum_{S=1}^{\infty} e^{i\vec{G}\cdot\vec{r}_s^\circ} e^{-W_s}$$

or

$$\psi_1(\vec{r},\vec{K}') = \left[e^{i\vec{K}'\cdot\vec{r}} e^{-W_0} e^{i\vec{G}\cdot\vec{r}_1^\circ} 1 + e^{-W} \sum_{S=2}^{\infty} [e^{i\vec{G}\cdot\vec{R}}]\, S\text{-}1\right]$$

where W_0 is the Debye Waller factor for the first layer, W is the Debye Waller factor for all of the other layers, $\vec{r}_1^\circ$ is the coordinate of the surface and $\vec{R}$ is the translational vector between layers. Making the definitions that $\alpha = e^{-W_0}$, $\beta = e^{-W}$, $\phi_0 = e^{i\vec{G}\cdot\vec{r}_1^\circ}$ and $\phi = e^{i\vec{G}\cdot\vec{R}}$, it may be shown that

$$\psi_1(\vec{r},\vec{K}') = e^{i\vec{K}'\cdot\vec{r}} [\alpha\phi_0 - \beta\phi/1\text{-}\phi]$$

The corresponding single scattering contribution to the intensity may be written as

$$I_1 = \left|\alpha\phi_0 - \frac{\beta\phi}{1-\phi}\right|^2$$

when all of the interplanar spacings are equivalent, this reduces to

$$I_1 = \alpha^2 - \alpha\beta + \frac{\beta^2}{2(1+\cos(\vec{G}\cdot\vec{R}))}.$$

This, of course, is essentially Darwin's result with the inclusion of the Debye-Waller factor previously considered by ALyon and Somorjai.[63]

Proceeding to higher order scattering events, the double scattering contribution to the total eigenfunction may be written as

$$\psi_2(\vec{r},\vec{K}) = e^{i(\vec{K}^\circ+\vec{G})\cdot\vec{r}} \left(\Sigma_s\, e^{i(\vec{G}-\vec{G}_1)\cdot\vec{r}_s^\circ}\, e^{-W_{12}}\right)\left(\Sigma_t\, e^{i\vec{G}_1\cdot\vec{r}_t^\circ}\, e^{-W_2}\right)$$

or

$$\psi_2(\vec{r},\vec{K}) = e^{i(\vec{K}^\circ+\vec{G})\cdot\vec{r}} \left(\alpha_1 - \frac{\beta_1\phi_1}{1-\phi_1}\right)\left(\alpha_2 - \frac{\beta_2\phi_2}{1-\phi_2}\right)$$

where it has been assumed that all ofthe interplanar spacings are equivalent and α_i and β_i have been defined in a manner similar to that for the kinematic case. The double diffraction contribution to the total intensity partakes of the form

$$I_2 = \left|\left(\alpha - \beta\,\frac{\phi^*}{1-\phi^*}\right)\left(\alpha_1-\beta_1\,\frac{\phi_1}{1-\phi_1}\right)\left(\alpha_2-\beta_2\,\frac{\phi_2}{1-\phi_2}\right)\right| .$$

where α and β correspond to the singly scattered amplitude and the α_i and β_i correspond to the doubly scattered amplitude. This term has a particularly interesting form when applied to fractional order beams arising from the presence of a surface structure. These beams are forbidden in the bulk of the crystal. One may therefore make the simplifying assumption that scattering into these beams can only occur at the surface. When this is the case, I_2 reduces to

$$I_2 = \left|\alpha\,\alpha_2\,\beta_1\,\frac{\phi_1}{1-\phi}\right|$$

The terms α and α_2 correspond to scattering events at the surface layer wherethe electron is diffracted into back scattered fractional order beams. The term $(\beta_1\,\phi_1/1-\phi_1)$ corresponds to scattering events that can occur in the bulk of the crystal between the incident and some intermediate integral order beam. It may be seen that if the surface species is loosely bonded relative to the bulk species, then the intensities of the fractional order beams should exhibit a stronger temperature dependence when double diffraction occurs than would be observed for th e integral order beams.

This of course, is also true for the kinematic contribution where

$$I_1 = |\alpha|^2.$$

It may be shown that higher order contributions to the total intensity will be of the form

$$I_n = \left|\pi_{i=1}^{n+1} \left(\alpha_i - \beta_i \frac{\phi_i}{1-\phi_i}\right)\right|$$

The inclusion of the Fourier coefficients of the expansion of the potential would lead to terms of the form

$$\alpha_i V_G^{\circ} \phi_0 - \beta_i V_G \frac{(V_0^{\circ} V_0)^2 \phi_i}{1 - V_0^2 \phi_i}$$

where V_0 and V_0° were essentially the forward scattered amplitudes or transmission coefficients for the bulk and surface layers respectively and V_G and V_G° were essentially the scattering amplitudes between the initial and the final beams again for the bulk and the surface layers respectively.

The actual calculation of the temperature dependence of LEED intensities using these equations was not performed. However, it was calculated with a step wise scattering procedure described in Appendix II. Several different situations were considered. In the first case, the intensities were calculated for the classical Bragg maxima in the (00) beam using fifteen scattering events. The higher order diffraction beams were suppressed, and multiple scattering was allowed to occur only between the transmitted and the specularly reflected beams as is described in the two beam case in Appendix II. Calculations were performed for two different scattering potentials; a screened Coulombic potential with $\lambda = 1.5\text{Å}^{-1}$ and a screened Coulombic potential with $\lambda = 0.1\text{Å}^{-1}$. It was first assumed that the effective Debye temperature for the surface was

identical with that for the bulk. The plots of the natural logarithm of the intensity vs the temperature were found to give straight lines over the temperature range 100 to 600°C. Both potentials gave very similar results. For aluminum, the hypothetical Bragg maximum at 81 and eV gave an effective Debye temperature, determined from these plots with simple kinematic model, very close to the bulk value. The values for θ_0 for the Bragg maxima at 9 and 37 eV were somewhat lower, being depressed less than 6% of the 81 eV value. As depressions more on the order of 30% are usually observed experimentally, it may be concluded that simply multiple scattering of this type is inadequate to generate the decrease in the effective Debye temperature of the magnitude generally observed.

It was then assumed that the effective Debye temperature for the first layer was one half that of the bulk and similar calculations were performed. As before, the two different potentials gave very similar answers. Again, the ln I vs T curves were straight lines in the 100 to 600°C region. The effective Debye temperature "experimentally" determined for this model were considerably lower than those found when all layers were assumed to be identical. The 81 eV value was depressed by about 25% from that for the identical layer situation. The 9 eV value was only about two thirds of the identical layer 81 eV value. It may therefore be concluded that decreasing the effective Debye temperature of the first layer does give results which are similar to those observed experimentally.

The effect of multiple scattering on the temperature dependence of non-kinematic multiple scattering maxima was investigated. Calculations were performed for the double diffraction $K_z^{00} + K_z^{10} = G_z$ peak that occurs in the specularly reflected beam at 31 eV for aluminum with a screened

Coulombic potential with $\lambda = 0.1\text{Å}^{-1}$. When it was assumed that all of the layers were identical, the ln I_{00} vs T curve was straight, and the effective Debye temperature from this plot was determined to be somewhat larger than the 37 eV value obtained when all of the higher order beams were suppressed in the identical layer model. However, when it was assumed that the first layer had an effective Debye temperature that was one half of the bulk value, considerable curvature was noted in the ln I_{00} vs T curve. Here, the average effective Debye temperature was again somewhat higher than the corresponding 37 eV value obtained from the non-identical layer model with suppression of the higher order beams.

This double diffraction condition has been discussed above. There, it was concluded that when all of the layers were identical, the determined effective Debye Waller temperature should be identical with that from single scattering. The fact that the multiple scattering value calculated at 31 eV is larger than that at 37 eV indicates that scattering events higher than the second order was contributing to the calculated value. As mentioned before, in a real situation the determined value may be either greater than or less than the actual value depending upon the detailed nature of the scattering potential.

From these considerations and calculations, it may be concluded that strong multiple scattering will have a non-negligible effect on the validity of the Debye temperature calculated from experimental data with the assumption of only kinematic scattering. However, these calculations would seem to indicate that multiple scattering alone is insufficient to produce the apparent depression of the effective Debye temperature of the magnitude that is observed at low energies and that the rms atomic displacements of the surface atoms are indeed larger than those of the bulk.

ACKNOWLEDGEMENTS

First and foremost, I would like to express my special gratitude to Professor Gabor A. Somorjai for his inspiration and unflagging enthusiasm in the guidance of this project. To the Department of Chemistry and the Inorganic Materials Research Division of the Lawrence Radiation Laboratory, I am indebted for the academic, technical and financial support that I have recieved during my studies here. I am deeply grateful for having had the opportunity to meet and work with all of the members of my research group. A special thanks goes to Richard M. Goodman for his support and cooperation as well as for the time and effort that he expended in teaching me many of the fine points of low energy electron diffraction. To Whalun Szeto, Theodore M. French and J. Gordon Davy, I am also very grateful for the many hours of discussion that so often provided insight into dim corners. For their effort and technical assistance, Emery I. Kozak, L. Albert West and particularly Fredrick J. Szalkowski have more than earned my gratitude. My sincere personal thanks goes to my family and my friends, particularly Catherine Y. Lou and the "Wednesday nighters" for their understanding and friendship that have made my stay here more enjoyable than tolerable. Finally, I would like to thank the staff, especially Jane Ball and Pat Shand for maintaining a sense of humor while typing this overly long thesis.

This work was supported by the United States Atomic Energy Commission.

REFERENCES

1. C. Davisson and L. H. Germer, Proc. Natl. Acad. 14, 619(1928).
2. (a) E. G. McRae, J. Chem. Phys. 45, 3258 (1966); (b) Surface Sci. 8, 14 (1967) (c) Fundamentals of Gas Surface Interactions (Academic Press, N. Y., 1967) p. 116.
3. E. G. McRae, Surface Sci 11, 479 (1968).
4. E. G. McRae, Surface Sci 11, 492 (1968).
5. E. G. McRae and Winkler, Surface Sci. 14, 407 (1969).
6. D. S. Boudreaux and V. Heine, Surface Sci. 8, 426 (1967).
7. K. Kambe, Z. Naturforsch. 22a, 22 (1967).
8. K. Kambe, (a) Z. Naturforsch 22a, 322 (1967); (b) Z. Naturforsch, 22a 422 (1967); (c) Z. Naturforsch, 23a, 1280 (1968).
9. J. L. Beeby, J. Phys. C. (Proc. Phys. Soc) 1, [2] 82 (1968).
10. Y. H. Ohtsuki, J. Phys. Soc Japan, 24, [5] (1968).
11. P. M. Marcus and D. W. Jepsen, Phys. Rev. Letters, 20, 925 (1968).
12. F. Hoffman and H. P. Smith, Phys. Rev. Letters, 19, [26] 1472 (1967).
13. G. Carpart, Surface Sci. 13, 361 (1969).
14. G. Gafner, Proceedings of the Fourth Internation Materials Symposium, Berkeley, 1968, ed. by G. A. Somorjai.
15. C. Kittel, Introduction to Solid State Physics, (John Wiley and Sons, Inc., New York, 1956) 2nd ed.
16. Hirabayashi and Takeishi, Surface Sci. 4, 150 (1966).
17. H. Bethe, Ann. Pays. 87, 55 (1928).
18. M. Von Laue, Phys. Rev. 37, 53 (1931).
19. E. Merzbacher, Quantum Mechanics, John Wiley and Sons Inc., 1961.
20. C. G. Darwin, Phil. Mag., 27, 315 (1914).
21. R. L. Park and H. H. Madden, Jr., Surface Sci. 11, (2), 188 (1968).

22. J. J. Lander in Advances in Solid State Chemistry, Vol. II, MacMillan Co., New York, 1965.

23. H. Morgenaue and G. M. Murphy, The Mathematics of Physics and Chemistry, Van Nostrand Co, Inc. Princeton, N. Y. (1957).

24. R. M. Goodman, H. H. Farrell and G. A. Somorjai, J. Phys. Chem. 49, 692 (1968).

25. E. Bauer, Colloque Intern. CNRS 1965 No. 152, p. 19.

26. Varien, Low Energy Electron Diffraction System No. 981-0000, 611 Hansen Way, Palo Alto, California.

27. Phillips Metalonics, Impregnated Cathode, Type B, 88 S. Columbus Ave., Mt. Vernon, N. Y.

28. H. B. Lyon, Thesis, University of California, Berkeley, 1967.

29. Gamma Scientific, No. 2000 (with fiber optics and variable aperture [6' → 3°], San Diego.

30. A. Mattera, R. M. Goodman and G. A. Somorjai, Surface Sci. 7, 26 (1967).

31. P. Palmberg, (private communication).

32. F. L. Zsalkowski (private communication).

33. I. Bergstrom and C. Nordling, Alpha-Beta and Gamma Ray Spectroscopy, Vol. 2, North Holland Publishing Co, Amsterdam, 1965, ed. Kai Siegbahn.

34. T. M. French (private communication).

35. F. Jona, J. Phys. Chem. Solids, 28, (1967) 2155.

36. S. M. Bedair, F. Hoffman and H. P. Smith, J. Appl. Phys. 39 4026 (1968).

37. E. E. Huber and C. T. Kirk, Surface Sci. 5, (1966) 447.

38. E. E. Huber and C. T. Kirk, Surface Sci. 8, (1967) 453.

39. M. W. Roberts and B. R. Wells, Surface Sci. 8, (1967) 453.

40. R. M. Goodman, Thesis, University of California, Berkeley (1969).

41. (a) A. U. MacRae and L. H. Germer, Ann. N. Y. Acad. Sci. 101, 627 (1963) (b) G. Gafner, Surface Sci 2, 534 (1964).

42. H. E. Farnsworth, Phys. Rev. 43, 900 (1933).

43. H. E. Farnsworth, Phys. Rev. 40, 684 (1932).

44. R. L. Park, J. Appl. Phys. 37, 295 (1966).

45. H. E. Farnsworth, et al. J. Appl. Phys. 29, 1150 (1958).

46. M. Onchi and H. E. Farnsworth, Surface Sci. 11, 203 (1968).

47. V. Heine, Proceedings of the Fourth International Materials Symposium Berkeley, 1968, ed. by G. A. Somorjai.

48. W. A. Harrison, Pseudopotentials in the Theory of Metals (Benjamin Co. New York, 1966).

49. J. B. Pendry, to be published, J. Phys. C. (1969).

50. A. Gervais, R. M. Stern, M. Menes, Acta Cryst. A24, 191 (1968).

51. R. L. Park and H. E. Farnsworth, J. Chem. Phys. 43, [7] 2351 (1965).

52. J. E. Boggio and H. E. Farnsworth, Surface Sci. 3, 62 (1964).

53. A. J. Pignocco and G. E. Pellissier, Surface Sci. 7, 261 (1967).

54. (a) H. E. Farnsworth and K. Hayek, Sup. Al Nuevo Cimiento, V,[2] 451 (1967); (b) K. Hayek and H. E. Farnsworth and R. C. Park, Surface Sci. 10, 429 (1968).

55. T. W. Hass and A. G. Jackson, J. Chem. Phys. 44 [8], 2921 (1965).

56. L. H. Germer, R. M. Stern, and A. U. MacRae, Metals Surface (American Society for Metals, Metals Park, Ohio), 1963, p. 287.

57. C. A. Hauk and H. E. Farnsworth, Surface Sci. 1, 378 (1964).

58. A. J. Pignocco and G. E. Pellissier, J. Electrochem. Soc. 112 [12], 1188 (1965).

59. J. K. Viji and P. F. Packnan, J. Chem. Phys. 50[3], 1343 (1969).

60. J-5-BKY-CC66, Cal Comp Plotter Subroutine - Chippewa Fortran.

61. J. M. Ziman, Principles of the Theory of Solids, (Cambridge University Press, London, 1964).

62. E. R. Jones, J. T. McKinney, M. B. Webb, Phys. Rev. 151, 476 (1966).

63. H. B. Lyon and G. A. Somorjai, J. Chem. Phys. 46, 2539 (1967).

64. R. M. Goodman, H. H. Farrell, and G. A. Somorjai, J. Chem. Phys. 48, 1046 (1968).

TECHNICAL INFORMATION DIVISION
LAWRENCE RADIATION LABORATORY
UNIVERSITY OF CALIFORNIA
BERKELEY, CALIFORNIA 94720